Numeričko modeliranje termokemijskih procesa unutar cementnog kalcinatora s ciljem čišće proizvodnje cementa

Mikulčić, Hrvoje

Doctoral thesis / Disertacija

2015

Degree Grantor / Ustanova koja je dodijelila akademski / stručni stupanj: **University of Zagreb, Faculty of Mechanical Engineering and Naval Architecture / Sveučilište u Zagrebu, Fakultet strojarstva i brodogradnje**

Permanent link / Trajna poveznica: https://urn.nsk.hr/urn:nbn:hr:235:318265

Rights / Prava: In copyright/Zaštićeno autorskim pravom.

Download date / Datum preuzimanja: **2024-05-08**

FACULTY OF MECHANICAL ENGINEERING AND NAVAL ARCHITECTURE

HRVOJE MIKULČIĆ

NUMERICAL MODELLING OF THERMO-CHEMICAL PROCESSES INSIDE A CEMENT CALCINER FOR A CLEANER CEMENT PRODUCTION

DOCTORAL THESIS

Zagreb, 2015

Sveučilište u Zagrebu

FAKULTET STROJARSTVA I BRODOGRADNJE

HRVOJE MIKULČIĆ

NUMERIČKO MODELIRANJE TERMO-KEMIJSKIH PROCESA UNUTAR CEMENTNOG KALCINATORA S CILJEM ČIŠĆE PROIZVODNJE CEMENTA

DOKTORSKI RAD

Zagreb, 2015

FACULTY OF MECHANICAL ENGINEERING AND NAVAL ARCHITECTURE

HRVOJE MIKULČIĆ

NUMERICAL MODELLING OF THERMO-CHEMICAL PROCESSES INSIDE A CEMENT CALCINER FOR A CLEANER CEMENT PRODUCTION

DOCTORAL THESIS

SUPERVISOR:

Prof.dr.sc. NEVEN DUIĆ

Zagreb, 2015

FAKULTET STROJARSTVA I BRODOGRADNJE

HRVOJE MIKULČIĆ

NUMERIČKO MODELIRANJE TERMO-KEMIJSKIH PROCESA UNUTAR CEMENTNOG KALCINATORA S CILJEM ČIŠĆE PROIZVODNJE CEMENTA

DOKTORSKI RAD

Mentor:

Prof.dr.sc. Neven Duić

Zagreb, 2015

BIBLIOGRAPHY DATA

TABLE OF CONTENTS

III

PREFACE

Repetitio est mater studiorum

ACKNOWLEDGEMENT

SUMMARY

The present cement production is facing two main problems. The first one is the production of large amount of greenhouse gases, around 5 % of world's anthropogenic CO_2 emissions, and second one is the high fuel prices, mainly coal. The cement producers are therefore under increasing pressure to reduce their fossil fuel consumption and associated greenhouse gases emissions. It was found that partial substitution of coal by alternative fuels like waste derived fuels and biomass may play a major role in the reduction of CO_2 emissions. As waste disposal at landfills is the last option in the waste management strategy, energy recovery of waste derived fuels, commonly known as solid recovered fuels – SRF, in the cement industry has a high potential.

Incineration of high share of SRF in cement calciners still faces significant challenges, mainly because it is well known that the use of alternative fuels in existing pulverized burners alters the flame shape, the temperature profile inside the furnace, and the burnout of the fuels used. A possibility for the ex-ante control and investigation of the incineration process are computational fluid dynamics - CFD simulations. CFD simulations have shown to be a powerful tool during the development and optimisation of chemical engineering processes and involved apparatuses. They can show some important flow characteristics and mixing phenomena, which cannot be experimentally investigated, and because of that CFD together with experiments and theory, has become an integral component of combustion research.

The main focus of this work was to achieve a physically accurate and numerically efficient method for simulation of thermo-chemical processes occurring inside a cement calciner. This implied good knowledge of state-of-the-art solid fuel combustion models, such as coal, biomass and solid recovered fuel combustion model, as well as proper definition of the endothermic calcination process. In order to correctly numerically study the role and interaction of solid fuel combustion and limestone calcination within cement calciner, new and improved physical and chemical models were introduced. To verify the accuracy of the modelling approach, the new models were extensively analysed, and the numerical predictions of each new model was compared with experimental data. To represent the applicability of the modelling approach, three different three dimensional geometries of real industrial cement calciners were used for the numerical simulations.

SAŽETAK

Trenutna proizvodnja cementa suočena je s dva značajna problema. Prvi je proizvodnja velike količine stakleničkih plinova, oko 5 % ukupnih globalnih CO_2 emisija ljudskog podrijetla, a drugi je visoka cijena goriva, uglavnom ugljena. Proizvođači cementa su stoga pod sve većim pritiskom da smanje potrošnju fosilnih goriva i s njima povezanim emisijama stakleničkih plinova. Utvrđeno je da je djelomična zamjena ugljena alternativnim gorivima, poput biomase i goriva dobivenih obradom otpada, može imati važnu ulogu u smanjenju CO_2 emisija. Kako je zbrinjavanje otpada na odlagalištima zadnja opcija u strategiji upravljanja otpadom, energetska oporaba goriva dobivenog obradom otpada, poznatijeg kao kruto gorivo iz otpada (*engl.* solid recovered fuel - SRF), ima veliki potencijal u cementnoj industriji.

Spaljivanje visokog udjela SRF-a u cementnim kalcinatorima još se uvijek suočava sa značajnim izazovima, poglavito jer je dobro poznato da upotreba alternativnih goriva u postojećim plamenicima mijenja oblik plamena, profil temperatura unutar peći, te izgorenost samog goriva koje se koristi. Korištenjem računalne dinamike fluida (engl. computational fluid dynamics - CFD) moguće je prethodno ispitivati i kontrolirati proces izgaranja različitih vrsta goriva. CFD simulacije su se tokom godina pokazale kao moćan alat za razvoj i optimizaciju kemijskih procesa te samih uređaja unutar kojih se te kemijske reakcije odvijaju. One mogu pokazati neke važne karakteristike strujanja fluida i miješanja više faza koje je teško eksperimentalno istražiti i stoga je CFD, zajedno sa eksperimentima i teorijom, postao sastavni dio istraživanja procesa izgaranja goriva.

Glavna tema ovog rada bila je postizanje fizički točne i numerički učinkovite metode za simuliranje termo-kemijskih procesa koji se odvijaju unutar cementnog kalcinatora. To je podrazumijevalo dobro poznavanje najmodernijih modela izgaranja krutih goriva kao što su modeli za izgaranje ugljena, biomase i goriva iz čvrstog otpada, kao i pravilno definiranje endotermnog procesa kalcinacije. Kako bi se ispravno numerički proučavala uloga i interakcija izgaranja krutih goriva i termičkog raspadanja vapnenca unutar cementnog kalcinatora, upotrijebljeni su novi i poboljšani fizikalni i kemijski modeli. Nadalje, kako bi se provjerila točnost numeričkog modeliranja, novi modeli su se opsežno analizirali, a numerički dobiveni rezultati svakog novog modela su bili uspoređeni s dostupnim eksperimentalnim podacima. Primjenjivost razvijenog numeričkog modeliranja prikazana je na tri različite trodimenzionalne geometrije realnih industrijskih cementnih kalcinatora, koje su se koristile za detaljne numeričke simulacije.

PROŠIRENI SAŽETAK

Ključne riječi: Numeričko modeliranje, kalcinacija, izgaranje, ugljen, biomasa, plastika, kruto gorivo iz otpada

U posljednjih pet desetljeća ubrzano povećanje koncentracije stakleničkih plinova (*engl.* greenhouse gases - GHG) u atmosferi, koji su uglavnom industrijskog podrijetla, rezultiralo je globalnim klimatskim promjenama. Stoga je čišća i održiva industrijska proizvodnja postala sve važnija. Dobro je poznata činjenica kako je CO_2 najznačajniji od svih stakleničkih plinova, te da samo cementna industrija sudjeluje s 5% u ukupnim globalnim CO_2 emisijama ljudskog podrijetla, potrebno je kontinuirano poboljšavati energetsku učinkovitost u procesu proizvodnje cementa [1]. Trenutno najefikasnija tehnologija u proizvodnji cementa je suhi proces u rotacionoj peći s višestupanjskim predgrijačem sirovine te cementnim kalcinatorom. Potonji predstavlja komoru za izgaranje koja se nalazi prije rotacione peći, a u kojoj se sirovina, većinom sačinjena od vapnenca, podvrgava procesu kalcinacije. Kalcinacija, ili termička razgradnja vapnenca, je snažna endotermna reakcija koja zahtijeva veliku količinu topline, ukazujući na potrebu istovremenog provođenja kalcinacije i egzotermnog izgaranja goriva [2]. Kontroliranje ova dva termo-kemijska procesa je vrlo važno iz razloga što imaju direktan utjecaj na kvalitetu cementa, nastajanje polutanata te općenito energetsku učinkovitost procesa proizvodnje cementa. Razni su pristupi kontroli i poboljšanju energetske učinkovitosti industrijskih ložišta. Korištenje računalne dinamike fluida (*engl.* computational fluid dynamics - CFD) i simulacija da se ispita i poboljša interakcija termo-kemijskih procesa postaje sve važnije [3]. Zajedno s teorijom i eksperimentima, CFD simulacije postale su integralni dio istraživanja komora za izgaranja. Rezultati dobiveni simulacijama mogu se iskoristiti za optimizaciju turbulentnog reaktivnog strujanja, geometrije komore izgaranja, te konačno za povećanje energetske učinkovitosti, čineći proizvodnju cementa održivijom.

Razvoj prikladnih komora izgaranja je često vrlo zahtjevan, vremenski dug te skup proces. Istraživanje termo-kemijskih procesa koji se odvijaju unutar komore za izgaranje moguće je postići simulacijama. Rane detaljne informacije, parametarske analize i početni zaključci koji se dobivaju putem simulacija vrlo su važne kod rukovanja komorama za izgaranje. Tijekom godina CFD je postao integralna komponenta istraživanja izgaranja koja se koristi u procesu razvoja komora za izgaranje, povećavajući razumijevanje kompleksnih fenomena koji se unutar njih odvijaju. Doduše, simulacije termo-kemijskih procesa u cementnim kalcinatorima

još su uvijek suočene s ozbiljnim izazovima. U cilju boljeg razumijevanja fenomena miješanja, procesa izmjene mase i topline te strujanja fluida istraživani su razni cementni kalcinatori. U radu Huanpeng i sur. [4] prikazana je numerička studija utjecaja raznih parametara na dinamiku dvofaznog strujanja u cementnom kalcinatoru, gdje su predstavljena transportna svojstva krute faze kinetičkom teorijom zrnatog strujanja. Numerička analiza nastajanja NO, CO i CO_2 u cementnom kalcinatoru pokazana je u radu Huang i sur. [5]. Ova studija je pokazala dobro poklapanje rezultata dobivenih numeričkim putem s provedenim mjerenjima za izgorenost čestica ugljena i razgradnju vapnenca. Numeričko istraživanje procesa u cementnim kalcinatorima provedeno je u studiji Hillers i sur. [6], gdje je prikazano modeliranje turbulencije, zračenja, procesa kalcinacije, izgaranja ugljena i nastajanja NO_x. Pokazano je da CFD ima velik potencijal u kontroli štetnih emisija i štednji goriva. Utjecaj struje primarnog zraka i promjera gorionika na dvofazno strujanje plinovite i krute faze u cementnom kalcinatoru razmatrano je u studiji Zheng i sur. [7]. Studija je pokazala da navedeni parametri imaju snažan utjecaj na strukturu strujanja i koncentraciju čestica. Hu i sur. [8] su simulirali trodimenzionalni model dvostrukog ložišta i kalcinatora koristeći Eulerov pristup za plinovitu fazu te Lagrangeov pristup za krutu fazu. Rad je pokazao dobro predviđanje izgorenosti i brzine razgradnje vapnenca tokom istovremenog ubrizgavanja dvije vrste ugljena i vapnenca. U radu Huang i sur. [9] prikazana je trodimenzionalna simulacija novog tipa vrtložnog kalcinatora. Razvijena je nova metoda za računanje interakcije čestica i zidova kao i novi model udjela smjese da bi se što preciznije opisali transportni fenomeni u kalcinatoru. Rezultati su pokazali dobro poklapanje s mjerenjima razgradnje vapnenca, izgorenosti ugljena i izlaznom temperaturom iz kalcinatora. Fidaros i sur. [10] predstavili su matematički model i studiju utjecaja parametara na strujanje fluida i transportne fenomene u cementnom kalcinatoru. Rad je pokazao dobro slaganje rezultata temperature, brzine i raspodjele čestica na izlazu iz kalcinatora gdje su postojali rezultati mjerenja. Dou i sur. [11] u svojem su radu istraživali izgaranje ugljena i razgradnju vapnenca unutar cementnog kalcinatora, te su pokazali da se za povećanje razgradnje vapnenca i optimiziranje temperature unutar kalcinatora, smjer tercijarnog zraka na gorioniku mora prilagoditi tangencijalno, te da ulaz vapnenca mora biti postavljen nasuprot ulazu ugljena. Ha i sur. [12] istraživali su utjecaj veličine čestica ugljena na razgradnju vapnenca unutar cementnog kalcinatora. Rad je pokazao da izgaranje sitnijih čestica ugljena ima zanemariv utjecaj na razgradnju vapnenca. Bluhm-Drenhaus i sur. [13] su povezivanjem metode računalne dinamike fluida i metode diskretnih elemenata istraživali prijenos mase i topline. Studija je pokazala da razvijena metoda daje detaljan uvid u fizikalne fenomene koji se odvijaju u komori i daje nove

mogućnosti za optimizaciju rada komore. Nance i sur. [14] koristeći simulacije, istraživali su prijenos mase i topline u novo dizajniranom cementnom kalcinatoru. Rad je pokazao da predložena metoda može uvelike pomoći u optimizaciji rada i geometrije kalcinatora. Jianxiang i sur. [15] koristeći metodu velikih vrtloga i kinetičku teoriju zrnatog strujanja za krutu fazu, istraživali su fenomen miješanja vapnenca i ugljena. Rad je pokazao da parametri rada kalcinatora trebaju biti postavljeni vrlo precizno kako bi proizvodnja bila stabilna i učinkovita. Sve navedene studije pokazuju potrebu za dodatnim istraživanjem i razvojem cementnih kalcinatora. Važno je ukazati da je većina ovdje navedenih CFD studija svoje rezultate uspoređivala s mjerenjima provedenima na izlazu iz kalcinatora. Zbog pomanjkanja mjerenih podataka vezanih uz karakteristike strujanja te kemijskih i fizikalnih procesa unutar kalcinatora, ovakav pristup je valjan za predviđanje emisija polutanata, brzine razgradnje vapnenca i stupnja izgorenosti čestica ugljena. S aspekta detalja u području gorionika, stijenki komore i ostalih područja s interesantnim fenomenima strujanja i miješanja, te radi optimizacije ključnih fizikalnih i kemijskih procesa unutar kalcinatora, novi pristup koji uključuje odvojene modele procesa kalcinacije i izgaranja različitih krutih goriva u prahu, poboljšava dostupnu metodu CFD simulacija. Zbog visoke pouzdanosti modela koji su odvojeno validirani, ovim pristupom je moguće postići potrebnu točnost navedenih detalja kemijskih i fizikalnih procesa unutar cementnih kalcinatora. Nadalje, važno je napomenuti da su sve navedene studije provedene za slučaj izgaranja ugljena u cementnim kalcinatorima, te se nije analiziralo korištenje alternativnih goriva, npr. biomase ili krutog goriva iz otpada.

CILJ I HIPOTEZA

Hipoteza ovog istraživanja je da se kombinacijom Euler-Langrangeove metode višefaznog strujanja, te prilagođenih difuzijsko-kinetičkih modela kalcinacije, izgaranja ugljene prašine, biomase i razvijenim modelom krutog goriva iz otpada, moguće dovoljno točno numerički simulirati termo-kemijski procesi unutar cementnog kalcinatora. Rezultati dobiveni pomoću ovog modela omogućuju razvoj učinkovitijih kalcinatora. Cilj ovog istraživanja je bio razvoj novih učinkovitih modela koji su potvrdili hipotezu usporedbom rezultata simulacije i dostupnih eksperimentalnih podataka.

Rezultat ovog istraživanja je bolje razumijevanje utjecaja su-spaljivanja alternativnih goriva i ugljena unutar cementnog kalcinatora, i njegovog utjecaja na proces kalcinacije. Posebna se pažnja posvetila modeliranju procesa kalcinacije, gdje su se u obzir uzeli utjecaji lokalne temperature, tlaka razgradnje, difuzije i ostalih utjecajnih fizikalnih značajki. Osobiti znanstveni doprinos predstavlja korištenje modela izgaranja alternativnih goriva koji su u ovom istraživanju prilagođeni ulozi sekundarnog goriva, uz ugljen kao primarnog goriva. Novi pristup modeliranju, predstavljen u ovom istraživanju, također ukazuje na nove mogućnosti vođenja procesa i proizvodnju efikasnije opreme za ekološki održiviju proizvodnju cementa.

METODE I POSTUPCI

Da bi se napravilo istraživanje utjecaja raznih parametara na brzinu razgradnje čestica vapnenca, izgorenosti čestica goriva i nastajanja štetnih polutanata u cementnom kalcinatoru, sve važne termo-kemijske reakcije, kao što su kalcinacija, izgaranje ugljena, biomase i krutog goriva iz otpada, moraju biti modelirane. U ovom istraživanju, kao i u većini inženjerskih pristupa danas, koristila se Euler-Langrangeova metoda rješavanja višefaznog strujanja. U ovom pristupu krute čestice su predstavljene konačnim brojem grupa čestica, koje se nazivaju parcelama [16]. Pretpostavlja se da su u jednoj parceli sadržane čestice slične veličine i fizikalnih svojstava. Putanja svake parcele unutar polja strujanja računa se pomoću Lagrangeove sheme, što pretpostavlja da su reprezentativne parcele praćene korištenjem skupa jednadžbi koje opisuju njihovu dinamiku dok se kreću kroz izračunato polje strujanja. Povezivanje krute i plinovite faze uzima se u obzir uvođenjem izvorskih članova za izmjenu mase, kemijskih vrsta , momenta i energije. Langrangeova faza se računa između dva vremenska proračuna Eulerove faze, eksplicitnom integracijskom metodom, te se tako dobivaju izvorski članovi za Eulerovu fazu. Jednako tako, rješenje Eulerove faze daje parametre okoline za Langrangeovu fazu [17].

Razvijeni matematički modeli koji se koriste za proračun procesa kalcinacije, izgaranja ugljena, biomase i krutog goriva iz otpada koristili su modul Lagrangeovog spreja unutar korištenog programskog paketa, gdje se termo-kemijske reakcije odvijaju unutar čestice, kao i između čestice i plinovite faze. Kemijske reakcije unutar plinovite faze računate su pomoću

rješavača koji koristi obične diferencijalne jednadžbe, te su one predstavljale dodatni ponor ili izvorski član za transportne jednadžbe kemijskih vrsta i entalpije u plinovitoj fazi. Razvijeni modeli, zajedno s termo-fizikalnim svojstvima vapnenca, vapna i komponenti ugljena, biomase i krutog goriva iz otpada, te modela zračenja čestica, integrirana su u komercijalni CFD kod AVL FIRE® pomoću korisničkih funkcija napisanih u programskom jeziku FORTRAN, kako bi se proces kalcinacije i izgaranja simulirao na ispravan način.

Ovo istraživanja provedeno je u nekoliko koraka. Kao što je prije navedeno, cilj je bio razvoj nove metode za ispitivanje su-spaljivanja alternativnih goriva s ugljenom unutar cementnog kalcinatora zbog boljeg razumijevanja, poboljšanja i optimizacije procesa kalcinacije.

Prvi korak istraživanja je bio razvoj i provjera točnosti modela procesa kalcinacije. Ispitivali su se glavni utjecaji na ovaj proces. Cilj ovog koraka je bio dobivanje informacija i saznanja o procesu kalcinacije i utjecaju raznih radnih uvjeta na isti.

Drugi korak je bio istraživanje, implementacija i provjera točnosti modela izgaranja ugljena i biomase. Ispitivali su se utjecaji sušenja, pirolize, izgaranja koksa i izgaranja hlapljivih tvari. Pod ovim korakom provedeno je i istraživanje i provjera točnosti modela izgaranja krutog goriva iz otpada. Ovdje se također ispitivao utjecaj sušenja, pirolize, izgaranja koksa, izgaranja hlapljivih tvari, međutim ispitivala se i razgradnja plastičnog udjela u otpadu. Cilj ovog koraka je bio dobivanje informacija i saznanja o procesu izgaranja različitih krutih goriva, te utjecaju raznih radnih uvjeta na isti.

Unutar oba navedena koraka istraživanja ispitivao se također i utjecaj diskretizacije računske domene na dobivene rezultate.

Konačno, svi zaključci iz prethodnih koraka bili su primijenjeni u CFD simulaciji tri različita industrijska cementna kalcinatora. Gdje je bilo moguće, rezultati simulacija su uspoređeni s dostupnim mjernim podacima, te je izložena opsežna analiza rezultata. Detaljni opisi tri različite geometrije realnih industrijskih cementnih kalcinatora, koje su se koristile za detaljne numeričke simulacije nalazi se u priloženim radovima PAPER 2, 4 i 6.

Cjelokupna metoda rješavanja višefaznog strujanja, te način na koji se povezuju Eulerova i Langrangeova faza, opisan je u poglavlju 2. NUMERICAL MODELLING. Pod istim poglavljem nalazi se detaljan opis modela kalcinacije te modeli izgaranja svakog od

prethodno navedenih krutih goriva. Više detalja vezano za modeliranje reaktivnog višefaznog strujanja nalazi se u priloženim radovima PAPERS 1-6.

KEYWORDS

Numerical modelling

Calcination process

Combustion

Coal

Biomass

Plastic

Solid Recovered Fuel

KLJUČNE RIJEČI

Numeričko modeliranje

Kalcinacija

Izgaranje

Ugljen

Biomasa

Plastika

Kruto gorivo iz otpada

LIST OF ABBREVIATIONS

CFD	Computational Fluid Dynamics
DTF	Drop Tube Furnace
EU	European Union
GHG	Greenhouse Gases
IEA	International Energy Agency
IFRF	International Flame Research Foundation
IPFR	Intensified Plug Flow Reactor
LES	Large Eddy Simulation
MSW	Municipal Solid Waste
ODE	Ordinary Differential Equation
PP	Polypropylene
SRF	Solid Recovered Fuels
UNFCCC	United Nations Framework Convention on Climate Change
WtE	Waste to Energy

NOMENCLATURE

A	sphere surface, m^2
A_{geom}	sphere surface, m^2
A_p	particle surface, m^2
A_{pn}	projected area of an n-particle, m^2
A_{por}	overall reaction surface, m^2
$\overline{c}_p$	specific heat capacity of coal or biomass, ash and char mixture, J kg^{-1} K^{-1}
$\tilde{c}_p$	specific heat capacity at constant pressure, J kg^{-1} K^{-1}
c_{pCaCO_3}	specific heat capacity of limestone, J kg^{-1} K^{-1}
c_{pCaO}	specific heat capacity of lime, J kg^{-1} K^{-1}
c_{pi}	specific heat capacity of gas component, J kg^{-1} K^{-1}
$c_{pPPvapour}$	specific heat capacity of polypropylene vapour, J kg^{-1} K^{-1}
C_p	water vapour concentration at the particle surface, kg mol m^{-3}
C_g	concentration of water vapour in the gas, kg mol m^{-3}
d	particle diameter, m
d'	mean particle diameter, m
d_p	particle diameter, m
d_{part}	particle diameter, m
d_{pore}	pore diameter, m
D	diffusion coefficient, m^2 s^{-1}
D_{bin}	binary diffusion coefficient, m^2 s^{-1}
D_{knu}	Knudsen diffusion coefficient, m^2 s^{-1}
D_0	oxygen diffusion coefficient, dimensionless
D_w	diffusion coefficient of water vapour in the gas, m^2 s^{-2}
E	internal energy, J kg^{-1}
E_a	activation energy for polypropylene decomposition, J mol^{-1}
E_{a1}	activation energy for devolatilisation, J mol^{-1}

E_{a2}	activation energy for char oxidation, J mol^{-1}
E_p	particle emission, W m^{-3}
f	reaction enthalpy factor, dimensionless
f_m	mechanism factor, dimensionless
f_{CO}	carbon monoxide factor, dimensionless
F_{idr}	drag force vector, N
F_{ig}	force including effects of gravity and buoyancy vector, N
g_i	gravitational acceleration vector, m s^{-2}
G	incident radiation, W m^{-2}
h_{latent}	latent heat, J kg^{-1}
ΔH_R	reaction enthalpy, J mol^{-1}
k	overall reaction rate, kg m^{-2} s^{-1}
$\hat{k}$	overall reaction rate, kg s^{-1}
k_{ch}	chemical reaction rate, mol m^{-2} s^{-1}
$\tilde{k}_{ch}$	chemical reaction rate, kg m^{-2} s^{-1}
$\bar{\bar{k}}_{ch}$	chemical reaction rate, s^{-1}
k_d	overall devolatilisation reaction rate, s^{-1}
k_D	reaction rate, mol m^{-2} s^{-1} Pa^{-1}
k_{ox}	overall char oxidation reaction rate, s^{-1}
k_{ph}	physical reaction rate, kg m^{-2} s^{-1}
k_w	mass transfer coefficient, m s^{-1}
k_0	pre-exponential factor for polypropylene decomposition, s^{-1}
$k_{0,1}$	devolatilisation pre-exponential factor, s^{-1}
$k_{0,2}^{ch}$	char oxidation pre-exponential factor, s^{-1}
k_1	devolatilisation reaction rate, s^{-1}
k_2	char oxidation reaction rate, s^{-1}
k_2^{ch}	char oxidation chemical reaction rate, kg m^{-2} s^{-1} Pa-1
k_2^{ph}	char oxidation physical reaction rate, kg m^{-2} s^{-1} Pa-1

m_{ash}	ash mass, kg
m_C	char mass, kg
$m_{coal/biomass}$	coal or biomass mass, kg
m_{CaCO_3}	limestone mass, kg
m_{CaO}	lime mass, kg
m_i	i-th gas component mass, kg
m_p	particle mass, kg
$\dot{m}_{ash}$	mass transfer of ash, kg s^{-1}
$\dot{m}_{C+}$	increase of char mass due to devolatilisation, kg s^{-1}
$\dot{m}_{C-}$	decrease of char mass due to char oxidation, kg s^{-1}
$\dot{m}_{coal/biomass}$	coal or biomass mass change, kg s^{-1}
$\dot{m}_{CO}$	mass transfer of carbon monoxide, kg s^{-1}
$\dot{m}_{CO_2}$	mass transfer of carbon dioxide, kg s^{-1}
$\dot{m}_{CaCO_3}$	mass transfer of limestone, kg s^{-1}
$\dot{m}_{CaO}$	mass transfer of lime, kg s^{-1}
$\dot{m}_i$	mass transfer of i-th gas component, kg s^{-1}
$\dot{m}_{O_2}$	mass transfer of oxygen, kg s^{-1}
$\dot{m}_p$	mass transfer of a particle, kg s^{-1}
$\dot{m}_{PPvapour}$	mass transfer of polypropylene vapour, kg s^{-1}
$\dot{m}_{Y_k}$	mass transfer of k-th gas component due to devolatilisation, kg s^{-1}
M_{AB}	average molecular weight, g mol^{-1}
M_C	char molecular weight, g mol^{-1}
M_{CO}	carbon monoxide molecular weight, g mol^{-1}
M_{CO_2}	carbon dioxide molecular weight, g mol^{-1}
M_{CaCO_3}	limestone molecular weight, g mol^{-1}
M_{CaO}	lime molecular weight, g mol^{-1}
$M_{coal/biomass}$	coal or biomass molecular weight, g mol^{-1}
M_{H_2O}	water vapour molecular weight, g mol^{-1}

M_{O_2}	oxygen molecular weight, g mol^{-1}
M_{Y_k}	k-th gas component molecular weight, g mol^{-1}
n	particle spread parameter, dimensionless
n_p	number of particles per parcel, dimensionless
p	total pressure, Pa
p_{CO_2}	carbon dioxide partial pressure, Pa
p_{eq}	equilibrium carbon dioxide partial pressure, Pa
p_{O_2}	oxygen partial pressure, Pa
p_{ref}	referent pressure, Pa
p_{sat}	saturation pressure, Pa
R	universal gas constant, J mol^{-1} K^{-1}
R_{CO_2}	carbon dioxide gas constant, J kg^{-1} K^{-1}
Re_p	particle Reynolds number, dimensionless
S_C	mass source, kg s^{-1}
S_E	energy source, W m^{-3}
S_M	momentum source, N m^{-3}
S_{Y_k}	k-th gas component source, kg s^{-1}
Sc	Schmidt number, dimensionless
Sh	Sherwood number, dimensionless
t	time, s
T	temperature, K
T_0	reference temperature, K
T_g	gas temperature, K
T_p	particle temperature, K
$\dot{T}_p$	rate change of particle temperature, K s^{-1}
u_{ip}	particle velocity vector, m s^{-1}
v_i, v_j	velocity vector, m s^{-1}
X_{H_2O}	water vapour molar fraction, dimensionless

y_C	mass fraction of char remaining in the particle, dimensionless
$y_{coal/biomass}$	mass fraction of coal or biomass remaining in the particle, dimensionless
Y_k	k-th gas component mass fraction, dimensionless

Greek letters

α	convective heat transfer coefficient , W m^{-2} K^{-1}
Γ	diffusion coefficient, dimensionless
δ_{ij}	Cronecker symbol, dimensionless
ε	correction factor, dimensionless
ε	emissivity, dimensionless
ε_p	void fraction (porosity), dimensionless
η	pore efficiency factor, dimensionless
λ	thermal conductivity, W m^{-1} K^{-1}
μ	dynamic viscosity, Pa s
ν_C	char stoichiometry number from devolatilisation, dimensionless
ν_{Y_k}	k-th gas component stoichiometry number from devolatilisation, dimensionless
ρ	density, kg m^{-3}
σ	Stefan-Boltzmann's constant, W m^{-2} K^{-4}
σ_{AB}	characteristic length, m
τ_{ij}	stress tensor, Pa
τ_p	tortuosity, dimensionless
ω_d	diffusion collision integral, dimensionless

LIST OF FIGURES

LIST OF TABLES

1 INTRODUCTION

1.1 Background

Over the past five decades rapid increases in the concentrations of greenhouse gases - GHG in the atmosphere, mainly coming from the industrial sector, have resulted in global climate changes. Climate change problems are addressed by two major international agreements: the 1992 United Nations Framework Convention on Climate Change (UNFCCC) and the 1997 Kyoto Protocol [18]. The ultimate objective of these agreements is to stabilise GHG concentrations in the atmosphere at a level that would prevent dangerous anthropogenic interference with the global climate system. The latest report from the scientific panel on anthropogenic global warming indicates that remarkable and joint global action is required to reduce CO_2 emissions. Meaning the longer we wait to address this issue, the more difficult, technologically challenging and expensive it becomes [19].

It is well known that over 80 % of global CO_2 emissions are caused by industry and transport activities and due to this reason, there is a need to decarbonise transport and industrial production [20]. In 2008, the electricity and heat generation sector was responsible for 41 %, transport sector for 22 %, and industry for 20 % of anthropogenic CO_2 emissions [1]. From these 20 % of global CO_2 emissions related to industry, cement industry accounts for approximately a quarter of total CO_2 emissions in industry [21]. This means that cement industry as an energy intensive industrial sector, alone generates approximately 5 % of anthropogenic CO_2 in the world [1],[22].

In recent years, there have been numerous studies worldwide discussing energy conservation policies, estimating the CO_2 mitigation potential, and considering technology evaluation for the cement industry. Some of these studies investigated the effect of mitigation measures at the global level, such as the study conducted by the International Energy Agency - IEA [23]. However, the majority of these studies evaluated the environmental impact of cement production at national and regional levels. The effect of mitigation measures on the regional level, like those in the EU were analysed by Pardo et al. [24] and Moya et al. [25]. The United States' cement industry was analysed in the study by Xu et al. [26]. However due to the rapid economic growth and vast urbanization, the majority of the studies related to the

1

cement industry are for the developing countries like China [27]-[29], South Africa [30], Turkey [31], Iran [32], India [33], Thailand [34], and Vietnam [35]. The reason for these is most easily seen in Table 1 where the global cement production for 2012 is given. Table 1 shows that the vast majority of cement production is located in developing countries, especially in Asia.

Table 1 Global cement production in 2012 [36].

Country	Production (million tons)	Share in the world production
China	2150	58.1%
India	250	6.7%
United States	74	2.0%
Brazil	70	1.9%
Iran	65	1.8%
Vietnam	65	1.8%
Turkey	60	1.6%
Russian Federation	60	1.6%
Japan	52	1.4%
South Korea	49	1.3%
Egypt	44	1.2%
Saudi Arabia	43	1.2%
Mexico	36	1.0%
Germany	34	0.9%
Thailand	33	0.9%
Pakistan	32	0.9%
Italy	32	0.9%
Indonesia	31	0.8%
Spain	20	0.5%
Other (rounded)	500	13.5%
World total (rounded)	3700	-

The importance of cement production in these developing economies can also be observed when comparing the annual CO_2 emissions from cement production in industrialised countries

2

and developing countries. In the EU, the cement industry contributes to about 4.1 % of total CO_2 emissions [24]. This share varies from one EU country to another, in EU's most developed country Germany, this share is even lower, and the cement industry accounts for 2.9 % of Germany's CO_2 emissions [37]. This is similar for the cement industry in United States, where cement production is responsible for about 2 % of total CO_2 emissions [38]. Whereas in the China, world's largest cement producing country and world's largest emitter of GHG emissions, 15 % of total CO_2 emissions are related to cement production [39][40]. All of these studies stated that there is a great challenge in attempting to approach sustainability in the cement industry.

1.2   Cement production process

The best available technology, the one with the lowest energy consumption, for the cement manufacturing today, is the use of a rotary kiln together with multi-stage cyclone preheater system and a calciner. Figure 1 illustrates the stages of the cement production process. As can be seen, cement manufacturing is a complex process which consists of several sub-processes. There are four sub-processes in the cement manufacturing process that have the most influence on final cement quality and fuel consumption. These four sub-processes are: raw material preheating, calcination, clinker burning, and clinker cooling [10]. Prior to the raw material preheating, the raw material is collected, crushed, mixed with additives and transported to the cyclone preheating system.

The cyclone preheating systems have been developed to enhance the heat exchange process between the raw material and the flue gases. The preheating system takes place prior to the calciner and the rotary kiln and can have several stages, depending on how many cyclones are used. At each stage of the preheating system, e.g. in each cyclone, the principle of the heat exchange is the same. Raw material is heated by moving counter-flow of the hot flue gases coming from the rotary kiln. This counter-flow movement effect is due to the particle separation phenomena occurring within the gas cyclones. The separation of the solid particles from the gas is done by the highly tangential flow entering the cyclone. The centrifugal force acting on the particles directs them to the wall, separating them from the flow, and due to the gravitational force the particles slide to the lower part of the cyclone. In contrast to the solid particles the gas flow has a different behaviour. Firstly the gas swirls downwards in the outer cyclone part, where the separation is done, and then in the lower part

3

of the cyclone where the axial velocity reverses, the gas starts to swirl upwards in the inner cyclone region. This process is repeated until the raw material goes through all the cyclones [41].
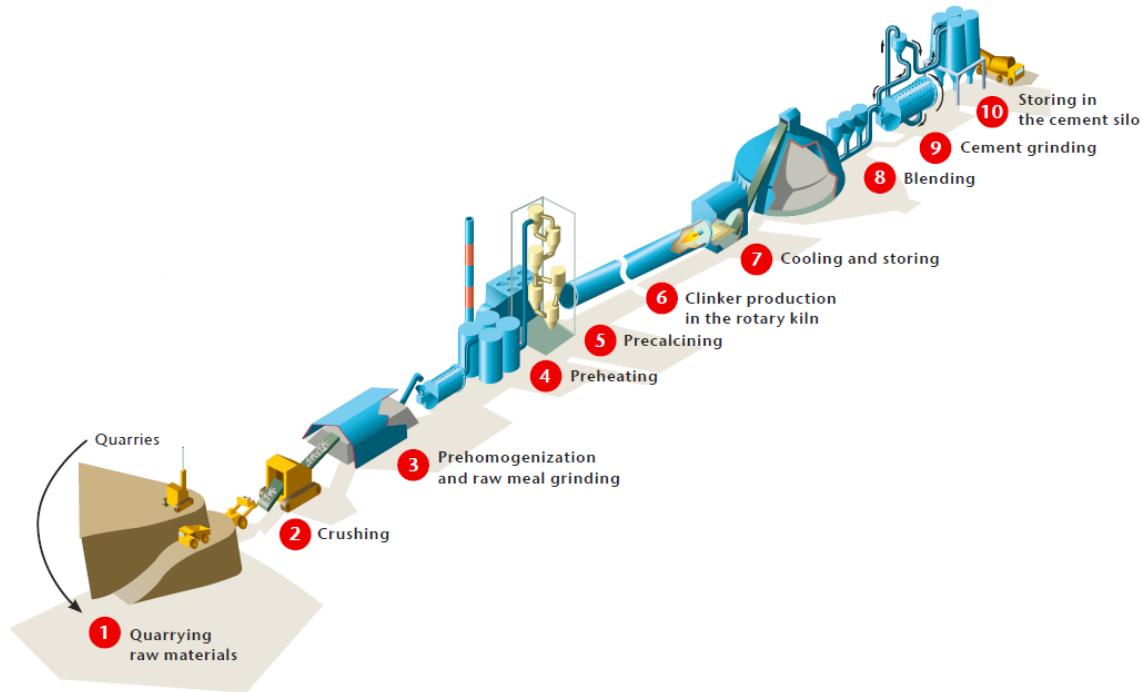
Figure 1 Cement manufacturing process [23].

After preheating, raw material enters the cement calciner. Cement calciner, is a combustion unit found prior to the rotary kiln, and inside of it, the raw material, mainly composed of limestone, undergoes the calcination process. The calcination process is a strongly endothermic reaction that requires combustion heat released by the fuel, indicating that endothermic limestone calcination and exothermic fuel combustion proceed simultaneously [2]. According to Szabo et al. [42] a decrease in energy consumption by 8-11% can be achieved when a rotary kiln is used together with a calciner. This decrease is due to the fact that cement calciners have lower operating temperatures than rotary kilns. To ensure a temperature of 850°C, needed for a stable calcination process, cement calciners use heat from the combustion of solid fuels along with the exhaust gases from a rotary kiln [43].

Clinker burning is the highest energy demanding process in cement production. It occurs after the calcination process. The clinker is produced in a rotary kiln which rotates at speed 3-5 revolutions per minute, and is positioned at an angle of 3-4 degrees to the horizontal line. This angle causes the material to slide and tumble down through the hotter zones towards the

flame. The temperature of 1450˚C ensures the clinker formation. After the clinkering process in the rotary kiln is finished, the cement clinker is rapidly cooled down to 100-200˚C [44]. This process is done rapidly to prevent undesirable chemical reactions. Blending of clinker with different additives follows the clinker cooling process. At that point the composition of the final product - cement is obtained. Afterwards the cement is milled, stored in the cement silo, and distributed to consumers.

1.3   Motivation and general overview

Coal as an abundant resource, is the most used solid fossil fuel in industry and power generating sector worldwide, albeit its CO_2 emission is higher than that of other fossil fuels [45]. The utilization of coal has however over the past decade started to face arising environmental challenges, mainly because coal-fired plants are the biggest contributor to CO_2 emissions. Consequently, extensive efforts have been devoted to develop cleaner and more efficient technologies for the utilization of coal.

Partial substitution of coal by alternative fuels like waste derived fuels and biomass has attracted attention worldwide, mainly because biomass and the biogenic fraction of waste derived fuels are considered CO_2-neutral [46]. Depletion of fossil fuels, rising of their prices and the Kyoto Protocol, are more and more directing plant operators towards renewable energy. In that sense, the displacing of fossil fuels with renewable fuels is gaining on importance in all industrial sectors [47].

The present cement production is facing two main problems. The first one is the production of large amount of greenhouse gases, and second one is the high fuel prices, mainly coal. The cement producers are therefore under increasing pressure to reduce their fossil fuel consumption and associated greenhouse gases emissions. Due to the huge amount of concrete used throughout the world as construction material, especially in the developing countries, researchers are searching for ways to reduce the cost of cement production and CO_2 emissions related to cement production. There are several measures, which applied to the cement manufacturing processes can reduce its environmental impact and improve its competitiveness. However, it was found that partial substitution of coal by alternative fuels like waste derived fuels and biomass may play a major role in the reduction of CO_2 emissions [48]. Figure 2 shows the IEA comparison of the fuel consumption for cement production for

industrialized and developing countries [49]. The figure shows the actual consumption in 2012 and the projection for year 2025. As can be seen, in both industrialized and developing countries, it is expected that the share of consumed coal and oil will decrease and that the share of natural gas and electricity will stay at the same level or slightly increase. The only fuel that will have a considerable increase in consumption will be biofuels and waste derived fuels. The reason for this expected increase in consumption of biofuels and waste derived fuels firstly is because these fuels are entirely or at least in part considered CO_2-neutral, and secondly because partial substitution of coal by alternative solid fuels like waste derived fuels and biomass in existing pulverized coal fired furnaces can be achieved with small investment costs. This method of partial substitution of coal by alternative solid fuels is recognized as one of the most convenient and advantageous methods for GHG mitigation [50].
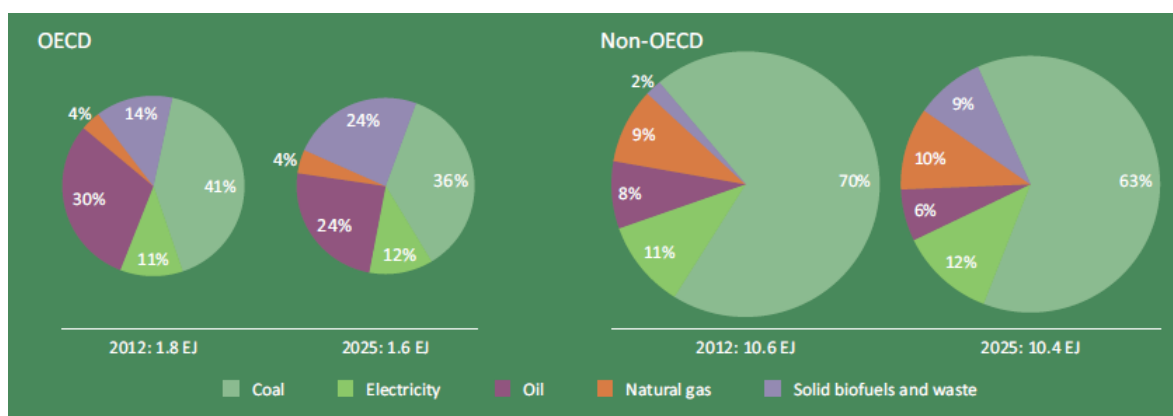
Figure 2 Projection of energy consumption by fuel in cement industry worldwide [49].

At the European Union level, there is a great potential for the use of solid waste derived fuels in the cement industry. As waste disposal at landfills is the last option in the waste management strategy, energy recovery of waste derived fuels, commonly known as solid recovered fuels – SRF, in the cement industry has a high potential [22]. Municipal solid waste - MSW is generated in large amounts worldwide and has a significant environment impact, as for example atmospheric emissions and effluents from landfills [51]. This MSW generation burdens the local communities for collection, handling and disposal, and due to this reason waste management has become a significant problem [52]. Traditional landfill method is also facing the problem of land shortage. Therefore, waste to energy - WtE methods, including incineration, pyrolysis and gasification are drawing more and more attentions [53]. Energy recovery of SRF in cement combustion units has one major advantage compared to regular combustion of SRF in incinerators. Due to the need for high combustion temperatures during

the cement production and supply of fresh air within the cement calciner and rotary kiln, a complete combustion of the waste is ensured. Furthermore, any ash that is produced as a by-product of the combustion process falls to the floor of the rotary kiln, reacts with the raw material and exits the rotary kiln as clinker, so there is no liquid or solid residue to contend with. As a result, the process is clean and favourable for the environment [54]. This is not the case when the alternative fuels are combusted in incinerators or co-combusted in utility boilers. The ash from such applications needs to be disposed of in a different way, meaning that there is still a solid residue to contend with [55].

Although partial substitution of coal by alternative solid fuels is recognized as a method for GHG mitigation, and is gaining in significance worldwide, due to different volatile and fix carbon content than that of coal, and especially because of the heterogeneous content in SRF (paper, cardboard, textile, plastic, etc.), alternative solid fuels may influence the operation and performance of a pulverized coal fired furnace. Therefore, combustion of biomass and SRF, and their co-combustion with coal continues to be a challenge to the scientific community and practicing engineers worldwide [56].

The development of appropriate combustion units is often very demanding, and time and cost consuming. A possibility for the ex-ante control and investigation of the thermo-chemical processes occurring inside combustion units are CFD simulations. Early comprehensive information, parametric studies and initial conclusions that can be gained from CFD simulations are very important in handling modern combustion units. Over the years CFD has become an integral component of combustion research. It has been used in the development process for understanding the complex phenomena occurring within the combustion units. Furthermore, CFD modelling of furnaces co-combusting alternative fuels is essential in order to reveal potential problems that may occur during their combustion and to mitigate potential negative effects [57]. However, CFD simulations of the thermo-chemical processes occurring within cement calciners still face significant challenges. With the aim of better understanding of the mixing phenomena, heat exchange processes and fluid flow in different types of cement calciners have been investigated. Huanpeng et al. [4] performed a numerical study for the effect of different parameters on the dynamics of the two-phase flow in a cement calciner. The study represented the transport properties of the solid phase with the kinetic theory of granular flow. Huang et al. [5] numerically analyzed the formation of NO, CO and CO_2 in a cement calciner. The study showed that numerical predictions for burn-out of coal particles, limestone decomposition, are in good agreement with the measured results. Hillers et al. [6]

numerically investigated processes that occur in cement calciners, e.g. they modelled the turbulence, radiation, calcination process, coal combustion, and NO_x formation. The study showed that CFD shows a great potential regarding emission control and fuel savings. Zheng et al. [7] studied the effects of primary jet velocity and throat diameter on the two-phase gas-solid flow inside a cement calciner. The study showed that for the simulated cement calciner, these two effects have a strong influence on flow structure and particle concentration. Hu et al. [8] simulated a three-dimensional model of a dual combustor and calciner, by using the Eulerian frame for the gaseous phase and a Lagrangean frame for the solid phase. The work showed that the burn-out and the decomposition ratio during the simultaneous injection of two types of coal and limestone were well predicted. Huang et al. [9] performed a three-dimensional simulation of a new type swirl-spray calciner. A new method for particle-wall boundary condition and a new four-mixture-fraction model were developed to describe the transport phenomena in a calciner. The work showed that predicted results for limestone decomposition, coal burnout and the temperature at the exit of the calciner agreed well with measured results. Fidaros et al. [10] presented a mathematical model and a parametric study of fluid flow and transport phenomena in a cement calciner. The work showed good prediction capabilities for temperature, velocity and distribution of particles at the calciner exit, where measurements exist. Dou et al. [11] investigated the coal combustion and the decomposition of raw material inside a cement calciner. The work showed that in order to increase the raw material decomposition and optimise the temperature inside the calculated cement calciner, the direction of the tertiary inlet needs to be tangentially adjusted, and that the raw material inlet needs to be opposite the coal inlet. Ha et al. [12] studied the separation of coal particles and its corresponding influence on the decomposition of limestone inside a cement calciner. The study showed that by combusting finer coal particles a negligible influence can be observed on the decomposition of limestone. Bluhm- Drenhaus et al. [13] by using a coupled fluid dynamic-discrete element method investigated the heat and mass transfer inside a lime shaft kiln. The study showed that the developed procedure gives detailed insight into physical phenomena related to kiln operating conditions and it furthermore opens up new possibilities to its optimization. Nance et al. [14] using the mineral interactive computational fluid dynamics investigated the "Hot-Reburn" conditions inside a cement calciner. The work showed that the proposed method greatly assists in the optimization of a cement calciner's operating conditions and design. Jianxiang et al. [15] using the LES simulation approach and the kinetic theory of granular flow, investigated the mixing of particles and the stability of production for the simulated cement calciner. The study showed

that operating parameters need to be set up very precisely to have an efficient and a stable production. All these studies show that there is still a need for further research and development of cement calciners. However here should be noted that most of these CFD studies evaluated their numerical predictions with measurement data obtained on the calciner's exit. Due to the lack of measurement data for flows characteristics, and physical and chemical processes inside cement calciners, this approach is satisfactory when looking at pollutant emissions, decomposition ratio for limestone and burnout ratio for char particles. When it comes to the details about burner region, wall region or other regions with interesting flow phenomena, the mixing phenomena and the optimisation of key physical and chemical processes inside cement calciners, the new approach, with separately validated models for calcination process and combustion of different pulverized solid fuels, improves the available CFD simulation methodology. Due to the high reliability of separately validated models, appropriate accuracy needed for the investigation of named details and optimisation of key physical and chemical processes within cement calciners can be achieved with the new approach. Furthermore, here should be noted that all of these CFD studies investigated only the coal combustion inside cement calciners, and none of them analysed the use of alternative fuels, i.e. biomass or solid recovered fuel.

1.4   Objective and hypotheses of research

The hypothesis of this research is that by combining the Euler-Lagrange method for the multiphase flow with attuned diffuse-kinetic models for the calcination process, combustion of pulverized coal, biomass and the developed solid recovered fuel model, a sufficiently accurate numerical simulation of the thermo-chemical processes occurring inside of the cement calciner is feasible. The results obtained by using this model enable the development of a more efficient calciner. The aim of this research was to develop new efficient models that confirm the hypothesis by comparing the simulation results and the available experimental data.

1.5   Scientific contribution

The result of this research is the better understanding of co-firing of alternative fuels with coal inside the cement calciners, and its influence on the calcination process. Special attention was

given to the modelling of the calcination process. For the calcination process, the effects of temperature, decomposition pressure, diffusion, and pore efficiency were taken into account. Furthermore, attention was also given to the models of alternative fuel combustion, in contrast to the commonly used coal combustion model. Additional contribution is that the new approach for the investigation of calcination and co-firing processes provides results that can be used by cement plant operators to make the cement production more sustainable. Furthermore, the obtained results can be used by manufacturers of pyroprocessing equipment to produce more efficient combustion equipment.

2 NUMERICAL MODELLING

In order to investigate the influence of different parameters on the decomposition rate of limestone particles, burnout rate of fuel particles, and pollutant emissions from a cement calciner, all relevant thermo-chemical reactions must be treated, i.e. the calcination process, the combustion of coal, biomass and solid recovered fuel. In this study, and in the most engineering applications today, the Eulerian-Lagrangian method for solving the multi-phase flow phenomena was used. In this approach, the solid particles are represented by finite numbers of particle groups, called parcels [16]. It is assumed that all the particles within one parcel are identical in size and that they have the same physical properties. The motion and transport of the parcels, through the cement calciner, were tracked through the flow field using a Lagrangian formulation, while the gas phase was described by solving conservation equations using an Eulerian formulation. The trajectory of each parcel within the flow field was calculated using the Lagrangian scheme, which means that representative particles were tracked by using a set of equations that describe their dynamic behaviour as they move through the calculated flow field. The coupling between the solid and the gaseous phases was taken into account by introducing appropriate source terms for interfacial mass, chemical species, momentum and energy exchange. Lagrangian phase was solved in between two Eulerian phase time steps, with an explicit integration method, providing the source terms for the Eulerian phase. Vice versa the solution of the Eulerian phase provided the ambient conditions for the Lagrangian phase [17].

The developed mathematical models used for the calculation of the calcination process, coal, biomass and solid recovered fuel combustion were treated in the Lagrangian spray module, where thermo-chemical reactions occur inside a particle as well as between the particle and the gas phase. The chemical reactions inside the gas phase were treated via an ODE solver providing additional sink and source terms for the species and enthalpy transport equations in the gas phase [17]. The developed models together with thermo-physical properties of the limestone, the lime and the components of the coal, biomass and solid recovered fuel particles, as well as a particle radiation model, were integrated into the commercial CFD code AVL FIRE$^{®}$ via user-functions written in the FORTRAN programming language, in order to simulate the calcination and combustion process properly.

This research was performed in several steps. As it has been said previously, the aim was to get a new procedure for the investigation of the co-firing of coal and alternative inside a cement calciner, which will provide better understanding, improvement and optimisation of the calcination process.

First step was the development and validation of the calcination reaction model. The major effects that have a direct influence on the calcination process were investigated. The aim of this step was to gain some information and expertise about the calcination process and effect of different operating conditions on it.

Second step was the research, implementation and validation of the coal and biomass combustion model. The effects of drying, devolatilisation process, combustion of char, and combustion of volatiles were investigated. Additional work that was performed under this step was the development and validation of the solid recovered fuel combustion model. Here the effects of drying, devolatilisation process, combustion of char, combustion of volatiles, but also the decomposition of the plastic fraction was investigated. The aim of this step was to gain some information and expertise about the combustion of different solid fuels and effect of different operating conditions on it.

For both mentioned steps, the influence of space discretization step, i.e. mesh resolution on the results, was examined.

Finally, all findings from previous steps were applied on a CFD simulation of three different real industrial cement calciners configurations. Simulation results were compared with available measurement data and an extensive analysis was given.

The overall procedure used, including the coupling of the Eulerian and the Lagrangian frame of reference, is described below. For details see the appended PAPERS 1-6. The modelling approach for the calcination process and combustion of each solid fuel is given in detail.

2.1 Continuous phase

The continuous phase is described by solving conservation equations using the Eulerian formulation. These equations are based on the conservation laws for mass, momentum and

energy. They are solved by using the finite volume approach. The differential form of mass conservation equation is:

$$\frac{\partial \rho}{\partial t} + \frac{\partial (\rho v_j)}{\partial x_j} = S_C .$$

(1)

The differential form of momentum conservation equation is:

$$\frac{\partial (\rho v_i)}{\partial t} + \frac{\partial (\rho v_j v_i)}{\partial x_j} = -\frac{\partial p}{\partial x_i} + \frac{\partial}{\partial x_j}\left[\mu(\frac{\partial v_j}{\partial x_i} + \frac{\partial v_i}{\partial x_j} - \frac{2}{3}\frac{\partial v_k}{\partial x_k}\delta_{ij})\right] + \rho g_i + S_M ,$$

(2)

with *i,j,k* denoting coordinate indices, and where the terms in the square brackets on the right side represent the stress tensor:

$$\tau_{ji} = \mu(\frac{\partial v_j}{\partial x_i} + \frac{\partial v_i}{\partial x_j} - \frac{2}{3}\frac{\partial v_k}{\partial x_k}\delta_{ij}) .$$

(3)

The differential form of energy conservation equation is:

$$\frac{\partial (\rho E)}{\partial t} + \frac{\partial (\rho v_j E)}{\partial x_j} = -p\frac{\partial v_j}{\partial x_j} + \frac{\partial}{\partial x_j}(\lambda\frac{\partial T}{\partial x_j}) + \tau_{ji}\frac{\partial v_i}{\partial x_j} + S_E .$$

(4)

Additionally to the conservation equations, for *n* species the following species transport equation is solved:

$$\frac{\partial}{\partial t}(\rho Y_l) + \frac{\partial}{\partial x_j}(\rho v_j Y_l) = \frac{\partial}{\partial x_j}(\Gamma\frac{\partial Y_l}{\partial x_j}) + S_{Y_l}, \quad l = 1,...,n.$$

(5)

The source terms S on the right side of each conservation equation and in the species transport equation are used for the coupling of the continuous and solid phase, e.g. the coupling of the Eulerian and the Lagrangian frame of reference, due to heterogeneous reactions. Additionally the source term in the species transport equation is due to the production or consumption of species mass fraction by homogeneous reactions in the continuous phase. The conservation equations are solved with a finite volume method providing the temporal evolution and spatial distribution of velocities, temperatures and concentrations. Gas phase chemistry can be defined via input files containing the desired gas phase reactions and is treated via a separate chemistry solver between the time steps of the gas phase solve [17].

13

2.2 Solid phase

Lagrangian frame of reference is used to describe the motion and transport of the solid particles through the flow field. The Lagrangian phase is treated by distributing the total mass of particles into a number of computational parcels containing particles with identical physical properties known as Discrete Droplet Model [16]. This allows the reducing of the computational effort by treating only one representative particle per parcel. As the parcels move through the calculated flow field, the trajectory of each representative particle is calculated from its corresponding differential equation for momentum conservation:

$$m_p \frac{du_{ip}}{dt} = F_{idr} + F_{ig}. \tag{6}$$

Here m_p is the particle mass, u_{ip} is the particle velocity vector, F_{ig} is a force including the effects of gravity and buoyancy, and F_{idr} is the drag force, given by:

$$F_{idr} = D_p \cdot u_{irel}. \tag{7}$$

Here u_{irel} represents the particle relative velocity vector, and D_p is the drag function, defined as:

$$D_p = \frac{1}{2} \rho_g A_p C_D |u_{irel}|, \tag{8}$$

where ρ_g is the gas density, A_p is the cross-sectional area of the particle, and C_D is the drag coefficient which is generally a function of the particle Reynolds number Re_p.

From the various formulations in literature for the drag coefficient of a single sphere, FIRE uses the following formulation from Schiller and Naumann [17]:

$$C_D = \begin{cases} \dfrac{24}{\text{Re}_p} \left(1 + 0.15\,\text{Re}_p^{0.687}\right) & \text{Re}_p < 10^3 \\ 0.44 & \text{Re}_p \geq 10^3 \end{cases} \tag{9}$$

Further energy and mass conservation equations are solved for each particle as described in the following sections taking into account all necessary thermo-chemical reactions of solid

particles. The thermo-chemical reactions occur inside a particle as well as between particle components and continuous phase species.

2.3 Calcination process model

In general the calcination process can be presented by the following equation:

$$CaCO_3(s) \xrightarrow{\;+\;178\;kJ/mol\;} CaO(s) + CO_2(g). \tag{10}$$

In this study the mathematical model of the calcination process, based on the chemical reaction scheme published by Silcox et al. [58], is extended with the effects of diffusion limitation of the overall rate and the pore diffusion effectiveness factor. The calcination model involves three rate-limiting processes: a) heat transfer to the particle, b) mass transfer of CO_2 from the reaction interface through the porous layer and particle boundary layer to the surrounding, and c) the kinetics of the chemical reaction.

The calcination process starts only if the partial pressure of carbon dioxide in the gas surrounding the limestone surface is less than the decomposition pressure of limestone [59]. The decomposition pressure p_{eq} and the chemical reaction rate k_{ch} of the calcination process determined by Silcox et al. [58] are:

$$p_{eq} = 4.137 \times 10^{12} \exp(-\frac{20474}{T}), \tag{11}$$

$$k_{ch} = k_D (p_{eq} - p_{CO_2}), \tag{12}$$

where p_{CO_2} is the partial pressure of carbon dioxide at the reaction surface of limestone and k_D is the reaction rate calculated by the following expression:

$$k_D = 1.22 \exp(-\frac{4026}{T}) \times 10^{-5}. \tag{13}$$

Based on the Eq. (11) and Eq. (13), Eq. (12) for the chemical reaction rate of the calcination process, can be written in the following form:

$$k_{ch} = 5.0 \cdot 10^7 \exp(-\frac{24500}{T}) - 1.22 \cdot 10^{-5} \exp(-\frac{4026}{T}) p_{CO_2} \cdot \frac{A_{por}}{A_{geom}}. \tag{14}$$

Major effects such as temperature, CO_2 partial pressure and enhanced overall surface due to porosity are taken into account in this equation. The surface increase is modelled as A_{por}/A_{geom}, where A_{por} is the overall reaction surface (representing the surface of internal pores and the outer surface of the sphere), and A_{geom} is the surface of the particle (sphere). The surface increase is depending on porosity, pore diameter and topology of the porous structure, and in this work it was used as a matching parameter for the specific type of limestone with typical values ranging from 1 to 5. This parameter has some initial value depending on type of limestone, but starting with this value it will also evolve during the reaction by shrinking and cracking processes as well as by sintering. Since the latter processes partly increase and partly decrease the surface the assumption of a mean average or balanced value is supported.

The physical reaction rate k_{ph} of the calcination process is determined from

$$k_{ph} = \frac{12D \cdot Sh}{R_{CO_2} d_{part} T} \cdot p_{ref}, \tag{15}$$

which represents the mechanism of diffusion limitation [60]. Due to high CO_2 concentration in the pore system and in the particle surrounding the partial pressure of CO_2 is assumed to be high as well and the reference pressure p_{ref} in Eq. (14) is assumed to be close to ambient pressure. Following Schneider [60] the Sherwood number is taken as 2, since limestone particles are small and rapid velocity equilibration can be assumed. The term D represents the diffusion coefficient that consists of binary and Knudsen diffusion coefficient [61] and is calculated as:

$$D = \left[\frac{1}{D_{bin}} + \frac{1}{D_{knu}} \right]^{-1}. \tag{16}$$

For the binary diffusion coefficient the following correlation demonstrated by Reid et al. [62] is used:

$$D_{bin} = \frac{0.0266 T^{1.5}}{p M_{AB}{}^{0.5} \sigma_{AB}^2 \omega_d}, \tag{17}$$

while the Knudsen diffusion coefficient [13] is calculated as:

$$D_{knu} = \frac{d_{pore}}{3} \left[\frac{8 R_{CO_2} T}{\pi} \right]^{0.5}. \tag{18}$$

The overall reaction rate of the calcination process, which is the compound of the physical and the chemical reaction rate, based on Levenspiel [63] is calculated as:

$$k = \left[\frac{1}{k_{ph}} + \frac{1}{\eta \cdot \tilde{k}_{ch}} \right]^{-1}, \tag{19}$$

where $\tilde{k}_{ch}$ is the chemical reaction rate in $\left[\text{kg m}^{-2} \text{ s}^{-1} \right]$ and η is the effect of pore efficiency on the chemical reaction rate of calcination process. Here the pore efficiency coefficient η is applied globally to the chemical reaction rate assumed to take place inside the complex topology of the porous structure. The coefficient η is given by Froment and Bischoff [64] as:

$$\eta = \frac{\tanh \left[\frac{d}{6} \sqrt{\frac{\bar{\bar{k}}_{ch}}{\varepsilon D}} \right]}{\left[\frac{d}{6} \sqrt{\frac{\bar{\bar{k}}_{ch}}{\varepsilon D}} \right]}, \tag{20}$$

where $\bar{\bar{k}}_{ch}$ is the chemical reaction rate in $\left[\text{s}^{-1} \right]$ and the correction factor ε given by Bluhm-Drenhaus et al. [13] applied to the diffusion coefficient D is:

$$\varepsilon = \frac{\varepsilon_p}{\tau_p^2}. \tag{21}$$

In Eq. (21) ε_p denotes the void fraction of the limestone particle with higher values favouring diffusion, τ_p denotes the tortuosity, which can be regarded as a measure for the complexity of the pore structure hindering the diffusion of the reacting gases inside the porous structure of the grains.

Mass exchange from the calcination reaction is calculated for the limestone, lime and carbon dioxide. The mass transfer rate of limestone is calculated by the following equation:

$$\dot{m}_{CaCO_3} = -\hat{k},$$
(22)

where $\hat{k}$ is the overall reaction rate of the calcination process in $\left[\text{kg s}^{-1}\right]$ and from stoichiometry the mass transfer of lime and carbon dioxide are:

$$\dot{m}_{CaO} = \hat{k}\frac{M_{CaO}}{M_{CaCO_3}},$$
(23)

$$\dot{m}_{CO_2} = \hat{k}\frac{M_{CO_2}}{M_{CaCO_3}}.$$
(24)

Enthalpy exchange from the calcination reaction (convective enthalpy, enthalpy transfer from reaction enthalpy, transfer of enthalpy with the mass leaving the particle) is calculated separately for the particle and for the gas temperature.

For the enthalpy conservation of a solid particle the following equation can be written:

$$\left(m_{CaCO_3}c_{pCaCO_3} + m_{CaO}c_{pCaO}\right)\dot{T}_p + \dot{m}_{CaCO_3}c_{pCaCO_3}T_p + \dot{m}_{CaO}c_{pCaO}T_p = \frac{f\,\Delta H_R\dot{m}_{CaCO_3}}{M_{CaCO_3}} + \alpha A\left(T_g - T_p\right) - \dot{m}_{CO_2}\tilde{c}_pT_p,$$
(25)

where f is a factor which represents the fraction of reaction enthalpy taken from the particle and $\tilde{c}_p$ is the difference of molar specific heat capacities of limestone and lime, divided by the molecular weight of carbon dioxide. In the calculations performed within this study, the factor f has been taken as 0.5 assuming that the reaction enthalpy is provided at equal parts from both particles and gaseous surrounding. However, a sensitivity study showed that at least for small particles the effect of parameter f on the calcination rate is not significant, i.e. $f = 0$ assuming that all enthalpy is taken immediately from the gas phase did not change the results.

Similar to the enthalpy balance for the solid particle, the enthalpy of the gas phase is:

$$\sum m_i (c_{pi} + \tfrac{dc_{pi}}{dT} T) \dot{T}_g + \dot{m}_{CO_2} c_{pCO_2} T_g = \left(\frac{-(1-f) \Delta H_R \dot{m}_{CaCO_3}}{M_{CaCO_3}} + \alpha A (T_p - T_g) \right) n_p + \dot{m}_{CO_2} \tilde{c}_p T_p,$$

(26)

From these equations the rate of change of particle and gas temperatures are calculated. The mass and enthalpy balance equations given above are applied in each cell of the computational domain during the integration of the Lagrangian particle phase for updating the gas and particle properties and are solved by time step subcycling using the DVODE solver [17]. This is done within every two gas phase time steps. Additionally from these equations the source terms for species mass and enthalpy are collected transferring the impact of the chemical reactions from the particles to the Eulerian solver.

2.4   Coal / Biomass combustion model

The pulverized coal / biomass combustion model includes four steps: drying, devolatilisation, char burning, and combustion of volatiles. The four step process for combustion of biomass and coal particles has been reported in several recent studies [65]-[68]. The coal particle first undergoes the drying process (Eq. 27), after which the devolatilisation starts (Eq. 28).

$$wet\ \mathrm{Coal(s)} \xrightarrow{\ H_2O\ evaporation\ } dry\ \mathrm{Coal(s)},$$

(27)

$$dry\ \mathrm{Coal(s)} \xrightarrow{\ devolatilisation\ } Volatiles(g) + Char(\mathrm{s}),$$

(28)
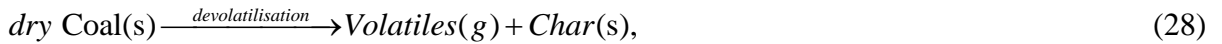
During the devolatilisation an important loss of weight occurs, due to the release of volatile matter. The quantity and composition of volatiles depend on the coal and biomass ingredients, its particle size and temperature. After the devolatilisation only char and ash are left in the solid particle. Parallel to the devolatilisation, depending on the particle size and temperature, char oxidizes to CO or CO_2, and afterwards only ash is left. Afterwards the ash particle is considered inert, only the residual ash heating still occurs.

2.4.1. Moisture evaporation

The model for the moisture evaporation considers two types of evaporation cases. The first one is the evaporation of water vapour due to the difference in water vapour concentration at the particle surface and in the gas, and the second one is the boiling process. The boiling process starts when the particle reaches the water boiling temperature, i.e. 100°C. It is

assumed that during the boiling process particle temperature remains the same, until the entire capillary bounded water evaporates [69].

The mass flux of water vapour is determined from difference in water vapour concentration at the particle surface and in the gas is determined from:

$$\dot{m}_p = \frac{d_p^2 \pi}{10^3} M_{H_2O} k_w (C_p - C_g).$$
(29)

For the water vapour concentration at the particle surface C_p it is assumed that the water vapour partial pressure at the particle surface is equal to the water saturation pressure p_{sat}, at the particle temperature T_p:

$$C_p = \frac{p_{sat}}{RT_p},$$
(30)

and the water vapour concentration in the gas C_g is given by the following equation:

$$C_g = X_{H2O} \frac{p}{RT}.$$
(31)

The Sherwood number correlation by Ranz and Marshall [70],[71] is used to calculate the mass transfer coefficient k_w:

$$Sh = \frac{k_w d_p}{D_w} = 2.0 + 0.6 \mathrm{Re}_p^{1/2} Sc^{1/3}.$$
(32)

The Schmidt number is calculated according the following equation:

$$Sc = \frac{\mu}{\rho D_w}.$$
(33)

The enthalpy balance of the drying particle below the water boiling temperature is calculated from the following expression:

$$m_p c_p \frac{dT_p}{dt} = \alpha A_p (T_g - T_p) + \varepsilon_p \sigma A_p (T_g^4 - T_p^4) + \dot{m}_p h_{latent},$$
(34)

and afterwards, during the boiling process, while the temperature is constant, the mass transfer is calculated according to:

$$\dot{m}_p = -\frac{\alpha A_p (T_g - T_p) + \varepsilon \sigma A (T_g^4 - T_p^4)}{h_{latent}}. \tag{35}$$

During the drying process the water vapour mass flux becomes a source of water vapour in the water vapour species transport equation, and also the water vapour mass flux multiplied by the latent heat becomes a source in the energy equation.

When the particle reaches the water boiling temperature, i.e. 100°C, the boiling process starts, meaning that during the whole boiling process particle temperature remains the same, until the entire capillary bounded water is evaporated [69].

2.4.2. Devolatilisation and char combustion

After the drying process the dry coal / biomass particles further heats up, and with increasing temperature the devolatilisation process starts. The volatile matter is released from the particle and char is produced. Instantly as char is produced, its oxidation starts, meaning that the devolatilization and char oxidation occur in parallel.

Numerically, the dry particle is composed of three parts: coal / biomass; char; ash. The mass balance of the dry particle is expressed by the following equation:

$$m_p = m_{coal/biomass} + m_C + m_{ash}. \tag{36}$$

As explained, coal / biomass particles undergo devolatilisation, the volatile matter is released and char is produced. Numerically the change of the coal / biomass particle mass can be expressed as:

$$\dot{m}_{coal/biomass} = -\dot{m}_{C+} - \sum_{l=1}^{n} \dot{m}_{Y_l} / n_p, \tag{37}$$

where the first term on the right hand side is the char production and the second term on the right hand side of the equation is the sum of production rates of all volatile species per particle.

The char mass changes, due to char production during devolatilisation, and due to char consumption during the char oxidation. This is calculated as:

$$\dot{m}_C = \dot{m}_{C+} + \dot{m}_{C-}. \tag{38}$$

The ash is assumed to be inert, and its mass does not change:

$$\dot{m}_{ash} = 0. \tag{39}$$

The overall particle mass changes due to the mass lost during the devolatilisation, and the char oxidation:

$$\dot{m}_p = -\sum_{l=1}^{n} \dot{m}_{Y_l} / n_p + \dot{m}_{C-}. \tag{40}$$

The change of the mass fraction of coal / biomass in the overall particle mass equals the devolatilisation reaction rate:

$$\frac{d}{dt}\left(\frac{m_{coal/biomass}}{m_p}\right) = -k_d. \tag{41}$$

After the term in brackets on the left hand side of Eq. 41 is derived, the following expression is obtained:

$$\dot{m}_{coal/biomass} = -k_d m_p + \left(\frac{m_{coal/biomass}}{m_p}\right)\dot{m}_p, \tag{42}$$

and here the change of coal/biomass mass is in the dependency with the devolatilisation reaction rate and a correction according to overall mass loss of the particle.

For the devolatilisation rate k_d, a unified single rate expression is used, meaning that the devolatilisation rate is in a first order dependency to the amount of coal / biomass mass fraction remaining in the particle (Eq. 43) holding for all volatiles.

$$k_d = -k_1 y_{coal/biomass} \tag{43}$$

Here for the kinetic rate k_1, an Arrhenius type expression which includes a pre-exponential factor $k_{0,1}$ and an activation energy E_{a1} is used:

$$k_1 = k_{0,1} \exp\left(-E_{a1} / RT_p\right) \tag{44}$$

The values of the devolatilisation kinetic constants, e.g. the pre-exponential factor and the activation energy for different coals and biomass are obtained from the literature, depending on which coal or biomass is modelled [72]-[74].

As now the change of coal / biomass mass during the devolatilisation is known (Eq. 42), the corresponding increase of char mass, and mass of each volatile species depends on the stoichiometry of the devolatilisation, and can be written in the following forms:

$$\dot{m}_{C+} = -\left|v_C\right|\left(\frac{M_C}{M_{coal/biomass}}\right)\dot{m}_{coal/biomass},$$

(45)

$$\dot{m}_{Y_n} = -\left|v_{Y_l}\right|\left(\frac{M_{Y_l}}{M_{coal/biomass}}\right)\dot{m}_{coal/biomass}\,n_p.$$

(46)

As soon as some char is produced, char is oxidized to form CO and CO_2 taking into account the mechanism factor f_m [75],[76]:

$$C + \frac{1}{f_m}O_2 \xrightarrow[-110kJ/mol]{-395kJ/mol} \left(2 - \frac{2}{f_m}\right)CO + \left(\frac{2}{f_m} - 1\right)CO_2.$$

(47)
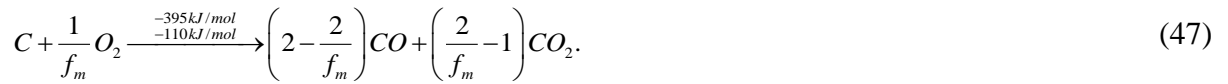
The mechanism factor f_m depends on char particle size and temperature, ranges between 1 and 2. It determines the shift from CO_2 to CO production with increasing temperature and decreasing particle diameter in Eq. 47 and is calculated by the following expressions [76]:

$$f_m = \frac{2f_{CO} + 2}{f_{CO} + 2}; \qquad d_p < 50\mu m,$$

(48)

$$f_m = \frac{2f_{CO} + 2}{f_{CO} + 2} - \frac{f_{CO}(d_p - 50)}{(f_{CO} + 2)\cdot 950}; \qquad 50\mu m < d_p < 1000\mu m.$$

(49)

Here the Arthur's law [77] is used to define f_{co}:

$$f_{CO} = 2500\cdot\exp(-6240/T).$$

(50)

The decrease of the char mass fraction in the overall particle mass equals the char oxidation reaction rate:

$$\frac{d}{dt}\left(\frac{m_{C-}}{m_p}\right) = -k_{ox}.$$

(51)

After the term in brackets on the left hand side of Eq. 51 is derived, the following expression is obtained:

23

$$\dot{m}_{C-} = -k_{ox}m_p + \left(\frac{m_C}{m_p}\right)\dot{m}_p. \tag{52}$$

Here the decrease of the char mass in the overall particle mass is in the dependency with the char oxidation reaction rate and again a correction for overall mass loss.

In this study the overall char oxidation reaction rate is modelled according to the kinetics / diffusion limited reaction model of Baum and Street [78]. The model assumes that the reaction rate of char oxidation is limited either by the oxygen's diffusion into the particle's mass expressed by the value of k_2^{ph}, or by the kinetics of the heterogeneous reaction itself expressed by the value of k_2^{ch}, presented in Eqs. 53–56:

$$k_{ox} = -k_2 A_p p_{O_2} y_c, \tag{53}$$

$$k_2 = \frac{k_2^{ch} \cdot k_2^{ph}}{k_2^{ch} + k_2^{ph}}, \tag{54}$$

$$k_2^{ch} = k_{0,2}^{ch} \cdot \exp\left(-E_{a2}^{ch} / RT\right), \tag{55}$$

$$k_2^{ph} = \frac{24 \cdot f_m \cdot D_0}{R \cdot d_p \cdot T_0^{1.75}} T^{0.75} \cdot 10^5. \tag{56}$$

Here also the values of the kinetic constants for the char oxidation are obtained from the literature [73],[74] , depending on which coal or biomass is modelled.

From char oxidation (Eq. 47) there is also the decrease in the oxygen mass, and increase in carbon monoxide and carbon dioxide mass. These mass changes are sink / source terms to the continuous phase equations and according to the stoichiometry of the Eq. 47 these mass changes can be expressed as:

$$\dot{m}_{O_2} = \frac{1}{f_m}\left(\frac{M_{O_2}}{M_C}\right)\dot{m}_{C-}n_p, \tag{57}$$

$$\dot{m}_{CO} = -\left(2 - \frac{2}{f_m}\right)\left(\frac{M_{CO}}{M_C}\right)\dot{m}_{C-}n_p, \tag{58}$$

$$\dot{m}_{CO_2} = \left(1 - \frac{2}{f_m}\right)\left(\frac{M_{CO_2}}{M_C}\right)\dot{m}_{C-}n_p.$$ (59)

Finally, based on Eq. 46 and Eq. 52, the change of the overall particle mass expressed by Eq. 40, can be written in the following form:

$$\dot{m}_p = -\Sigma\dot{m}_{Y_k}/n_p + \dot{m}_{C-} = \frac{m_p(1 - \frac{M_C|v_C|}{M_{coal/biomass}})k_d + m_p k_{ox}}{(1 - \frac{m_C}{m_p} - \frac{m_{coal/biomass}}{m_p}(1 - \frac{M_C|v_C|}{M_{coal/biomass}}))}.$$ (60)

The local mass and enthalpy transfer processes between Lagrangian parcels and their computational residence cell inside gas phase time steps of the Navier-Stokes solver are resolved in more detail with a time-step sub-cycling method. For this purpose simplified enthalpy and mass balances are solved for each parcels and each cell during the time-step sub-cycling. These neglect, e.g., convective heat and mass transfer from neighbouring cells and local thermal radiation effects inside the cell. However, these are considered and updated again in the next solution step of the Eulerian gas phase solver after sources from Lagrangian phase have been added. Enthalpy exchange during the devolatilisation and char oxidation (enthalpy transfer from reaction enthalpy, convective enthalpy) is calculated separately for the particle and for the gas temperature.

For the enthalpy conservation of a solid particle the following equation can be written:

$$\dot{T}_p = \frac{1}{m_p c_p}\left(\frac{-f\Delta H_R \dot{m}_{C-}}{M_C} + \alpha A\left(T_g - T_p\right)\right).$$ (61)

Similar to the enthalpy balance for the particle, the enthalpy of the continuous phase is:

$$\dot{T}_g = \frac{\left[\left(\frac{-(1-f)\Delta H_R \dot{m}_{C-}}{M_C} - \alpha A\left(T_g - T_p\right)\right)n_p + \sum\dot{m}_i c_{pi}(T_p - T_g)\right]}{\sum m_i(c_{pi} + \frac{dc_{pi}}{dT}T)}.$$ (62)

From these equations the rate of change of particle and gas temperatures are calculated. The mass and enthalpy balance equations given above are applied in each cell of the computational domain during the integration of the Lagrangian particle phase for updating the gas and particle properties and are solved by time step subcycling using DVODE solver [17]. Furthermore from these equations the source terms for species mass and enthalpy are

collected transferring the impact of the thermo-chemical reactions from the particles to the Eulerian solver.

2.4.3. Volatile combustion

For the homogeneous gas phase reactions of volatile oxidation, a detailed chemistry approach is used. The source terms in each species transport equations (Eq. 5) and in the continuous phase mass, momentum and energy conservation equation (Eqs. 1-2 and Eq. 4), are calculated according to the Arrhenius law, meaning that the reaction rates of each homogeneous reaction depends on species concentrations and temperature. The modelled homogeneous reactions include tar oxidation (here C_6H_6 was chosen as tar representative), CO oxidation (Görner [76]), NOx formation and the combustion of methane, which is treated via the four step Jones-Lindstedt mechanism [79]. Eq. 63 represents the tar (C_6H_6) oxidation, whereas Eq. 64 and Eqs. 65-68 represent the CO oxidation and the four step Jones-Lindstedt mechanism for methane combustion.

$$C_6H_6 + 3O_2 \longrightarrow 6CO + 3H_2 \tag{63}$$

$$CO + \frac{1}{2}O_2 \longrightarrow CO_2 \tag{64}$$

$$CH_4 + \frac{1}{2}O_2 \longrightarrow CO + 2H_2 \tag{65}$$

$$CH_4 + H_2O \longrightarrow CO + 3H_2 \tag{66}$$

$$CO + H_2O \longrightarrow CO_2 + H_2 \tag{67}$$

$$H_2 + \frac{1}{2}O_2 \longrightarrow H_2O \tag{68}$$

Generally, it is considered that the main NO formation mechanism in coal-fired systems is the fuel-NO formation mechanism. Fuel-NO is formed from the nitrogen bounded in the coal. During the devolatilisation nitrogen is released as HCN and NH_3, which react with oxygen containing species in the flame and produce NO [80]. Fuel-NO formation from HCN and NH_3 is treated by the De Soete mechanism [81] represented by Eqs. 69-72:

$$4HCN + 5O_2 \longrightarrow 4NO + 4CO + 2H_2O \tag{69}$$

$$4HCN + 6NO \longrightarrow 5N_2 + 4CO + 2H_2O \tag{70}$$

$$NH_3 + O_2 \longrightarrow NO + H_2O + 0.5H_2 \tag{71}$$

$$NH_3 + NO \longrightarrow N_2 + H_2O + 0.5H_2 \tag{72}$$

2.5   Plastic combustion model

The thermal decomposition of different polymers has been at the centre of studies for several years [82]. It has been reported that the plastic waste consist mainly of four polymers: polyethylene (PE), polypropylene (PP), polystyrene (PS), and polyvinylchloride (PVC) [83]. In this study for the plastic combustion model a reaction scheme for dealing with polymers structured as C_nH_{2n}, e.g. PE, and PP has been designed. It has been reported that these three plastic polymers heat-up and combust differently than PVC [84]. For PE, PP and PS a single-step mechanism for the decomposition can be assumed, however when PVC is combusted, a two-step mechanism for decomposition has to be considered, since during PVC decomposition also molecularly bounded chloride is released. For the validation of the plastic combustion model, only polypropylene is used. The reason for this is that currently no experimental data for the validation of other plastic combustion models exist [85]. Therefore, the current plastic combustion model is based on the PP's combustion behaviour. However future research activities may include validation of the presented plastic combustion model with other commercial polymers.

It has been reported that experimental data clearly indicates that polypropylene degrades in a single stage process [86]. This is described with the following equation for the mass change of the PP particle:

$$\dot{m}_p = -k_0 e^{\frac{-E_a}{RT_p}} m_p. \tag{73}$$

The values of the polypropylene decomposition kinetic constants, e.g. the pre-exponential factor and the activation energy are obtained from the literature [87]. Here it is assumed that the PP particle decomposes directly to the gas phase as PP vapour, without any intermediate liquid phase. Therefore, the source for the continuous phase equations from a computational parcel with n_p particles is:

$$\dot{m}_{PPvapour} = -\dot{m}_p n_p. \tag{74}$$

The enthalpy conservation of a PP particle can be written as:

$$\dot{T}_p = \frac{1}{m_p c_p} \left(\Delta H_R \dot{m}_p + \alpha A \left(T_g - T_p \right) + \varepsilon \sigma A \left(T_g^{\,4} - T_p^{\,4} \right) \right). \tag{75}$$

Similar to the enthalpy balance for the particle, the enthalpy of the continuous phase is:

$$\dot{T}_g = \frac{\left[-\alpha A \left(T_g - T_p \right) n_p + \dot{m}_{PPvapour} c_{PPvapour} \left(T_p - T_g \right) \right]}{\sum m_i (c_{pi} + \frac{dc_{pi}}{dT} T)}. \tag{76}$$

The PP vapour is combusted in the continuous phase according to the Westbrook and Dryer [88] global reaction mechanism:

$$C_3 H_6 + 3 O_2 \rightarrow 3 CO + 3 H_2 O \tag{77}$$

$$CO + 0.5 O_2 \rightarrow CO_2 \tag{78}$$
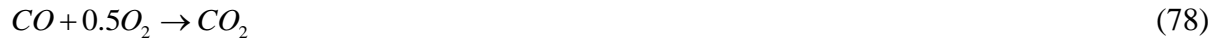
2.6 Solid recovered fuel combustion model

A high calorific value waste material that is not suitable for composting and cannot be landfilled has the potential of being used in energy recovery. Some of these high calorific value waste materials include paper, cardboard, and all sorts of plastics, textile and wood. From these materials SRF is produced [89]. SRF has different proportions of biodegradable materials and materials of fossil origin. The composition depends on the origin of waste and its pre-treatment. The fact that SRF contains a considerable amount of biodegradable materials and is also a less expensive fuel, explains its increasing usage in industry [90]. Furthermore, the benefit of using SRF is also the possibility of using SRF in existing pulverized fuel burners used in power plants and industrial furnaces. The biodegradable part of SRF is considered as a renewable fuel as its properties are similar to the ones of the biomass fuels, whereas the fossil part is predominately composed of plastic materials [91].

In this study due to the complex and inhomogeneous composition of SRF, the modelling approach from Agraniotis et al. [85] is used to describe the SRF combustion. SRF is modelled as a mixture of two different fractions, the biodegradable and the plastic fraction. Each

28

fraction undergoes a different combustion procedure. The biodegradable fraction uses the coal / biomass combustion model, whereas the plastic fraction uses the polypropylene combustion model, both previously elaborated. Following the same study [85] it is assumed that plastic fraction accounts for 20% of SRF's mass.

3 SELECTED RESULTS AND DISCUSSION

3.1 Single particle tests

For the plausibility checks and the quantitative checks of balances, the models for the calcination process, coal / biomass and polypropylene combustion presented above were tested on a single particle in a single mesh cube. Different types of initial conditions were set-up (e.g., temperature, carbon dioxide content, particle diameter) to test the numerical model.

For calculations of a single limestone particle, which results are shown in Figures 3 and 4, initial particle diameter was set to 10 μm, the porosity factor, i.e. A_{por} / A_{geom}, was set to 5, and there was no carbon dioxide present in the single mesh cube.
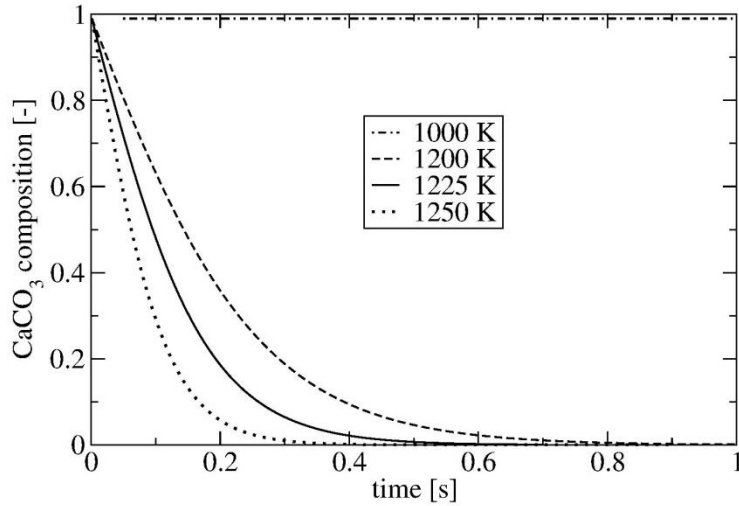
Figure 3 Calcination process at lower reaction temperatures.

Figure 3 shows the influence of lower reaction temperatures on the calcination process, i.e. decomposition of limestone, and Figure 4 shows the influence of higher reaction temperatures on the calcination process. From these two figures it is clear that the temperature

increase results with an increase of limestone decomposition which represents a reasonable physical trend.
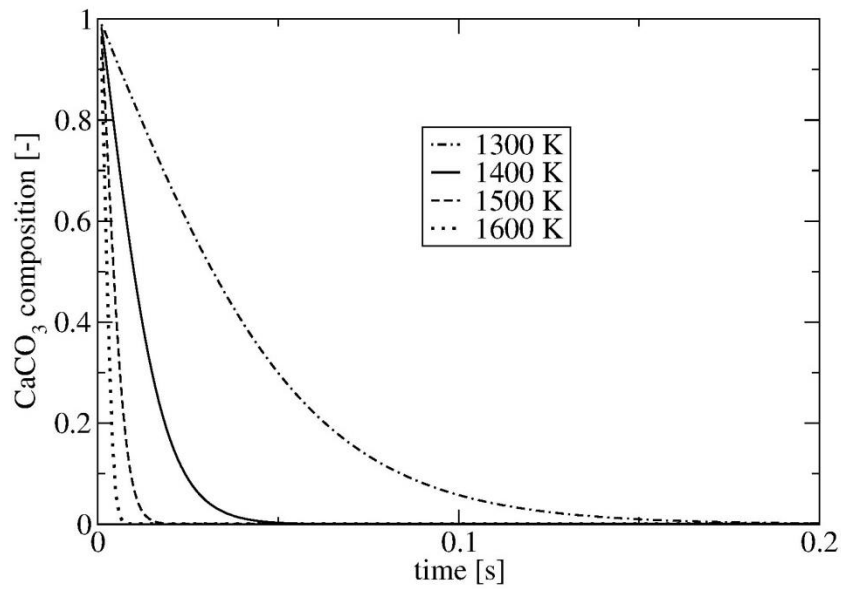
Figure 4 Calcination process at higher reaction temperatures.
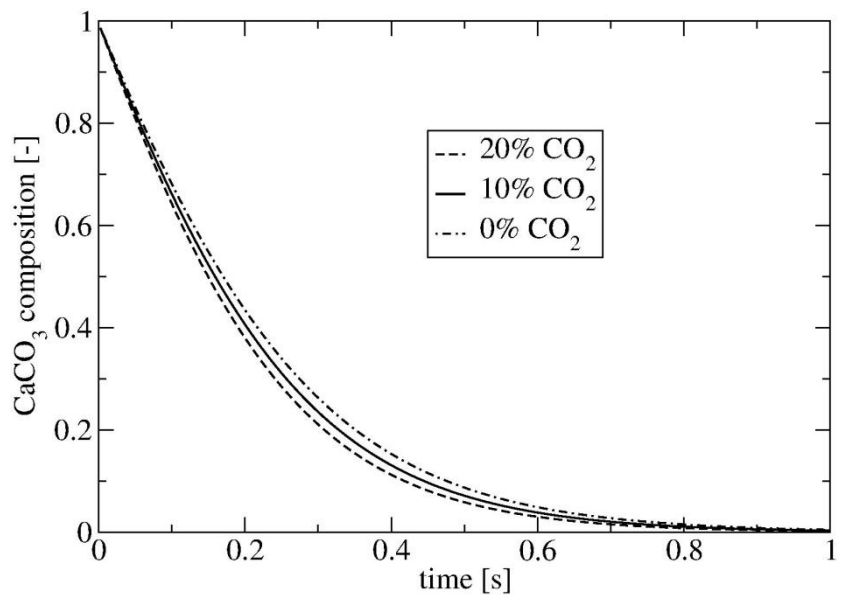
Figure 5 Influence of CO$_2$ content on the calcination process.

Figure 5 shows the influence of carbon dioxide content on the calcination process. As can be seen the increase of carbon dioxide content reduces the limestone decomposition. The initial limestone particle diameter for this figure was 10 μm, porosity factor was set to 5, the gas temperature was set to 1200 K and the carbon dioxide was the variable parameter.
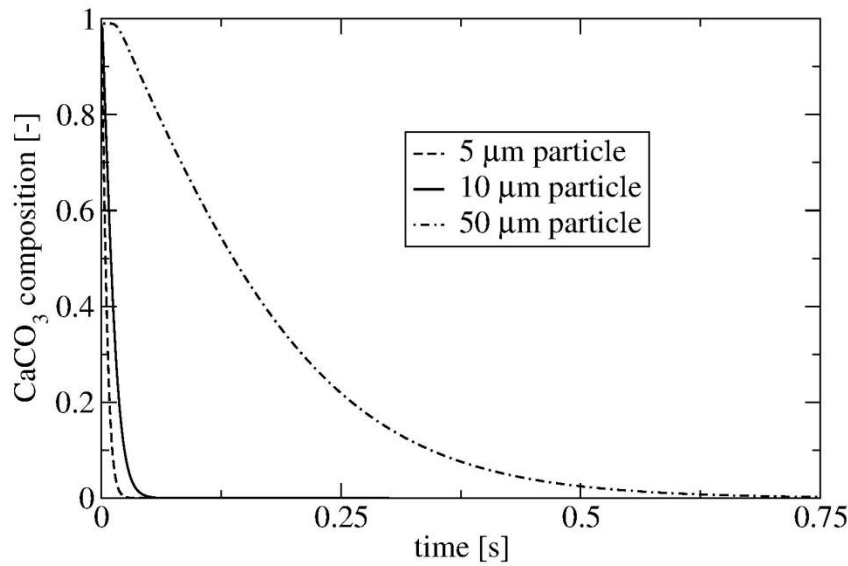
Figure 6 Influence of limestone particle size on the calcination process.

Figure 6 shows the influence of particle size on the calcination process. As can be seen bigger limestone particles need more time to decompose than the small particles. For this figure the initial gas temperature was set to 1400 K, the porosity factor was set to 5 and initially there was no carbon dioxide.

Results gained from the single limestone particle tests show that the right range of particle temperatures is covered, that the conversion of limestone depends on the carbon dioxide content and that the reaction kinetics of the calcination process are able to obtain reasonable trends.

For calculation of a single biomass particle, which results are shown in Figure 7, initial particle diameter was set to 100 μm, the initial particle temperature was set to 50 °C, the initial particle moisture content was set to 15%, and the ambient temperature in the single

mesh cube was set to 1400 °C. Figure 7 shows the evolution of different biomass particle components. As can be seen first the moisture evaporates and its mass fraction decreases to zero. At the same time, the biomass fraction is increased. Afterwards the devolatilisation starts, the dry biomass releases the volatile matter, its mass fraction decreases, and correspondingly the mass fraction of char increases. Parallel to the devolatilisation, the char is oxidized, and therefore the mass fraction of ash in the particle increases rapidly. When the devolatilisation is complete, the char mass fraction reaches the maximum value, after which due to the char oxidation the char mass fraction steadily decreases and the ash mass fraction increases.
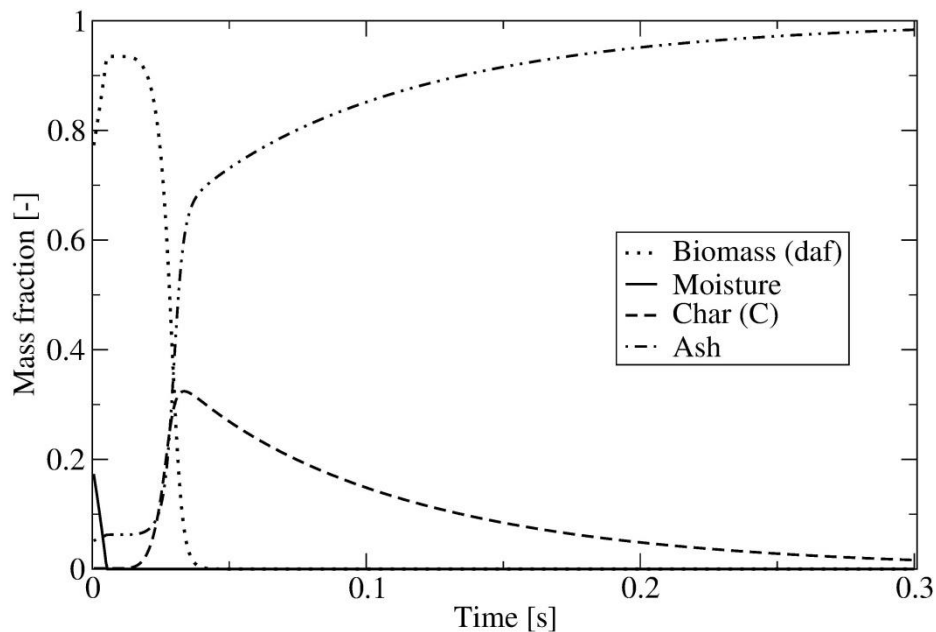
Figure 7 Evolution of biomass particle components.

In Figure 8 the biomass particle with same initial conditions as in Figure 7 was analysed. Figure 8 shows the influence of different ambient temperatures in the single mesh cube, on the decrease of the biomass particle diameter. It can be observed that first the biomass diameter decreases due to moisture evaporation, then during devolatilisation and simultaneous char oxidation the diameter is strongly reduced. Furthermore, it can be seen that higher temperature causes faster shrinking of the biomass particle.

33
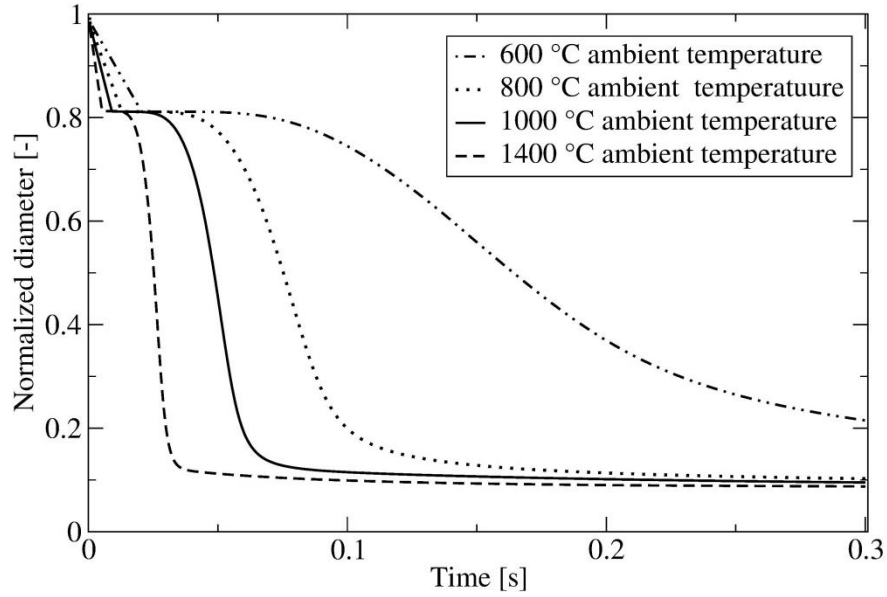
Figure 8 Biomass particle diameter in relation to the different ambient temperatures.

In Figure 9, biomass particles of different size, with the initial particle temperature of 50 °C, the initial particle moisture content of 15%, and the ambient temperature in the single mesh cube of 1000 °C were analysed. The particle heats up until it completely combusts, after which it cools down to the cell ambient temperature. As can be expected, smaller particles tend to heat up faster than the bigger particle. It can also be seen that during the boiling process particle temperature remains the same.
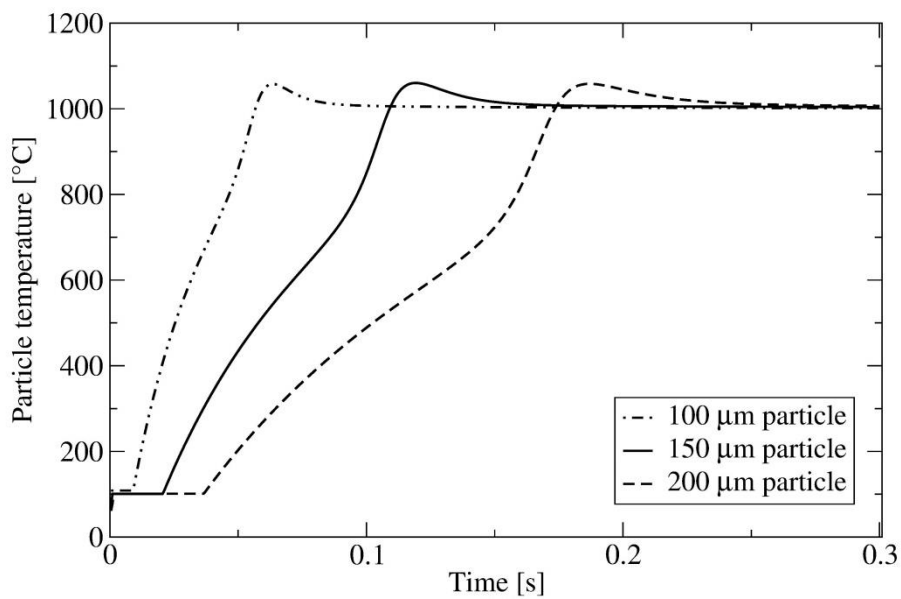
Figure 9 Heat up of different biomass particle sizes.

For calculations of a single polypropylene particle, which results are shown in Figure 10, the initial particle temperature was set to 50 °C, and the ambient temperature in the single mesh cube was set to 1000 °C. Figure 10 shows the polypropylene particle mass loss during the simulated time. As can be observed, as expected smaller particles decompose quicker than the bigger particles. What can also be observed is that the mass of the polypropylene does not change until the decomposition starts.
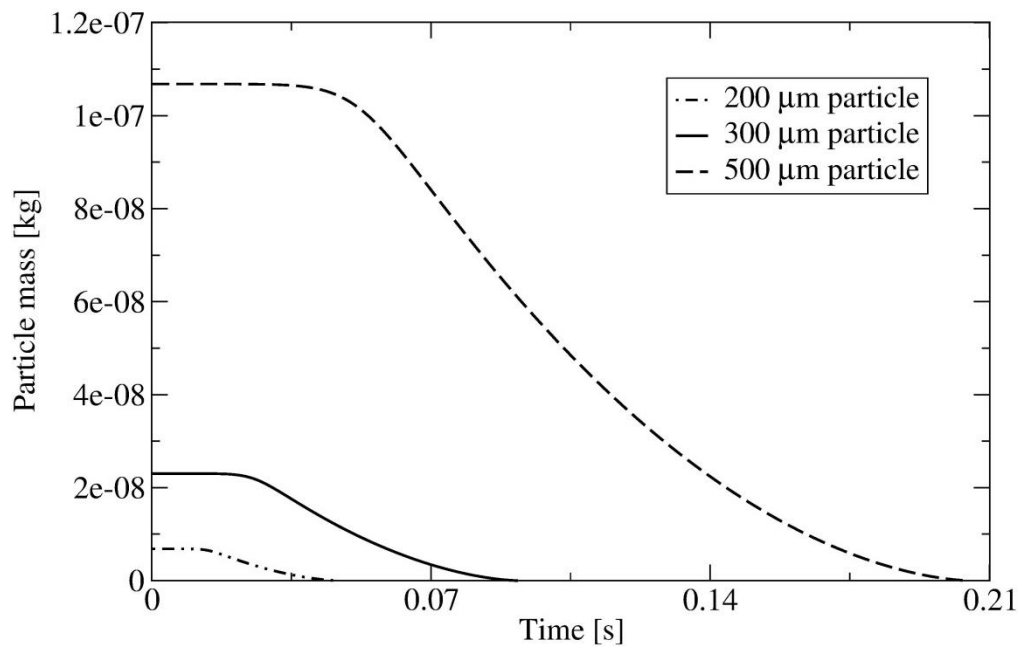
Figure 10 Polypropylene particle's mass loss over time.

Figure 11 shows the increase of the polypropylene particle temperature during the simulation time. Here it can be seen that the polypropylene particle's temperature steadily increases until the decomposition process starts. Then the temperature increase slows down due to the mass exchange consuming the reaction enthalpy. At the end of the decomposition process the temperature again starts to increase more rapidly due to decreasing particle size and mass, until the moment where all polypropylene has decomposed. These phenomena are better visible with increasing particle size.
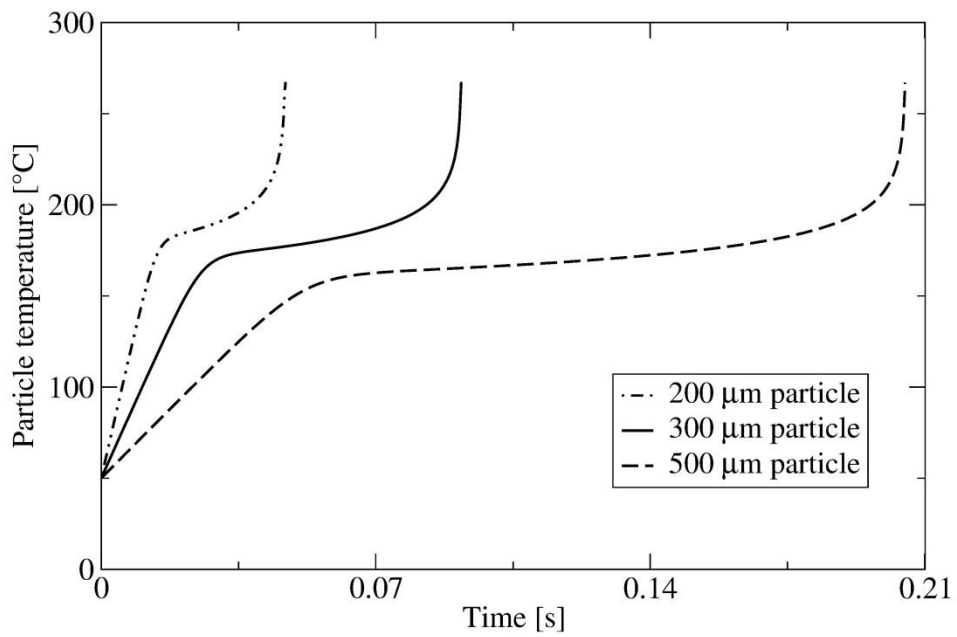
Figure 11 Polypropylene particle's temperature over time.

Figure 12 shows the relation between polypropylene particle mass and temperature. It can be seen that bigger particles start to decompose quicker than smaller particles. What can also be seen in this figure is that within certain temperature range particles lose most of their mass.
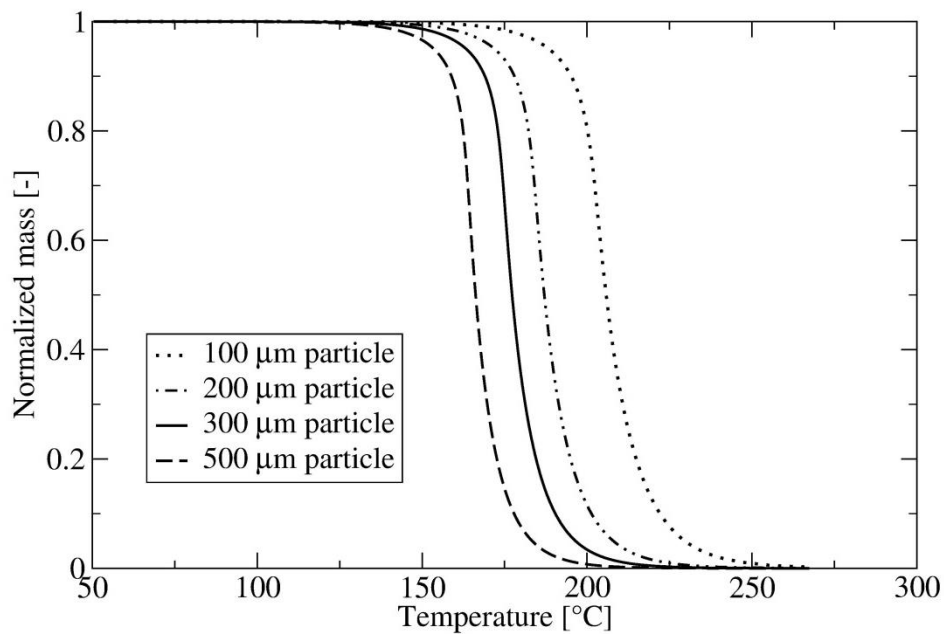
Figure 12 Polypropylene particle's mass loss in relation to the temperature increase.

Results gained from the single particle tests for biomass and polypropylene particles, show that different particle sizes and ambient temperatures have an expected effect on the heat-up and decomposition history of the particles. Furthermore, it has been shown that the reaction kinetics of the biomass combustion yields reasonable trends.

3.2   Validation test cases

In order to reduce the influence of turbulence and other flow characteristics on the calcination and combustion process, each of the presented models was validated by simulating experiments done in drop tube furnaces (DTF). The available measurement data were used for comparison with numerical predictions. In Table 2, the operating conditions and the simulated mesh sizes for the mesh dependency tests, for each drop tube experiment, are summarized. More details about the drop tube experiments can be found in the references named in Table 2, and in appended PAPER 1.

Table 2 Drop tube furnace experiments operating conditions, and mesh size.

	Limestone* [92]	Coal [73]	Biomass [74]	Polypropylene [85]	Solid recovered fuel [74]
Furnace temperature [°C]	1200	1100	1100	1300	1100
Chamber diameter [m]	0.08	0.038	0.05	0.2	0.05
Chamber length [m]	2.0	1.2	1.2	2.5	1.2
Solid feed rate [g/h]	600	22	25	498	25
Solid inlet temperature [°C]	20	25	25	25	25
Air flow rate	22 $[m_N^3/h]$	8.2 [L/min]	22 [L/min]	Primary air 1.950 Secondary air 2.957 [kg/h] Tertiary air 1.371	22 [L/min]
Air inlet temperature [°C]	1200	25	25	25	25
3D mesh dependency tests (number of hexahedral cells)					
Reference mesh	10,800	12,800	16,800	32,600	16,800
Coarser mesh	5,600	9,600	12,900	24,600	12,900
Finer mesh	26,500	15,600	23,000	40,800	23,000

*Only calcination experiment C3, one out of six analysed experimental set-ups from the PhD thesis of Mohr [92], is given in Table 2, for more details see PAPER 1.

The calcination model was validated by simulating the International Flame Research Foundation (IFRF) pipe reactor IPFR (intensified plug flow reactor), for which measurements of limestone conversion exist [92]. Several experiments with different operating conditions have been done. This sensitivity analysis gives some more information about the influence of various parameters (CO_2 content, temperature, mass flow, etc.) on the calcination reaction rate. The experimental data forms the basis for the evaluation of the calcination model and its simulation behaviour.

The predicted conversion of limestone to lime, for different set-ups, was compared with the calculations from Mohr's doctoral dissertation and the reported experimental data [92].
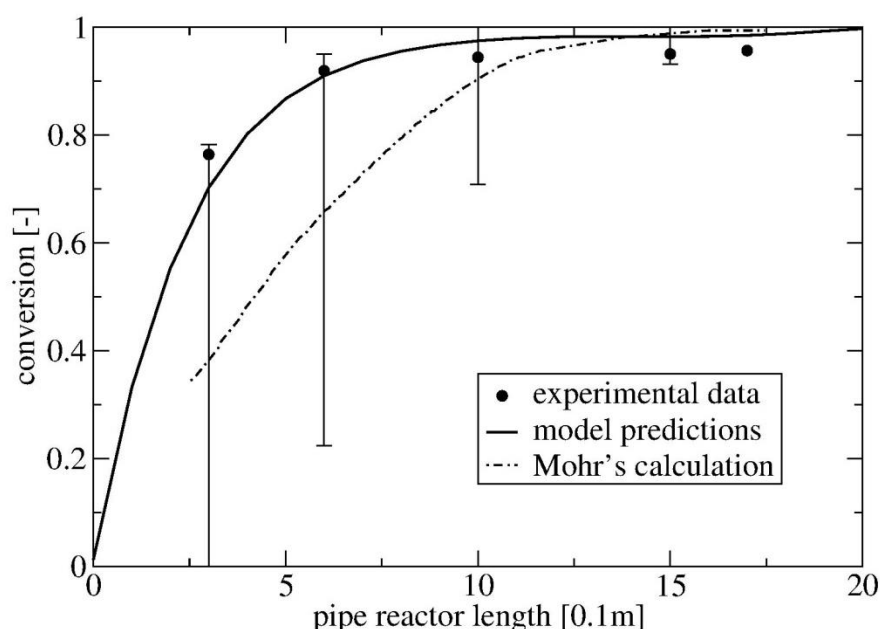
Figure 13 Comparison of limestone conversion for the C3 experimental set-up.

Figure 13 shows the comparison of limestone conversion for the C3 experimental set-up between the reported experimental data and the numerical predictions. As can be seen the experimental measurements and the numerical results obtained by the calcination model are in good agreement. In Figure 13 also the calculation from the PhD thesis of Mohr [92] is shown. Despite the model presented is simpler than the Mohr model, e.g. regarding details of evolution of the porous structure and detailed description of sintering processes, the overall agreement with the experimental data could be improved. This might be due to the additional uncertainties in Mohr's model introduced by unknown model parameters of the detailed sub-

models and complex interactions between them, which would need an even broader experimental data base for adjustment. In contrast to this the simpler model can be more easily controlled and matched and thus is judged to be sufficiently accurate for CFD simulations of the overall calcination process.
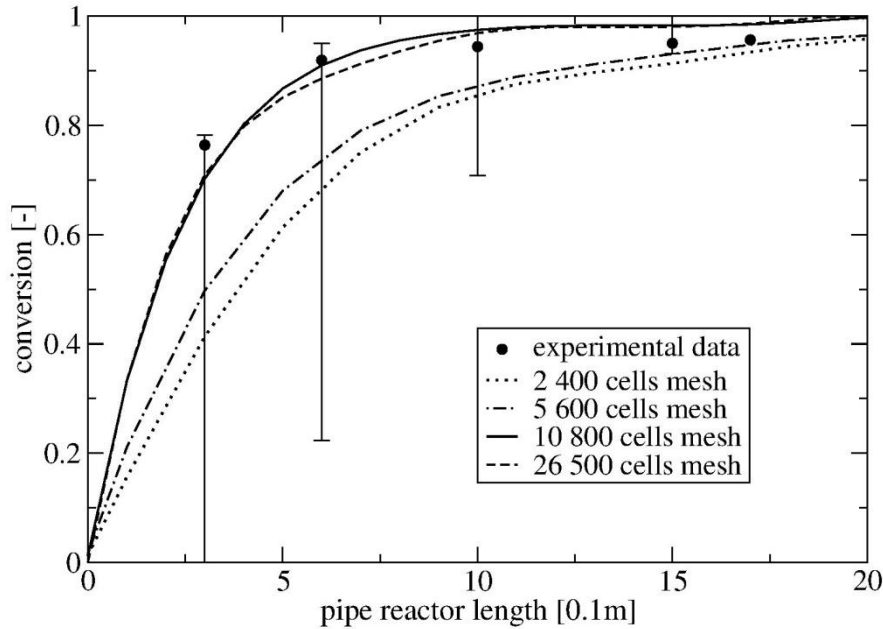
Figure 14 Influence of mesh size on the results for the C3 experiment.

Fig. 14 shows the influence of mesh size on the results for the C3 experiment. Comparison of the coarsest grid (dotted line) and the coarse grid (dash dot line) shows significant differences in the results, while the difference between intermediate (continuous line) and fine grid (dashed line) is already considerably smaller. The conversion rate of these two grids (continuous and dashed line) is almost identical. Thus with respect to the experimental uncertainty the grid with 10 800 cells has been regarded as sufficient.

For the coal combustion model validation, combustion of unsieved coal in air was simulated, and the numerical predictions for oxygen concentration, temperature and particle burnout were compared with the experimental data. For particle burnout, the expression reported in the literature [73] was used to determinate the simulation burnout rate. Unsieved coal's proximate and ultimate analysis, as well as its particle size distribution can be found in literature [73].
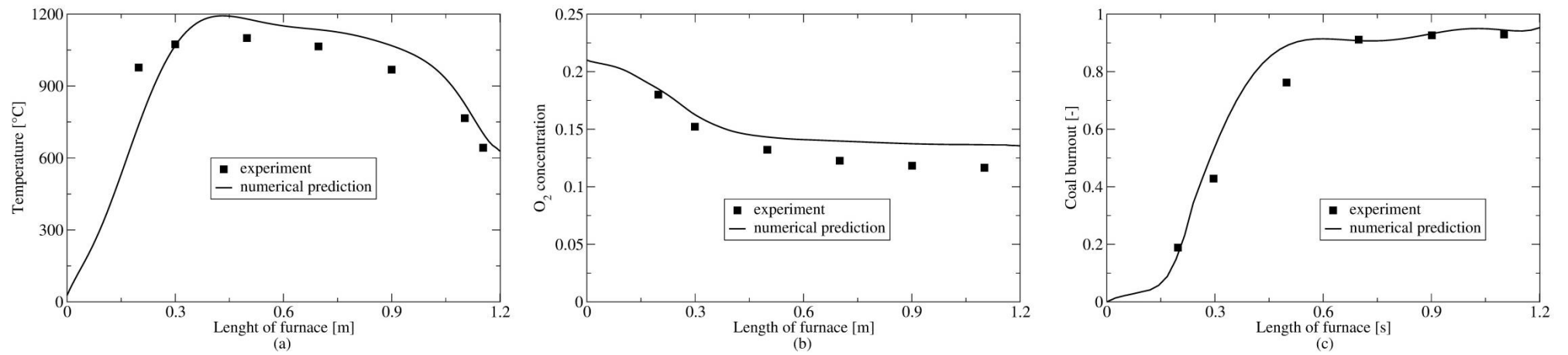
Figure 15 Validation of coal combustion model: (a) temperature profile along the furnace; (b) oxygen concentration along the furnace; (c) burnout rate along the furnace.

In Figure 15 the comparison of the coal combustion model numerical predictions with experimental measurements is shown. Figure 15(a) shows the temperature along the furnace axis. It can be observed that the numerical prediction follows the experimental trend. Figure 15(b) shows the oxygen concentration along the furnace, and here the numerical prediction shows satisfying agreement with the experimental data. Figure 15(c) shows the burnout rate along the furnace. For the burnout rate, the expression from literature [73] was used. According to this expression the burnout rate of the solid fuel is calculated by comparing the initial and final ash mass fraction in the particle. As can be seen the numerical prediction here follows well the experimental trend.

For the biomass and SRF combustion model validation, combustion of milled pine branches, that represents the biomass, and combustion of SRF in the same DTF was simulated. The available experimental data for temperature and particle burnout were compared with numerical predictions. Pine branches and SRF proximate and ultimate analysis, as well as its particle size distribution can be found in literature [74].

In Figure 16 the comparison of biomass combustion model numerical predictions with experimental data is shown. Figure 16(a) shows the comparison of numerical prediction and experimental data for temperature along the furnace. As can be seen the model predicts the temperature quite well. In Figure 16(b) the burnout rate along the furnace is shown. As can be seen, here also the numerical prediction follows well the experimental trend.
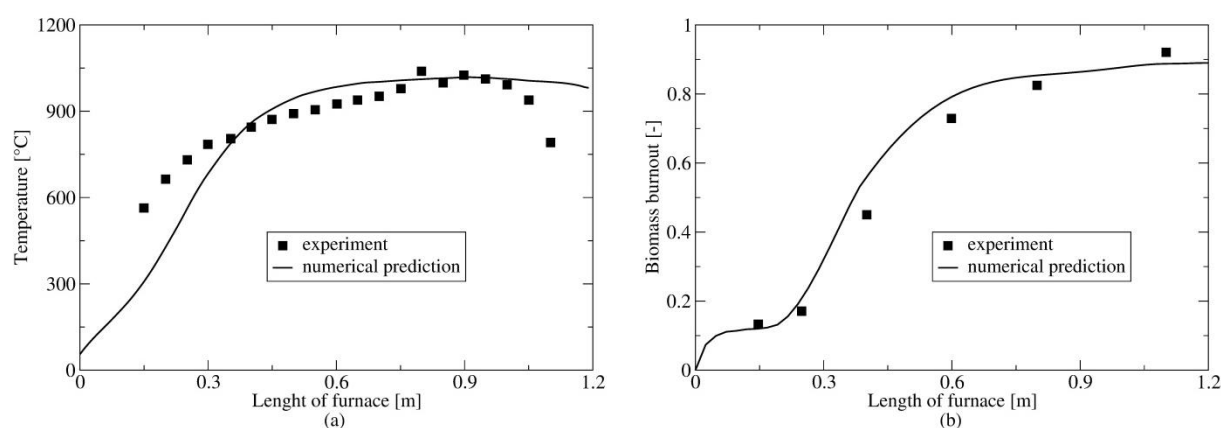
Figure 16 Validation of biomass combustion model: (a) temperature profile along the furnace; (b) burnout rate along the furnace.

42

For the polypropylene combustion model validation, combustion of polypropylene in an electrically heated DTF was simulated. The furnace burner has a central inlet, where polypropylene together with the primary air enters, and two concentric inlets for the secondary and tertiary air. All air streams enter the furnace without any swirl [93]. The numerical predictions for oxygen and carbon dioxide concentration profiles along the furnace axis were compared with the experimental data reported in literature [84]. Proximate and ultimate analysis of polypropylene, as well as its particle size distribution can be found in literature [85].

In Figure 17 the comparison of polypropylene combustion model numerical predictions with experimental data is shown. Figure 17(a) shows the oxygen, and Figure 17(b) carbon dioxide concentration comparison along the furnace. It can be seen that for both species numerical predictions are in good agreement with the experimental data.
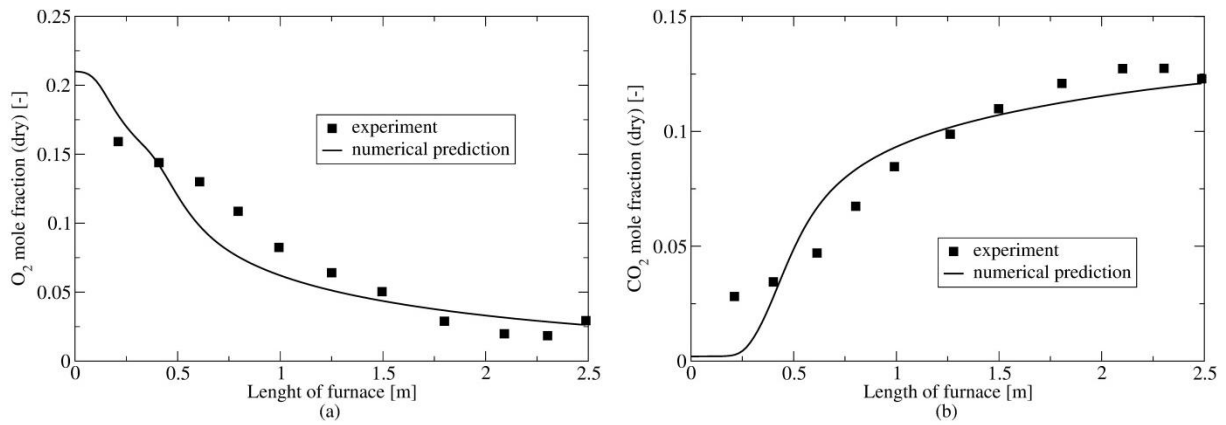
Figure 17 Validation of polypropylene combustion model: (a) oxygen concentration along the furnace; (b) carbon dioxide concentration along the furnace.

Figure 18 shows the comparison of SRF combustion model numerical predictions with the experimental measurements. In Figure 18(a) the temperature and in Figure 18(b) the burnout rate along the furnace is shown. As can be observed the numerical predictions of the SRF combustion model are also in quite good agreement with experimental data.
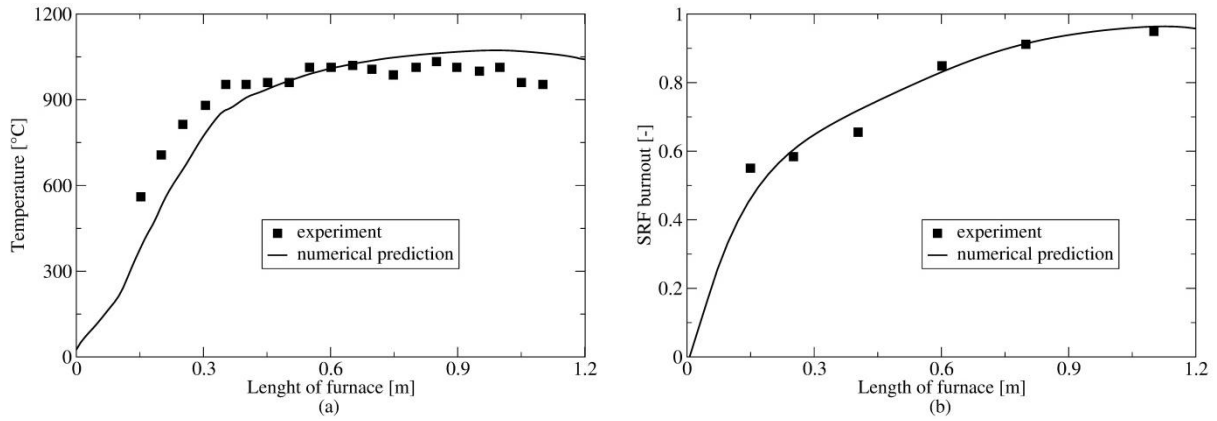
Figure 18 Validation of SRF combustion model: (a) temperature profile along the furnace; (b) burnout rate along the furnace.

In Figure 19 the influence of mesh size on presented combustion models is shown. The mesh dependency tests were done in detail for all presented combustion models, and they show that mesh size has a very small impact on the obtained results. In Figure 19 for each solid fuel only one quantity is analysed. Thus, the influence of mesh size on the numerical prediction of the: temperature profile along the furnace for the coal combustion model is given in Figure 19(a); temperature profile for the biomass combustion model is given in Figure 19(b); oxygen concentration for the polypropylene combustion model is given in Figure 19(c); burnout rate for the SRF combustion model is given in Figure 19(d).
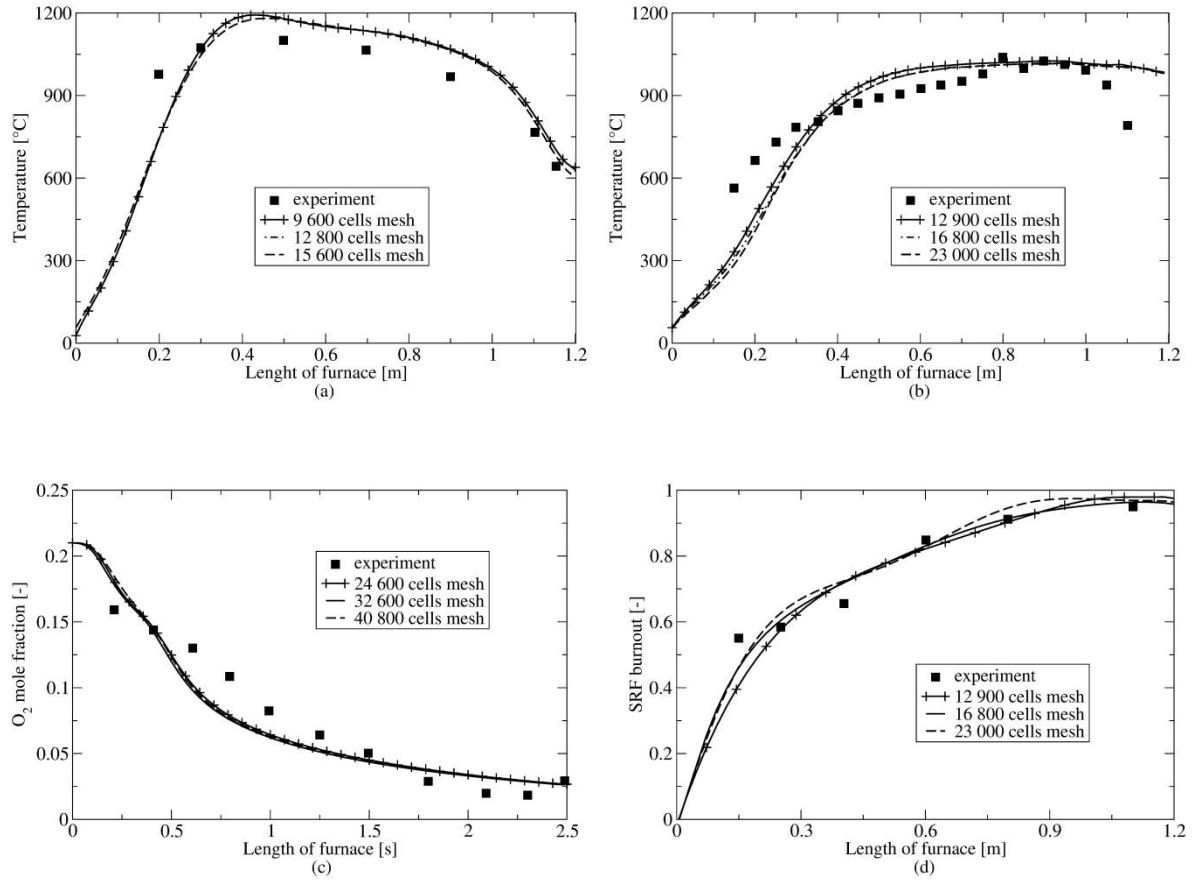
Figure 19 Influence of mesh size on presented combustion models: (a) temperature profile along the furnace for the coal combustion model; (b) temperature profile for the biomass combustion model; (c) oxygen concentration for the PP combustion model; (d) burnout rate for the SRF combustion model.

3.3 Large scale cement calciner simulations

To demonstrate the application of the validated calcination and combustion models for different solid fuels, three complex three dimensional geometries of industrial cement calciners were simulated. In the following, the results of the CFD simulations for two different real industrial cement calciners are given. The results show some interesting features of the flow, which help to understand the operating conditions of the simulated calciners. The calciners operating conditions and the computational details of each CFD simulation, as well as the results for the third calciner, are given in PAPERS 2-6.

In Figure 20 the geometries and boundary conditions for two different industrial cement calciners are shown.

The calciner on the left hand side of the Figure 20 is 75 m high in total. The lower part of the calciner consists of two vertical tubes, of which one is used as the tertiary air inlet, and the other is used as an inlet for the hot flue gases coming from the rotary kiln. At the bottom of each of these tubes, inlets for coal and pre-dried limestone are positioned. Both tubes have an approximate diameter of 2 m, and they connect at the height of 25 m to form a rectangular shaped junction, where tertiary air and hot flue gases coming from the rotary kiln, together with the introduced limestone and coal particles, are mixed. After the rectangular shaped junction a single vertical tube, with diameter of 3.1 m, serves to direct the flow to the top of the calciner. The top of the calciner is designed in a way that it, by using the swirling effect, directs the upward stream to a downward stream. Finally after the flow is directed downwards, a tube, with diameter of 3.1 m, is used to direct the fluid flow together with now already calcined raw material to the outlet of the calciner. The outlet of the calciner corresponds to the inlet of the fifth preheater cyclone, where measurement data are obtained. The boundary conditions used for the numerical simulation of the calciner on the left hand side of the Figure 20 are given in Table 3.

The calciner shown on the right hand side of Figure 20 consists of two vertical cylinder parts and a cylinder connecting them. On the top of the first vertical cylinder the swirl burner is positioned, and in the second vertical cylinder the hot gas stream from the rotary kiln is used to enhance the calcination process. At the bottom of the second vertical cylinder a converging-diverging section is used to increase the velocity of the incoming hot stream from the rotary kiln. The entire model is 24 m high, with the diameter of the first cylindrical part, the burner chamber, of 5.5 m, and with the diameter of the second cylindrical part of 4.5 m. The connecting cylinder is positioned at 60˚ angles and is 4 m in diameter. At the top of the first vertical cylinder two limestone and two tertiary air inlets are positioned diametrically opposite each other. The top of the second vertical cylinder is the calciner's outlet. The boundary conditions used for the numerical simulation of the calciner on the right hand side of the Figure 20 are given in Table 4.

In Figures 21 to 26 the results of the 3D CFD simulations of the cement calciner shown on the left hand side of Figure 20 are given, whereas in Figures 27 to 31 the results of the 3D CFD simulations of the cement calciner shown on the right hand side of Figure 20 are given.

Table 3 Boundary conditions for the calciner shown on the left hand side of Figure 20.

Notation		Mass flow rate [kg/h]	T [°C]	ρ [kg/m^3]	d_p [kg/m^3]	O_2 [mass %]	N_2 [mass %]	CO_2 [mass %]
Limestone and coal inlet 1	Coal	5800	70	1300	50			
	Limestone	126000	780	3100	50			
Limestone and coal inlet 2	Coal	1380	70	1300	50			
	Limestone	21000	780	3100	50			
Tertiary air inlet		20690	780	1.292		28	71.8	0.2
Hot gas from rotary kiln inlet		48275	1060	1.292		8	72	20
Outlet	Static Pressure	10^5 Pa						

Table 4 Boundary conditions for the calciner shown on the right hand side of Figure 20.

	T [°C]	Coal case (100% Coal Combustion)	Biomass case (Biomass 10% thermal share)	PP case (PP 10% thermal share)	SRF case (SRF 10% thermal share)
		Mass flow rate [kg/h]			
Limestone 1+2	720	147900			
Tertiary air 1	950	49600			
Tertiary air 2	950	49600			
Primary air	80	16200			
Secondary air	950	33065			
Coal	60	14811	13330	13330	13330
Biomass / SRF Biodegradable	60	-	2240	-	1793
PP / SRF PP	60	-	-	878	176
Hot gas from rotary kiln	1100	110600			
Outlet (Static Pressure)		10^5 Pa			
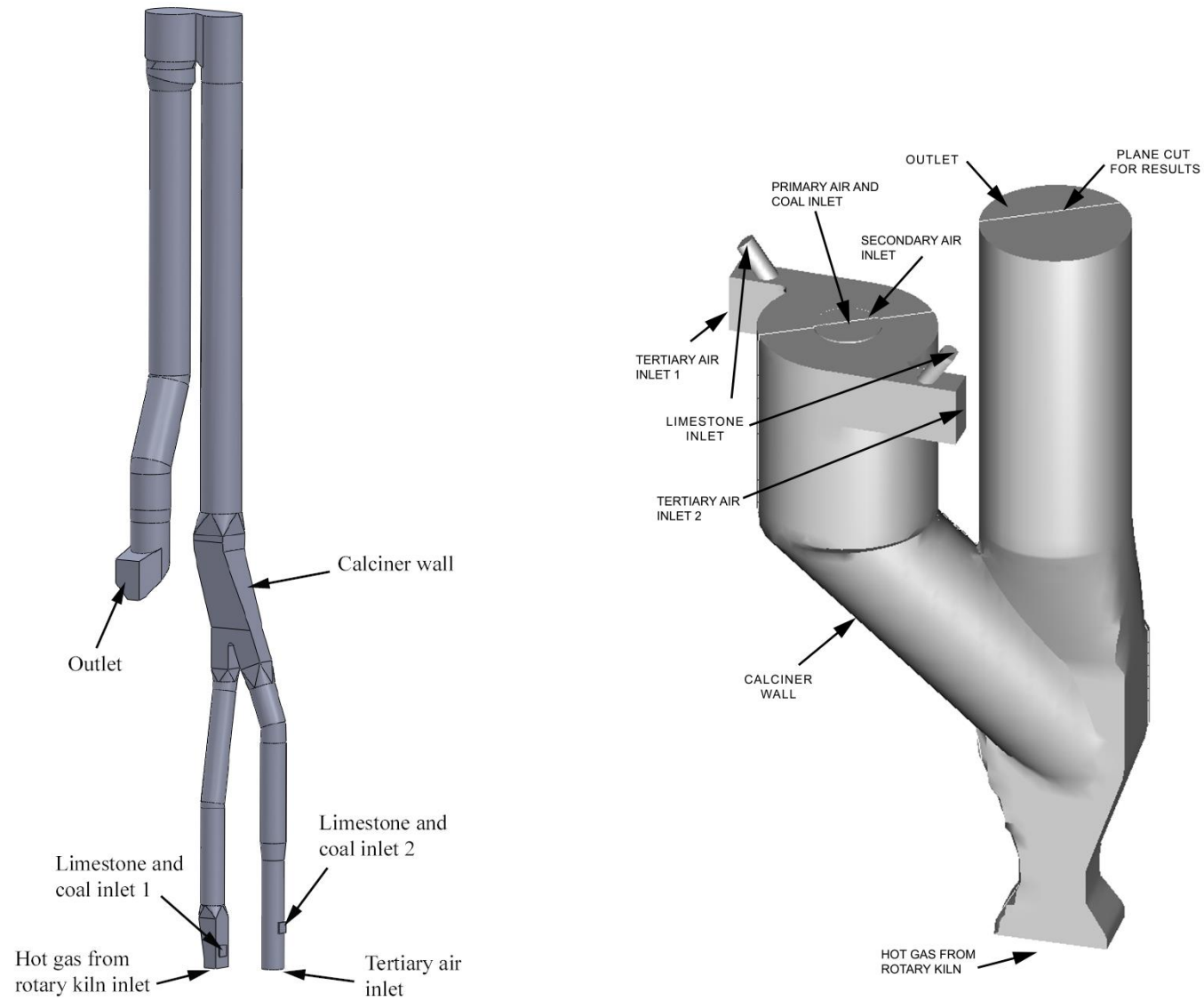
Figure 20 Geometries and boundary conditions for two different types of industrial cement calciners.

Figure 21 shows the flow streamlines inside the first calculated calciner. As can be observed, in the lower part of the calciner, in the tertiary air tube and the hot flue gases coming from the rotary kiln tube, the flow streams are stable and uniform, and going upwards. Both streams join together in the rectangular shaped junction, after which they form one stream that is going upwards to the top of the calciner. In this part of the calciner the majority of the limestone thermal degradation, e.g. calcination process, occurs. At the top of the calciner, where the fluid flow changes the direction, from an upward to a downward direction, the flow becomes highly swirled. The reason for this highly swirled flow is the big mass flow of the stream that is coming to the top of the calciner and the design of the calciner's top, that by using the swirling effect effectively changes the flow direction. After the flow is directed downwards, the flow gradually loses its swirling effect and together with now already calcined raw material goes to the outlet of the calciner. Understanding of the flow characteristics inside the calciner is of crucial importance for plant operators, since the flow characteristics give a good estimation of the particle residence time. The particle residence time is important, since limestone and fuel particles need several seconds to fully decompose and burn.
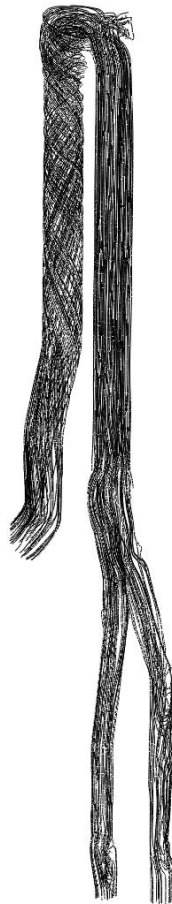
Figure 21 Flow streamlines inside the first calculated calciner.

50

Figure 22 shows, from the left hand side to the right hand side, the position of limestone particles and its degradation at 2, 4, 6 and 8 s of particle residence time. For each particle residence time, the limestone mass fraction in particles is shown. It can be seen that limestone particles need several seconds to fully decompose.
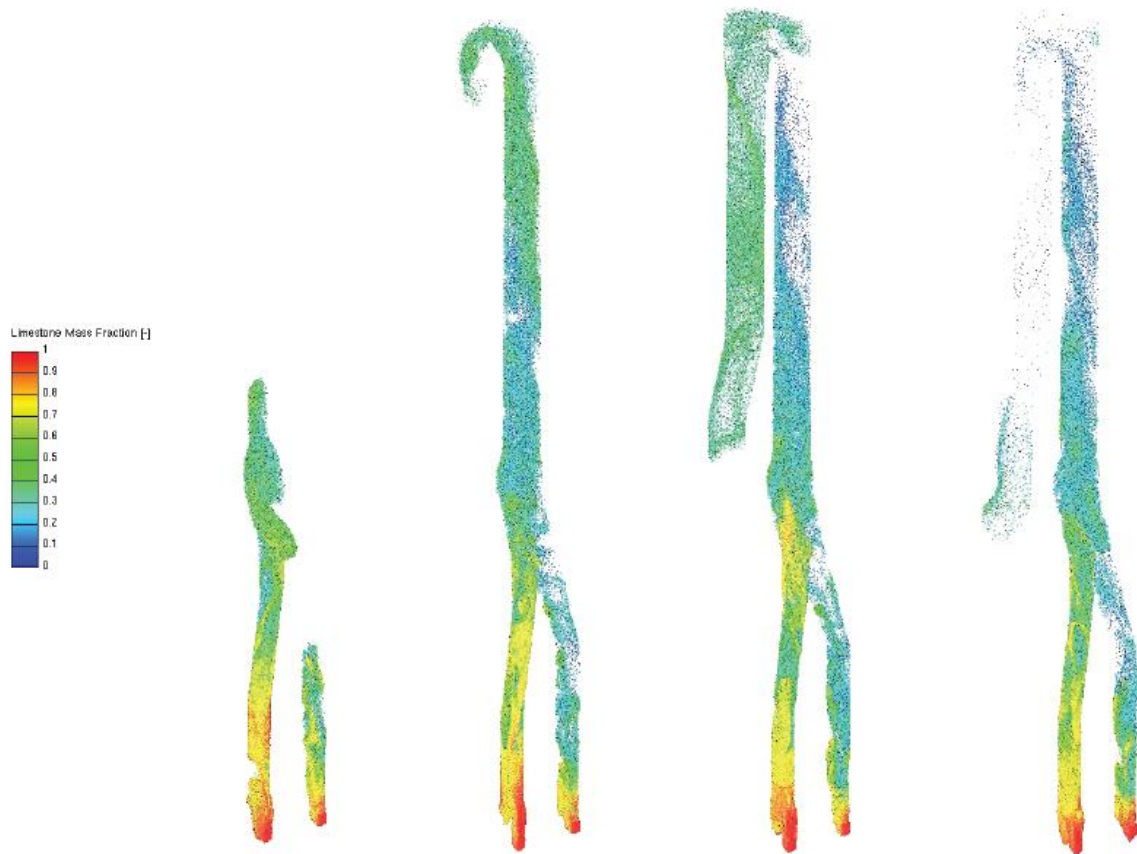
Figure 22 Limestone degradation at different particle residence time: 2 s (left); 4 s (second from left); 6 s (second from right); 8 s (right).

Figure 23 shows, from the left hand side to the right hand side, the position of produced lime particles at 2, 4, 6 and 8 s of particle residence time. For each particle residence time, the lime mass fraction in particles is shown. When compared to Figure 22, the corresponding increase of the lime mass fraction at different particle residence time can be observed. In this figure, like in the previous one, it can be observed that the calcination process needs several seconds to finish.
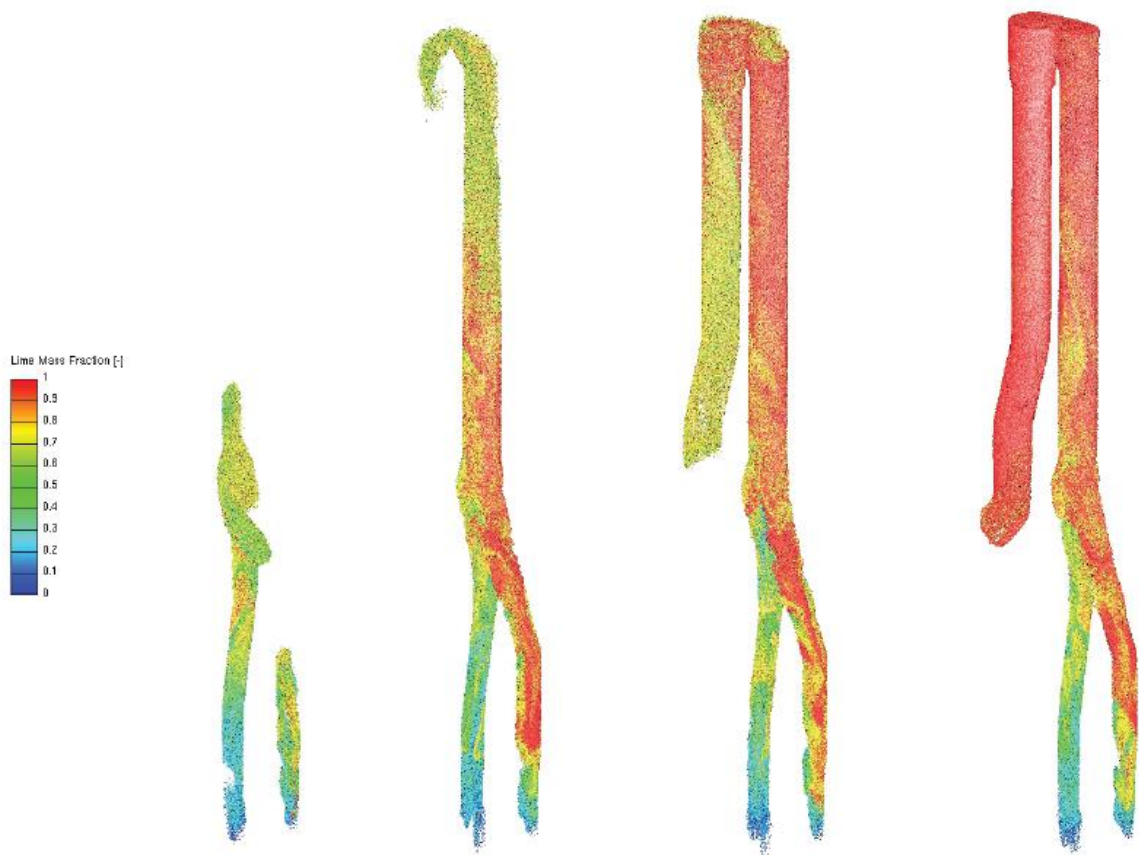
Figure 23 Lime production at different particle residence time: 2 s (left); 4 s (second from left); 6 s (second from right); 8 s (right).

Figure 24 shows, from the left hand side to the right hand side, the position of char particles in the lower calciner part at 2, 4, 6 and 8 s of particle residence time. For each particle residence time, the char mass fraction in particles is shown. As can be observed, char particles combust in the lower part of the calciner, e.g. in two vertical tubes, of which one is used as the tertiary air inlet, and the other is used as an inlet of hot flue gases coming from the rotary kiln. Here it can be seen that unlike the calcination process, the char oxidation is a faster reaction and it does not need several seconds to fully react.
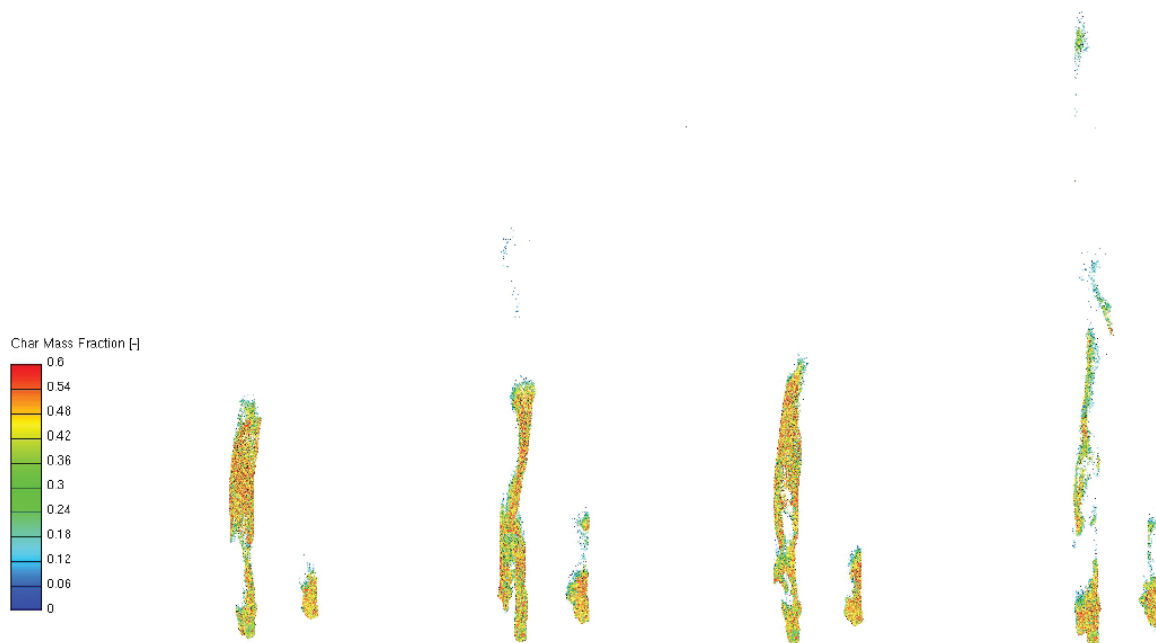
Figure 24 Char oxidation at different particle residence time: 2 s (left); 4 s (second from left); 6 s (second from right); 8 s (right).

Due to the complex geometry of the calculated calciner, it is difficult to represent the concentration of species and the temperature field. For that reason, the back view of the calciner is shown in Figure 25 and Figure 26. In Figures 25 and 26 the quasi stationary state simulation results are shown. Figure 25 shows the combustion process inside the calculated calciner. The char mass fraction in particles is presented on the left hand side, in middle the temperature field is presented, and on the right side the ash mass fraction in particles is presented. Also the distribution of char and ash particles inside the calculated calciner is shown. The 'empty' regions for char mass fraction indicate the regions where conversion of char to CO, CO_2, and ash, to a large extent, has already been completed. In this figure the decrease of char mass fraction and the corresponding increase of ash mass fraction towards the outlet can be observed. Also, it can be seen that since the calcination process is a strong endothermic reaction, throughout the cement calciner the temperature field is uniform and there are no extreme temperature peaks inside the calciner. It can be seen that the char particles are concentrated close to the inlets, and that the ash particles are found in the whole calciner.

Figure 25 Combustion process inside the calculated calciner.

Figure 26 shows the thermal degradation of limestone inside the calculated calciner. On the left hand side the limestone mass fraction in particles is shown, in middle the CO_2 mass fraction is shown, and on the right hand side of the figure the produced lime mass fraction in particles is shown. It can be observed that as expected the limestone particles decompose from bottom of the calciner to its top and exit. The corresponding increase of the lime mass fraction can be observed on the right hand side of the figure. The mass fraction of lime in the particle increases as raw material particles move to the top of the calciner and its exit. The CO_2 mass fraction, shown in the middle of the figure shows that the highest concentrations are located at

the bottom of the calciner where the combustion of coal occurs, and between the rectangular junction and the top of the calciner where most of the calcination process occurs.

Figure 26 Calcination process inside the calculated calciner.

Comparison of numerically obtained results with experimental data is essential for the validation of the numerical model used. The measurement equipment of this fully operating industrial calciner was placed on its outlet. On the outlet of the calciner, coal burnout rate, limestone degradation rate and the outlet temperature was measured. In Table 3, the comparison of measurement data and numerical predictions is shown. As can be seen, the numerical predictions are in good correlation with the measured data. Coal burnout rate is the same, whereas for the limestone degradation rate and the outlet temperature numerical predictions are slightly higher, but still in good agreement with the measured data.

Table 5 Comparison of measurement data and numerical predictions.

	Measurement Data	Numerical Predictions
Coal Burnout Rate [-]	1.0	0.999
Limestone Degradation Rate [-]	0.957	0.983
Outlet Temperature [K]	1,188	1,213

In Figure 27 the temperature field inside the second calciner, shown on the right hand side of Figure 20, for the four calculated combustion cases is shown. In this figure from left to right the temperature fields for the reference coal case, biomass co-combustion case, PP co-combustion case, and SRF co-combustion case are shown. The figure shows that in all cases throughout the calciner the temperature is more or less uniform and around 1200 K, except in the near burner region. This is due to the strong endothermic calcination reaction, where limestone particles using the available enthalpy in the gas phase thermally decompose. Furthermore, it can be seen that there are some differences in the temperature field in the near burner region. In the coal case and in the SRF case the temperature in the near burner region are approximately the same, however this is not the case for the biomass and the PP case. It can be observed that in biomass case, where biomass is co-combusted with coal, a decrease in the middle of the temperature pick is present. This is due to the higher moisture content in the biomass particle than that of coal, and consequently the drying of biomass particles. In the PP case, where PP is co-combusted with coal, the biggest difference in the temperature field when compared to the reference case can be seen. Due to the rapid PP decomposition and combustion the temperature is much higher in this case, meaning that special care needs to be taken, in order not to increase the wall thermal load in this calciner part. In contrast to other combustion units where only fuel is combusted, in the calciner due to the intensive mixing of fuel and limestone particles and the mentioned calcination reaction, there is no classical flame shape.

Figure 27 Temperature fields inside the calciner for the four calculated cases: (a) coal case; (b) biomass co-combustion case; (c) PP co-combustion case; (d) SRF co-combustion case.
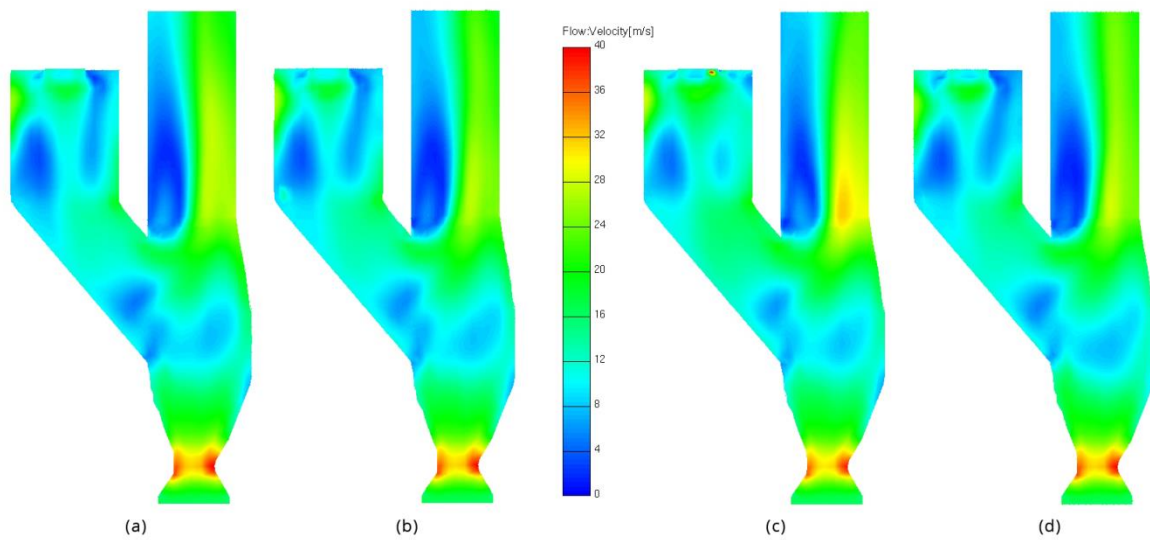
Figure 28 Velocity fields inside the calciner for the four calculated cases: (a) coal case; (b) biomass co-combustion case; (c) PP co-combustion case; (d) SRF co-combustion case.

Figure 28 shows the velocity field inside the calciner for the four calculated combustion cases. In this figure from left to right the temperature fields for the reference coal case,

57

biomass co-combustion case, PP co-combustion case, and SRF co-combustion case are shown. The figure shows that in all cases the highest velocity is in the bottom of the calciner, where the high velocity stream of exhaust gases coming from the rotary kiln enters. What can also be seen from this figure is that in the PP case, a slightly higher velocity in the right vertical cylinder part can be observed. This might indicate danger of enhanced erosion in the respective region of the vessel.
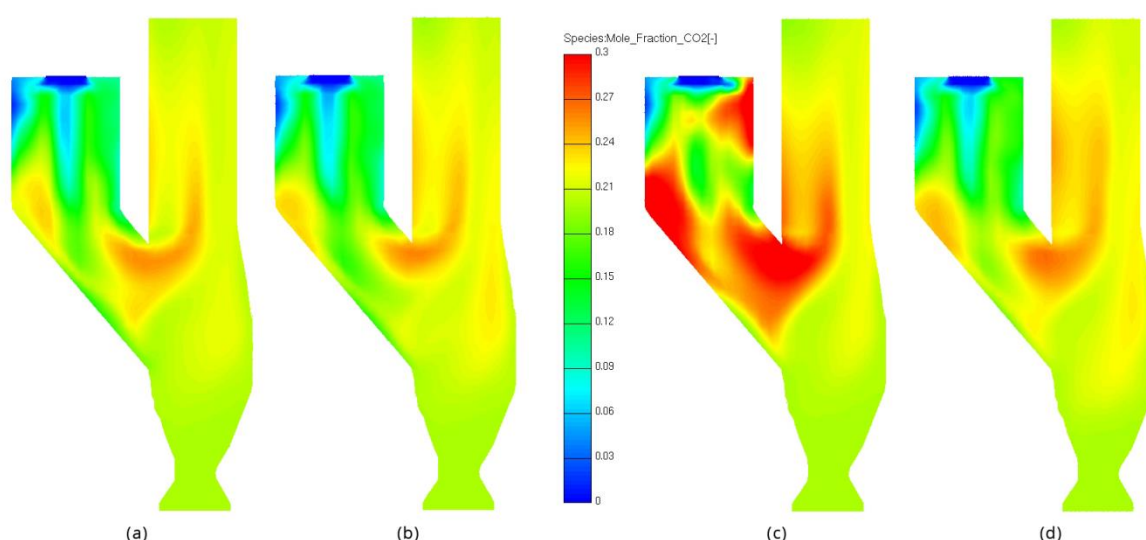
Figure 29 CO$_2$ mole fraction inside the calciner for the four calculated cases: (a) coal case; (b) biomass co-combustion case; (c) PP co-combustion case; (d) SRF co-combustion case.

Figure 29 shows the CO$_2$ mole fraction inside the calciner for the four calculated combustion cases. In this figure from left to right the CO$_2$ mole fraction for the reference coal case, biomass co-combustion case, PP co-combustion case, and SRF co-combustion case are shown. The figure clearly shows the difference in the CO$_2$ concentrations for all calculated cases. In the biomass and SRF case, a slight difference from the coal case can be observed, however in PP case significance in the results can be observed. Since calcination reaction is predominantly a temperature driven process, and it was shown that the PP case has higher temperatures in the near burner region, calcination process start sooner than in other cases. Therefore in this case limestone sooner decomposes and sooner releases the bounded CO$_2$ having higher concentrations of CO$_2$. This is valuable information for plant operators, since it

is known that the calcination process can extinguish the combustion process, so special care has to be taken not to have too quick limestone decomposition.

In Figure 30 the H_2O mole fraction inside the calciner for the four calculated combustion cases is shown. In this figure from left to right the temperature fields for the reference coal case, biomass co-combustion case, PP co-combustion case, and SRF co-combustion case are shown. It can be seen that in the biomass and SRF case, where fraction of fuel is biomass, higher concentrations of H_2O are present. The higher concentration is related to evaporation of moisture from the biomass particles.
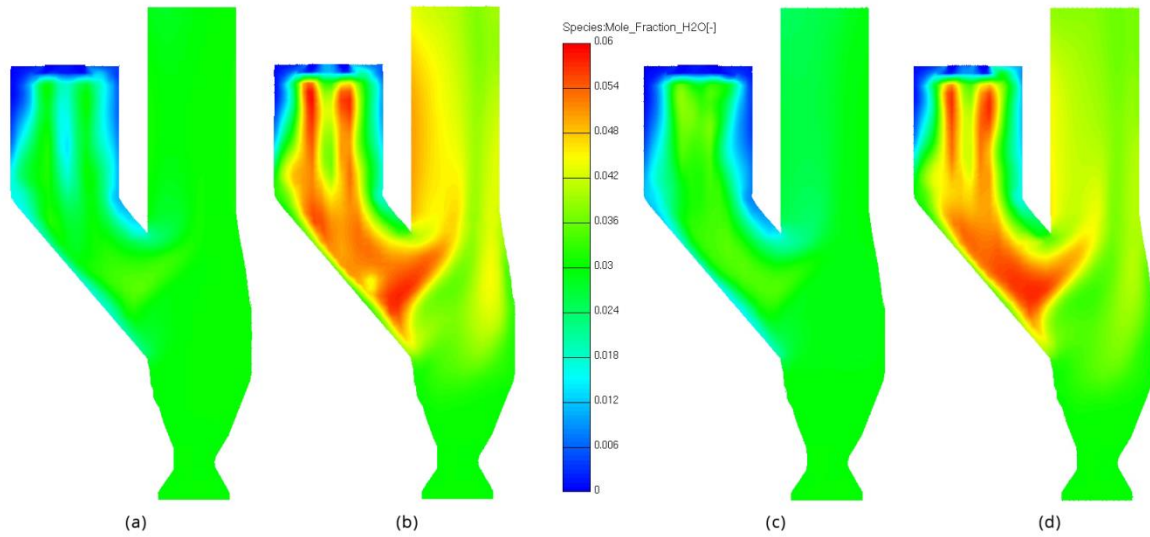
Figure 30 H_2O mole fraction inside the calciner for the four calculated cases: (a) coal case; (b) biomass co-combustion case; (c) PP co-combustion case; (d) SRF co-combustion case.
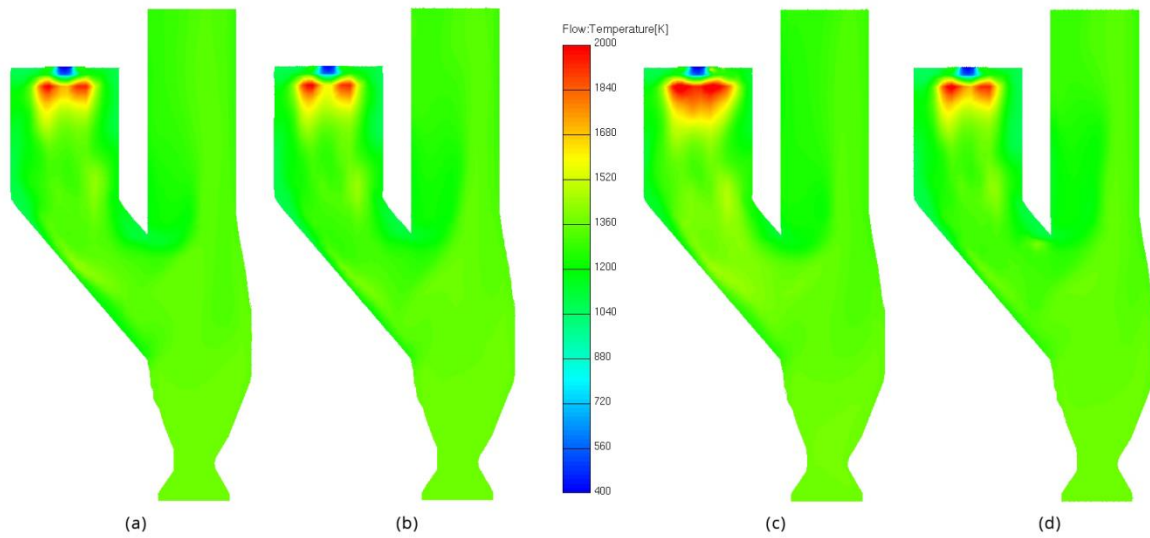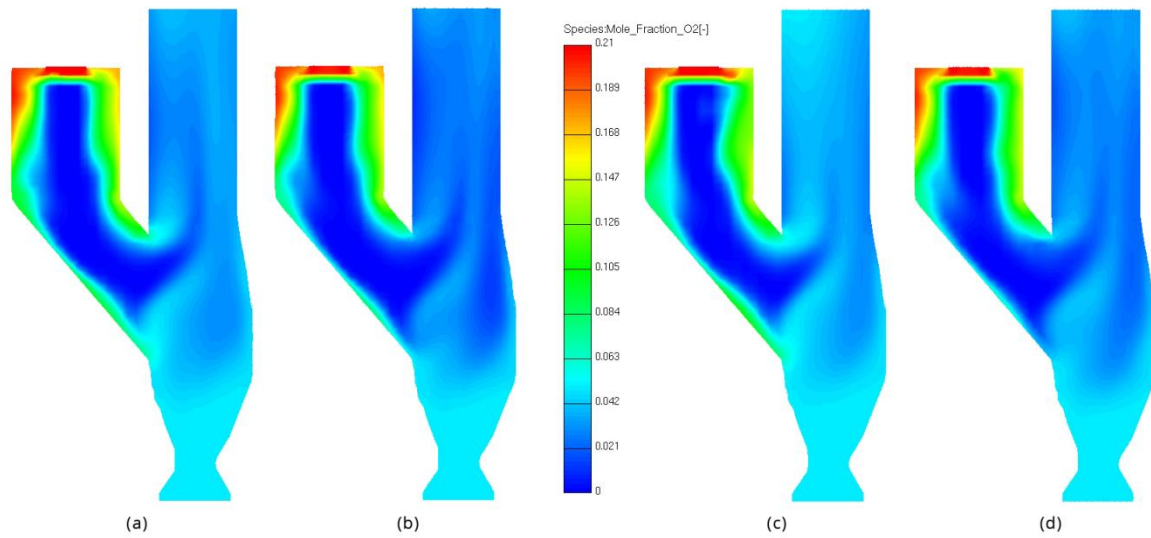
Figure 31 O$_2$ mole fraction inside the calciner for the four calculated cases: (a) coal case; (b) biomass co-combustion case; (c) PP co-combustion case; (d) SRF co-combustion case.

Figure 31 shows the O$_2$ mole fraction inside the calciner for the four calculated combustion cases. It can be observed that in all cases the concentrations of O$_2$ are similar, meaning that oxygen is consumed similarly in all cases.

The results presented herein show that computer simulation method can serve as an advanced tool to analyse and improve understanding of complex turbulent reacting flow in real cement calciner. The proposed models and methods can assist plant operators and practical engineers in the optimization of cement calciner's operating conditions, which are crucial to ensure better plant efficiency and reduction of pollutant emissions.

4 CONCLUSIONS AND FUTURE WORK

Depletion of fossil fuels, rising of their prices, global warming and GHG emissions reduction are becoming important issues to be dealt with. Coal as the most used solid fossil fuel in industry and power generating sector, is being partially substituted by alternative solid fuels like biomass and solid recovered fuel worldwide. Due to different combustion characteristics of these alternative solid fuels coal partial substitution continues to be a challenge to the scientific community and practicing engineers worldwide.

Investigations of various thermo-chemical reaction techniques, which can be used to reduce carbon dioxide emission, have become a major area of the current research. Computer modelling of the calcination process and alternative fuel combustion provides a valuable tool that can be used for the investigation and better understanding of particle kinetics and pollutant emissions from cement combustion systems.

The main objectives of this study were to:
- present the modelling approach for the calcination process, and for the combustion of pulverized coal, biomass, plastic, and solid recovered fuel;
- validate the modelling approach for the calcination process and for each combustion model;
- demonstrate the large scale application of the presented and validated models.

The numerical models for the calcination process and for the pulverised solid fuel combustion were implemented into a commercial CFD code AVL FIRE$^{®}$, taking into account the major effects that influence these processes. The numerical models were described in detail in order to accurately explain the thermo-chemical processes that govern the calcination and the combustion process.

For validation of the modelling approach, simple three dimensional geometries of drop tube furnaces were used for the simulations. From the results shown it can be concluded that the presented models are in a good agreement with the reported experimental measurements.

Validated models were used to simulate complex three dimensional geometries of three different industrial cement calciners. The results obtained by these simulations can be used for the better understanding of the thermo-chemical reaction occurring inside the calculated calciners, and their improvement, confirming the hypothesis of this work.

By using the presented combustion models for the evaluation of different co-combustion modes, time consuming and costly experimental studies can be avoided. Therefore it can be concluded that numerical simulations are a useful tool that can be used for studying and improvement of different co-combustion concepts in existing pulverized fuel combustion units. Furthermore, it should also be mentioned that the presented models can be used for the investigation of some practical engineering options. Such practical engineering investigations include for instance the investigation of:

- the temperature hot spots in near wall regions, in order to reduce the thermal load on the wall;
- the particle mixing phenomena, in order to increase the reaction rate of limestone thermal degradation;
- the length of different units, in order to ensure complete limestone decomposition and fuel oxidation;
- the complete combustion versus complete calcination, in order to reduce fuel consumption;
- the danger of erosion in high velocity regions close to the wall, in order to minimize the wall erosion effects;
- the influence of different thermal shares of different alternative fuels, in order to have a stable manufacturing process;
- the influence of various air streams of the process, in order to minimize the thermal loses;
- the concentration of NO, CO and other pollutants, in order to reduce the environmental impact of the manufacturing process.

The presented modelling approach however has some bottlenecks. One of these bottlenecks is the calculation time. Due to the very detailed approach, when it comes to the particle reactions, the large scale full 3D simulation of cement calciners can take from two weeks to a month, depending on the size of the calciner. Here it should also be mentioned that the reason for the long calculation time could partly be related to very small time scales of the chemical reactions involved, which therefore need a high temporal resolution. A promising

measure for speed-up of calculations here would be the tabulation of chemistry. Another bottleneck of the modelling approach is the mesh size of the cement calciner. This is related to the calculation time, and because of that coarser meshes needed to be used in order to obtain results with such long calculation time. Thus, the reduction of the calculation time is needed in order to speed up the calculations and to use high resolution grids. This will be done in future work.

For the presented coal and biomass combustion model, future work will involve the investigation of unknown amount and composition of pyrolysis gases from the various coals and biomasses. An optional solution will be to couple a commercial pyrolysis software tool, which depends on the temperature and on the composition of different coals / biomasses, with the presented model.

Further investigation of detailed models for the N-chemistry and also for the reaction schemes of hydrocarbons from pyrolysis could also be of interest.

Future work also includes the investigation of different aerodynamic characteristics, e.g. different drag forces acting on particles of different size and shape, and different particle heat-up rates, e.g. temperature profiles in particles of bigger size. The temperature profiles in solid fuel particles of bigger size and particle-particle collision model would be beneficial for simulations of grate fired furnaces, which is a technology extensively used in waste incinerators.

As for the calcination model, implementation of the sintering model is one point of future work, in order to simulate all the thermo-chemical reactions occurring in the rotary kiln, and not just the flame. The other point of future work regarding the calcination model can be investigation of limestone particles of bigger size. This would be beneficial for the simulation of the lime kilns that are used in paper and pulp industry.

5 LITERATURE

[1] Benhelal E, Zahedi G, Shamsaei E, Bahadori A. Global strategies and potentials to curb CO_2 emissions in cement industry. J Clean Prod 2013;51:142-161.

[2] Chen J, Yao H, Zhang L. A study on the calcination and sulphation behaviour of limestone during oxy-fuel combustion. Fuel 2012;102:386–395.

[3] Klemeš JJ, Varbanov PS, Pierucci S, Huisingh D. Minimising emissions and energy wastage by improved industrial processes and integration of renewable energy. J Clean Prod 2010;18:843-847.

[4] Huanpeng L, Wentie L, Jianxiang Z, Ding J, Xiujian Z, Huilin L. Numerical study of gas–solid flow in a precalciner using kinetic theory of granular flow. Chem Eng J 2004;102:151-160.

[5] Huang L, Lu J, Wang S, Hu Z. Numerical simulation of pollutant formation in precalciner. Can J Chem Eng 2005;83:675-684.

[6] Hillers M, Severin T, Görner K, Scherer V. Process optimization for a precalciner facility of the cement industry. VDI Berichte 2005;1888:553-558. (in German)

[7] Zheng J, Lu H, Sun X, He Y, Ding J, Wang S. Hydrodynamic modeling of gas-particle flows in D-D calciners. Ind Eng Chem Res 2005;44:3033-3041.

[8] Hu Z, Lu J, Huang L, Wang S. Numerical simulation study on gas–solid two-phase flow in pre-calciner. Commun Nonlinear Sci Numer Simul 2006;11:440-451.

[9] Huang L, Lu J, Xia F, Li W, Ren H. 3-D mathematical modeling of an in-line swirl-spray precalciner. Chem Eng Process 2006;45:204-213.

[10] Fidaros DK, Baxevanou CA, Dritselis CD, Vlachos NS. Numerical modelling of flow and transport processes in a calciner for cement production. Powder Techn 2007;171:81-95.

[11] Dou H, Chen Z, Huang J. Numerical study of the coupled flow field in a Double-spray calciner. Conference Proceedings - 2009 International Conference on Computer Modeling and Simulation, ICCMS 2009, art. no. 4797367, 119-123.

[12] Ha S, Li Y, Zhang H, Shi H-Y, Zhu C. Study on a separation technology for more efficient utilization of pulverized coals in cement plants. Fuel Process Techn 2010;91:1261-1266.

64

[13] Bluhm-Drenhaus T, Simsek E, Wirtz S, Scherer V. A coupled fluid dynamic-discrete element simulation of heat and mass transfer in a lime shaft kiln. Chem Eng Sci 2010;65:2821-2834

[14] Nance G, Abbas T, Lowes T, Bretz J. Calciner design for lower CO and NOx using MI-CFD analysis to optimize "Hot-Reburn" conditions. IEEE Cement Industry Technical Conference 2011. art. no. 5934552.

[15] Jianxiang Z, Tingzhi Y, Jing Y. Numerical simulation of gas and solid flow behaviour in the pre-calciner with large eddy simulation approach. Energy Procedia 2012;17:1535-1541.

[16] Dukowicz JK. A particle-fluid numerical model for liquid sprays. J Comp Physics 1980;35:229-253.

[17] FIRE v2014 Manuals, 2014, Graz, Austria

[18] IPCC, 2013: Climate Change 2013: The Physical Science Basis. Contribution of Working Group I to the Fifth Assessment Report of the Intergovernmental Panel on Climate Change [Stocker, T.F., D. Qin, G.-K. Plattner, M. Tignor, S.K. Allen, J. Boschung, A. Nauels, Y. Xia, V. Bex and P.M. Midgley (eds.)]. Cambridge University Press, Cambridge, United Kingdom and New York, NY, USA, p. 1535

[19] IPCC Press Release, 2014/19/PR, 2014. http://www.ipcc.ch/pdf/ar5/pr_wg3/20140413_pr_pc_wg3_en.pdf, accessed February 24, 2015.

[20] Klemeš JJ, Varbanov PS, Huisingh D. Recent cleaner production advances in process monitoring and optimization. J Clean Prod 2012;34:1–8.

[21] Marques M, Neves-Silva R. Decision support for energy savings and emissions trading in industry. J Clean Prod 2015;88:105-115.

[22] Usón AA, López-Sabirón AM, Ferreira G, Sastresa EL. Uses of alternative fuels and raw materials in the cement industry as sustainable waste management options. Renew Sustain Energy Rev 2013;23:242-260.

[23] IEA (International Energy Agency) Cement Technology Roadmap 2009: Carbon emissions reductions up to 2050. http://www.iea.org/publications/freepublications/publication/Cement_Roadmap.pdf, accessed February 24, 2015.

[24] Pardo N, Moya JA, Mercier A. Prospective on the energy efficiency and CO_2 emissions in the EU cement industry. Energy 2011;36:3244–3254.

[25] Moya JA, Pardo N, Mercier A. The potential for improvements in energy efficiency and CO_2 emissions in the EU27 cement industry and the relationship with the capital budgeting decision criteria. J Clean Prod 2011;19:1207–1215.

[26] Xu T, Galama T, Sathaye J. Reducing carbon footprint in cement material making: Characterizing costs of conserved energy and reduced carbon emissions. Sustain Cities Soc 2013;9:54-61.

[27] Li C, Nie Z, Cui S, Gong X, Wang Z, Meng X. The life cycle inventory study of cement manufacture in China. J Clean Prod 2014;72:204-211.

[28] Wang Y, Höller S, Viebahn P, Hao Z. Integrated assessment of CO_2 reduction technologies in China's cement industry. Int J Greenh Gas Control 2014;20:27-36.

[29] Xu J-H, Fleiter T, Fan Y, Eichhammer W. CO_2 emissions reduction potential in China's cement industry compared to IEA's Cement Technology Roadmap up to 2050. Appl Energy 2014;130:592–602.

[30] Swanepoel JA, Mathews EH, Vosloo J, Liebenberg L. Integrated energy optimisation for the cement industry: A case study perspective. Energy Convers Manag 2014;78:765-775.

[31] Ekincioglu O, Gurgun AP, Engin Y, Tarhan M, Kumbaracibasi S. Approaches for sustainable cement production – A case study from Turkey. Energy Build 2013;66:136-142.

[32] Ostad-Ahmad-Ghorabi MJ, Attari M. Advancing environmental evaluation in cement industry in Iran. J Clean Prod 2013;41:23-30.

[33] Morrow WR, Hasanbeigi A, Sathaye J, Xu T. Assessment of energy efficiency improvement and CO_2 emission reduction potentials in India's cement and iron & steel industries. J Clean Prod 2014;65-131-141.

[34] Hasanbeigi A, Menke C, Price L. The CO_2 abatement cost curve for the Thailand cement industry. J Clean Prod 2010;18:1509-1518.

[35] Nguyen QA, Hens L. Environmental performance of the cement industry in Vietnam: the influence of ISO 14001 certification. J Clean Prod 2015;96:362–378.

[36] Oh D-Y, Noguchi T, Kitagaki R, Park W-J. CO_2 emission reduction by reuse of building material waste in the Japanese cement industry. Renew Sustain Energy Rev 2014;38:796–810.

[37] Brunke J-C, Blesl M. Energy conservation measures for the German cement industry and their ability to compensate for rising energy-related production costs. J Clean Prod 2014;82:94-111.

[38] Worrell E, Galitsky C. 2008. Energy Efficiency Improvement and Cost Saving Opportunities for Cement Making, An ENERGY STAR[®] Guide for Energy and Plant Managers. Lawrence Berkeley National Laboratory: Berkeley, CA (LBNL-54036-Revision).

[39] Chen W, Hong J, Xu C. 2014. Pollutants generated by cement production in China, their impacts, and the potential for environmental improvement. J Clean Prod doi: 10.1016/j.jclepro.2014.04.048

[40] Wang Y, Zhu Q, Geng Y. Trajectory and driving factors for GHG emissions in the Chinese cement industry. J Clean Prod 2013;53:252-260.

[41] Mikulčić H, Vujanović M, Ashhab MS, Duić N. Large eddy simulation of a two-phase reacting swirl flow inside a cement cyclone. Energy 2014;75:89-96.

[42] Szabó L, Hidalgo I, Ciscar JC, Soria A. CO_2 emission trading within the Europian Union and Annex B coutries: the cement industry case. Energy Policy 2006;34:72-87.

[43] Mikulčić H, Vujanović M, Fidaros DK, Priesching P, Minić I, Tatschl R, Duić N, Stefanović G. The application of CFD modelling to support the reduction of CO_2 emissions in cement industry. Energy 2012;45:464-473.

[44] Methodology for the free allocation of emission allowances in the EU ETS post 2012. Sector report for the cement industry. http://ec.europa.eu/clima/policies/ets/cap/allocation/docs/bm_study-cement_en.pdf, accessed February 24, 2015.

[45] Wang G, Silva RB, Azevedo JLT, Martins-Dias S, Costa M. Evaluation of the combustion behaviour and ash characteristics of biomass waste derived fuels, pine and coal in a drop tube furnace. Fuel 2014;117:809–824.

[46] Lu H, Robert W, Peirce G, Ripa B, Baxter LL. Comprehensive study of biomass particle combustion. Energy Fuels 2008;22:2826–2839.

[47] Ariyaratne WKH, Melaaen MC, Tokheim L-A. Determination of biomass fraction for partly renewable solid fuels. Energy 2014;70:465-472.

[48] Mikulčić H, Vujanović M, Markovska N, Filkoski RV, Ban M, Duić. CO_2 emission reduction in the cement industry. Chem Eng Trans 2013;35:703-708.

[49] IEA - Tracking Clean Energy Progress 2015 http://www.iea.org/publications/freepublications/publication/Tracking_Clean_Energy_Progress_2015.pdf, accessed February 24, 2015.

[50] Wagland ST, Kilgallon P, Coveney R, Garg A, Smith R, Longhurst PJ, Pollard SJT, Simms N. Comparison of coal/solid recovered fuel (SRF) with coal/refuse derived fuel (RDF) in a fuidised bed reactor. Waste Manag 2011;31:1176-1183.

[51] Talebi G, Van Goethem M. Synthesis gas from waste plasma gasification for fueling lime kiln. Chem Eng Trans 2014;37:619-624.

[52] Al-Salem SM, Lettieri P, Baeyens J. The valorization of plastic solid waste (PSW) by primary to quaternary routes: From re-use to energy and chemicals. Prog Energy Combust Sci 2010;36:103-129.

[53] Zhou H, Long YQ, Meng AH, Li QH, Zhang YG. Classification of municipal solid waste components for thermal conversion in waste-to-energy research. Fuel 2015;145:151–157.

[54] Najjar YSH, Waite D. 2014. Energy conservation and waste utilization in the cement industry serve the green technology and environment. Int J Sustain Eng doi:10.1080/19397038.2014.991775

[55] Wang X, Tan H, Niu Y, Pourkashanian M, Ma L, Chen E, Liu Y, Liu Z, Xu T. 2011. Experimental investigation on biomass co-firing in a 300 MW pulverized coal-fired utility furnace in China. Proc 33th Int Symposium Combust., The Combustion Institute, 2725–2733.

[56] Wu H, Glarborg P, Frandsen FJ, Dam-Johansen K, Jensen PA, Sander B. Co-combustion of pulverized coal and solid recovered fuel in an entrained flow reactor – General combustion and ash behaviour. Fuel 2011;90:1980-1991.

[57] Ma L, Gharebaghi M, Porter R, Pourkashanian M, Jones JM, Williams A. Modelling methods for co-fired pulverised fuel furnaces. Fuel 2009;88:2448-2454.

[58] Silcox GD, Kramlich JC, Pershing DW. A mathematical model for the flash calcination of dispersed $CaCO_3$ and $Ca(OH)_2$ particles. Ind Eng Chem Res 1989;28:155-160.

[59] Stanmore BR, Gilot P. Review - calcination and carbonation of limestone during thermal cycling for CO_2 sequestration. Fuel Process Techn 2005;86:1707-1743.

[60] Schneider M. 2003. Experimentelle und mathematische Modellierung der Festbettvergasung am Beispiel der Gleichstromvergasung von Holzhackschnitzeln. PhD-Thesis TU Dresden, Germany

[61] Kern C, Jess A. Verkokung and Koksabbrand in heterogenen Katalysatoren. Chemie Ingenieur Technik 2006: 78, No.8.

[62] Reid RC, Prausnitz JM, Polling BE. 1988. The Properties of Gases and Liquids, fourth ed. McGraw-Hill Book Company, New York, p.582

[63] Levenspiel O. 1972. Chemical Reaction Engineering, second ed. J. Wiley and Sons, New York, p.482

[64] Froment G, Bischoff K. 1990. Chemical Reactor Analysis and Design, second ed. J. Wiley and Sons, New York, p.160

[65] Lee H, Choi S. An observation of combustion behavior of a single coal particle entrained into hot gas flow. Combust Flame 2015;162:2610–2620.

[66] Williams A, Jones JM, Ma L, Pourkashanian M. Pollutants from the combustion of solid biomass fuels. Prog Energy Combust Sci 2012;38:113-137.

[67] Yang YB, Sharifi VN, Swithenbank J, Ma L, Darvell LI, Jones JM, Pourkashanian M, Williams A. Combustion of a single particle of biomass. Energy Fuel 2008;22:306-316.

[68] Hayhurst AN. The kinetics of the pyrolysis or devolatilisation of sewage sludge and other solid fuels. Combust Flame 2013;160:138–144.

[69] Ma L, Jones JM, Pourkashanian M, Williams A. Modelling the combustion of pulverized biomass in an industrial combustion test furnace. Fuel 2007;86:1959-1965.

[70] Ranz WE, Marshall WR Jr. Evaporation from drops, Part I. Chem Eng Prog 1952;48:141–146.

[71] Ranz WE, Marshall WR Jr. Evaporation from drops, Part II. Chem Eng Prog 1951;48:173–180.

[72] Toporov D, Bocian P, Heil P, Kellermann A, Stadler H, Tschunko S, Förster M, Kneer R. Detailed investigation of a pulverized fuel swirl flame in CO_2/O_2 atmosphere. Combust Flame 2008;155:605–618.

[73] Wang G, Zander R, Costa M. Oxy-fuel combustion characteristics of pulverized-coal in a drop tube furnace. Fuel 2014;101:452-460.

[74] Wang G, Silva RB, Azevedo JLT, Martins-Dias S, Costa M. Evaluation of the combustion behaviour and ash characteristics of biomass waste derived fuels, pine and coal in a drop tube furnace. Fuel 2014;117:809-824.

[75] Singer SL, Ghoniem AF. Comprehensive gasification modeling of char particles with multi-modal pore structures. Combust Flame 2013;160:120–137.

[76] Görner K. Technical combustion systems: fundamentals, modelling, simulation, Berlin, Heidelberg, Springer-Verlag, 1991, p. 180-194.

[77] Arthur JA. Reactions between carbon and oxygen. Trans Faraday Soc 1951;47:164-178.

[78] Baum MM, Street PJ. Predicting the combustion behaviour of coal particles. Combust Sci Techn 1971;3:231–243.

[79] Jones WP, Lindstedt RP. Global reaction scheme for hydrocarbon combustion. Combust Flame 1988;73:233-249.

[80] Molina A, Murphy JJ, Winter F, Haynes BS, Blevins LG, Shaddix CR. Pathways for conversion of char nitrogen to nitric oxide during pulverized coal combustion. Combust Flame 2009;156:574-587.

[81] De Soete GG. 1975. Overall reaction rates of NO and N_2 formation from fuel nitrogen. Proc 15th Int Symposium Combust., The Combustion Institute, 1093-1102.

[82] Peterson JD, Vyazovkin S, Wight CA. Kinetics of the thermal and thermo-oxidative degradation of polystyrene, polyethylene and poly(propylene). Macromol Chem Phys 2001;202:775-784.

[83] Al-Salem SM, Lettieri P, Baeyens J. The valorization of plastic solid waste (PSW) by primary to quaternary routes: From re-use to energy and chemicals. Prog Energy Combust Sci 2010;36:103-129.

[84] Deeg C, Schneider M, Schnell U, Scheffknecht G. A method for modelling the co-combustion of solid recovered fuels in pulverised fuel power plants, VDI-Berichte 2007;1988:345-354.

[85] Agraniotis M, Nikolopoulos N, Nikolopoulos A, Grammelis P, Kakaras E. Numerical investigation of solid recovered fuels' co-firing with brown coal in large scale boilers – evaluation of different co-combustion modes. Fuel 2010;89:3693–3709.

[86] Gersten J, Fainberg V, Hetsroni G, Shindler Y. Kinetic study of the thermal decomposition of polypropylene, oil shale, and their mixture. Fuel 2000;79:1679-1686.

[87] Westerhout RWJ, Waanders J, Kuipers JAM, van Swaaij WPM. Kinetics of the low-temperature pyrolysis of polyethene, polypropene, and polystyrene modelling, experimental determination, and comparison with literature models and data. Ind Eng Chem Res 1997;36:1955-1964.

[88] Westbrook CK, Dryer FL. Simplified reaction mechanisms for the oxidation of hydrocarbon fuels in flames. Comb Sci Techn 1981;27:31-43.

[89] Garg A, Smith R, Hill D, Longhurst PJ, Pollard SJT, Simms, NJ.An integrated appraisal of energy recovery options in the United Kingdom using solid recovered fuel derived from municipal solid waste Waste Manag 2009;29:1189-1197.

[90] Ariyaratne WKH, Asgautsen Ø, Melaaen MC, Eine K, Tokheim L.-A. Determination of fossil fraction of refuse derived fuel by the selective dissolution method in calorific value basis: Development of simplified method. Fuel 2012;98:41-47.

[91] Dunnu G, Panopoulos KD, Karellas S, Maier J, Touliou S, Koufodimos G, Boukis I, Kakaras E. The solid recovered fuel Stabilat®: Charracteristics and fluidised bed gasification tests. Fuel 2012;93:273-283.

[92] Mohr M. 2001. Numerische Simulation der simultanen Reaktion von Kalkstein und Kohle bei der Zementherstellung. PhD-Thesis, University of Ruhr, Bochum, Germany.

[93] Hilber T. 2008. UPSWING: an advanced waste treatment concept compared to the state-of-the-art, PhD-Thesis, University of Stuttgart, Stuttgart, Germany.

6 CURRICULUM VITAE

HRVOJE MIKULČIĆ mag.ing.mech. was born on the 8th of April 1985 in Zagreb, Croatia. In 2004 he finished High School "XV. Gimnazija" in Zagreb and started his studies on the Faculty of Mechanical Engineering and Naval Architecture (FMENA), University of Zagreb. He finished the undergraduate studies in mechanical engineering in 2008, and the same year started with the graduate studies in mechanical engineering, which he finished with honours – FMENA Medal in 2009. From 2009 he has been employed at the Faculty of Mechanical Engineering and Naval Architecture, University of Zagreb, at the Department of Power Engineering, Energy and Environment as research assistant and PhD student. He has been working on the research project "Numerical modelling of multiphase flow and combustion processes" financed by the Austrian Institute for internal combustion engines AVL List GmbH.

Since 2009 he has also been working on the national scientific project: Smart energy storage for sustainable development of energy systems, financed by the Ministry of Science, Education and Sport of the Republic of Croatia.

He is member of the Adria Section of Combustion Institute, of the International Centre for Sustainable Development of Energy, Water and Environment Systems (SDEWES Centre), and of the European Research Community on Flow, Turbulence and Combustion.

He is an author of 24 scientific papers, of which 10 in scientific journals (CC/SCI). His current Scopus *h*-index is 5. He serves as a Reviewer for Applied Energy, Energy Conversion and Management, Journal of Cleaner Production, International Journal of Heat and Mass Transfer, International Journal of Food Engineering and JSDEWES journals. He has been awarded Recognized Reviewer Status by Elsevier. Since 2011 he has been involved in the organization of SDEWES conferences and from 2012 he serves as a PR officer of the International Centre for Sustainable development of Energy, Water and Environment Systems.

List of published scientific journal papers:

- Mikulčić H, Vujanović M, Duić N. *Improving the Sustainability of Cement Production by Using Numerical Simulation of Limestone Thermal Degradation and Pulverized*

Coal Combustion in a Cement Calciner. Journal of Cleaner Production 2015;88:262-271.

- Wang X, Xu Z, Wei B, Zhang L, Tan H, Yang T, Mikulčić H, Duić N. *The Ash Deposition Mechanism in Boilers Burning Zhundong Coal with High Contents of Sodium and Calcium: a Study from Ash Evaporating to Condensing.* Applied Thermal Engineering. 2015;80:150-159.

- Mikulčić H, von Berg E, Vujanović M, Duić N. *Numerical Study of Co-firing Pulverized Coal and Biomass inside a Cement Calciner.* Waste Management & Research 2014;32:661-669.

- Mikulčić H, Vujanović M, Ashhab MS, Duić N. *Large Eddy Simulation of a Two-Phase Reacting Swirl Flow inside a Cement Cyclone.* Energy 2014;75:89-96.

- Mikulčić H, Vujanović M, Markovska N, Filkoski, RV, Ban M, Duić N. *CO_2 Emission Reduction in the Cement Industry.* Chemical Engineering Transactions 2013;35:703-708.

- Mikulčić H, von Berg E, Vujanović M, Priesching P, Tatschl R, Duić N. *Numerical analysis of cement calciner fuel efficiency and pollutant emissions.* Clean Technologies and Environmental Policy 2013;15:489–499.

- Mikulčić H, Vujanović M, Duić N. *Reducing the CO_2 emissions in Croatian cement industry.* Applied Energy 2013;101:41-48.

- Mikulčić H, von Berg E, Vujanović M, Priesching P, Tatschl R, Duić N. *CFD analysis of a cement calciner for a cleaner cement production.* Chemical Engineering Transactions 2012;29:1513-1518.

- Mikulčić H, Vujanović M, Fidaros DK, Priesching P, Minić I, Tatschl R, Duić N, Stefanović G. *The application of CFD modelling to support the reduction of CO_2 emissions in cement industry.* Energy 2012;45:464-473.

- Mikulčić H, von Berg E, Vujanović M, Priesching P, Perković L, Tatschl R, Duić N. *Numerical Modelling of Calcination Reaction Mechanism for Cement Production.* Chemical Engineering Science 2012;69:607-15.

7 SUMMARY OF PAPERS

PAPER 1

Mikulčić H, von Berg E, Vujanović M, Priesching P, Perković L, Tatschl R, Duić N. *Numerical modelling of calcination reaction mechanism for cement production.* Chem Eng Sci 2012;69:607-615.

Calcination is a thermo-chemical process, widely used in the cement industry, where limestone is converted by thermal decomposition into lime CaO and carbon dioxide CO2. The focus of this paper is on the implementation and validation of the endothermic calcination reaction mechanism of limestone in a commercial finite volume based CFD code. This code is used to simulate the turbulent flow field, the temperature field, concentrations of the reactants and products, as well as the interaction of particles with the gas phase, by solving the mathematical equations which govern these processes. For calcination, the effects of temperature, decomposition pressure, diffusion, and pore efficiency were taken into account. A simple three dimensional geometry of a pipe reactor was used for numerical simulations. To verify the accuracy of the modelling approach, the numerical predictions were compared with experimental data, yielding satisfying results and proper trends of physical parameters influencing the process.

In this paper the simulations were performed by Mikulčić. Von Berg, Priesching and Tatschl set up the framework in AVL FIRE[®] for solid particle reactions, and Perković set up the framework for the particle radiation model. The paper was written by Mikulčić and reviewed by von Berg, Vujanović and Duić.

PAPER 2

Mikulčić H, Vujanović M, Fidaros DK, Priesching P, Minić I, Tatschl R, Duić N, Stefanović G. *The application of CFD modelling to support the reduction of CO_2 emissions in cement industry.* Energy 2012;45:464-473.

The cement industry is one of the leading producers of anthropogenic greenhouse gases, of which CO_2 is the most significant. Recently, researchers have invested a considerable amount of time studying ways to improve energy consumption and pollutant formation in the overall cement manufacturing process. One idea involves dividing the calcination and clinkering processes into two separate furnaces. The calcination process is performed in a calciner while the clinkering process takes place in a rotary kiln. As this is new technology in the cement manufacturing process, calciners are still in the research and development phase. The purpose of this paper is to demonstrate the potential of CFD to support the design and optimization of calciners, whose use appears to be essential in reduction of CO_2 emission during cement production. The mathematical model of the calcination process was developed, validated and implemented into a commercial CFD code, which was then used for the analysis. From the results obtained by these simulations, researchers will gain an in-depth understanding of all thermo-chemical reactions in a calciner. This understanding can be used to optimize the calciner's geometry, to make production more efficient, to lower pollutant formation and to subsequently reduce greenhouse gas emissions.

In this paper the simulations were performed by Mikulčić. Fidaros provided the geometry detailes and calciner operating conditions. Priesching and Tatschl set up the framework in AVL FIRE® for solid particle reactions. Minić explained the cement production process. The paper was written by Mikulčić and reviewed by Vujanović, Duić and Stefanović.

PAPER 3

Mikulčić H, Vujanović M, Duić N. *Reducing the CO_2 emissions in Croatian cement industry.* Appl Energy 2013;101:41-48.

Cement industry is one of the largest carbon emitting industrial sectors. It is responsible for about 5% of anthropogenic CO_2 in the world. Therefore, it is a relevant industrial sector for CO_2 emission regulation strategies. Bearing in mind the importance of cement industry in Croatia, and because of the fact that Croatia will soon become an EU member state, the present paper analyses the potential to reduce CO_2 emission in the Croatian cement industry. There are several measures that can reduce CO_2 emissions from the cement manufacturing process: the use of waste heat as an alternative source of energy; CO_2 capture and storage

technologies; reduction of clinker to cement ratio; the use of alternative and biomass fuels; the use of alternative raw materials; an energy efficient combustion process. The most energy efficient technology for cement manufacturing today is the use of a rotary kiln together with a multi-stage preheater and a calciner. Since the use of cement calciners is a relatively new technology, further improvement of their operating conditions is still needed. This paper also highlights the results of research in the field of computational fluid dynamic (CFD) simulations that are used for the investigation of process and combustion emissions. The above mentioned measures together with numerical investigations can reduce the effect of cement manufacturing in Croatia on the environment and can make it more competitive with cement manufacturers from the EU.

In this paper the simulations were performed by Mikulčić, Vujanović collected the data about the cement industry in Croatia and calculated the CO_2 emissions. The paper was written by Mikulčić and reviewed by Vujanović and Duić.

PAPER 4

Mikulčić H, von Berg E, Vujanović M, Priesching P, Tatschl R, Duić N. *Numerical analysis of cement calciner fuel efficiency and pollutant emissions.* Clean Techn Environ Policy 2013;15:489–499.

Efficient mixing of pulverized fuel and limestone particles inside cement calciners is important due to the reason that the calcination process directly affects the final fuel consumption. The focus of this paper is on the numerical analysis of cement calciner's operating conditions and pollutant emissions. The paper analyzes the influence of different amounts of fuel, mass flow of the tertiary air and the adiabatic wall condition on the decomposition rate of limestone particles, burnout rate of coal particles, and pollutant emissions of a newly designed cement calciner. Numerical models of calcination process and pulverized coal combustion were developed and implemented into a commercial computational fluid dynamics code, which was then used for the analysis. This code was used to simulate turbulent flow field, interaction of particles with the gas phase, temperature field, and concentrations of the reactants and products, by solving the set of conservation equations for mass, momentum and enthalpy that govern these processes. A three dimensional geometry

of a real industrial cement calciner was used for numerical simulations. The results gained by these numerical simulations can be used for the optimization of cement calciner's operating conditions, and for the reducing of its pollutant emissions.

In this paper the simulations were performed by Mikulčić, Vujanović calculated the different operating conditions, and von Berg and Priesching set up the framework in AVL FIRE® used for the analysis the obtained results. The paper was written by Mikulčić and reviewed by von Berg, Tatschl and Duić.

PAPER 5

Mikulčić H, von Berg E, Vujanović M, Duić N. Numerical study of co-firing pulverized coal and biomass inside a cement calciner. Waste Manag Res 2014;32:661-669.

The use of waste wood biomass as fuel is increasingly gaining significance in cement industry. Combustion of biomass and particularly co-firing of biomass and coal in existing pulverized-fuel burners still faces significant challenges. A possibility for the ex-ante control and investigation of the co-firing process are Computational Fluid Dynamics - CFD simulations. The purpose of this paper is to present a numerical analysis of co-firing pulverized coal and biomass in a cement calciner. Numerical models of pulverized coal and biomass combustion were developed and implemented into a commercial computational fluid dynamics code FIRE, which was then used for the analysis. A three dimensional geometry of a real industrial cement calciner was used for the analysis. Three different co-firing cases were analysed. The results obtained from this study can be used for assessing different co-firing cases, and for improving the understanding of the co-firing process inside the calculated calciner.

In this paper the simulations were performed by Mikulčić, Vujanović calculated the operating conditions for different fuel substitution rates. The paper was written by Mikulčić and reviewed by von Berg and Duić.

PAPER 6

Mikulčić H, Vujanović M, Duić N. *Improving the Sustainability of Cement Production by Using Numerical Simulation of Limestone Thermal Degradation and Pulverized Coal Combustion in a Cement Calciner.* J Clean Prod 2015;88:262-271.

The cement industry sector is one of the largest carbon emitting industrial sectors, and due to the effect of global warming sustainable cement production is increasingly gaining on importance. Controlling the combustion of coal and the thermal degradation of limestone, the two main thermo-chemical processes that occur inside a cement calciner, is of significant importance, since these processes have a direct influence on the cement quality, pollutant formation and overall energy efficiency of the cement manufacturing process. One of the possibilities for the improvement and control of these thermo-chemical processes are Computational Fluid Dynamics - CFD simulations. The results gained from these simulations are being increasingly used to enhance the efficiency of cement production, since they improve the understanding of the flow characteristics and transport phenomena taking place inside the cement calciner. The purpose of this paper is to present that a more energy efficient and sustainable cement production can be achieved by deploying CFD simulations in the process of cement production. The numerical models of limestone thermal degradation, also known as the calcination process, and pulverized coal combustion were developed and implemented within the commercial computational fluid dynamics code FIRE, which was then used for the analysis. The developed models are based on the solution of Navier-Stokes equations for the gas phase, and on the Lagrangean dynamics for the discrete particles. A three dimensional complex geometry of a real industrial cement calciner was used for the CFD simulation. The information obtained from this numerical simulation, such as the distribution of particles, distribution of temperatures and the concentrations can be used for better understanding of particle kinetics and pollutant emissions from the given cement calciner and also for its further investigation and optimization.

In this paper the simulations were performed by Mikulčić, Vujanović obtained the geometry, the operating conditions and the measurement data. The paper was written by Mikulčić and reviewed by Vujanović and Duić.

PAPER 1
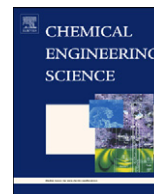
Numerical modelling of calcination reaction mechanism for cement production

Hrvoje Mikulčić [a,*], Eberhard von Berg [b], Milan Vujanović [a], Peter Priesching [b], Luka Perković [a], Reinhard Tatschl [b], Neven Duić [a]

[a] Faculty of Mechanical Engineering and Naval Architecture, University of Zagreb, Ivana Lučića 5, 10000 Zagreb, Croatia
[b] AVL-AST, Hans List Platz 1, Graz, Austria

ARTICLE INFO

ABSTRACT

Calcination is a thermo-chemical process, widely used in the cement industry, where limestone is converted by thermal decomposition into lime CaO and carbon dioxide CO_2. The focus of this paper is on the implementation and validation of the endothermic calcination reaction mechanism of limestone in a commercial finite volume based CFD code. This code is used to simulate the turbulent flow field, the temperature field, concentrations of the reactants and products, as well as the interaction of particles with the gas phase, by solving the mathematical equations, which govern these processes. For calcination, the effects of temperature, decomposition pressure, diffusion and pore efficiency were taken into account. A simple three-dimensional geometry of a pipe reactor was used for numerical simulations. To verify the accuracy of the modelling approach, the numerical predictions were compared with experimental data, yielding satisfying results and proper trends of physical parameters influencing the process.

1. Introduction

During the cement manufacturing process, large amounts of carbon dioxide are emitted. There are two processes from which carbon dioxide is produced. One of the processes is the combustion of the fossil fuel and the other is the calcination reaction. Because of the effect of global warming and particularly because carbon dioxide is one of the primary greenhouse gases, in-depth understanding of these processes is relevant for the development of effective cement production and reduction of carbon dioxide emission.

Calcination is a strongly endothermic process where limestone (calcium carbonate) $CaCO_3$ is converted by thermal decomposition into lime (calcium oxide) CaO and carbon dioxide CO_2. The process of calcination (thermal decomposition of a limestone particle) in a cement calciner can be divided into three stages (Bes, 2006): (a) heat energy transported by calciner gases (i.e. combustion products and exhaust gases from the rotary kiln) supplied to the limestone particle by convection and radiation, pre-heats the particle from the ambient temperature to the decomposition temperature. The decomposition temperature reported in the literature (Stanmore and Gilot, 2005) is in the temperature range from 600 °C to 900 °C, depending on the type of limestone; (b) at the decomposition temperature, when the pressure of carbon dioxide produced by the decomposition of limestone at the particle surface is greater than the partial pressure of carbon dioxide in the surrounding gas, the process of calcination begins, making a lime shell around the limestone core; (c) by conduction the heat passes through the porous layer increasing the internal temperature, which causes continued calcination. The released carbon dioxide diffuses through the porous layer to the surface and by convection is released into the calciner. As long as the particle temperature increases and the partial pressure of CO_2 is below the decomposition pressure, the process of calcination will continue until all the limestone is converted into lime.

The calcination process that takes place in a calciner for cement production is of particular importance because it affects energy consumption and pollutant emissions. A calciner is a separate furnace used prior to the rotary cement kiln, where the limestone, pulverised coal and rotary kiln exhaust gases are mixed. Thus, an in-depth understanding of the physical and chemical processes in the calciner is relevant for the development of effective cement production.

Recently, because of the increased reductions in carbon dioxide emissions as well as reductions of other pollutant emissions

(Vujanović et al., 2007), different types of calciners with different operating conditions have been studied. Fidaros et al. (2007) presented a numerical model and a parametric study of the gaseous flow and the transport phenomena that take place in a vertical industrial low NO_x calciner, showing good prediction capabilities of velocity, temperature and distribution of particles. Iliuta et al. (2002b) developed a mathematical model for an in-line low-NO_x calciner based on reaction-diffusion approach for calcination and combustion. Also Iliuta et al. (2002a) reported the effect of different operating conditions in an in-line low-NO_x calciner in their parametric study, showing that the influence of different operating conditions has an impact on the level of calcination, burn-out and NO emission. Hu et al. (2006) used a three-dimensional Eulerian–Lagrangean model to simulate a dual combustor and precalciner to predict the burn-out rate of coal and the decomposition rate of limestone. Huang et al. (2006) carried out a three-dimensional simulation of an in-line swirl-spray precalciner with a new method for particle-wall boundary condition and with a four-mixture-fraction model to describe the multi-component mutual transportation in a precalciner. Huanpeng et al. (2004) used a two-dimensional model to study the impact of various parameters on the dynamics of the two-phase flow in a precalciner, representing the transport properties of the solid phase with the kinetic theory of granular flow. All of these studies show that there is a great potential in research and the development of calciners, especially regarding the thermo-chemical reactions that take place in the calciner, e.g. calcination, combustion and pollutant formation. Although there have been numerous studies about the calcination reaction mechanism, the basis of current calcination mathematical models was completed during the mid-1980's. Borgwart (1985) investigated the calcination kinetics and demonstrated that heat and mass transfer in a particle determines the reaction rate. He also reported that the maximum calcination reaction rate is achieved when the limestone particle size is minimised, because the mass transport of CO_2 through the product layer has a lesser influence on the rate of decomposition. His results provided useful data for the rates of limestone decomposition. Dennis and Hayhurst (1987) ran a series of experiments in a fluidized bed, and by changing the gas pressure and temperature found the influence of CO_2 partial pressure on the rate of calcination. Campbell et al. (1970) and Hills (1968) found that the decomposition of limestone is controlled by the mass transfer through the product layer and by the heat transfer. Ingraham and Marier (1963) found that the decomposition rate depends linearly on the difference between the equilibrium pressure of the calcination process and the CO_2 pressure at the reaction surface. Darroudi and Searcy (1981) found that at CO_2 partial pressures below 0.01 bar the rate is practically independent, whereas at higher pressure values a linear dependency was found. Silcox et al. (1989) used the experimental data produced by Borgwardt to develop a mathematical model of the calcination of limestone. Hu and Scaroni (1996) investigated the influence of particle size on the rate of calcination and found that for particles bigger than 20 μm and gas flow temperatures above 1473 K heat transfer and pore diffusion are the rate-controlling factors. For particles smaller than 10 μm and gas flow temperatures below than 1073 K they found that chemical kinetics are the rate-controlling factors. Most of the authors (Garcia-Labiano et al., 2002; Hu and Scaroni, 1996; Khinast et al., 1996) consider the mass transfer of CO_2 from the reaction interface through the porous lime layer to the surface of the particle and the chemical reaction as the rate-controlling factors. Garcia-Labiano et al. (2002), along with their experiment, demonstrated different behaviours of different types of limestone during the calcination process. As a result of this finding they stated that the appropriate mathematical model for calcination, the shrinking core or the changing grain size model, must be used to

appropriately define the reaction rate parameters of the particular type of limestone. A study by Mohr (2001) describes in detail the mathematical model of the calcination process, showing the impact of various parameters on the rate of calcination. Following Mohr's study, Hillers (2008) investigated the influence of numerical turbulence models on the calcination results using the same calcination model.

The purpose of this paper is to present a numerical model of the calcination process implemented into a commercial CFD code that is detailed enough to contain the relevant physical and chemical processes e.g., Arrhenius rate approach, pressure limitation, diffusion resistance, porosity, tortuosity, pore size and pore efficiency. The latter features are treated with parameters understood as averages over the grain topology and size. Thus this procedure avoids uncertain additional assumptions needed for more detailed sub-models, but is still sufficiently accurate and simple enough to run on meshes of appropriate size and resolution as it is needed for detailed CFD simulations of realistic industrial calcination devices. This balance is regarded as characteristic feature of the approach presented. To verify the accuracy of the modelling approach, the numerical predictions were compared with the experimental data that are given in the literature (Mohr, 2001).

2. Numerical model

2.1. Continuous phase

The fundamental equations of continuum mechanics are based on the conservation laws for mass, momentum and energy. The general form of the time averaged conservation equation for any dependent variable φ of the continuous phase in the differential form is

$$\frac{\partial}{\partial t}(\rho\varphi) + \frac{\partial}{\partial x_j}(\rho\varphi u_j) = \frac{\partial}{\partial x_j}\left(\Gamma_\varphi \frac{\partial \varphi}{\partial x_j}\right) + S_\varphi, \tag{1}$$

where ρ is the density, u_j Cartesian velocity, Γ_φ diffusion coefficient and S_φ is the source term of the dependent variable φ.

2.2. Calcination reaction mechanism

In the CFD-code used in this study, the motion and transport of the solid particles are tracked through the flow field using the Lagrangian formulation, while the gas phase is described by solving conservation equations using the Eulerian formulation. Solid particles are discretized into finite numbers of particle groups, known as parcels, which are assumed to have same size and also the same physical properties. The parcels are tracked as they move through the calculated flow field using a set of equations that describe their dynamics. The coupling between the parcels and the gaseous phase is taken into account by introducing appropriate source terms for mass, momentum and enthalpy exchange (Vujanović, 2010).

The mathematical model used for the calcination calculation is treated in the Lagrangian spray module, where thermo-chemical reactions occur inside a particle as well as between particle components and gas phase species. The described calcination model was integrated into the commercial CFD code FIRE, using FIRE's user-defined functions capability. User functions, written in FORTRAN programming language, were linked with the AVL's FIRE code (Baburić et al., 2004, 2005; Vujanović et al., 2009), providing prediction of calcination process on one hand and retaining all the usual FIRE features on the other. In general the

calcination process can be presented by the following equation:
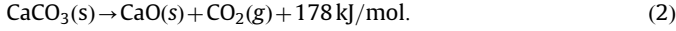
$$CaCO_3(s) \rightarrow CaO(s) + CO_2(g) + 178 \, kJ/mol. \tag{2}$$

In this study the mathematical model of the calcination process, based on the chemical reaction scheme published by Silcox et al. (1989), is extended with the effects of diffusion limitation of the overall rate and the pore diffusion effectiveness factor. The calcination model involves three rate-limiting processes: (a) heat transfer to the particle, (b) mass transfer of CO_2 from the reaction interface through the porous layer and particle boundary layer to the surrounding and (c) the kinetics of the chemical reaction.

The calcination process starts only if the partial pressure of carbon dioxide in the gas surrounding the limestone surface is less than the decomposition pressure of limestone (Stanmore and Gilot, 2005). The decomposition pressure P_{eq} and the chemical reaction rate k_{ch} of the calcination process determined by Silcox et al. (1989) are

$$p_{eq} = 4.137 \times 10^{12} \exp\left(-\frac{20474}{T}\right) \, [Pa], \tag{3}$$

$$k_{ch} = k_D(p_{eq} - p_{CO_2}) \, [mol \, m^{-2} \, s^{-1}], \tag{4}$$

where p_{CO_2} is the partial pressure of carbon dioxide at the reaction surface of limestone and

$$k_D = 1.22 \exp\left(-\frac{4026}{T}\right) \times 10^{-5} \, [mol \, m^{-2} \, s^{-1} \, Pa^{-1}]. \tag{5}$$

Based on the Eqs. (2) and (4), Eq. (3) for the chemical reaction rate of the calcination process can be written in the following form:

$$k_{ch} = 5.0 \times 10^7 \exp\left(-\frac{24500}{T}\right) - 1.22$$
$$\times 10^{-5} \exp\left(-\frac{4026}{T}\right) p_{CO_2} \frac{A_{por}}{A_{geom}} \, [mol \, m^{-2} \, s^{-1}]. \tag{6}$$

Major effects such as temperature, CO_2 partial pressure and enhanced overall surface due to porosity are taken into account in this equation. The surface increase is modelled as A_{por}/A_{geom}, where A_{por} is the overall reaction surface (representing the surface of internal pores and the outer surface of the sphere), and A_{geom} is the surface of the particle (sphere). The surface increase is dependent on porosity, pore diameter and topology of the porous structure, which are not known in detail for the limestone considered in the experiments discussed below. Thus in this work it is used as a matching parameter for the specific type of limestone with typical values ranging from 1 to 5. This parameter has some initial value depending on type of limestone, but starting with this value it will also evolve during the reaction by shrinking and cracking processes as well as by sintering. Since the latter processes partly increase and partly decrease the surface the assumption of a mean average or balanced value is supported.

As illustrated in Fig. 1 partial pressure of CO_2 greatly influences the reaction rate. At higher temperatures and lower CO_2 partial pressure the rate of change of the reaction rate is much faster than for lower temperature and higher CO_2 partial pressure values. For the above diagram the effect of porosity was not taken into account, i.e., the value of A_{por}/A_{geom} was set to 1.

The physical reaction rate k_{ph} of the calcination process is determined from

$$k_{ph} = \frac{12DSh}{R_{CO_2} d_{part} T} p_{ref} \, [kg \, m^{-2} \, s^{-1}], \tag{7}$$

which represents the mechanism of diffusion limitation (Schneider, 2003). Due to high CO_2 concentration in the pore system and in the
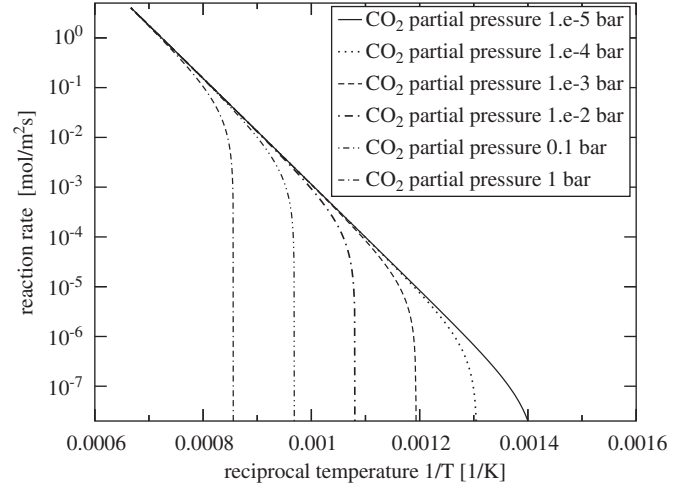

Fig. 1. Effect of CO_2 partial pressure on the chemical reaction rate.

particle surrounding the partial pressure of CO_2 is assumed to be high as well and the reference pressure p_{ref} in Eq. (6) is assumed to be close to ambient pressure. Following Schneider (2003) the Sherwood number is taken as 2, since limestone particles are small and rapid velocity equilibration can be assumed. The term D represents the diffusion coefficient that consists of binary and Knudsen diffusion coefficient (Kern and Jess, 2006) and is calculated as

$$D = \left[\frac{1}{D_{bin}} + \frac{1}{D_{knu}}\right]^{-1} \, [m^2 \, s^{-1}]. \tag{9}$$

For the binary diffusion coefficient the following correlation demonstrated by Reid et al. (1988) is used:

$$D_{bin} = \frac{0.0266T^{1.5}}{pM_{AB}^{0.5}\sigma_{AB}^2\omega_d} \, [m^2 \, s^{-1}], \tag{9}$$

while the Knudsen diffusion coefficient (Bluhm-Drenhaus et al., 2010) is calculated as

$$D_{knu} = \frac{d_{pore}}{3}\left[\frac{8R_{CO_2}T}{\pi}\right]^{0.5} \, [m^2 \, s^{-1}]. \tag{10}$$

The overall reaction rate of the calcination process, which is the component of the physical and the chemical reaction rate, based on Levenspiel (1972) is calculated as

$$k = \left[\frac{1}{k_{ph}} + \frac{1}{\eta \tilde{k}_{ch}}\right]^{-1} \, [kg \, m^{-2} \, s^{-1}], \tag{11}$$

where $\tilde{k}_{ch}$ is the chemical reaction rate in $[kg \, m^{-2} \, s^{-1}]$ and η is the effect of pore efficiency on the chemical reaction rate of calcination process. Here the pore efficiency coefficient η is applied globally to the chemical reaction rate assumed to take place inside the complex topology of the porous structure. The coefficient η is given by Froment and Bischoff (1990) as

$$\eta = \frac{\tanh\left[\frac{d}{6}\sqrt{\frac{\bar{\bar{k}}_{ch}}{\varepsilon D}}\right]}{\left[\frac{d}{6}\sqrt{\frac{\bar{\bar{k}}_{ch}}{\varepsilon D}}\right]}, \tag{12}$$

where $\bar{\bar{k}}_{ch}$ is the chemical reaction rate in $[s^{-1}]$ and the correction factor ε given by Bluhm-Drenhaus et al. (2010) applied to the diffusion coefficient D is

$$\varepsilon = \frac{\varepsilon_p}{\tau_p^2}, \tag{13}$$

where ε_p denotes the void fraction of the limestone particle with higher values favouring diffusion, τ_p denotes the tortuosity, which can be regarded as a measure for the complexity of the pore structure hindering the diffusion of the reacting gases inside the porous structure of the grains.

Fig. 2 illustrates the impact of the chemical reaction rate and the physical limitation on the overall reaction rate of the calcination process. It is clear that at higher temperatures, physical limitation has a significant influence on the overall calcination rate. Since the experimental conditions of Mohr's experiment are covering the transition region shown in Fig. 2, the diffusion limitations must be taken into account in the simulations.

Mass exchange from the calcination reaction is calculated for the limestone, lime and carbon dioxide. The mass transfer rate of limestone is calculated by the following equation:

$$\dot{m}_{CaCO_3} = -\widehat{k} \; [\text{kg s}^{-1}], \tag{14}$$

where $\widehat{k}$ is the overall reaction rate of the calcination process in [kg s^{-1}] and from stoichiometry the mass transfer of lime and carbon dioxide are

$$\dot{m}_{CaO} = \widehat{k} \frac{M_{CaO}}{M_{CaCO_3}} \; [\text{kg s}^{-1}], \tag{15}$$

$$\dot{m}_{CO_2} = \widehat{k} \frac{M_{CO_2}}{M_{CaCO_3}} \; [\text{kg s}^{-1}]. \tag{16}$$

Enthalpy exchange from the calcination reaction (convective enthalpy, enthalpy transfer from reaction enthalpy, transfer of enthalpy with the mass leaving the particle) is calculated separately for the particle and for the gas temperature.

For the enthalpy conservation of a solid particle the following equation can be written:

$$(m_{CaCO_3}c_{pCaCO_3} + m_{CaO}c_{pCaO})\dot{T}_p + \dot{m}_{CaCO_3}c_{pCaCO_3}T_p + \dot{m}_{CaO}c_{pCaO}T_p$$
$$= \frac{f\Delta H_R \dot{m}_{CaCO_3}}{M_{CaCO_3}} + \alpha A(T_g - T_p) - \dot{m}_{CO_2}\tilde{c}_p T_p, \tag{17}$$

where f is a factor, which represents the fraction of reaction enthalpy taken from the particle and $\tilde{c}_p$ is the difference of molar specific heat capacities of limestone and lime, divided by the molecular weight of carbon dioxide. In the calculations shown below the factor f has been taken as 0.5 assuming that the reaction enthalpy is provided at equal parts from both particles and gaseous surrounding. However, a sensitivity study showed that at least for small particles the effect of parameter f on the calcination rate is not significant, i.e. $f=0$ assuming that all

enthalpy is taken immediately from the gas phase did not change the results.

Similar to the enthalpy balance for the solid particle, the enthalpy of the gas phase is

$$\sum m_i \left(c_{pi} + \frac{dc_{pi}}{dT}T \right) \dot{T}_g + \dot{m}_{CO_2}c_{pCO_2}T_g$$
$$= \left(\frac{-(1-f)\Delta H_R \dot{m}_{CaCO_3}}{M_{CaCO_3}} + \alpha A(T_p - T_g) \right) n_p + \dot{m}_{CO_2}\tilde{c}_p T_p. \tag{18}$$

From these equations the rate of change of particle and gas temperatures are calculated. The mass and enthalpy balance equations given above are applied in each cell of the computational domain during the integration of the Lagrangian particle phase for updating the gas and particle properties and are solved by time step subcycling using DVODE solver. This is done within every two gas phase time steps. Complex chemistry systems in FIRE solver are usually treated by pre-tabulation or similar methods (Ban and Duić, 2011), but in this case the calcination process, represented by one reaction (see Eq. (2)), is calculated directly. Additionally from these equations the source terms for species mass and enthalpy are collected transferring the impact of the chemical reactions from the particles to the Eulerian solver.

2.3. Radiative heat transfer

The radiative heat transfer and the effects of particle radiation from the limestone particles is modelled with the P-1 radiation model (Sazhin et al., 1996; Brewster and Kunitomo, 1984):

$$\nabla(\Gamma\nabla G) = (a + a_p)G - 4\pi \left(a\frac{\sigma T^4}{\pi} + E_p \right) \; \left[\frac{W}{m^3}\right], \tag{19}$$

where the term on the left hand side represents the change of the incident radiation. The first term on the right hand side represents the absorption, from the continuous phase and the particles, and the second term on the right hand side represents the emission, again from the continuous phase and the particles.

For the particle emission E_p the following correlation is used:

$$E_p = \frac{1}{\Delta V} \sum_{n=1}^{N} \varepsilon_{pn} A_{pn} \frac{\sigma T^4}{\pi} \left[\frac{W}{m^3}\right], \tag{20}$$

while the particle absorption coefficient is calculated as

$$a_p = \frac{1}{\Delta V} \sum_{n=1}^{N} \varepsilon_{pn} A_{pn} \left[\frac{1}{m}\right]. \tag{21}$$

The diffusion coefficient Γ is calculated as

$$\Gamma = \frac{1}{3(a + a_p + \sigma_p)} [m], \tag{22}$$

and for the particle scattering factor σ_p the following correlation is used:

$$\sigma_p = \frac{1}{\Delta V} \sum_{n=1}^{N} (1 - f_{pn})(1 - \varepsilon_{pn}) A_{pn} \left[\frac{1}{m}\right]. \tag{23}$$

The source term that is directly introduced into the enthalpy equation as a radiative heat source is calculated as follows:

$$-\nabla q_r = -4\pi \left(a\frac{\sigma T^4}{\pi} + E_p \right) + (a + a_p)G \left[\frac{W}{m^3}\right]. \tag{24}$$

3. Single particle test and results

For the plausibility checks and the quantitative checks of balances, presented model of the calcination process was tested on a single particle in a single mesh cube. Different types of initial
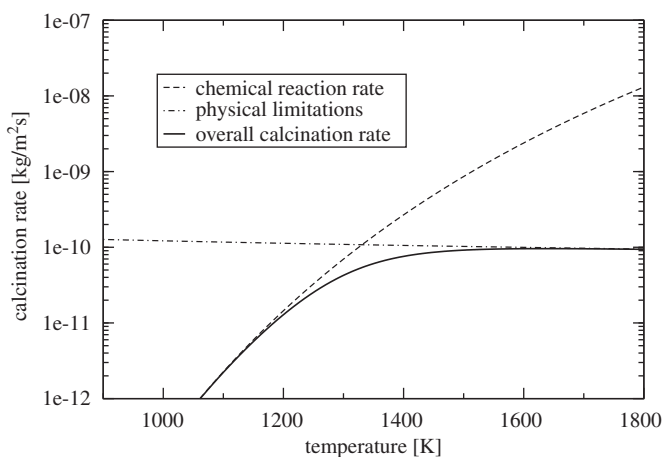

Fig. 2. Impact of the chemical reaction rate and the physical limitations on the overall reaction rate.

conditions were set-up (e.g., temperature, carbon dioxide content, particle diameter) to test the presented numerical model.

For calculations of a single particle, the results of which are shown in Figs. 3 and 4, initial particle diameter was set to 10 μm, the porosity factor, i.e. A_{por}/A_{geom}, was set to 5 and there was no carbon dioxide present in the single mesh cube.

Fig. 3 shows the influence of lower reaction temperatures on the calcination process, i.e. decomposition of limestone, and Fig. 4 shows the influence of higher reaction temperatures on the calcination process. From these two figures it is clear that the temperature increase results with an increase of limestone decomposition, which represents a reasonable physical trend.

Fig. 5 shows the influence of carbon dioxide content on the calcination process. As can be seen the increase of carbon dioxide content reduces the limestone decomposition. The initial particle diameter for this figure was 10 μm, porosity factor was set to 5, the gas temperature was set to 1200 K and the carbon dioxide was the variable parameter.

Fig. 6 shows the influence of particle size on the calcination process. As can be seen bigger limestone particles need more time to decompose than the small particles. For this figure the initial gas temperature was set to 1400 K, the porosity factor was set to 5 and initially there was no carbon dioxide.
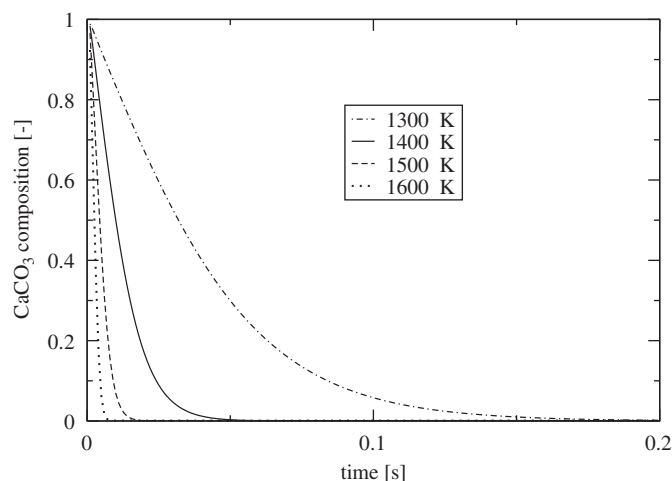
Fig. 5. Influence of CO_2 content on the calcination process.

Fig. 6. Influence of particle size on the calcination process.

Results gained from the single particle tests show that the right range of particle temperatures is covered, that the conversion of limestone depends on the carbon dioxide content and that the reaction kinetics of the calcination process are able to obtain reasonable trends. Additional studies regarding the effects of pore diameter and porosity still need to be done in further work.

4. Validation test—calcination process in a pipe reactor

The calcination model was validated by simulating the International Flame Research Foundation (IFRF) pipe reactor IPFR (intensified plug flow reactor), for which measurements of limestone conversion exist (Mohr, 2001). Several experiments with different operating conditions have been done. This sensitivity analysis gives some more information about the influence of various parameters (CO_2 content, temperature, mass flow, etc.) on the calcination reaction rate.

4.1. Experimental data

The IPFR is a laboratory reactor (Fig. 7) made up of a 2 m long tube with a steady radial and axial temperature profile (electrically heated walls). Different gas velocities and gas compositions as well as powder mass flows can be adjusted and a sampling device to monitor the progress of reaction along the tube axis is available. This pipe reactor works up to a temperature of 1400 °C.

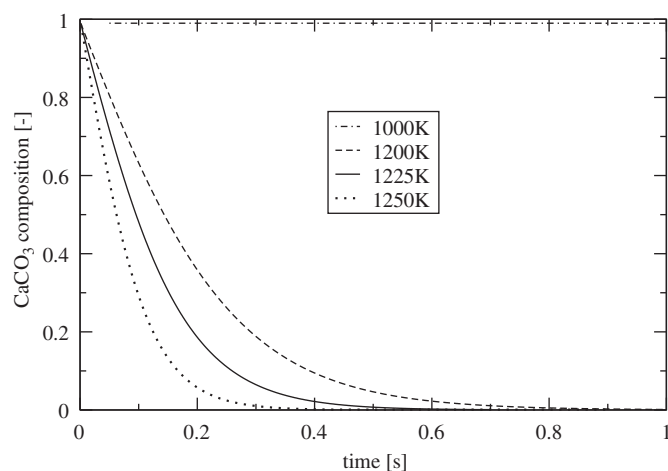**Fig. 3.** Calcination process at lower reaction temperatures.

Fig. 4. Calcination process at higher reaction temperatures.

Fig. 7. Construction of IPFR pipe reactor (Mohr, 2001).

Table 1
Experimental settings (Mohr, 2001).

Parameter	Unit	Calcination					
		C1	C2	C3	C4	C5	C6
$\dot{V}_g$	m_N^3/h	35.1	31.1	22.0	21.0	22.0	28.3
O_2	Vol%				5		
CO_2	Vol%			14		19	8.5
H_2O	Vol%				9.5		
$\dot{T}_g$	°C	1000	1100	1200	1350	1200	
$\dot{m}_{CaCO_3}$	g/h	900		600			

Reaction pipe dimensions:

Length: $l = 2000$ mm
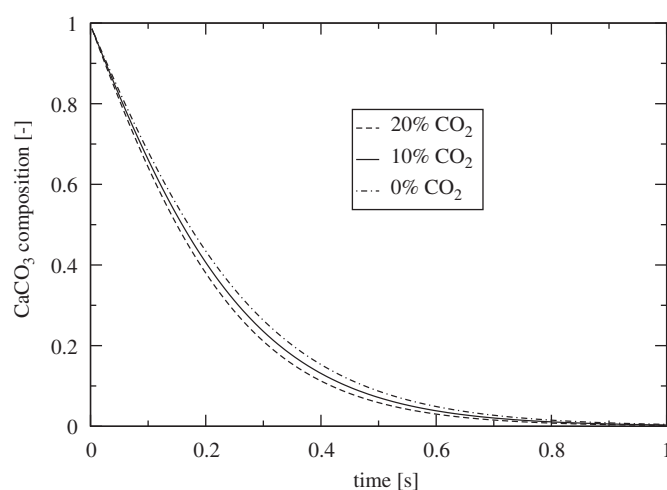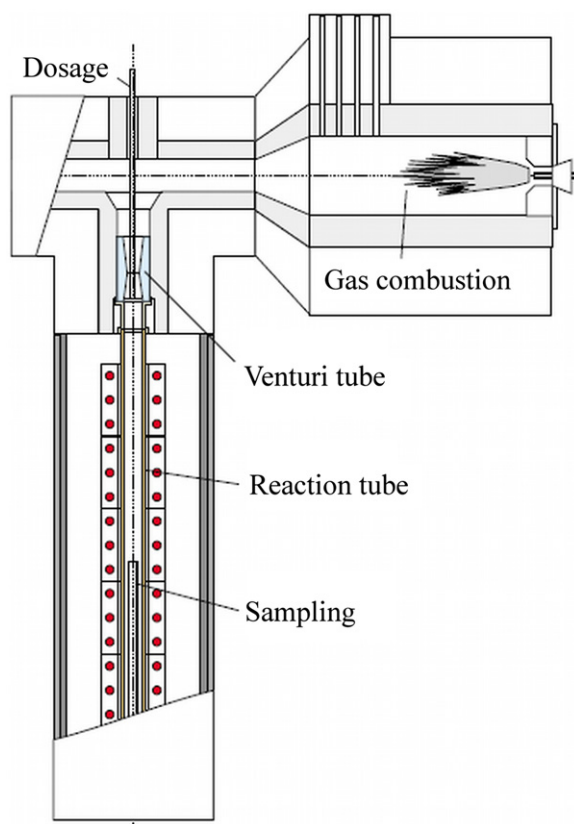Inner diameter: $D_1 = 80$ mm
Outer diameter: $D_2 = 117$ mm

The experimental data forms the basis for the evaluation of the calcination model and its simulation behaviour. The experiments were performed according to Table 1.

Finally following the procedure of Mohr (2001) a Rosin–Rammler distribution is assumed for limestone particle size distribution, with the mean particle diameter $d' = 10.68\,\mu m$, the smallest diameter $0.1\,\mu m$, the largest diameter $62.93\,\mu m$ and the spread parameter $n = 0.653$.

Rosin–Rammler distribution function is

$$R(d) = \exp\left[-\left(\frac{d}{d'}\right)^n\right]. \qquad (25)$$

4.2. Numerical simulation

In the simulation 10,800 cells were employed to discretize the computational domain, extending from 0 to 2000 mm in axial direction and from 0 to 80 mm in radial direction, representing the reaction tube (Fig. 7). For the validation test six different set-ups were calculated according to Table 1. The differencing scheme used for momentum and continuity balances was Central Differencing, and for turbulence, energy balances and scalar transport equations an Upwind scheme was applied. Turbulence was modelled by the standard $k-\varepsilon$ model.

4.3. Results and discussion

The predicted conversion of limestone to lime, for different set-ups, was compared with the calculations from Mohr's doctoral dissertation and the reported experimental data (Mohr, 2001). Fig. 8 shows the influence of pore diameter on the results for the C3 experiment. It is clear that with higher values of pore diameter conversion of limestone to lime is higher. Fig. 9 shows the influence of void fraction on the results for the C3 experiment. As can be seen higher values of void fraction increase the conversion of limestone to lime. Fig. 10 shows the influence of tortuosity on the results for the C3 experiment. It is clear that higher values of tortuosity give slower conversion effect. The rest of the figures show the
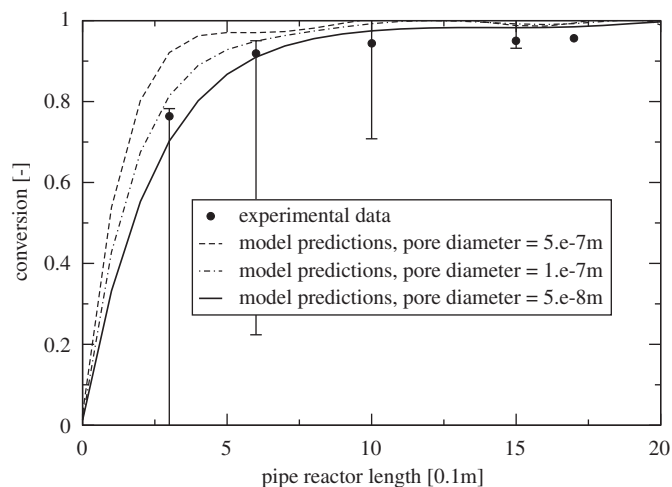

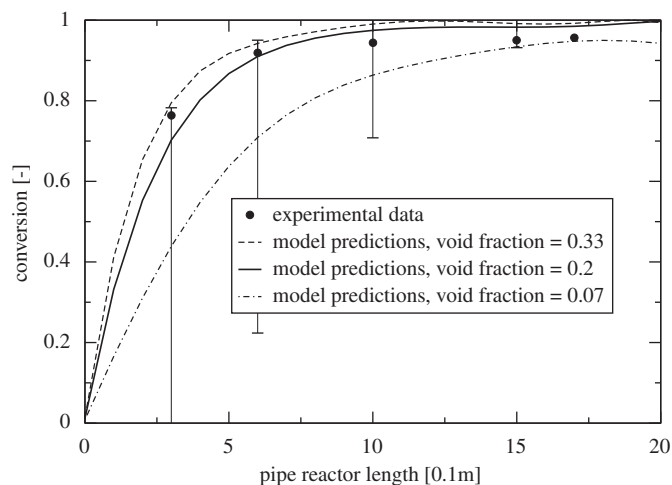**Fig. 8.** Influence of pore diameter on the results for the C3 experiment.

Fig. 9. Influence of void fraction on the results for the C3 experiment.
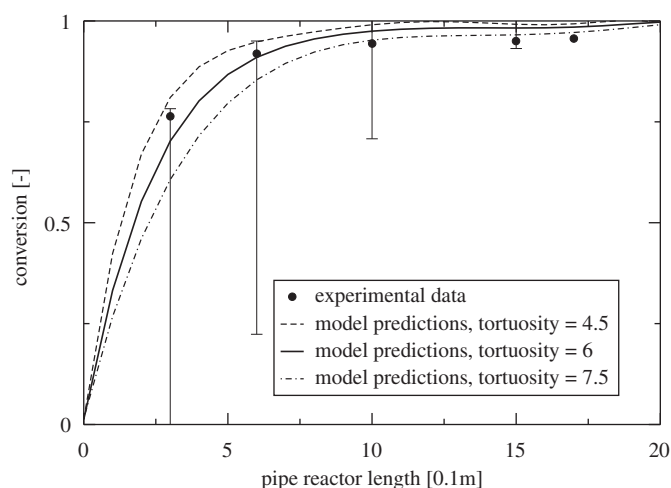
Fig. 10. Influence of tortuosity on the results for the C3 experiment.

Fig. 11. Influence of mesh size on the results for the C3 experiment.

comparison of the predicted limestone conversion, using the combined reaction rate with pore diffusion, with Mohr's calculation and the experimental measurements along the pipe reactor for all set-ups presented in Table 1. All of the calculations have been done with the same set of model parameters using the value of 6 for tortuosity (Wang et al., 2005), 0.2 for void fraction and $5e-8m$ for pore diameter. In the literature (Bluhm-Drenhaus et al., 2010; Stanmore and Gilot, 2005) higher values for the void fraction in the range of 0.36–0.68 are given. The lower value of 0.2 assumed in this work can be justified by sintering processes as described by Hillers (2008), which can reduce again the porosity considerably to values down to 0.05 depending on temperature and particle residence time.

As can be noted the experimental measurements and the numerical results obtained by the calcination model are in good agreement. From the shown results it is clear that the presented model follows the influence of temperature as can be concluded from comparison of C1 and C2 as well as C3 and C4, which differ by temperature only. The effect of reduced conversion with increasing carbon dioxide content varied in C3 and C5, which is not that clearly visible, but the calculated curves are anyway close to the experimental mean values and always within the experimental uncertainty range. Further comparing C5 and C6 the same trend of reduced conversion with increasing gas mass flow can be detected in both experiments as well as in the calculations. This occurs despite the reduction of the carbon dioxide content at the same time, which should enhance conversion. Thus the effect can be understood by the reduced particle residence time connected with enhanced gas mass flow.

Fig. 11 shows the influence of mesh size on the results for the C3 experiment. Comparison of the coarsest grid (dotted line) and the coarse grid (dash dot line) shows significant differences in the results, while the difference between intermediate (continuous line) and fine grid (dashed line) is already considerably smaller. The conversion rate of these two grids (continuous and dashed line) is almost identical. Thus with respect to the experimental uncertainty the grid with 10,800 cells has been regarded as sufficient.

In Figs. 12–17 also the calculations from the Ph.D. thesis of Mohr (2001) are shown. Despite the fact that the model presented is simpler than the Mohr model, e.g. regarding details of evolution of the porous structure and detailed description of sintering processes, the overall agreement with the experimental data could be improved. This might be due to the additional uncertainties in Mohr's model introduced by unknown model parameters of the detailed sub-models and complex interactions
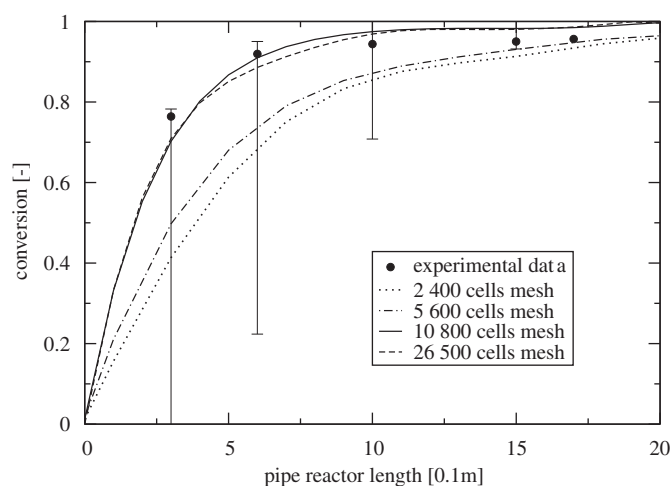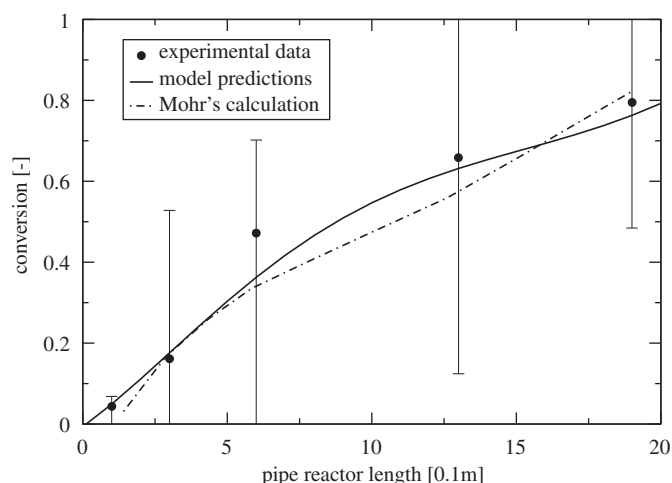
Fig. 12. Comparison of C1 set-up.
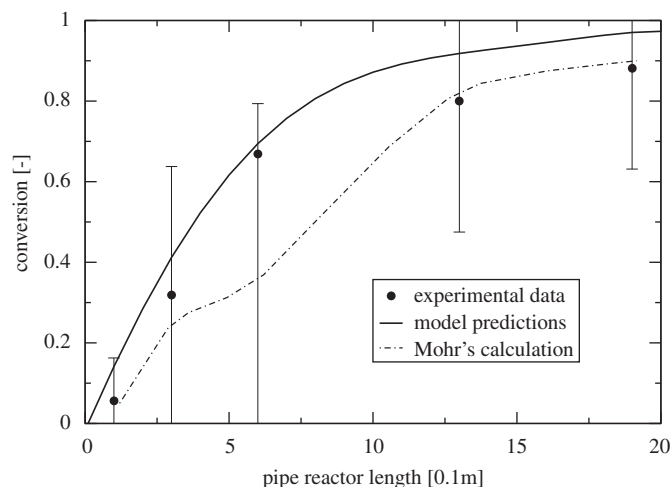
Fig. 13. Comparison of C2 set-up.

between them, which would need an even broader experimental data base for adjustment. In contrast to this the simpler model can be more easily controlled and matched and thus is judged to be sufficiently accurate for CFD simulations of the overall calcination process. Nevertheless the refined models from the literature are the valuable basis for further model extensions.

Fig. 14. Comparison of C3 set-up.

Fig. 17. Comparison of C6 set-up.

Fig. 15. Comparison of C4 set-up.

Fig. 16. Comparison of C5 set-up.

various thermo-chemical reaction techniques, which can be used to reduce carbon dioxide emission, have become a major area of the current research. Computer modelling of the calcination process provides a valuable tool that can be used for the investigation and better understanding of particle kinetics and pollutant emissions from cement combustion systems.

The numerical model of the calcination process was implemented into a commercial CFD code FIRE, taking into account the effects of temperature, decomposition pressure, diffusion and pore efficiency. The model is detailled enough to contain the relevant physical and chemical processes, yet simple enough to run on the realistic industrial meshes needed for detailed CFD simulations of calcination devices. From the results shown it can be concluded that the presented model of the calcination process is in a good agreement with the reported experimental measurements. Thus, it can be used for the investigation and optimisation of calcination devices for cement production. This will be done in future work.

Nomenclature

|	
a	absorption coefficient, m^{-1}
a_p	particle absorption coefficient, m^{-1}
A	sphere surface, m^2
A_{geom}	sphere surface, m^2
A_{pn}	projected area of an n-particle, m^2
A_{por}	overall reaction surface, m^2
$\tilde{c}_p$	specific heat capacity, $J\,kg^{-1}\,K^{-1}$
c_{pCaCO_3}	specific heat capacity of limestone, $J\,kg^{-1}\,K^{-1}$
c_{pCaO}	specific heat capacity of lime, $J\,kg^{-1}\,K^{-1}$
c_{pi}	specific heat capacity of gas component, $J\,kg^{-1}\,K^{-1}$
d	particle diameter, m
d'	mean particle diameter, m
d_{part}	particle diameter, m
d_{pore}	pore diameter, m
D	diffusion coefficient, $m^2\,s^{-1}$
D_{bin}	binary diffusion coefficient, $m^2\,s^{-1}$
D_{knu}	Knudsen diffusion coefficient, $m^2\,s^{-1}$
E_p	particle emission, $W\,m^{-3}$
f	reaction enthalpy factor, dimensionless
f_{pn}	scattering factor of n-th particle, dimensionless
G	incident radiation, $W\,m^{-2}$
ΔH_R	reaction enthalpy, $J\,mol^{-1}$
k	overall reaction rate, $kg\,m^{-2}\,s^{-1}$
$\widehat{k}$	overall reaction rate, $kg\,s^{-1}$

5. Conclusion

The formation of carbon dioxide in cement production systems has created increasing environmental concerns because of the reductions in carbon dioxide emissions. Thus, investigations of

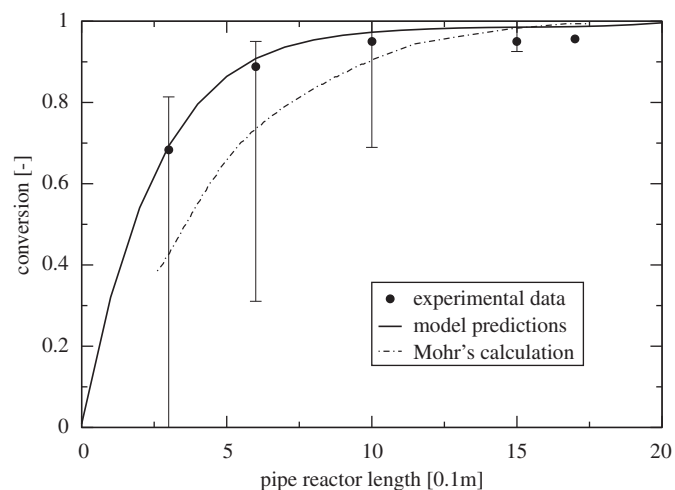|	
k_{ch}	chemical reaction rate, mol m^{-2} s^{-1}
$\underline{\tilde{k}}_{ch}$	chemical reaction rate, kg m^{-2} s^{-1}
$\bar{k}_{ch}$	chemical reaction rate, s^{-1}
k_D	reaction rate, mol m^{-2} s^{-1} Pa^{-1}
k_{ph}	physical reaction rate, kg m^{-2} s^{-1}
m_{CaCO_3}	limestone mass, kg
m_{CaO}	lime mass, kg
$\dot{m}_{CO_2}$	mass transfer of CO_2, kg s^{-1}
$\dot{m}_{CaCO_3}$	mass transfer of limestone, kg s^{-1}
$\dot{m}_{CaO}$	mass transfer of lime, kg s^{-1}
m_i	gas component mass, kg
M_{AB}	average molecular weight, g mol^{-1}
M_{CO_2}	CO_2 molecular weight, g mol^{-1}
M_{CaCO_3}	limestone molecular weight, g mol^{-1}
M_{CaO}	lime molecular weight, g mol^{-1}
n	particle spread parameter, dimensionless
n_p	number of particles per parcel, dimensionless
p	total pressure, Pa
p_{CO_2}	CO_2 partial pressure, Pa
p_{eq}	equilibrium CO_2 partial pressure, Pa
p_{ref}	referent pressure, Pa
q_r	radiation flux, W m^{-2}
R	Rosin–Rammler distribution function, dimensionless
R_{CO_2}	CO_2 gas constant, J kg^{-1} K^{-1}
S_φ	source term of the dependent variable φ
Sh	Sherwood number, dimensionless
T	temperature, K
T_g	gas temperature, K
T_p	particle temperature, K
u_j	Cartesian velocity, m s^{-1}

Greek letters

α	convective heat transfer coefficient, W m^{-2} K^{-1}
Γ	diffusion coefficient, m
Γ_φ	diffusion coefficient of the dependent variable φ
ε	correction factor, dimensionless
ε_p	void fraction (porosity), dimensionless
ε_{pn}	emissivity of n-th particle, dimensionless
φ	dependent variable
η	pore efficiency factor, dimensionless
ρ	density, kg m^{-3}
σ	Stefan–Boltzmann's constant, W m^{-2} K^{-4}
σ_{AB}	characteristic length, 10^{-8} m
σ_p	particle scattering factor, m^{-1}
τ_p	tortuosity, dimensionless
ω_d	diffusion collision integral, dimensionless

References

Baburić, M., Raulot, A., Duić, N., 2004. Implementation of discrete transfer radiation method into SWIFT computational fluid dynamics code. Therm. Sci. 8, 293–301.

Baburić, M., Duić, N., Raulot, A., Coelho, P.J., 2005. Application of the conservative discrete transfer radiation method to a furnace with complex geometry. Numer. Heat Transfer Part A Appl. 48, 297–313.

Ban, M., Duić, N., 2011. Adaptation of n-heptane autoignition tabulation for complex chemistry mechanisms. Therm. Sci. 15, 135–144.

Bes, A., 2006. Dynamic Process Simulation of Limestone Calcination in Normal Shaft Kilns. Ph.D. Thesis. Otto-von-Guericke-University, Magdeburg.

Bluhm-Drenhaus, T., Simsek, E., Wirtz, S., Scherer, V., 2010. A coupled fluid dynamic-discrete element simulation of heat and mass transfer in a lime shaft kiln. Chem. Eng. Sci. 65, 2821–2834.

Borgwart, R.H., 1985. Calcination kinetics and surface area of dispersed limestone particles. AIChE J. 31, 103–111.

Brewster, M.Q., Kunitomo, T., 1984. The optical constants of coal, char and limestone. ASME J. Heat Transfer 106, 678–683.

Campbell, F.R., Hills, A.W.D., Paulin, A., 1970. Transport properties of porous lime and their influence on the decomposition of porous compacts of calcium carbonate. Chem. Eng. Sci. 25 (1970), 929–942.

Darroudi, T., Searcy, A.W., 1981. Effect of CO_2 pressure on the rate of decomposition of calcite. J. Phys. Chem. 85, 3971–3974.

Dennis, J.S., Hayhurst, A.N., 1987. The effect of CO_2 on the kinetics and extent of calcinations of limestone and dolomite particles in fluidised beds. Chem. Eng. Sci. 42, 2361–2372.

Fidaros, D.K., Baxevanou, C.A., Dritselis, C.D., Vlachos, N.S., 2007. Numerical modelling of flow and transport processes in a calciner for cement production. Powder Technol. 171, 81–95.

Froment, G., Bischoff, K., 1990. Chemical Reactor Analysis and Design, second ed. J. Wiley and Sons, New York (pp. 160).

Garcia-Labiano, F., Abad, A., de Diego, L.F., Gayan, P., Adanez, J., 2002. Calcination of calcium-based sorbents at pressure in a broad range of CO_2 concentrations. Chem. Eng. Sci. 57, 2381–2393.

Hillers, M., 2008. Modellierung der Turbulenzmodulation einer hochbeladenen reaktiven Zweiphasenströmung am Beispiel des Zementherstellungsprozesse. Ph.D. Thesis. University Duisburg-Essen.

Hills, A.W.D., 1968. The mechanism of the thermal decomposition of calcium carbonate. Chem. Eng. Sci. 23, 297–320.

Hu, N., Scaroni, A.W., 1996. Calcination of pulverised limestone particles under furnace injection conditions. Fuel 75, 177–186.

Hu, Z., Lu, J., Huang, L., Wang, S., 2006. Numerical simulation study on gas–solid two-phase flow in pre-calciner. Commun. Nonlinear Sci. Numer. Simulation 11, 440–451.

Huang, L., Lu, J., Xia, F., Li, W., Ren, H., 2006. 3-D mathematical modeling of an in-line swirl-spray precalciner. Chem. Eng. Process. 45, 204–213.

Huanpeng, L., Wentie, L., Jianxiang, Z., Ding, J., Xiujian, Z., Huilin, L., 2004. Numerical study of gas–solid flow in a precalciner using kinetic theory of granular flow. Chem. Eng. J. 102, 151–160.

Iliuta, I., Dam-Johansen, K., Jensen, A., Jensen, L.S., 2002a. Modeling of in-line low-NO$_x$ calciners—a parametric study. Chem. Eng. Sci. 57, 789–803.

Iliuta, I., Dam-Johansen, K., Jensen, L.S., 2002b. Mathematical modeling of in-line low-NO$_x$ calciner. Chem. Eng. Sci. 57, 805–820.

Ingraham, T.R., Marier, P., 1963. Kinetic studies on the thermal decomposition of calcium carbonate. Can. J. Chem. Eng. 41, 170–173.

Kern, C., Jess, A., 2006. Verkokung und Koksabbrand in heterogenen Katalysatoren. Chem. Ing. Tech. 8, 78.

Khinast, J., Krammer, G.F., Brunner, Ch., Staudinger, G., 1996. Decomposition of limestone: the influence of CO_2 and particle size on the reaction rate. Chem. Eng. Sci. 51, 623–634.

Levenspiel, O., 1972. Chemical Reaction Engineering, second ed. J. Wiley and Sons, New York (pp. 482).

Mohr, M., 2001. Numerische Simulation der simultanen Reaktion von Kalkstein und Kohle bei der Zementherstellung. Ph.D. Thesis. University of Ruhr, Bochum.

Reid, R.C., Prausnitz, J.M., Polling, B.E., 1988. The Properties of Gases and Liquids, fourth ed. McGraw-Hill Book Company, New York (pp. 582).

Sazhin, S.S., Sazhina, E.M., Faltsi-Saravelou, O., Wild, P., 1996. The P-1 model for thermal radiation transfer: advantages and limitations. Fuel 75, 289–294.

Schneider, M., 2003. Experimentelle und mathematische Modellierung der Festbettvergasung am Beispiel der Gleichstromvergasung von Holzhackschnitzeln. Ph.D. Thesis. TU, Dresden.

Silcox, G.D., Kramlich, J.C., Pershing, D.W., 1989. A mathematical model for the flash calcination of dispersed CaCO$_3$ and Ca(OH)$_2$ particles. Ind. Eng. Chem. Res. 28, 155–160.

Stanmore, B.R., Gilot, P., 2005. Review—calcination and carbonation of limestone during thermal cycling for CO_2 sequestration. Fuel Process. Technol. 86, 1707–1743.

Vujanović, M., Duić, N., Galović, A., 2007. Three-dimensional numerical simulation of the nitrogen oxides formation in an oil-fired furnace. Strojarstvo 49, 165–171.

Vujanović, M., Duić, N., Tatschl, R., 2009. Validation of reduced mechanisms for nitrogen chemistry in numerical simulation of a turbulent non-premixed flame. React. Kinet. Catal. Lett. 96, 125–138.

Vujanović, M., 2010. Numerical Modeling of Multiphase Flow in Combustion of Liquid Fuel. Ph.D. Thesis. University of Zagreb.

Wang, R., Pavlin, T., Rosen, M.S., Mair, R.W., Cory, D.G., Walsworth, R.L., 2005. Xenon NMR measurements of permeability and tortuosity in reservoir rocks. Magn. Reson. Imaging 23, 329–331.

PAPER 2

The application of CFD modelling to support the reduction of CO_2 emissions in cement industry

Hrvoje Mikulčić [a,*], Milan Vujanović [a], Dimitris K. Fidaros [b], Peter Priesching [c], Ivica Minić [d], Reinhard Tatschl [c], Neven Duić [a], Gordana Stefanović [d]

[a] Faculty of Mechanical Engineering and Naval Architecture, University of Zagreb, Ivana Lučića 5, 10000 Zagreb, Croatia
[b] Centre for Research and Technology-Thessaly, Institute of Technology and Management of Agricultural ecosystems, Technology Park of Thessaly, 1st Industrial Area of Volos, 38500 Volos, Greece
[c] AVL − AST, Hans List Platz 1, Graz, Austria
[d] Faculty of Mechanical Engineering, University of Niš, Aleksandra Medvedeva 14, 18 000 Niš, Serbia

ABSTRACT

The cement industry is one of the leading producers of anthropogenic greenhouse gases, of which CO_2 is the most significant. Recently, researchers have invested a considerable amount of time studying ways to improve energy consumption and pollutant formation in the overall cement manufacturing process. One idea involves dividing the calcination and clinkering processes into two separate furnaces. The calcination process is performed in a calciner while the clinkering process takes place in a rotary kiln. As this is new technology in the cement manufacturing process, calciners are still in the research and development phase. The purpose of this paper is to demonstrate the potential of CFD to support the design and optimization of calciners, whose use appears to be essential in reduction of CO_2 emission during cement production. The mathematical model of the calcination process was developed, validated and implemented into a commercial CFD code, which was then used for the analysis. From the results obtained by these simulations, researchers will gain an in-depth understanding of all thermo-chemical reactions in a calciner. This understanding can be used to optimize the calciner's geometry, to make production more efficient, to lower pollutant formation and to subsequently reduce greenhouse gas emissions.

© 2012 Elsevier Ltd. All rights reserved.

1. Introduction

The cement industry has a significant effect on the environment. It is responsible for 5% of the world's anthropogenic CO_2 emissions, and therefore it is an important sector for CO_2 mitigation strategies [1,2]. Around 50% of CO_2 emissions produced during the cement manufacturing process come from the thermal decomposition of limestone, also known as the calcination process. Additionally, 40% comes from the combustion process [3]. CO_2 emission mitigation options include various process and combustion efficiency improvements. One of these improvements comes from controlling the calcination process during the cement production process. Calcination is a strong endothermic reaction, during which limestone

($CaCO_3$) thermally decomposes into lime (CaO) and carbon dioxide (CO_2). In addition to the influence on cement quality, calcination also affects fuel consumption and pollutant emissions [4]. One possibility for the control and investigation of the calcination process is a Computational Fluid Dynamics (CFD) simulation. Early comprehensive information, parametric studies and initial conclusions that can be gained from CFD simulations are very important in handling modern cement technology requirements. Together with experiments and theory, CFD has become an integral component of calciner research. It has been used in the development process for understanding the complex phenomena occurring within the calcination and combustion processes. For instance, results gained from CFD simulations of the calcination process in the calciner can be used for the optimization of a calciner design. The result is a calciner with a higher performance. This higher performing calciner will then have an influence on the final cement quality, fuel consumption and pollutant emissions.

With the aim of understanding all chemical reactions, the heat exchange processes and fluid flow, different cement calciners have been studied. Fidaros et al. [4] presented a numerical model and

* Corresponding author. Tel.: +385 1 6168 494; fax: +385 1 6156 940.
E-mail addresses: hrvoje.mikulcic@fsb.hr (H. Mikulčić), milan.vujanovic@fsb.hr (M. Vujanović), dfeid@cereteth.gr (D.K. Fidaros), peter.priesching@avl.com (P. Priesching), ivica.minic@gmail.com (I. Minić), reinhard.tatschl@avl.com (R. Tatschl), neven.duic@fsb.hr (N. Duić), goca@masfak.ni.ac.rs (G. Stefanović).

a parametric study of flow and transport phenomena that take place in an industrial calciner. This work shows good prediction capabilities for velocity, temperature and distribution of particles. Iliuta et al. [5] investigated the effect of different operating conditions on the level of calcination, burn-out and NOx emissions of an in-line low NOx calciner. This work made a sensitivity analysis of the model with respect to aerodynamics, combustion and calcination parameters. Huanpeng et al. [6] studied the impact of various physical parameters on the dynamics of the two-phase flow in a precalciner. This work used the kinetic theory of granular flow to represent the transport properties of the solid phase in a 2D model. Hu et al. [7] used a 3D model for a dual combustor and precalciner. An Eulerian frame was used for the continuous phase and a Lagrangean frame for the solid phase. The burn-out and the decomposition ratio during the simultaneous injection of two types of coal and limestone were predicted. Bluhm-Drenhaus et al. [8] studied the heat and mass transfer related to the chemical conversion of limestone to lime in a shaft kiln. CFD was used to model the transport of mass, momentum and energy in the continuous phase, while the discrete element method (DEM) was used to model the mechanical movement and the conversion reactions of the solid materials. Using a cement calciner in the cement production process is relatively new technology. Consequently, all of these studies show the need for further improvements of cement calciners.

In addition to studies investigating the chemical and physical processes in cement production, several studies investigated the potential of CO_2 emission reduction. In general, CO_2 emissions due to fossil fuel combustion in cement production systems can be reduced by using more energy efficient technologies in the existing production process [9,10]. Fidaros et al. [3] showed a parametric analysis of a solar calciner, using CFD as a research tool. The study also showed how CO_2 emissions can be decreased because the required heat comes from solar energy. Therefore, fossil fuels are not needed for the calcination process. Koumboulis and Kouvakas [11] demonstrated their dynamically adjustable controller for calciner exhaust gases, showing that, with a controlled calciner outlet temperature, the desirable precalcination degree can be achieved. They also showed that the corresponding energy consumption can be lowered according to the fuel used for the process. Kääntee et al. [12] investigated the use of alternative fuels in the cement manufacturing process. This research provided useful data for optimizing the manufacturing process by using different alternative fuels with lower calorific value than those used in classical configurations. Gartner [13] studied clinker chemistry to lower CO_2 emissions. This study showed that raw materials other than limestone could be used in cement production in order to reduce CO_2 emissions.

Due to the significance of the cement industry sector and increased environmental awareness [14], several studies, in different parts of the world, have demonstrated the energy efficiency of cement plants and CO_2 emissions reduction. Much of this work studied the improvement of the cement production process and options for CO_2 emission reduction. Pardo et al. [15] demonstrated the potential for improvement in energy efficiency of EU's cement industry and CO_2 emission reduction by the year 2030. Liu et al. [16] reported the potential for the renovation and building of new cement plants in China. Hasanbeigi et al. [17] demonstrated the abatement CO_2 cost curve for the Thai cement industry. The possibilities and costs of CO_2 abatement were identified, while considering the costs and CO_2 abatement for different technologies. Worrell et al. [18] presented an in-depth analysis of the US cement industry, showing the possibilities for energy saving and CO_2 emissions reduction, based on a detailed national technology database. This work emphasized that the most energy efficient

pyroprocessing cement manufacturing systems consist of pre-heaters, a calciner and a rotary kiln. Sheinbaum and Ozawa [19] reported the energy use and the CO_2 emissions in the Mexican cement industry, concluding that the focus of the energy and CO_2 emissions reduction should be on the use of alternative fuels. Szabó et al. [20] for the 2000–2030 period, presented the most important trends in world cement production, technology development and CO_2 emissions. The study showed that the most advanced dry-precalciner technologies are expected to be the most widely used by 2030. In addition, their work showed that global CO_2 emissions from the cement industry will increase by 50%.

The purpose of this paper is to present the potential of CFD-based CO_2 emission reduction in a Croatian cement plant. The best available technology for cement production, a dry rotary kiln together with preheating of the raw material and a cement calciner were used. In addition to the calculation of the CO_2 emission, a mathematical model of the calcination process was developed, validated and implemented into a commercial CFD code [21]. This calcination model was then used for numerical simulation of a specific calciner geometry which is reported in the literature [4].

1.1. Modern cement pyroprocessing unit

Fig. 1 illustrates the four main cement production processes which have the most influence on final cement quality and fuel consumption. These four processes are: raw material preheating, calcination, clinker burning, and clinker cooling [4]. Prior to the raw material preheating, the raw material is collected, crushed, mixed with additives and transported to the cyclone preheating system. Cyclone preheating systems (usually 3–4 cyclones) have been developed to improve the heat exchange process. Preheating occurs prior to the calciner and the rotary kiln, and has several stages. In every stage the principle is the same – raw material is moving
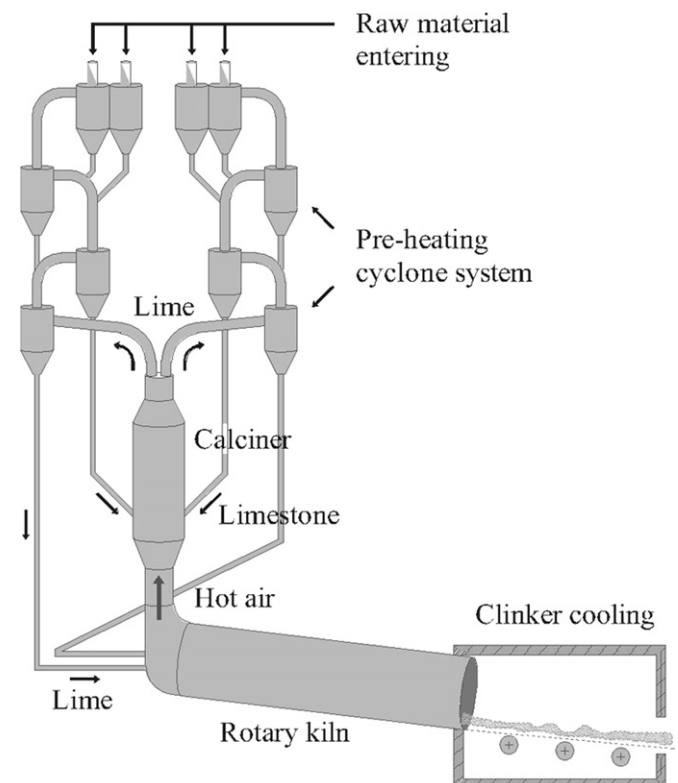

Fig. 1. General pyroprocessing unit of a cement production plant.

counter to hot exhaust gasses from the rotary kiln and in that way is heated. This process is repeated until the raw material goes through all cyclones.

After preheating, raw material enters the cement calciner, where the calcination process occurs. According to Szabó et al. [20] a decrease of energy consumption by 8–11% can be achieved when a rotary kiln is used together with a calciner. This decrease is due to the fact that cement calciners have lower temperatures than rotary kilns. To ensure a temperature of 850 °C, needed for a stabile calcination process, cement calciners use heat from the combustion of solid fuels along with the exhaust gases from a rotary kiln [22]. This is new technology in cement production. Therefore, cement calciners are not standard equipment in cement plants.

Clinker burning is the highest energy demanding process in cement production. It occurs after the calcination process. The clinker is produced in a rotary kiln which rotates 3–5 times per minute, and is positioned at an angle of 3–4°. This angle causes the material to slide and tumble down through the hotter zones towards the flame. The temperature of 1450 °C ensures the clinker formation. After the clinkering process in the rotary kiln is finished, the cement clinker is rapidly cooled down to 100–200 °C [23]. This process is done rapidly to prevent undesirable chemical reactions.

2. Theoretical background

2.1. Analytical calculation of CO_2 emissions

The analytical calculation of CO_2 emission was performed for a cement plant in Croatia. This particular cement plant uses a dry rotary kiln along with the preheating of the raw material in cement production. A calciner is not used at this plant. However, the plant operator is planning to increase the cement production while decreasing the CO_2 emissions. To ensure both criteria are satisfied, the plant operator is planning on modernizing the pyroprocessing unit and including a calciner. For that reason, the CO_2 emissions were calculated for a plant with and without a calciner. CO_2 is emitted from two different sources: the combustion of fossil fuels and the calcination process of limestone in which the clinker forming process also emits CO_2. The former refers to combustion CO_2 emissions, and the latter refers to process CO_2 emissions. Combustion CO_2 emissions are calculated on the basis of the fuel consumption [24]:

$$m_{CO_2(combustion)} = m_{fuel} \times H_d \times e_{fuel} \times O_x \tag{1}$$

Process CO_2 emissions, originating from the conversion of the raw material, are calculated on the basis of the produced cement clinker:

$$m_{CO_2(clinker)} = m_{clinker} \times e \times f \tag{2}$$

Table 1 shows the analytically calculated CO_2 emissions for this particular cement plant. From these results, it is clear that most of the CO_2 emissions come from the calcination process. Also, it should be noted that the amount of CO_2 coming from the calcination process cannot be reduced. CO_2 must be released during the calcination process ($CaCO_3 \rightarrow CaO + CO_2$). Thus, the major potential

for the reduction of CO_2 emissions will be in the design of the combustion processes (with or without a calciner).

As mentioned previously, CO_2 emissions can be reduced if a calciner is used prior to the rotary kiln [4,18,20]. In that case, a decrease of fuel consumption by 8–11% can be gained [20]. This means that with the reduction of the fuel consumption an overall reduction of 3–4% in CO_2 emissions (see Table 1) can be achieved.

2.2. Numerical simulation of a cement calciner

2.2.1. Mathematical model

To model a calciner, the decay of limestone to lime via release of carbon dioxide and the process providing the reaction enthalpy, e.g., the pyrolysis of pit coal to carbon and volatiles with subsequent heterogeneous oxidation of the carbon must be treated. The motion of solid particles is traced through the cement calciner by the Lagrangian formulation. The gas phase is solved by an Eulerian formulation [25]. The mathematical models for the calcination and combustion are treated in the Lagrangian spray module. The thermo-physical properties of the limestone, the lime and the components of the pit coal particles were entered into the commercial CFD code FIRE via user-functions [26–28]. The functions were written in the FORTRAN programming language. In general, the thermal decomposition of limestone into lime and carbon dioxide can be presented by the following equation:

$$CaCO_3(s) \rightarrow CaO(s) + CO_2(g) + 178 \text{ kJ/mol.} \tag{3}$$
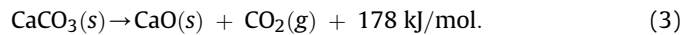
Calcination occurs when the partial pressure of carbon dioxide in the ambient gas is lower than the decomposition pressure of limestone. The decomposition pressure p_{eq} and the chemical reaction rate k_{ch} defined by Silcox et al. [29] are:

$$p_{eq} = 4.137 \times 10^{12} \exp\left(-\frac{20474}{T}\right) \quad [\text{Pa}], \tag{4}$$

$$k_{ch} = k_D \left(p_{eq} - p_{CO_2}\right) \quad \left[\text{mol m}^{-2}\text{s}^{-1}\right], \tag{5}$$

where p_{CO_2} is a partial pressure of carbon dioxide at the limestone reacting surface and

$$k_D = 1.22 \exp\left(-\frac{4026}{T}\right) \times 10^{-5} \quad \left[\text{mol m}^{-2}\text{s}^{-1}\text{Pa}^{-1}\right]. \tag{6}$$

Based on equations (4)–(6), the chemical reaction rate of the calcination process can be written as [21]:

$$k_{ch} = 5.0 \cdot 10^7 \exp\left(-\frac{24500}{T}\right) - 1.22 \cdot 10^{-5} \exp\left(-\frac{4026}{T}\right)$$
$$p_{CO_2} \cdot \frac{A_{por}}{A_{geom}} \quad \left[\text{mol m}^{-2}\text{s}^{-1}\right], \tag{7}$$

where the effects of temperature, partial pressure of CO_2 and surface porosity are taken into account.

The physical reaction rate k_{ph} in the calcination process is defined as [30]:

$$k_{ph} = \frac{12 D_{eff} \cdot Sh}{R_{CO_2} d_{part} T} \cdot p_{ref} \quad \left[\text{kg m}^{-2}\text{s}^{-1}\right], \tag{8}$$

taking into account the diffusion limitations of limestone.

The total reaction rate of the calcination process is the combination of the physical and the chemical reaction rate, and is represented as [31]:

Table 1
CO_2 emissions from a cement plant without and with a calciner.

Type of CO_2 emissions	Without a calciner	With a calciner
Process emissions [tCO_2 per annum]	241 000	241 000
Combustion emissions [tCO_2 per annum]	166 000	149 500–153 700
Total CO_2 emissions [tCO_2 per annum]	407 000	390 500–394 700

$$k = \left[\frac{1}{k_{ph}} + \frac{1}{\eta \cdot \tilde{k}_{ch}}\right]^{-1} \quad \left[\text{kg m}^{-2}\text{s}^{-1}\right], \tag{9}$$

where $\tilde{k}_{ch}$ is the chemical reaction rate in [kg m^{-2} s^{-1}] and η is dimensionless pore efficiency factor.

The coefficient η is described in the following equation [32]:

$$\eta = \frac{\tanh\left[\frac{d}{6}\sqrt{\frac{\bar{\bar{k}}_{ch}}{D_{eff}}}\right]}{\left[\frac{d}{6}\sqrt{\frac{\bar{\bar{k}}_{ch}}{D_{eff}}}\right]}, \tag{10}$$

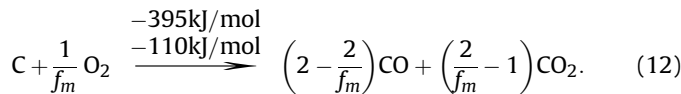where $\bar{\bar{k}}_{ch}$ is the chemical reaction rate in [s^{-1}].

The presented mathematical model of the calcination process was thoroughly tested and validated in our previous studies. For quantitative checks of balances, the presented mathematical model was tested on a single particle [21]. Results gained from the single particle tests show that the decomposition of limestone depends on the following achieving reasonable trends: CO_2 content, the right range of temperatures, and the reaction kinetics of the calcination process. The mathematical model of the calcination process was validated by simulating the International Flame Research Foundation pipe reactor [21], for which measurements of limestone decomposition exist. Several experimental set-ups with different operating conditions have been calculated. This analysis gives more information about the impact of various parameters (CO_2 content, temperature, mass flow, etc.) on the calcination process.

For coal combustion, a two stage process is taken into account. Usually, complex chemistry systems in the FIRE solver are treated by pre-tabulation or similar methods [33]. In this case the coal combustion is a two stage process and is calculated directly. The coal particle, which is composed of pit coal and ash is undergoing a first stage pyrolitic decomposition into volatiles and pure carbon. In a subsequent step, treated in parallel to the pyrolysis, the carbon is oxidized to CO and CO_2 taking into account a mechanism factor depending on temperature.

For the pit coal, a very simple composition represented via chemical formula C_3H_4 is assumed. The heterogeneous chemical reactions treated for the basic model are:

$$C_3H_4 \rightarrow 2C + CH_4, \tag{11}$$

and

$$C + \frac{1}{f_m}O_2 \xrightarrow[\substack{-110\text{kJ/mol}}]{\substack{-395\text{kJ/mol}}} \left(2 - \frac{2}{f_m}\right)CO + \left(\frac{2}{f_m} - 1\right)CO_2. \tag{12}$$

Here, f_m denotes the so-called mechanism factor [34], which ranges between 1 and 2. It causes predominant production of CO_2 in the low temperature range below approximately 900 K and predominant generation of CO for higher temperatures. The value of f_m depends on the particle temperature and size.

Further, additional homogeneous reactions are treated inside the gaseous phase for the oxidation of CO [34] and the combustion of methane, which is treated via the four step Jones−Lindstedt mechanism [35]:

$$CO + \frac{1}{2}O_2 \rightarrow CO_2 \tag{13}$$
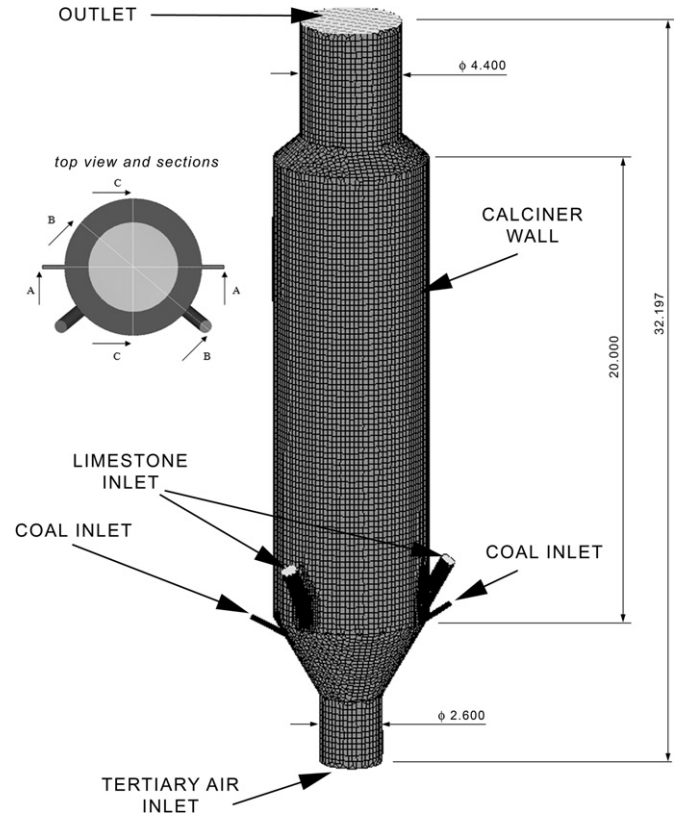
Fig. 2. Calciner boundary conditions and cross section views.

$$\begin{aligned} &CH_4 + \frac{1}{2}O_2 \rightarrow CO + 2H_2 \\ &CH_4 + H_2O \rightarrow CO + 3H_2 \\ &CO + H_2O \longleftrightarrow CO_2 + H_2 \\ &H_2 + \frac{1}{2}O_2 \rightarrow H_2O \end{aligned} \tag{14}$$
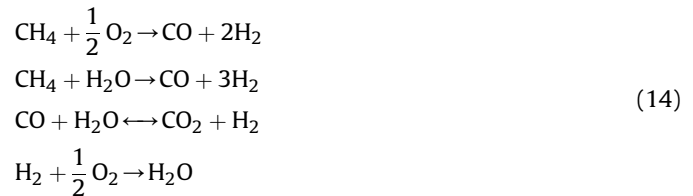
The homogeneous reactions inside the gaseous phase are treated within the general gas phase reactions module of the CFD code. The heterogeneous reactions cause mass transfer sinks and sources to the gas phase and particles. These are described by rate equations for pit coal consumption, for the carbon production from pyrolysis and for consumption from oxidation. As for the calcination, the total reaction rate is composed of a chemical rate following an Arrhenius approach and a physical rate introducing the rate limitation due to diffusion effects. Additional details of the model can be found in the literature [21].

2.2.2. Numerical simulation

The calciner geometry (Fig. 2), available in literature [4], was used to simulate the calcination process. The entire model is 32 m high, with three different cylinders and two conical sections connecting them. On the side of the calciner, there are two symmetric

Table 2
Initial conditions used for calciner calculation.

Pressure	0.1 [MPa]
Temperature	300 [K]
Gas composition	Air
Turbulent kinetic energy	0.001 [m^2/s^2]
Turbulent length scale	0.001 [m]
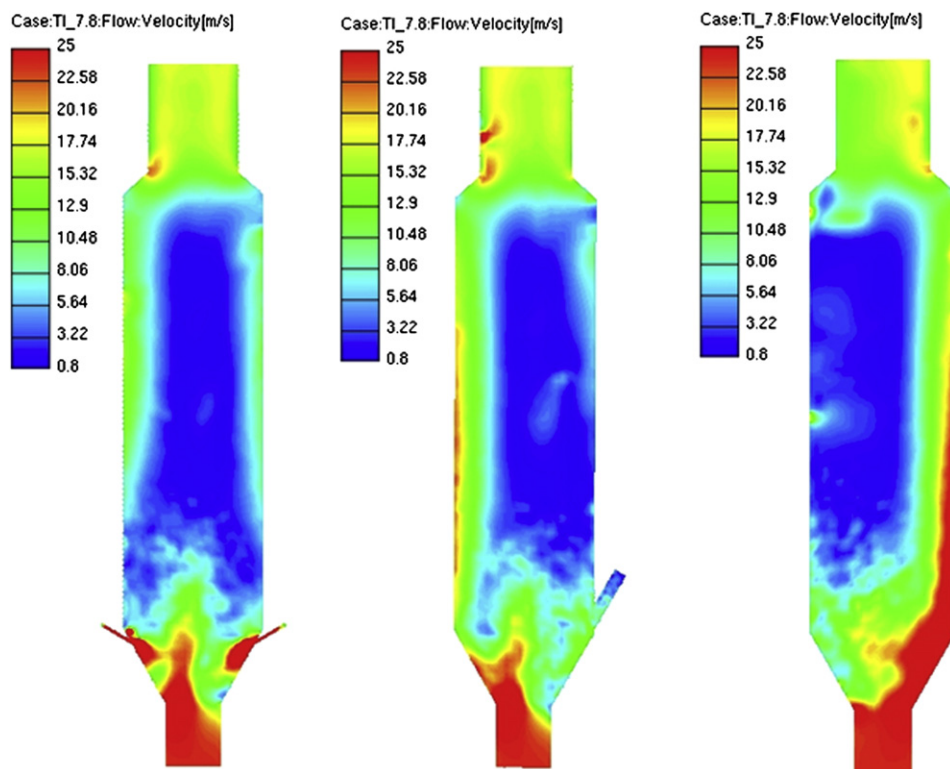
Fig. 3. Velocity distribution in vertical plane: section A-A (left); section B-B (middle); section C-C (right).

inlets for limestone. They are positioned at 60° angles and are 0.6 m in diameter. There are also two symmetric inlets for coal which are positioned at 30° angles and have a diameter of 0.2 m. The cylinder at the bottom of the calciner is 2.6 m in diameter and 3 m high. The centre cylinder represents the main volume where physico-chemical reactions take place. It is 6.6 m in diameter and 20 m high. The cylinder at the outlet is 4.4 m in diameter and 4.7 high. The total volume of the calciner is 850 m^3.
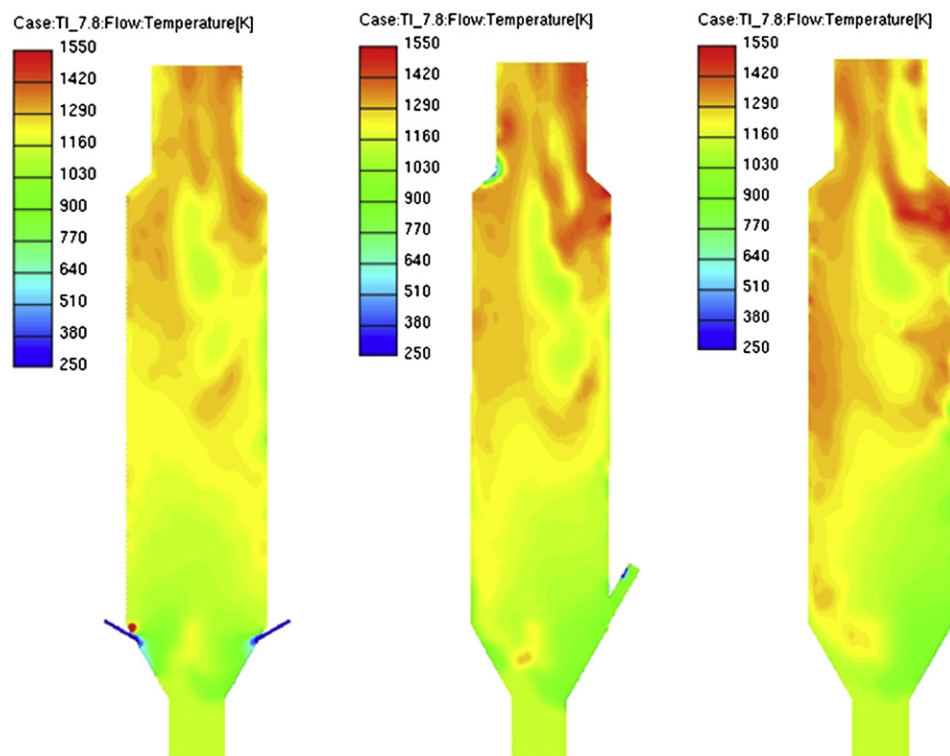
Fig. 4. Temperature field in vertical plane: section A-A (left); section B-B (middle); section C-C (right).
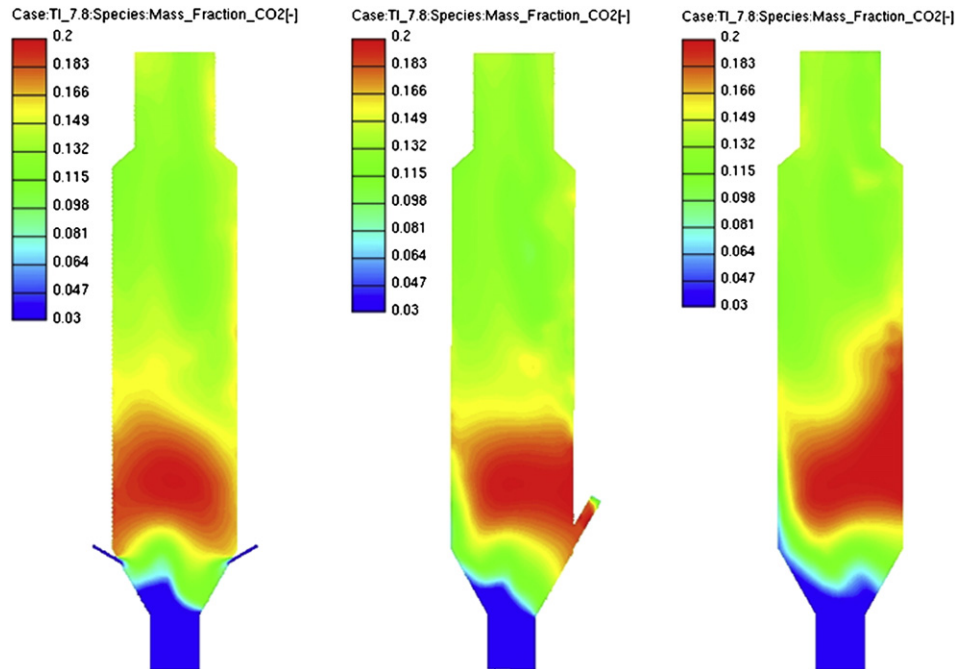
Fig. 5. CO$_2$ mass fraction in vertical plane: section A-A (left); section B-B (middle); section C-C (right).
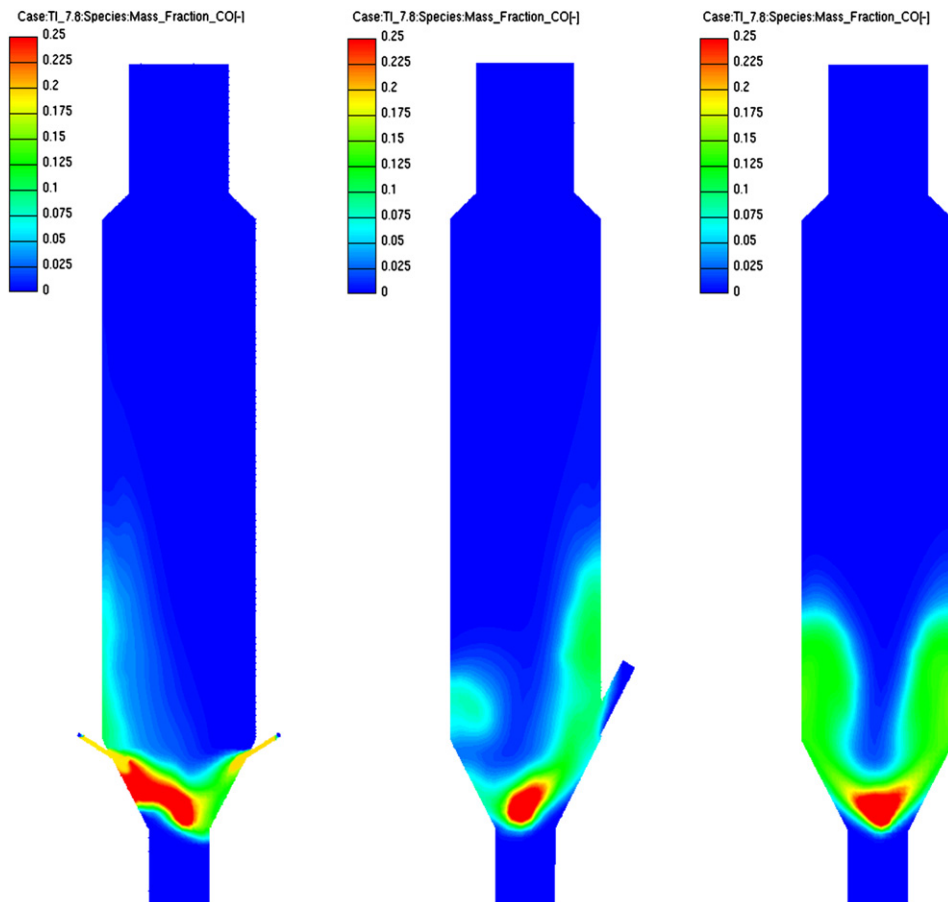
Fig. 6. CO mass fraction in vertical plane: section A-A (left); section B-B (middle); section C-C (right).
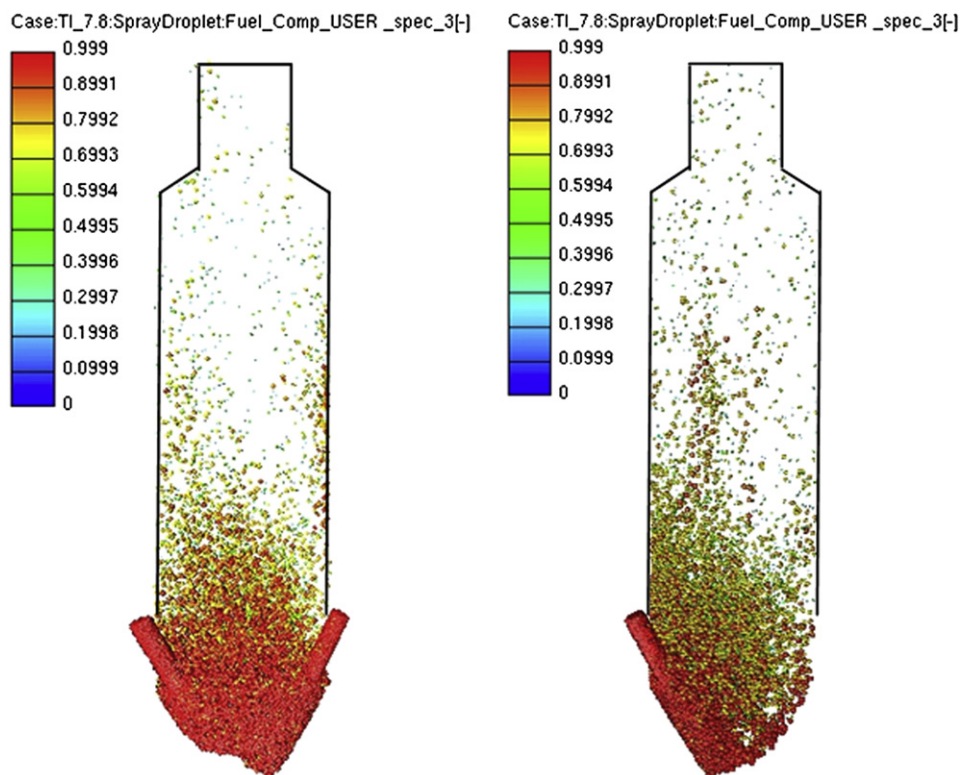
Fig. 7. Limestone (CaCO₃) particle: section A-A (left); section C-C (right).

The grid-size dependency for calcination calculation was analysed in our previous study [21]. Based on these results, 95 000 cells were employed to discretize the computational domain (Fig. 2) used in the simulation of the cement calciner. The calculation of the

values of variables at cell faces has a profound effect on the accuracy and the convergence, e.g., numerical stability, of the numerical method. For that reason, the differencing scheme used for momentum, continuity and enthalpy balances was MINMOD
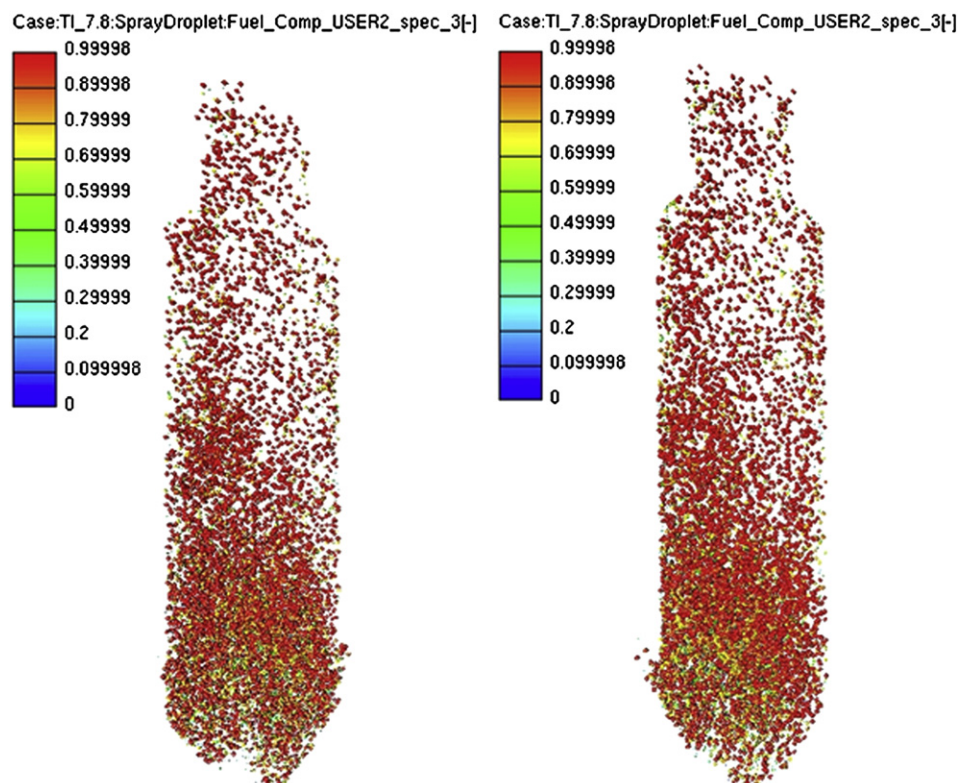
Fig. 8. Lime (CaO) particle: section A-A (left); section C-C (right).

Relaxed [36–38]. MINMOD Relaxed is a differencing scheme that combines advantages of the Upwind and the Central Differencing scheme. For the turbulence and scalar transport equations, an Upwind scheme was applied. The most favoured method for modelling turbulent flows in industrial applications is the Reynolds Averaged Navier–Stokes equations (RANS) with an appropriate turbulence model. Many turbulent models employ the concept of a turbulent viscosity or a turbulent diffusivity to approximate the turbulent Reynolds stresses and the turbulent heat fluxes. Turbulence was modelled by the standard $k–\varepsilon$ model. This is the most widely used turbulence model in CFD simulations of practical engineering applications. It is numerically robust, offering a reasonable compromise between computational effort and accuracy, and it is generally accepted that the $k–\varepsilon$ model yields reasonably realistic predictions of major mean-flow features in most situations [25,39]. For these reasons, the $k–\varepsilon$ model is used in this work. The tertiary air entered the domain with the velocity of 24 m/s, limestone with 1.5 m/s, coal with 11.5 m/s, and static pressure of 10^5 Pa was used for the outlet boundary condition. The boundary conditions used for the calciner simulation are given in Fig. 2, and the initial conditions used for the calciner calculation are summarized in Table 2.

2.2.3. Results and discussion

Fig. 2 also shows the top view of the calculated calciner with the cross section views that are presented in the following figures.

Fig. 3 shows the velocity field in three different cross sections for the calculated cement calciner. In the central part of the calciner, where the calcination reaction takes place, the velocity is around 3–5 m/s. As can be seen, a region with higher velocity occurs in the near wall region, and continues to the upper conical part and the outlet of the calciner. Section C–C clearly illustrates that the velocity in the region with the higher velocity is around 19–25 m/s, while in the middle of the calciner it is around 3–5 m/s. The main coal and raw material inlet are in the lower conical part of the calciner and from section C–C it can seen that the velocity in that part of the calciner is around 20 m/s. The Reynolds number on the inlet of the tertiary air is around 3.5×10^5.

Fig. 4 shows the temperature field in three different cross sections for the calculated cement calciner. As can be seen, the highest temperature occurs in the region where coal combustion is taking place. In that region, the average temperature is around 1200 °C. In the central part of the calciner, i.e. especially in the lower part and in the transition range to the combustion zone, where the limestone decomposition is taking place, the temperature is around 950 °C. This is the desirable temperature for the calcination process, slightly higher than the decomposition temperature of limestone, which ensures the process of calcination.

From Fig. 5 it is clear that the highest concentration of CO_2 is in the region where the decomposition of limestone is taking place, i.e. in the lower conical part of the calciner. It can also be seen that the concentration of CO_2 is decreasing towards the calciners outlet. This is due to the smaller limestone concentration.

Fig. 6 shows the concentration of CO in three different cross sections for the calculated cement calciner. It can be seen that the concentration of CO is highest in the lower part of the calciner. The
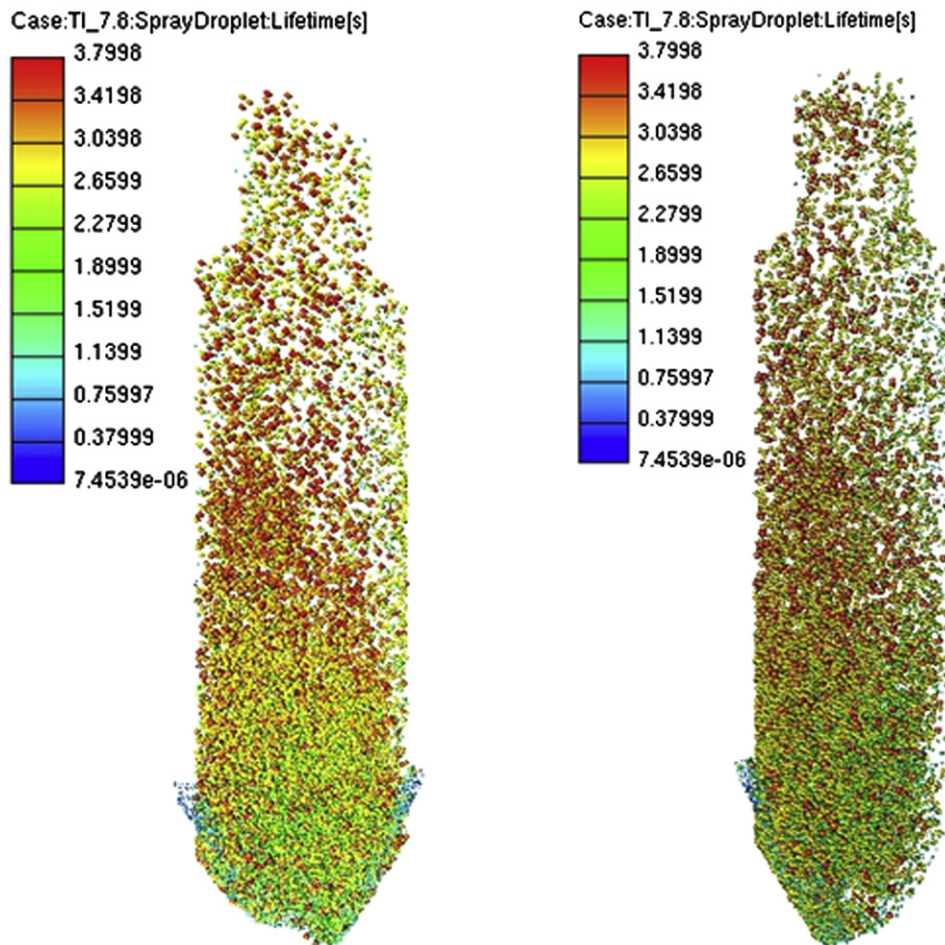

Fig. 9. Particle residence time section A-A (left); section C-C (right).

reason for this is the incomplete combustion of coal. It is harmful to have CO in the exhaust gases, however it can be seen that in the middle part of the calciner, CO further oxidises and forms CO_2.

Fig. 7 shows the portion of limestone in the entering raw material particle. Red represents 100% of limestone in the particle. The other colours represent a lower portion of limestone in the particle, with blue representing a fully decomposed limestone particle, i.e. a lime particle. For completeness, the overall contour of the limestone and lime particles is given. The 'empty' regions inside this contour indicate the regions where conversion, to a large extent, has already been completed. Also, it can be seen that the particles are carried with higher velocity, and consequently they are on one side of the calciner.

Fig. 8 shows the portion of lime in the entering raw material particle. Red represents 100% of lime in the particle, the rest of the colours represent a lower portion of lime in the particle. Also, from this figure it can be concluded that the particles are carried with the higher velocity, and consequently, they are mostly on one side of the calciner.

Fig. 9 shows the particle residence time. The coal particles are also shown. They are mainly located at the outer regions on the right side of the figure. It can be noted that the calculated residence time of both coal and lime/limestone particles is around 3.5 s.

There are no experimental data available for this calciner. Therefore, we could not compare the numerical predictions. However, validation of the calcination model, used for this calculation, was performed in our previous study [21]. The results achieved by this calculation demonstrate that the developed model for the calcination process [21] coupled with the commercial CFD code, is a suitable and promising tool for plant optimization. That was the focus of this study. Although the validation or the verification of a developed numerical model with experimental data is essential for such studies, it should be noted that the placement of the appropriate instrumentation for specific data recording and extraction (like fluid velocities components, peak spatial temperatures at high frequency rates) is not possible in fully operational devices. Also, for many reasons, related to production alteration rates and/or the altered fuel and raw material supply, the experiment's measurement repeatability is practically impossible under such conditions. Here it is worth noting that the measurement quantities acquired by the plant's measurement devices, motoring magnitudes like temperatures, fuel consumption, volumetric flows may, and should, be compared with the data provided by the simulations, as those data remain many times the only evidence in real working conditions.

The calcination process in a calciner is an energy saving process, which was also shown by the analytic calculation of CO_2 emissions. The cement calciner is supplied with appropriate quantity of fuel in order to achieve the calcination process. If this process takes place in the rotary cement kiln, the fuel supply should ensure that the main core temperature will exceed the 1450 or 1500 °C for length larger than 2/3 of total device in order to achieve firstly the calcination and then the clinkering process. The calcination process in a calciner is performed under significantly lower temperatures, approximately 850 °C, saving fuel and reducing the extra CO_2 which would be produced by extra fuel supply.

3. Conclusion

The CO_2 emissions created by the cement production systems have enhanced environmental concerns in the context of the present discussion on required CO_2 emission reduction efforts. From the analytical calculation of possible CO_2 reductions for a cement plant in Croatia, it is clear that a CO_2 emission reduction is possible by using a calciner prior to a rotary kiln. The present paper demonstrates that CFD can serve as an advanced tool to analyse and improve the understanding of all thermo-chemical reactions occurring in real industrial configurations. This understanding can further on be used for the optimization of cement calciner's geometry and operating conditions. By optimizing its operating conditions, a reduction of fuel consumption can be achieved, resulting in the reduction of CO_2 emissions. The presented mathematical model is detailed enough to predict velocity, temperature, and all relevant physical and chemical processes needed for a CFD simulation of a cement calciner. From the results shown, it can be concluded that the physical expectations are well described with the presented mathematical model. Thus, the presented simulation method can be applied for the investigation and optimization of cement calciners in order to improve energy efficiency and reduce greenhouse gas emissions.

Nomenclature

$m_{CO_2(combustion)}$	CO_2 combustion emissions, t
m_{fuel}	fuel consumption, t
H_d	lower calorific value, TJ/t
e_{fuel}	fuel emission factor, tCO_2/TJ
O_x	oxidation factor, dimensionless
$m_{CO_2(process)}$	CO_2 clinker production, t
$m_{clinker}$	clinker production, t
e	emission factor, tCO_2/t
f	conversion factor, dimensionless
A_{geom}	sphere surface, m^2
A_{por}	overall reaction surface, m^2
D	diffusion coefficient, $m^2\,s^{-1}$
k	overall reaction rate, $kg\,m^{-2}\,s^{-1}$
d	particle diameter, m
T	temperature, K
$\tilde{k}_{ch}$	chemical reaction rate, $kg\,m^{-2}\,s^{-1}$
k_{ch}	chemical reaction rate, $mol\,m^{-2}\,s^{-1}$
$\bar{k}_{ch}$	chemical reaction rate, s^{-1}
R_{CO_2}	CO_2 gas constant, $J\,kg^{-1}\,K^{-1}$
p_{CO_2}	CO_2 partial pressure, Pa
p_{eq}	equilibrium CO_2 partial pressure, Pa
d_{part}	particle diameter, m
k_{ph}	physical reaction rate, $kg\,m^{-2}\,s^{-1}$
k_D	reaction rate, $mol\,m^{-2}\,s^{-1}\,Pa^{-1}$
p_{ref}	referent pressure, Pa
Sh	Sherwood number, dimensionless
f_m	mechanism factor, dimensionless

Greek symbols

η	pore efficiency factor, dimensionless

References

[1] Stefanović G, Vučković G, Stojiljković M, Trifunović M. CO_2 reduction options in cement industry – the Novi Popovac case. Thermal Science 2010;14:671–9.
[2] Cement Technology Roadmap. Carbon emission reduction up to 2050. Available at: International Energy Agency http://www.iea.org/; 2009 [accessed 2.2.2011].
[3] Fidaros DK, Baxevanou CA, Vlachos NS. A parametric study of a solar calcinator using computational fluid dynamics. Energy Conversion and Management 2007;48:2784–91.
[4] Fidaros DK, Baxevanou CA, Dritselis CD, Vlachos NS. Numerical modeling of flow and transport processes in a calciner for cement production. Powder Technology 2007;171:81–95.
[5] Iliuta I, Dam-Johansen K, Jensen A, Jensen LS. Modeling of in-line low-Nox calciners – a parametric study. Chemical Engineering Science 2002;57: 789–803.
[6] Huanpeng L, Wentie L, Jianxiang Z, Ding J, Xiujian Z, Huilin L. Numerical study of gas–solid flow in a precalciner using kinetic theory of granular flow. Chemical Engineering Journal 2004;102:151–60.

[7] Hu Z, Lu J, Huang L, Wang S. Numerical simulation study on gas−solid two-phase flow in pre-calciner. Communications in Nonlinear Science and Numerical Simulation 2006;11:440−51.

[8] Bluhm-Drenhaus T, Simsek E, Wirtz S, Scherer V. A coupled fluid dynamic-discrete element simulation of heat and mass transfer in a lime shaft kiln. Chemical Engineering Science 2010;65:2821−34.

[9] Hayashi D, Krey M. Assessment of clean development mechanism potential of large-scale energy efficiency measures in heavy industries. Energy 2007;32: 1917−31.

[10] Akashi O, Hanaoka T, Matsuoka Y, Kainuma M. A projection for global CO_2 emissions from the industrial sector through 2030 based on activity level and technology changes. Energy 2011;36:1855−67.

[11] Koumboulis FN, Kouvakas ND. Indirect adaptive neural control for precalcination in cement plants. Mathematics and Computer in Simulation 2002;60: 325−34.

[12] Kääntee U, Zevenhoven R, Backam R, Hupa M. Cement manufacturing using alternative fuels and the advantages of process modeling. Fuel Processing Technology 2004;85:293−301.

[13] Gartner E. Industrially interesting approaches to "low-CO_2" cements. Cement and Concrete Research 2004;34:1489−98.

[14] Vujanović M, Duić N, Galović A. Three-dimensional numerical simulation of the nitrogen oxides formation in an oil-fired furnace. Strojarstvo 2007;49:165−71.

[15] Pardo N, Moya JA, Mercier A. Prospective on the energy efficiency and CO_2 emissions in the EU cement industry. Energy 2011;36:3244−54.

[16] Liu F, Ross M, Wang S. Energy efficiency of China's cement industry. Energy 1995;20(7):669−89.

[17] Hasanbeigi A, Menke C, Price L. The CO_2 abatement cost curve for Thailand cement industry. Journal of Cleaner Production 2010;18:1509−18.

[18] Worrell E, Martin N, Price L. Potentials for energy efficiency improvement in the US cement industry. Energy 2000;25:1189−214.

[19] Sheinbaum C, Ozawa L. Energy use and CO_2 emissions for Mexico's cement industry. Energy 1998;23(9):725−32.

[20] Szabó L, Hidalgo I, Ciscar JC, Soria A. CO_2 emission trading within the European Union and annex B countries: the cement industry case. Energy Policy 2006;34:72−87.

[21] Mikulčić H, von Berg E, Vujanović M, Priesching P, Perković L, Tatschl R, et al. Numerical modelling of calcination reaction mechanism for cement production. Chemical Engineering Science 2012;69(1):607−15.

[22] BAT Guidance Note on Cement Industry, CARDS. Project further approximation of croatian legislation with the environmental acquis. Available at: http://www.mzopu.hr/; 2004 [accessed 17.8.2010].

[23] Methodology for the free allocation of emission allowances in the EU ETS post. Sector report for the cement industry − Available at: http://ec.europa.eu/clima/studies/ets/benchmarking_en.htm; 2012 [accessed 27.1.2011].

[24] [In Croatian]. Zagreb, CroatiaInstructions for tracking and reporting of greenhouse gas emissions from the facility resulting from the activities listed in annex I of the regulation on greenhouse gas emission quotas and emissions trading; 2009.

[25] Vujanović M. Numerical modeling of multiphase flow in combustion of liquid fuel. PhD-thesis, University of Zagreb, Zagreb, Croatia; 2010.

[26] Baburić M, Duić N, Raulot A, Coelho PJ. Application of the conservative discrete transfer radiation method to a furnace with complex geometry. Numerical Heat Transfer, Part A, Applications 2005;48:297−313.

[27] Baburić M, Raulot A, Duić N. Implementation of discrete transfer radiation method into SWIFT computational fluid dynamics code. Thermal Science 2004;8:293−301.

[28] Vujanović M, Duić N, Tatschl R. Validation of reduced mechanisms for nitrogen chemistry in numerical simulation of a turbulent non-premixed flame. Reaction Kinetics and Catalysis Letters 2009;96:125−38.

[29] Silcox GD, Kramlich JC, Pershing DW. A mathematical model for the flash calcination of dispersed $CaCO_3$ and $Ca(OH)_2$ particle. Industrial Engineering Chemistry 1989;28:155−60.

[30] Schneider M. Experimentelle und mathematische Modellierung der Festbettvergasung am Beispiel der Gleichstromvergasung von Holzhackschnitzeln. PhD-thesis TU Dresden, Germany; 2003.

[31] Levenspiel O. Chemical reaction engineering. 2nd ed. New York: J. Wiley and Sons; 1972. p. 482.

[32] Froment G, Bischoff K. Chemical reactor analysis and design. 2nd ed. New York: J. Wiley and Sons; 1990. p. 160.

[33] Ban M, Duić N. Adaptation of n-heptane autoignition tabulation for complex chemistry mechanisms. Thermal Science 2011;15:135−44.

[34] Görner K. Technische Verbrennungssysteme, Grundlagen, Modelbildung, Simulation. Berlin, Heidelberg: Springer-Verlag; 1991.

[35] Jones WP, Lindstedt RP. Global reaction scheme for hydrocarbon combustion. Combustion and Flame 1988;73:233−49.

[36] FIRE_v2011_Manuals.

[37] Harten A. High resolution schemes using flux limiters for hyperbolic conservation laws. Journal of Computational Physics 1983;49:357−93.

[38] Harten A. High resolution schemes for hyperbolic conservation laws. Journal of Computational Physics 1991;49:225−32.

[39] Blazek J. Computational fluid dynamics: principles and applications. Amsterdam, London, New York, Oxford, Paris, Shannon, Tokyo: Elsavier; 2001.

PAPER 3
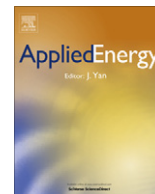
Reducing the CO₂ emissions in Croatian cement industry

Hrvoje Mikulčić *, Milan Vujanović, Neven Duić

Faculty of Mechanical Engineering and Naval Architecture, University of Zagreb, Ivana Lučića 5, 10000 Zagreb, Croatia

ARTICLE INFO

ABSTRACT

Cement industry is one of the largest carbon emitting industrial sectors. It is responsible for about 5% of anthropogenic CO_2 in the world. Therefore, it is a relevant industrial sector for CO_2 emission regulation strategies. Bearing in mind the importance of cement industry in Croatia, and because of the fact that Croatia will soon become an EU member state, the present paper analyses the potential to reduce CO_2 emission in the Croatian cement industry. There are several measures that can reduce CO_2 emissions from the cement manufacturing process: the use of waste heat as an alternative source of energy; CO_2 capture and storage technologies; reduction of clinker to cement ratio; the use of alternative and biomass fuels; the use of alternative raw materials; an energy efficient combustion process. The most energy efficient technology for cement manufacturing today is the use of a rotary kiln together with a multi-stage pre-heater and a calciner. Since the use of cement calciners is a relatively new technology, further improvement of their operating conditions is still needed. This paper also highlights the results of research in the field of computational fluid dynamic (CFD) simulations that are used for the investigation of process and combustion emissions. The above mentioned measures together with numerical investigations can reduce the effect of cement manufacturing in Croatia on the environment and can make it more competitive with cement manufacturers from the EU.

© 2012 Elsevier Ltd. All rights reserved.

1. Introduction

There is indisputable evidence that the build-up of man-made greenhouse gases in atmosphere cause changes in the global climate that will have increasingly severe human, environmental and economic impacts over the coming years [1]. Climate change problems are addressed by two major international agreements: the 1992 United Nations Framework Convention on Climate Change (UNFCCC) and the 1997 Kyoto Protocol. The ultimate objective of these agreements is to stabilise greenhouse gas concentrations in the atmosphere at a level that would prevent dangerous anthropogenic interference with the global climate system. The Republic of Croatia has been a party of the UNFCCC since 1996 and the Kyoto Protocol was ratified in 2007 with a commitment of limitation of greenhouse gas emission in the 2008–2012 period to the level of 95% of the 1990 base year [2]. In the post-Kyoto period, Croatia, as a future EU member state, has set itself the intermediate goal of reducing the overall greenhouse emissions by at least 20% by 2020, and the long-term goal of reducing its emission to 80% below 1990 levels by 2050. To reach this goal, increase of the energy efficiency comes first, followed by significant

increase of the use renewable energy sources for electricity generation, transportation and other sectors [3].

Cement industry is one of the largest carbon emitting industrial sectors in the world, being the third largest carbon emitting industrial sector in the EU [4]. It contributes to about 5% of world's anthropogenic CO_2 [5,6], in the EU it accounts about 4.1% of the total CO_2 emissions [7]. Since the EU has proved to be a frontrunner in implementing the emission reduction targets and addressing climate change, in 2005, the EU Emissions Trading Scheme (EU ETS) for greenhouse gases was launched [8]. Cement manufacturers within the EU are obliged to participate in this trading scheme, due to high CO_2 emissions. Cement production is not only a source of combustion related CO_2 emissions, but it is also the largest sources of industrial process related CO_2 emissions in Croatia, and therefore CO_2 reduction measures will be required to keep cement industry emissions in line with levels set in Kyoto and post-Kyoto period. During the cement manufacturing process almost 90% of CO_2 is emitted from two thermo-chemical processes which occur in the process of cement production. One is the calcination process, which contributes with 50% of CO_2 emission, and the other is the combustion of the solid fuels, which contributes with 40% of CO_2 emission. Remaining 10% of CO_2 are emitted during the transport of raw material and some other production processes. The only way to reduce the CO_2 emission from the calcination process is to use alternative raw materials, but so far there have been no such materials from which that kind of cement, with at least as

* Corresponding author. Tel.: +385 1 6168 494; fax: +385 1 6156 940.
E-mail addresses: hrvoje.mikulcic@fsb.hr (H. Mikulčić), milan.vujanovic@fsb.hr (M. Vujanović), neven.duic@fsb.hr (N. Duić).

good performance and durability characteristics as the current Portland-based cements, could be produced. Following this fact Gartner [9] studied the alternative hydraulic cements to lower CO_2 emissions. The study showed that with replacing the limestone with different raw materials for cement production, a CO_2 emission reduction can be achieved, but the product will be too expensive to the consumer. That is why, for now, the only way to reduce the CO_2 emission is to use more fuel efficient technologies. The best available technology, the one with the lowest energy consumption, for the cement manufacturing today, is the use of a rotary kiln together with a calciner. Szabo et al. [4] reported that an energy consumption decrease of 8–11% can be achieved if a cement calciner is used prior to the rotary kiln. The calciner is a separate furnace in which the calcination process occurs, and after that the material goes to the rotary kiln where the clinkering process occurs. This improvement in the energy consumption, by simply dividing the calcination and the clinkering process, can be calculated also as a CO_2 emission reduction.

Because cement calciners are relatively a new technology in the cement manufacturing process, further improvements of their operating conditions are needed. With the aim of improving the operating conditions, different calciners, as well as the chemical and physical processes occurring inside the calciner [10], have been studied. Huanpeng et al. [11] using a two-dimensional model and the kinetic theory of granular flow to represent the transport properties of the solid phase, studied the influence of different parameters on the dynamics of the two-phase flow in a calciner. Iliuta et al. [12] based on the reaction–diffusion approach for combustion and calcination developed a mathematical model for an in-line low-NO_x calciner. Fidaros et al. [13] demonstrated a numerical model and a parametric study of the gaseous flow and the transport processes taking place in a vertical industrial low NO_x calciner. The study showed good predictions for velocity, temperature and distribution of particles.

Aside from the studies investigating the cement production, due to the increased environmental awareness, several studies investigated environmental aspects and in particular, the potential of CO_2 emission reduction in this sector. Hence, in [14] relatively high economic and environmental effectiveness of climate change mitigation measures has been demonstrated for Macedonian industrial sector, including cement industry. Furthermore, Mokrzycki et al. [15] presented the economical and ecological benefits of using alternative fuels in Polish cement plants. The study, for the presented two cement plants, shows that combustion of alternative fuels is an environmentally friendly method of waste utilization. Mokrzycki and Uliasz-Bocheńczyk [16] demonstrated the types of alternative fuels that can be used for the combustion in the cement manufacturing process, showing that the use of wastes as alternative fuels also reduces energy costs of cement production. Fodor and Klemeš [17] studied the use of waste as an alternative fuel and discussed the applicability and limitations of current and developing waste-to-energy technologies. The study focuses on how the different technologies are being developed, to enable energy to be produced from different types of waste, while simultaneously minimizing emissions. Kääntee et al. [18] studied the use of alternative fuels in the cement manufacturing process. The study provides useful data for the optimization of the manufacturing process when alternative fuels, instead of conventional fossil fuels, are used for the combustion. Because shredder dust is an industrial by-product which must be disposed in an environmental friendly way, Kakimoto et al. [19] examined the effectiveness of the use of fine-grained shredder dust as a cement admixture. First they crushed the molten shredder dust and then mixed it with the ordinary Portland cement to form a new cement mortar. The new cement mortar was then tested, and the results of this test showed that the long-term strength of cement was not

deteriorated. Bassioni [20] reported that the use of up to 5% limestone as an admixture in the ordinary Portland cement, does not affect its performance, and in the same time minimizes the CO_2 emissions from the cement manufacturing process. In order to reduce the energy consumption in the cement manufacturing process, since approximately 40% of the total input energy is being lost, Wang et al. [21] studied the use of a cogeneration power plant in cement industry. The cogeneration plant in a cement plant could recover the heat lost through hot flue gases and cooler stack, and in that way generate electrical energy and reduce the CO_2 emissions from the cement manufacturing process. Since CO_2 emissions from the industrial sectors, one of them the cement industry, are major contributors to the global warming, Wang et al. [22] studied the capturing the CO_2 from the flue gases. Worrel et al. [23] made an in-depth analysis of the US cement industry, showing that the use of blended cement in cement manufacturing process is the most efficient method for CO_2 emission reduction. Jaber [24] reported that the cement industry in Jordan is the industrial sector with highest CO_2 emissions. To achieve an annual reduction of 90,000 tonnes of CO_2 emitted from Jordanian cement industry, an increase in the energy efficiency of the grinding and the calcination process is needed.

The purpose of this paper is to analyse the current status of Croatian cement industry and the possibilities of reducing the CO_2 emissions. The development of the Croatian cement industry was analysed with different scenarios. These scenarios show that there is a possibility for a more sustainable development of this industrial sector in Croatia. In addition, a previously developed mathematical model of the calcination process [10], which contains the relevant physical and chemical processes as, e.g., Arrhenius rate approach, pressure limitation, diffusion resistance, porosity, tortuosity, pore size and pore efficiency, was used for the numerical investigation of a cement calciner. By using this detailed mathematical model, a progress in understanding of the thermo-chemical processes occurring inside a calciner was made. The results gained by this numerical simulation show that CFD can be a useful tool for the optimization of the calciner's operating conditions. Hence, by using CFD and optimizing calciner's operating conditions, less fuel will be used, and therefore a decrease of CO_2 emissions will be achieved.

2. Cement production in Croatia

Production of cement and clinker in Croatian cement plants is based on the dry kiln process. There are five operating cement plants in Croatia (Table 1), which produce Ordinary Portland Cement. Three of them have multi-stage cyclone preheater plus a calciner in their kiln process, and rest two have a multi-stage cyclone preheater kiln process. The general decline in economic activity during the period 1991–1995, particularly because of the war in Croatia, led to a reduction in cement production. However, in 1996, cement production began to rise until 2003, while in the period 2003–2008 the production was almost at same level. The another decline in economic activity, primarily due to recession and the related economic downturn during the period 2008–2010, led

Table 1
Cement plants currently (2011) operating in Croatia.

Group	Plant
Cemex	Sveti Juraj
	Sveti Kajo
	10. kolovoz
Holcim	Koromačno
Nexe	Našice

Fig. 1. Cement production in Croatia.

Table 3
Typical electrical energy consumption during the cement manufacturing process [27].

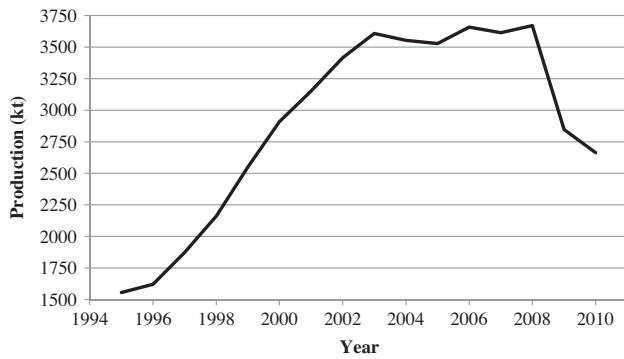| Sub-process/equipment	Electrical energy consumption (kW h/t cement)	Share (%)
Mining, crushing and stacking	1.50	2.00
Raw meal grinding and transport	18.00	24.00
Kiln feed, kiln and cooler	22.00	29.30
Coal mill	5.00	6.70
Cement grinding and transport	23.00	30.70
Packing	1.50	2.00
Lighting, pumps and services	4.00	5.30
Total	75.00	100.00

to a new reduction of cement production with approximately 2.6 million tonnes of produced cement, with an average clinker to cement ratio 0.77. Fig. 1 shows the production of cement in Croatia from 1995 to 2010.

In the operating cement plants (Table 1), various fossil fuels are used, mostly pulverized coal. Due to the increased environmental awareness, cement plant operators are starting to use alternative fuels. So far, used oil and tires have been mostly used as alternative fuels, and their share in the total fuel consumption of Croatian cement industry is around 2% [25], which is still a very modest share.

The energy efficiency of a cement plant is evaluated by comparing the specific energy consumption of that particular cement plant with the specific energy consumption of a benchmark. The specific energy consumption can also be used for the evaluating and tracking of any improvements in the energy efficiency of the production process. The average specific thermal energy consumption of a kiln process is shown in Table 2. It can be noted that the pre-heating of the raw material can reduce energy consumption significantly.

The values of electrical specific energy consumption for different sub-processes of the cement manufacturing process are shown in Table 3. It can be noted that grinding and transportation, together with the kiln and the cooler consume almost 85% electricity needed for the cement manufacturing process.

The reported [25] average value of the specific thermal energy consumption of Croatian cement industry is 3.4 GJ/t clinker and the specific electrical energy consumption is about 113 kW h/t cement.

Cement manufacturers contribute to approximately 4–9% of Croatian total greenhouse gases emissions [25]. Cement industry CO_2 emissions mainly come directly from the calcination process and the combustion of fossil fuels. An indirect amount of CO_2 comes from the consumption of electricity needed for the manufacturing process. As mentioned, approximately half of CO_2 emissions come from the calcination process (see Eq. (2)). In this study, the CO_2 emissions from the cement production systems in Croatia have been calculated for the period 1995–2010, according to the IPCC methodology [28]. The results (see Fig. 2) show that CO_2 emissions from cement manufacturing in Croatia, grew almost steadily until 2008 when the economic crisis started, and due to the decreased cement production, the CO_2 emissions from the cement production decreased.

3. Mitigation scenarios

Currently, the cement industry worldwide is facing increscent challenges in conserving raw material and energy resources, as well as reducing the CO_2 emissions from the cement manufacturing process [29]. There are several different effective measures which can reduce the CO_2 emissions from the cement manufacturing process. The most effective way is to capture CO_2 from the flue gases and store it. This can reduce carbon emissions by 65–70%, but due to high cost of this technology, and because so far only laboratory size CCS devices are available, CCS technologies have not yet found wide application in the industry [30]. Additionally to high cost of the CCS technologies, Roddy [31] analysed the development of CO_2 networks which can accommodate CO_2 emissions from industrial facilities. Another effective measure, which can reduce CO_2 emissions significantly, is the reduction of clinker to cement ratio with the addition of different additives. Replacing fossil fuels with alternative fuels may play a major role in the reduction of CO_2 emissions as well. The use of alternative raw materials can reduce CO_2 emissions as well. Improving the energy efficiency of the kiln process is also one of the possibilities of CO_2 emissions reduction. Most of these measures are influenced to a large extent by environmental policy and legal framework and integration of

Table 2
Specific thermal energy consumption of a kiln process [26].

| Kiln process	Thermal energy consumption (GJ/t clinker)
Wet rotary kiln	5.86–6.28
Dry long rotary kiln	4.60
Dry rotary kiln with 1-stage cyclone preheater	4.18
Dry rotary kiln with 2-stage cyclone preheater	3.77
Dry rotary kiln with 4-stage cyclone preheater	3.55
Dry rotary kiln with 4-stage cyclone preheater and calciner	3.14
Dry rotary kiln with 5-stage cyclone preheater, calciner and high efficiency cooler	3.01
Dry rotary kiln with 6-stage cyclone preheater, calciner and high efficiency cooler	<2.93
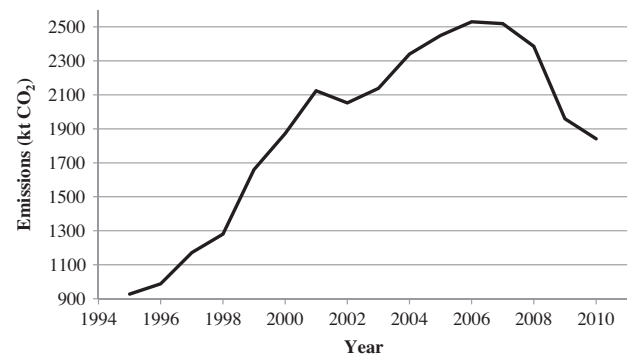
Fig. 2. CO_2 emissions from cement production.

these measures will only be possible if the policy framework will foster the cost-effective deployment of the best available technology.

The projected development of Croatian cement industry is presented through three different scenarios. The first scenario, BAU scenario, anticipates deployment of technological improvements that would have occurred regardless of the need to reduce CO_2 emissions, this can be considered as a "black" scenario. The other two scenarios, mitigation scenarios, integrate appropriate mitigation measures that will lessen the CO_2 emissions from cement production.

3.1. Specific mitigation costs

For the mitigation scenarios three different measures that reduce the CO_2 emissions from the cement manufacturing process were considered: (a) reduction of clinker to cement ratio; (b) the use of alternative fuels; (c) an energy efficient combustion process. The mitigation cost *MC* for each of the named measures was calculated according to the following equation:

$$MC = \frac{C_m - C_{BAU}}{E_{BAU} - E_m},\qquad(1)$$

where C_m is the equivalent annual cost of the mitigation scenario, C_{BAU} is the equivalent annual cost of the business as usual scenario, E_{BAU} is the annual CO_2 emission of the business as usual scenario, and E_m is the annual CO_2 emission of the mitigation scenario. When calculated, the specific cost of reduction of clinker to cement ratio is between (−0.4) and 0.5 €/t CO_2 reduced. For the use of alternative fuels the specific cost is between (−7) and (−5) €/t CO_2 reduced, while the specific cost of an energy efficient combustion process is between 8 and 17 €/t CO_2 reduced. From this figures it can be concluded that in the case of Croatian cement industry, named measures for CO_2 emissions reductions are economically viable.

3.2. Scenario definition

In these three scenarios an assumption was made that a steady growth of 2.5% in cement production will be achieved until 2020. The forecast for the development of the cement industry and the growth of cement production until 2020 was made based on the data obtained from the cement factories development plans.

3.2.1. Business as usual scenario

The BAU scenario is based on the exploitation of the existing resources, and includes the programs aimed at the market adjustments. The BAU scenario does not include the implementation of any measures to reduce CO_2 emissions. This scenario represents a reference level of CO_2 emissions, in relation to which, potential of CO_2 emissions reduction is calculated. The predicted CO_2 emissions for the BAU scenario until the year 2020 are shown in Fig. 3. From Fig. 3 it can be seen that according to the BAU scenario, in the period 2010–2020, an increase of 582 kt CO_2 in CO_2 emissions from the cement manufacturing process will be achieved.

3.2.2. First mitigation scenario

This scenario assumes the inclusion of mitigation measures to fulfil the CO_2 emissions reduction obligation. The first assumption of this scenario is that the specific energy consumption of a current benchmark will be achieved until the year 2020. The second one is that waste will be used as an alternative fuel for co-combustion in calciners and rotary kilns, and the last one is that an average clinker to cement ration of 0.7 will be achieved in 2020. The predicted CO_2 emissions for the first mitigation scenario until the year 2020, and the comparison with the BAU scenario, are shown in Fig. 4. From Fig. 4 it can be concluded that in the period 2010–2020, first
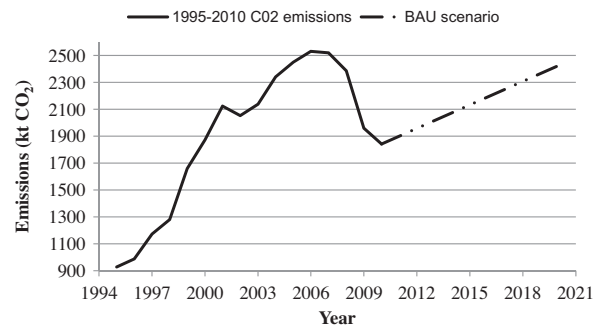

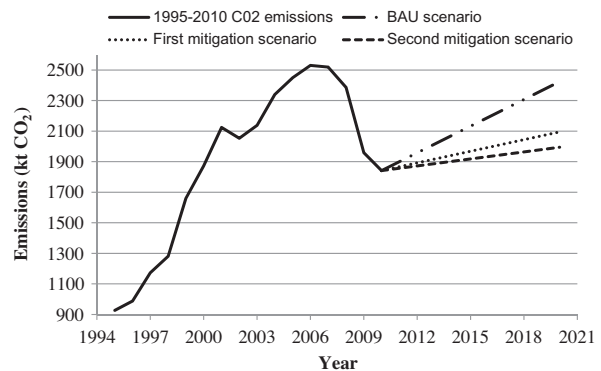**Fig. 3.** BAU scenario CO_2 emissions.

Fig. 4. Mitigation scenarios CO_2 emissions.

mitigation scenario in comparison with the BAU scenario decreases CO_2 emissions for 331 kt CO_2.

3.2.3. Second mitigation scenario

In this scenario assumption was made that even lower, to the one assumed in the first mitigation scenario, average clinker to cement ration of 0.65 will be achieved in 2020. The predicted CO_2 emissions for the second mitigation scenario until the year 2020, are also shown in Fig. 4. From Fig. 4 it can be seen that in the period 2010–2020, second mitigation scenario in comparison with the BAU scenario decreases CO_2 emissions for 429 kt CO_2.

4. Numerical investigation of a cement calciner

In order to reduce the atmospheric concentration of CO_2, an important environmental target for cement producers worldwide is the reduction of CO_2 emissions from their manufacturing process. As mentioned, there are several possibilities of CO_2 emissions reduction from the cement manufacturing process. Some of these measures are: the reduction of clinker to cement ratio; carbon capture and storage; use of alternative fuels; more energy efficient production, etc. The latter two can effectively be investigated with numerical simulations. To simulate the CO_2 emissions from the combustion of alternative fuels, models for the combustion of alternative fuels have to be developed. To have a more energy efficient combustion process, in-depth understanding of thermo-chemical processes, occurring in cement manufacturing devices, is needed. The understanding of the complex nature of combustion and calcination processes in experimental investigation is limited and can be significantly improved by computer simulation tools. Numerical models developed for cement calciners [10], can be used for numerical simulations of process and combustion emissions. Numerical simulations can be used to gain detailed knowledge

and required information about operation of devices in order to help cement manufactures to operate in a more energy efficient way. In this paper just the operating conditions for a cement calciner, for a more efficient cement production, is investigated.

4.1. Mathematical model

For an effective investigation of the operating conditions of a cement calciner the decomposition of limestone and the process providing the reaction enthalpy, e.g., the combustion of coal must be treated. The Lagrangian formulation is used for the motion and transport of solid particles through the cement calciner, and the Eulerian formulation is used for the solving of the gas phase [32]. The developed mathematical model [10] used for the calcination calculation is treated in the Lagrangian spray module, where thermo-chemical reactions occur inside a particle as well as between the particle and the gas phase. The developed calcination model was integrated into the commercial CFD code FIRE [33], and applied together with additional user functions for providing thermo-physical properties of limestone and lime as well as a particle radiation model [34–36]. The model takes into account the effects of temperature, decomposition pressure, diffusion, and pore efficiency. The model is detailed enough to contain the relevant physical and chemical processes, yet robust enough for detailed CFD simulations of calcination devices, i.e. cement calciners.

In general the calcination process can be presented by following equation:

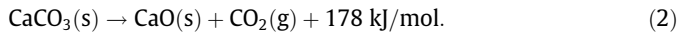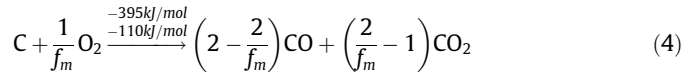$$CaCO_3(s) \rightarrow CaO(s) + CO_2(g) + 178 \text{ kJ/mol}. \tag{2}$$

Fig. 5 shows the validation of the developed calcination model. Large experimental error bars are due to the uncertainty in experimental measurements, however as can be seen, predicted numerical results are in good agreement with the mean experimental data. Thus, the developed calcinations model can be used for the investigation and optimization of calcination devices for cement production.

The coal combustion is modeled as a two stage process. Generally complex combustion systems, in FIRE solver, are treated by pre-tabulation or similar methods [37], but in this case the coal combustion is calculated directly. The coal particle, which is composed of pit-coal and ash, is first undergoing the pyrolitic decomposition into volatiles and char particle. In a subsequent step treated in parallel to the pyrolysis, the char particle is oxidized to CO and CO_2 taking into account a mechanism factor depending on temperature and particle size. A very simple composition, represented via chemical formula C_3H_4, for the pit coal is assumed. The treated heterogeneous chemical reactions are:

$$C_3H_4 \rightarrow 2C + CH_4, \tag{3}$$

and

$$C + \frac{1}{f_m}O_2 \xrightarrow[-110kJ/mol]{-395kJ/mol} \left(2 - \frac{2}{f_m}\right)CO + \left(\frac{2}{f_m} - 1\right)CO_2 \tag{4}$$

here f_m denotes the mechanism factor [38], which ranges between 1 and 2, causing predominant production of CO_2 for temperatures below about 900 K and predominant generation of CO for higher temperatures.

The homogeneous reactions of CO oxidation [38] and the combustion of methane, which is treated via the four step Jones–Lindstedt mechanism [39], are treated within the gaseous phase. Eq. (4) and (5) represent the CO oxidation and the four step Jones–Lindstedt mechanism for methane combustion.

$$CO + \frac{1}{2}O_2 \rightarrow CO_2 \tag{5}$$

$$\begin{aligned} CH_4 + \tfrac{1}{2}O_2 &\rightarrow CO + 2H_2 \\ CH_4 + H_2O &\rightarrow CO + 3H_2 \\ CO + H_2O &\leftrightarrow CO_2 + H_2 \\ H_2 + \tfrac{1}{2}O_2 &\rightarrow H_2O \end{aligned} \tag{6}$$
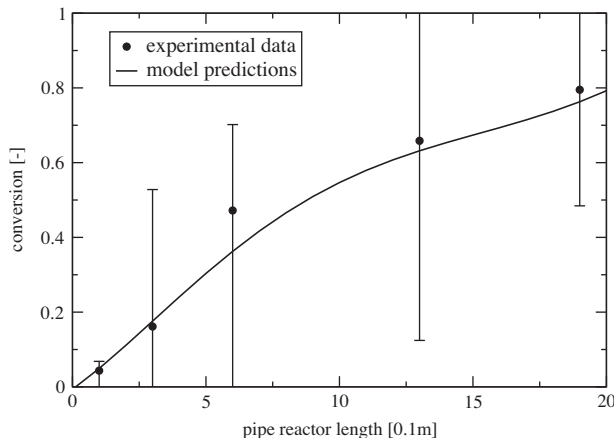
Fig. 5. Validation of the developed calcination model.

Fig. 6. Preview of flow characteristics inside a calciner.

The heterogeneous reactions cause mass transfer sources and sinks to the gas phase and particles, which are described by rate equations for pit coal consumption, char production from pyrolysis and consumption from oxidation.

4.2. Numerical simulation

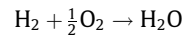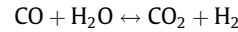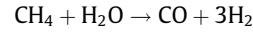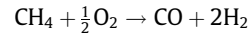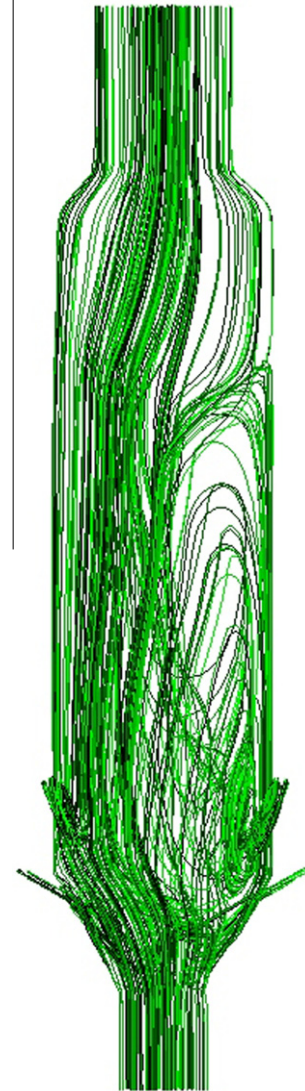Calciner geometry available in the literature [13], was used to investigate the thermo-chemical reactions occurring inside the calciner. The entire model is 32 m high, with three different diameters of cylinders, which make the calciner geometry, and two conical sections connecting them.

To discretize the computational domain 95000 cells were employed. The differencing scheme used for momentum and continuity balances was central differencing, and for turbulence, energy balances and scalar transport equations an Upwind scheme was applied. Turbulence was modeled by the standard $k - \varepsilon$ model. For practical engineering applications this is the most widely used turbulence model. It is numerically robust, and it is widely accepted that the $k - \varepsilon$ model yields reasonably realistic predictions of major mean-flow features in most situations.

5. Results and discussion

Fig. 6 shows the streamlines of the flow inside the calculated calciner. As can be seen, a region with recirculation occurs in the right part of the calciner, and afterwards continues with the higher velocity stream in the left part of the calciner to the upper outlet. Understanding of the flow characteristics inside a calciner is of essential importance for a plant operator, because limestone needs several seconds to completely decompose.

Fig. 7 shows the particle residence time. For a plant operator it is important to know the flow characteristics, particle residence time, and their distribution inside the calciner. It can be noted that the calculated residence time of particles inside of a calciner is around 3.5 s, and that the majority of the particles is in the lower part of the calciner. Together with the gaseous hot stream, particles go to the upper part of the calciner and exit the calciner.

Fig. 8 shows the temperature field for the calculated calciner. As can be seen, the highest temperature occurs in the region in the upper part of the calciner, where all limestone has already decomposed, and in that region the average temperature is around 1100 °C. In the central and in the lower part of the calciner, where the calcination takes place, the temperature is around 950 °C. This is the desirable temperature for the calcination process, which is slightly higher than the decomposition temperature of limestone, and that is why it ensures a stable calcination process.

From Fig. 9 it is clear that the highest concentration of CO_2 is in the lower part of the calciner, in the region where calcination takes place. What can also be seen from this figure is that the concentration of CO_2 decreases towards the calciner's outlet, because almost all of the limestone has decomposed.

Although the comparison of numerical predictions with experimental data is crucial for such kind of studies, experimental measurements are not available for this calciner. It should be noted that the placement of the appropriate instrumentation for specific data recording is not possible in a fully operational devices. Though there are no experimental data available for this calciner, the results obtained by this calculation show that the developed model for the calcination process [10] coupled with the commercial CFD code FIRE, is a suitable and promising tool for cement calciner optimization. Since energy efficiency is one of the mitigation measures for CO_2 emissions reduction, by using CFD as a tool for optimization
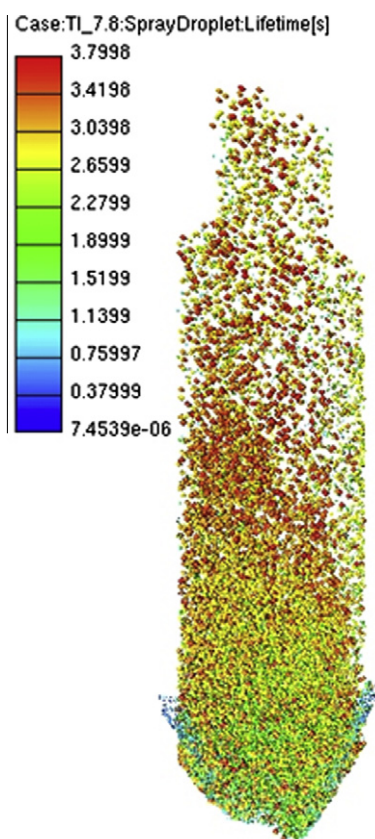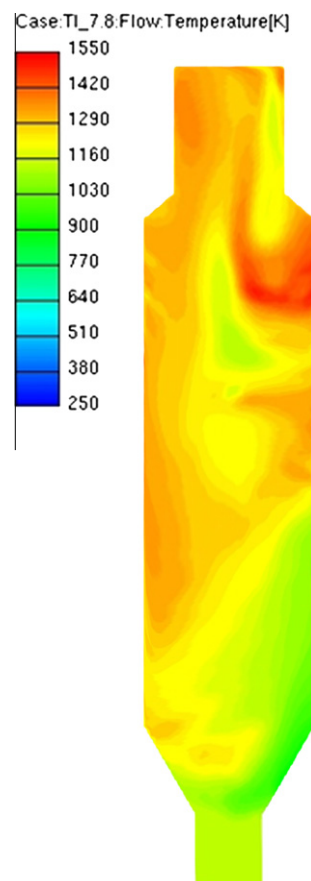

Fig. 7. Particle residence time.

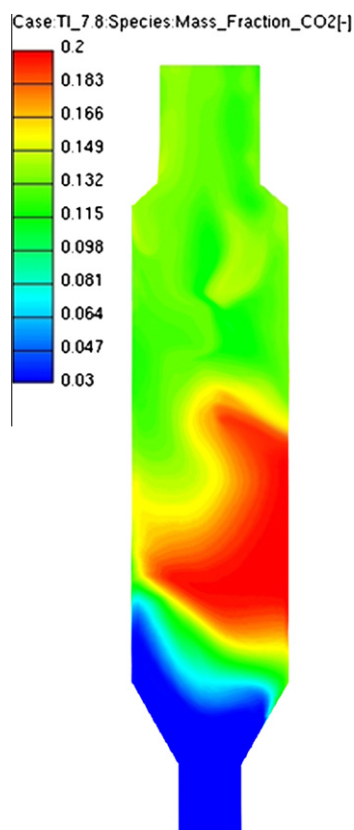Fig. 8. Temperature field in vertical plane.

Fig. 9. CO$_2$ mass fraction in vertical plane.

of calciner's operating conditions, a decrease of CO$_2$ emissions can be achieved. Results obtained by this study are essential for better understanding of achievable CO$_2$ emissions reductions and the understanding of thermo-chemical processes occurring inside a cement calciner.

6. Conclusion

Climate change is one of the most serious challenges facing modern society and a reduction of CO$_2$ emission in cement industry is one of the important measures for achieving the EU climate targets for 2020 and beyond. The paper analyses the potential for achieving CO$_2$ emission reduction in the Croatian cement industry. In the Croatian cement industry, there are three economically viable measures for reducing CO$_2$ emissions. The reduction of clinker to cement ratio by adding different additives, the replacement of fossil fuels with alternative and biomass fuels, and a further improvement in the energy efficiency of the existing kiln processes, are the economically viable measures which can decrease CO$_2$ emissions of the cement industry in Croatia. Three different scenarios were calculated to predict the achievable CO$_2$ emission reduction until the year 2020. The first scenario, BAU scenario, shows that if the current practices in Croatian cement industry are to be continued, an increase of 582 kt CO$_2$ in CO$_2$ emissions from the cement manufacturing process will be achieved until 2020. The other two scenarios, mitigation scenarios, show that if appropriate mitigation measures are to be used, a decrease of CO$_2$ emissions of 331 kt CO$_2$, for the first mitigation scenario in comparison with the BAU scenario, and a decrease of CO$_2$ emissions of 429 kt CO$_2$, for the second mitigation scenario in comparison with the BAU scenario, will be achieved until 2020. These figures show that the implementation of mentioned measures results in a considerable decrease of CO$_2$ emissions by 2020, thus

the mentioned measures are to be used to have a more sustainable cement production in Croatia.

Furthermore, since one of the named measures for CO$_2$ emissions reduction is energy efficient combustion process during the cement production, the paper highlights the results of research in the field of computational fluid dynamic (CFD) simulations. These results can be used for further investigation of CO$_2$ emissions coming from the calcination and combustion processes. The paper deals with the development of concepts for the numerical simulation of calcination and combustion processes, which are used to investigate and improve the understanding of the complex interacting physical and chemical phenomena occurring in calciner systems. The presented paper shows that CFD is a promising tool for the optimization of calciner geometry and operating conditions in order to increase the combustion efficiency and to reduce CO$_2$ emissions, both of which are essential in meeting future emission restrictions. The measures concerned here together with numerical investigations can reduce the effect of cement manufacturing in Croatia on the environment and can make it more competitive with cement manufacturers from the EU.

References

[1] IPCC Forth Assessment Report, <www.ipcc.ch/publications_and_data/publications_and_data_reports.shtml#1> [last accessed 09.02.12].
[2] Duić N, Juretić F, Zeljko M, Bogdan Ž. Croatia energy planning and Kyoto Protocol. Energy Policy 2005;33:1003–10.
[3] Vad Mathiesen B, Lund H, Karlsson K. 100% Renewable energy systems, climate mitigation and economic growth. Appl Energy 2011;88:488–501.
[4] Szabó L, Hidalgo I, Ciscar JC, Soria A. CO$_2$ emission trading within the European Union and Annex B countries: the cement industry case. Energy Policy 2006;34:72–87.
[5] Stefanović G, Vučković G, Stojiljković M, Trifunović M. CO$_2$ reduction options in cement industry – The Novi Popovac case. Therm Sci 2010;14:671–9.
[6] Fidaros DK, Baxevanou CA, Vlachos NS. A parametric study of a solar calcinator using computational fluid dynamics. Energy Convers Manage 2007;48:2784–91.
[7] Pardo N, Moya JA, Mercier A. Prospective on the energy efficiency and CO$_2$ emissions in the EU cement industry. Energy 2011;36:3244–54.
[8] Zhang YJ, Wei YM. An overview of current research on EU ETS: evidence from its operating mechanism and economic effect. Appl Energy 2010;87:1804–14.
[9] Gartner E. Industrially interesting approaches to "low-CO$_2$" cements. Cem Concr Res 2004;34:1489–98.
[10] Mikulčić H, von Berg E, Vujanović M, Priesching P, Perković L, Tatschl R, et al. Numerical modelling of calcination reaction mechanism for cement production. Chem Eng Sci 2012;69(1):607–15.
[11] Huanpeng L, Wentie L, Jianxiang Z, Ding J, Xiujian Z, Huilin L. Numerical study of gas–solid flow in a precalciner using kinetic theory of granular flow. Chem Eng J 2004;102:151–60.
[12] Iliuta I, Dam-Johansen K, Jensen LS. Mathematical modeling of in-line low-No$_x$ calciner. Chem Eng Sci 2002;57:805–20.
[13] Fidaros DK, Baxevanou CA, Dritselis CD, Vlachos NS. Numerical modelling of flow and transport processes in a calciner for cement production. Powder Technol 2007;171:81–95.
[14] Markovska N, Todorovski M, Bosevski T, Pop-Jordanov J. Cost and environmental effectiveness of climate change mitigation measures. In: Barbir F, Ulgiati S, editors. Sustainable energy production and consumption. Springer Science; 2008. p. 67–73.
[15] Mokrzycki E, Uliasz-Bocheńczyk A, Sarna M. Use of alternative fuels in the Polish cement industry. Appl Energy 2003;74:101–11.
[16] Mokrzycki E, Uliasz-Bocheńczyk A. Alternative fuels for the cement industry. Appl Energy 2003;74:95–100.
[17] Fodor Z, Klemeš JJ. Waste as alternative fuel – Minimising emissions and effluents by advanced design. Process Saf Environ Prot 2011. http://dx.doi.org/10.1016/j.psep.2011.09.004.
[18] Kääntee U, Zevenhoven R, Backman R, Hupa M. Cement manufacturing using alternative fuels and the advantages of process modelling. Fuel Process Technol 2004;85:293–301.

[19] Kakimoto K, Nakano Y, Yamasaki T, Shimizu K, Idemitsu T. Use of fine-grained shredder dust as a cement admixture after a melting, rapid-cooling and pulverizing process. Appl Energy 2004;79:425–42.

[20] Bassioni G. A study towards "greener" construction. Appl Energy 2010. http://dx.doi.org/10.1016/j.apenergy.2010.09.012.

[21] Wang J, Dai Y, Gao L. Exergy analyses and parametric optimizations for different cogeneration power plants in cement industry. Appl Energy 2009;86:941–8.

[22] Wang J, Manovic V, Wu Y, Anthony EJ. A study on the activity of CaO-based sorbents for capturing CO_2 in clean energy processes. Appl Energy 2010;87:1453–8.

[23] Worrell E, Martin N, Price L. Potentials for energy efficiency improvement in the US cement industry. Energy 2000;25:1189–214.

[24] Jaber JO. Future energy consumption and greenhouse gas emissions in Jordanian industries. Appl Energy 2002;71:15–30.

[25] Janeković G, Hublin A, Delija-Ružić V, Vešligaj D. Croatian cement industry and climate changes (In Croatian). Zagreb; 2007. <www.undp.hr/upload/file/208/104184/FILENAME/Studija_cement-klima.pdf> [last accessed 05.02.12].

[26] Ali MB, Saidur R, Hossain MS. A review on emission analysis in cement industries. Renew Sustain Energy Rev 2011;15:2252–61.

[27] Madlool NA, Saidur R, Hossain MS, Rahim NA. A critical review on energy use and savings in the cement industries. Renew Sustain Energy Rev 2011;15:2042–60.

[28] IPCC Good Practice Guidance and Uncertainty Management in National Greenhouse Gas Inventories. </www.ipcc-nggip.iges.or.jp/public/gp/english/> [last accessed 05.02.12].

[29] Schneider M, Romer M, Tschudin M, Bolio H. Sustainable cement production – present and future. Cem Concr Res 2011;41:642–50.

[30] Zhou W, Zhu B, Fuss S, Szolgayova J, Obersteiner M, Fei W. Uncertainty modeling of CCS investment strategy in China's power sector. Appl Energy 2010;87:2392–400.

[31] Roddy DJ. Development of a CO_2 network for industrial emissions. Appl Energy 2012;91:459–65.

[32] Vujanović M. Numerical modeling of multiphase flow in combustion of liquid fuel. PhD thesis, University of Zagreb, Zagreb, Croatia; 2010.

[33] FIRE_v2011_Manuals.

[34] Baburić M, Duić N, Raulot A, Coelho PJ. Application of the conservative discrete transfer radiation method to a furnace with complex geometry. Numer Heat Transfer Part A Appl 2005;48:297–313.

[35] Baburić M, Raulot A, Duić N. Implementation of discrete transfer radiation method into SWIFT computational fluid dynamics code. Therm Sci 2004;8:293–301.

[36] Vujanović M, Duić N, Tatschl R. Validation of reduced mechanisms for nitrogen chemistry in numerical simulation of a turbulent non-premixed flame. React Kinet Catal Lett 2009;96:125–38.

[37] Ban M, Duić N. Adaptation of N-heptane autoignition tabulation for complex chemistry mechanisms. Therm Sci 2011;15:135–44.

[38] Görner K. Technische verbrennungssysteme, grundlagen, modelbildung, simulation. Berlin, Heidelberg: Springer-Verlag; 1991.

[39] Jones WP, Lindstedt RP. Global reaction scheme for hydrocarbon combustion. Combust Flame 1988;73:233–49.

PAPER 4

ORIGINAL PAPER

Numerical analysis of cement calciner fuel efficiency and pollutant emissions

**Hrvoje Mikulčić · Eberhard von Berg ·
Milan Vujanović · Peter Priesching ·
Reinhard Tatschl · Neven Duić**

Abstract Efficient mixing of pulverized fuel and limestone particles inside cement calciners is important due to the reason that the calcination process directly affects the final fuel consumption. The focus of this paper is on the numerical analysis of cement calciner's operating conditions and pollutant emissions. The paper analyzes the influence of different amounts of fuel, mass flow of the tertiary air and the adiabatic wall condition on the decomposition rate of limestone particles, burnout rate of coal particles, and pollutant emissions of a newly designed cement calciner. Numerical models of calcination process and pulverized coal combustion were developed and implemented into a commercial computational fluid dynamics code, which was then used for the analysis. This code was used to simulate turbulent flow field, interaction of particles with the gas phase, temperature field, and concentrations of the reactants and products, by solving the set of conservation equations for mass, momentum, and enthalpy that govern these processes. A three-dimensional geometry of a real industrial cement calciner was used for numerical simulations. The results gained by these numerical simulations can be used for the optimization of cement calciner's operating conditions, and for the reducing of its pollutant emissions.

Keywords Numerical modeling · Cement calciner · Fuel efficiency · Pollutant emissions · Calcination process

Introduction

Large amounts of different anthropogenic greenhouse gases, especially CO_2, are emitted during the cement production process. Since it is well known that CO_2 is the most important greenhouse gas, and that cement industry alone contributes to 5 % of global anthropogenic CO_2 emissions, continuous improvement of energy efficiency in the cement production process is needed (Mikulčić et al. 2013). In order to make the cement industry more greener and lower the CO_2 emissions, increase of the energy efficiency comes first, followed by significant increase of the use of renewable energy sources for electricity generation, transportation, and other sectors, including process industry (Vad Mathiesen et al. 2011). Therefore, policy makers should uphold the good environmental practice in process industry, in order that the applied new technology avoids the use of additional energy, chemicals, and rare catalysts (Maroušek 2012). Aside from the studies investigating the CO_2 emissions coming from the cement manufacturing process, several studies investigated the economical and ecological benefits of waste-to-energy technologies, e.g., using alternative fuels in cement plants. Villar et al. (2012) studied the waste-to-energy technologies in cement industry, and other continuous process industries, showing how GHG emissions and energy use can be reduced. Fodor and

H. Mikulčić (✉) · M. Vujanović · N. Duić
Faculty of Mechanical Engineering and Naval Architecture,
University of Zagreb, Ivana Lučića 5, 10000 Zagreb, Croatia
e-mail: hrvoje.mikulcic@fsb.hr

M. Vujanović
e-mail: milan.vujanovic@fsb.hr

N. Duić
e-mail: neven.duic@fsb.hr

E. von Berg · P. Priesching · R. Tatschl
AVL – AST, Hans List Platz 1, Graz, Austria
e-mail: eberhard.von.berg@avl.com

P. Priesching
e-mail: peter.priesching@avl.com

R. Tatschl
e-mail: reinhard.tatschl@avl.com

Klemeš (2011) investigated the potential use of pre-treated municipal solid waste as an alternative fuel for heat, power, and cement production. Fodor and Klemeš (2012), additionally to the investigation of benefits of using alternative fuels for cement production, studied the applicability and limitations of current and still developing waste-to-energy technologies. The study showed the influence of different waste-to-energy technologies on the environment. Mislej et al. (2012) investigated the combustion behavior and the environmental effect of using alternative fuels for heat generation in cement kilns. The study showed that by using alternative fuels, no notable negative environmental effects can be observed. These studies showed that there is a great potential, especially environmental, of using alternative fuels in cement production.

In recent years, due to stringent environmental measures, a more energy efficient cement production technology, the dry rotary kiln with preheater and calciner technology, is widely replacing the less energy efficiency kiln processes, e.g., wet rotary kiln process, and especially the shaft kiln process (Zhang et al. 2011). Cement calciners are pyroprocessing units found prior to the rotary kiln. Inside of them two strong thermo-chemical reactions occur. The first one is the combustion of pulverized solid fuels, and the second one is a strong endothermic reaction known as the calcination process (Mikulčić et al. 2012a). Controlling of the mixing of these two reactions, inside the cement calciner, is of particular importance since it directly affects the fuel consumption. With the aim of better understanding of the mixing phenomena, heat exchange processes and fluid flow different types of calciners have been investigated. Giddings et al. (2000) numerically investigated the performance of a fully operating cement calciner. The work showed the usefulness of the CFD and some important fluid flow characteristics of the simulated calciner, which cannot be experimentally measured. Huanpeng et al. (2004) performed a numerical study for the effect of different parameters on the dynamics of the two-phase flow in a cement calciner. The study represented the transport properties of the solid phase with the kinetic theory of granular flow. Huang et al. (2005) numerically analyzed the formation of NO, CO, and CO_2 in a cement calciner. The study showed that numerical predictions for burnout of coal particles, limestone decomposition, are in good agreement with the measured results. Hu et al. (2006) simulated a three-dimensional model of a dual combustor and calciner, by using the Eulerian frame for the gaseous phase and a Lagrangian frame for the solid phase. Huang et al. (2006) performed a three-dimensional simulation of a new type swirl-spray calciner. A new method for particle–wall boundary condition and a new four-mixture-fraction model were developed to describe the transport phenomena in a calciner. The work showed that predicted results for

limestone decomposition, coal burnout and the temperature at the exit of the calciner agreed well with measured results. Fidaros et al. (2007) presented a mathematical model and a parametric study of fluid flow and transport phenomena in a cement calciner. The work showed good prediction capabilities for temperature, velocity, and distribution of particles at the calciner exit, where measurements exist. All these studies show that there is still a need for further research and development of cement calciners. However, here should be noted that most of these CFD studies evaluated their numerical predictions with measurement data obtained on the calciner's exit. Due to the lack of measurement data for flow characteristics, and physical and chemical processes inside cement calciners, this approach is satisfactory when looking at pollutant emissions, decomposition ratio for limestone and burnout ratio for char particles. When it comes to, the details about burner region, wall region, or other regions with interesting flow phenomena, the mixing phenomena and the optimization of key physical and chemical processes inside cement calciners, our approach, with separately validated models for calcination process and pulverized coal combustion, improves the available CFD simulation methodology. Due to the high reliability of separately validated models, appropriate accuracy needed for the investigation of named details and optimization of key physical and chemical processes within cement calciners can be achieved with our approach. Since good mixing of both pulverized fuel and limestone particles is essential for a more energy efficient, and thus a cleaner cement production, engineers need to have an in-depth understanding of all relevant reactions that occur inside cement calciners. The use of experimental methods to investigate these reactions is complex and expensive, and thus the use of numerical simulations is a more attractive way to obtain the necessary information. Moreover, results gained by the numerical simulations give more information about the flow and transport processes inside a cement calciner, which is very difficult to obtain experimentally.

The purpose of this paper is to present a numerical analysis of cement calciner's operating conditions and pollutant emissions. The paper analyzes the influence of different amounts of fuel, mass flow of the tertiary air, and the adiabatic wall condition on the decomposition rate of limestone particles, burnout rate of coal particles, and pollutant emissions of a newly designed cement calciner. A three-dimensional geometry of a cement calciner was simulated with a commercial finite volume-based CFD code FIRE. This code was used to simulate turbulent flow field, temperature field, concentrations of the reactants and products, as well as the interaction of particles with the gas phase. Numerical models for the calcination process and pulverized coal combustion, e.g., the process providing the

reaction enthalpy for limestone decomposition, were developed and implemented into the commercial computational fluid dynamics code, which was then used for the analysis. Based on these numerical simulations, interactions between the calcination process and pulverized coal combustion were studied, e.g., regarding cooling effects in the near wall regions, distribution of pollutants was analyzed, and particle trajectories of limestone and fuel were discussed. The results gained by these numerical simulations can be used for the optimization of cement calciner's operating conditions, and for the reducing of its pollutant emissions. Hence, by using numerical techniques and by optimizing cement calciner's operating conditions, less fuel is used, and therefore a more sustainable cement production is achieved.

Numerical model

In order to investigate the influence of different parameters on the decomposition rate of limestone particles, burnout rate of coal particles, and pollutant emissions from a cement calciner, all relevant thermo-chemical reactions must be treated, e.g., the calcination process and the combustion of pulverized coal. In this study, and in the most engineering applications today, the Eulerian–Lagrangian method for solving the multiphase flow phenomena is used. In this approach, the solid particles are represented by finite numbers of particle groups, called parcels. It is assumed that all the particles within one parcel are similar in size and that they have the same physical properties. The motion and transport of the parcels, through the cement calciner, are tracked through the flow field using a Lagrangian formulation, while the gas phase is described by solving conservation equations using a Eulerian formulation. The trajectory of each parcel within the flow field is calculated using the Lagrangian scheme, which means that representative parcels are tracked by using a set of equations that describe their dynamic behavior as they move through the calculated flow field. The coupling between the solid and the gaseous phases is taken into account by introducing appropriate source terms for interfacial mass, momentum, and energy exchange. Lagrangian phase is solved in between two Eulerian phase time steps, with explicit integration method, providing the source terms for the Eulerian phase. Vice versa the solution of the Eulerian phase provides the ambient conditions for the Lagrangian phase.

The developed mathematical models used for the calculation of the calcination process and pulverized coal combustion are treated in the Lagrangian spray module, where thermo-chemical reactions occur inside a particle as well as between the particle and the gas phase. The

developed models together with thermo-physical properties of the limestone, the lime and the components of the pit coal particles, as well as a particle radiation model, were integrated into the commercial CFD code via user-functions written in the FORTRAN programming language, in order to simulate the calcination and combustion process properly (Baburić et al. 2004).

Multiphase flow equations

The equations of continuum mechanics are based on the conservation laws for mass, momentum, and energy. The general form of the time averaged conservation equation for any dependent variable φ, of the continuous phase in the differential form is

$$\frac{\partial}{\partial t}(\rho\varphi) + \frac{\partial}{\partial x_j}(\rho\varphi u_j) = \frac{\partial}{\partial x_j}\left(\Gamma_\varphi \frac{\partial\varphi}{\partial x_j}\right) + S_\varphi, \tag{1}$$

where ρ is the density, u_j is the Cartesian velocity, Γ_φ is the diffusion coefficient, and S_φ is the source term of the dependent variable φ. The source term S_φ is used for the coupling of the Eulerian and the Lagrangian phase.

The momentum differential equation of a parcel is as follows:

$$m_p \frac{du_{ip}}{dt} = F_{idr} + F_{ig} + F_{ip} + F_{ib}, \tag{2}$$

where m_p is the particle mass, u_{ip} is the particle velocity vector, F_{ig} is a force including the effects of gravity and buoyancy, F_{ip} is the pressure force, F_{ib} summarizes other external forces, and F_{idr} is the drag force, given by

$$F_{idr} = D_p \cdot u_{irel}. \tag{3}$$

Here u_{irel} represents the particle relative velocity vector, and D_p is the drag function, defined as

$$D_p = \frac{1}{2}\rho_g A_p C_D |u_{irel}|, \tag{4}$$

where ρ_g is the gas density, A_p is the cross-sectional area of the particle, and C_D is the drag coefficient which is generally a function of the particle Reynolds number Re_p.

From the various formulations in literature for the drag coefficient of a single sphere, FIRE uses the following formulation from Schiller and Naumann (FIRE Manual 2011):

$$C_D = \begin{cases} \frac{24}{Re_p}\left(1 + 0.15Re_p^{0.687}\right) & Re_p < 10^3 \\ 0.44 & Re_p \geq 10^3 \end{cases} \tag{5}$$

Calcination process

The numerical model of the calcination process presented by the following equation:

$$CaCO_3(s) \xrightarrow{+178 kJ/mol} CaO(s) + CO_2(g), \qquad (6)$$
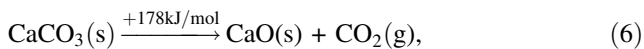
used in this study takes into account the effects of decomposition pressure, temperature, diffusion, and pore efficiency. The developed numerical model is detailed enough to contain the relevant physical and chemical processes, yet simple enough for detailed CFD simulations. The model of the calcination process was thoroughly tested and validated by simulating experiments performed in the International Flame Research Foundation pipe reactor, for which measurements of limestone decomposition exist, in our previous studies (Mikulčić et al. 2012b). The comparison of numerical predictions with the experimental conversion rates showed that the developed model predicted very well the influence of all of the relevant process parameters (temperature, CO_2 content, mass flow, etc.).

Pulverized coal combustion

The combustion of pulverized coal can be considered as a three-step process: devolatilisation process, combustion of char, and combustion of volatiles. The coal particle, composed of pit coal, sulfur, and ash, in first step at high temperatures undergoes the devolatilisation process. The devolatilisation process is the most important physicochemical change in the coal particle. During this step a significant loss of weight occurs, because of the release of volatile matter, the quantity and composition of which depend on the coal ingredients (see Eq. 7). A complex composition, represented via chemical formula $C_{50}H_{18}O_6N_2$, for the pit coal is assumed, which has been chosen to meet the elemental composition of a typical coal as given in the literature (Schnell 1991).

$$C_{50}H_{18}O_6N_2 \rightarrow 5CO + H_2O + CH_4 + H_2 + HCN + NH_3$$
$$+ 37C + C_6H_6. \qquad (7)$$
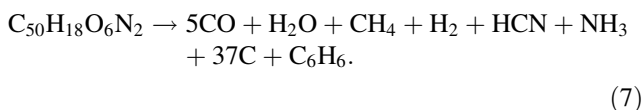
For devolatilisation process (see Eq. 7), a single rate expression is used meaning that the devolatilisation rate dc_{pc}/dt is in a first-order dependency on the amount of pit coal remaining in the particle (Eq. 8)

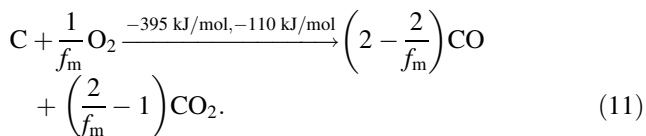$$\frac{dc_{pc}}{dt} = -k_1 y_{pc}. \qquad (8)$$

Here y_{pc} is the mass fraction of pit coal remaining in the particle and k_1 is the kinetic rate defined by an Arrhenius type expression including a pre-exponential factor $k_{0,1}$ and an activation energy E_1 (Eq. 9).

$$k_1 = k_{0,1} \exp(-E_1/RT_p) \qquad (9)$$

The values of the kinetic constants ($k_{0,1}$ is the pre-exponential factor and E_1 is the activation energy) for different

pit coal devolatilisation processes are obtained from the literature (Görner 1991).

Parallel to the devolitilisation, sulfur is oxidized to form SO_2 (Eq. 10), and the char is oxidized to form CO and CO_2 taking into account a mechanism factor depending on coal particle size and temperature (Eq. 11).

$$S + O_2 \rightarrow SO_2 \qquad (10)$$

$$C + \frac{1}{f_m}O_2 \xrightarrow{-395 kJ/mol, -110 kJ/mol} \left(2 - \frac{2}{f_m}\right)CO$$
$$+ \left(\frac{2}{f_m} - 1\right)CO_2. \qquad (11)$$

In Eq. 11, f_m represents the mechanism factor (Görner 1991), which ranges between 1 and 2, causing predominant generation of CO for temperatures higher of approximately 900 K, and predominant production of CO_2 for temperatures lower than 900 K.

Char combustion (Eq. 11) is modeled according to the kinetics/diffusion limited reaction model of Baum and Street (1971). The model assumes that the reaction rate of char combustion is limited either by the kinetics of the heterogeneous reaction k_2^{ch} or by the oxygen's diffusion into the particle's mass expressed by the value of k_2^{ph} as presented in Eqs. 12–15.

$$\frac{dc_c}{dt} = -k_2 A_p p_{ox} y_c \qquad (12)$$

$$k_2 = \frac{k_2^{ch} \cdot k_2^{ph}}{k_2^{ch} + k_2^{ph}} \qquad (13)$$

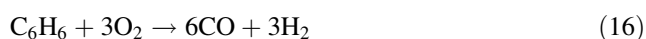$$k_2^{ch} = k_{0,2}^{ch} \cdot \exp(-E_2^{ch}/RT) \qquad (14)$$

$$k_2^{ph} = \frac{24 \cdot f_m \cdot D_0}{R \cdot d_p \cdot T_0^{1.75}} T^{0.75} \cdot 10^5 \qquad (15)$$

In Eq. 8, the char reaction rate dc_c/dt in terms of rate of change of mass fraction is given. Here y_c is the mass fraction of char remaining in the particle, A_p is the specific particle surface, p_{ox} is the oxygen partial pressure, and k_2 is the overall kinetic rate of char combustion. In Eq. 14, the kinetics of the heterogeneous reaction k_2^{ch} are defined as an Arrhenius type expression with a pre-exponential factor $k_{0,1}^{ch}$ and activation energy E_2^{ch}. In Eq. 15, D_0 is the oxygen diffusion coefficient, d_p is the particle diameter, and T_0 is the reference temperature. The values of the kinetic constants for the char combustion model are obtained from the literature (Görner 1991).

Named heterogeneous reactions (Eqs. 7, 10, and 11) cause mass transfer sources and sinks to the gas phase and particles, which are described by rate equations for sulfur and pit coal consumption, char production from devolitilisation and consumption from oxidation. After the completion of the char combustion, the particle is considered as

inert without any further chemical interaction with the gas phase.

The homogeneous reactions of volatiles released during the devolitilisation, are treated within the gas phase reactions module of the used CFD code. A detailed chemistry approach is used for each of the homogeneous reaction. The source terms accounting for the gas phase reactions in the species transport equations and in the gas phase energy equation are calculated with reaction rates depending on species concentrations and temperature, e.g., reaction rates are defined by an Arrhenius law. The modeled homogeneous reactions include tar (here C_6H_6 was chosen as tar representative), CO oxidation (Görner 1991), NOx formation, and the combustion of methane, which is treated via the four-step Jones–Lindstedt mechanism (Jones and Lindstedt 1988). Equation 16 represents the tar (C_6H_6) oxidation, whereas Eqs. 17 and 18a–18d represent the CO oxidation and the four-step Jones–Lindstedt mechanism for methane combustion.

$$C_6H_6 + 3O_2 \rightarrow 6CO + 3H_2 \tag{16}$$

$$CO + \frac{1}{2}O_2 \rightarrow CO_2 \tag{17}$$

$$CH_4 + \frac{1}{2}O_2 \rightarrow CO + 2H_2 \tag{18a}$$

$$CH_4 + H_2O \rightarrow CO + 3H_2 \tag{18b}$$

$$CO + H_2O \leftrightarrow CO_2 + H_2 \tag{18c}$$

$$H_2 + \frac{1}{2}O_2 \rightarrow H_2O \tag{18d}$$

Generally, it is considered that the main NO formation mechanism in coal-fired systems is the fuel-NO formation mechanism. Fuel-NO is formed from the nitrogen bounded in the coal. During the devolatilisation nitrogen is released as HCN and NH_3, which react with oxygen containing species in the flame and produce NO (Molina et al. 2009). Fuel-NO formation from HCN is treated by Eqs. 19a–19b (Görner 1991):

$$4HCN + 5O_2 \rightarrow 4NO + 4CO + 2H_2O, \tag{19a}$$

$$4HCN + 6NO \rightarrow 5N_2 + 4CO + 2H_2O, \tag{19b}$$
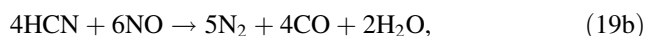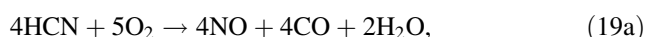
and the De Soete mechanism (De Soete 1975) is used to describe the fuel-NO formation from the NH_3:

$$NH_3 + O_2 \rightarrow NO + H_2O + 0.5H_2, \tag{20a}$$

$$NH_3 + NO \rightarrow N_2 + H_2O + 0.5H_2. \tag{20b}$$
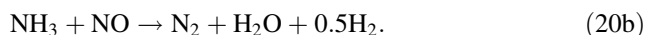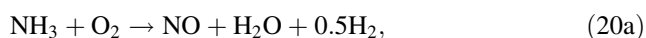
Computational details

The modeled calciner (Fig. 1) consists of two vertical cylinder parts and a cylinder connecting them. On the top of the first vertical cylinder the swirl burner is positioned, and in the second vertical cylinder the hot gas stream from the rotary kiln is used to enhance the calcination process. At the bottom of the second vertical cylinder, a converging–diverging section is used to increase the velocity of the incoming hot stream from the rotary kiln. The entire model is 24 m high, with the diameter of the first cylindrical part, the burner chamber, of 5.5 m, and with the diameter of the second cylindrical part of 4.5 m. The connecting cylinder is positioned at 60° angles and is 4 m in diameter. At the top of the first vertical cylinder, two limestone and two tertiary air inlets are positioned diametrically opposite each other. The top of the second vertical cylinder is the calciner's outlet.

The grid-size dependency was analyzed in our previous study (Mikulčić et al. 2012b), and based on these results, 47,000 cells were employed to discretize the computational domain (Fig. 1) used in the simulation of the cement calciner. The differencing scheme used for momentum, continuity, and enthalpy balances was MINMOD Relaxed
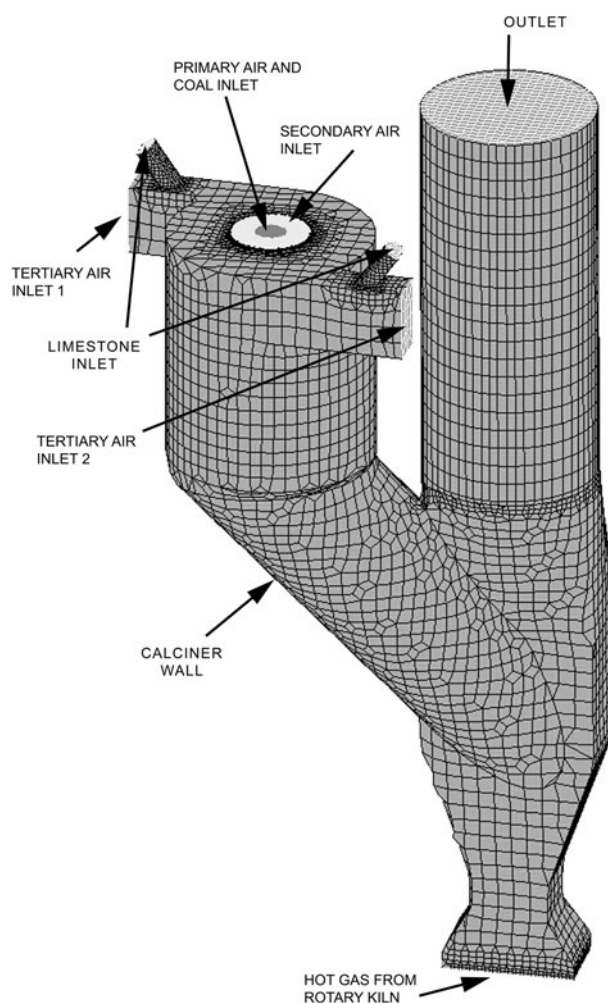

Fig. 1 Calciner geometry and boundary conditions

(FIRE Manual 2011), and for the turbulence and scalar transport equations, an Upwind scheme was applied. Turbulence was modeled by the standard $k - \varepsilon$ model. This is the most widely used turbulence model in CFD simulations of practical engineering applications, and it is generally accepted that the $k - \varepsilon$ model yields realistic predictions of major mean-flow features in most situations. The P-1 radiation model (Sazhin et al. 1996) was used to model the radiative heat transfer and the effects of particle radiation from the limestone and coal particles. The boundary conditions used for the cement calciner's reference case simulation are given in Table 1, and the variation of operating conditions for five other simulation cases are summarized in Table 2. The values for the reference simulation case were the input data that were provided to the authors. In Table 2, the written percentage marks the difference between the calculated case and the reference simulation case, and the dash symbols' that there is no difference between boundary conditions of the calculated case and the reference simulation case.

Results and discussion

Figure 2 shows the streamlines of the flow inside the calculated calciner for the reference case. As can be seen, in the left vertical cylinder part, the burner chamber part, and in the connecting cylinder, the flow is highly swirled. The reason for this highly swirled flow is the big mass flow of the tertiary air that enters at the top of the left vertical cylinder. The highly swirled flow enhances the mixing of pulverized limestone and coal particles, and due to that reason majority of the limestone decomposition, e.g., calcination process, occurs in this part of the calciner. What can also be observed is a small region with recirculation that occurs in the right vertical cylinder part of the calciner. Afterwards the recirculation region vanishes due to the high velocity stream coming from the bottom of the right vertical cylinder part. This high velocity stream is caused by the big mass flow of hot gases entering the calciner from the rotary kiln. All particles are due to the high velocity stream of hot gases from the rotary kiln, blown to the upper calciner outlet. For a plant operator or a practical engineer, understanding of the flow characteristics inside a calciner is of essential importance, since limestone and coal need several seconds to completely decompose and burnout.

Figure 3 shows the velocity field inside the calculated calciner for the reference case. The cross section is positioned 20 m from the bottom of the calciner. On the left hand side of the Fig. 3 the velocity field in the left vertical cylinder, near burner region together with tertiary air inlet is shown. As can be seen, in the near burner region, the flow is highly swirled. The highest velocities are in the outer cylinder part, due to the big mass flow of the tertiary air, and lower velocities can be observed in the center part of the cylinder, where the burner is positioned. Limestone particles are carried by the high velocity flow, and pulverized coal particles are carried by the lower velocity flow. On the right hand side of the Fig. 3 the velocity field in the right vertical cylinder, close to the calcirer's outlet, is shown. As can be observed, in the right vertical cylinder the flow is concentrated on one side. The highest velocities

Table 1 Reference simulation case boundary conditions

Notation	Mass flow rate (kg/h)	T (°C)	ρ (kg/m³)	d_p (μm)	O_2 (mass%)	N_2 (mass%)	CO_2 (mass%)
Limestone 1 + 2	147,900	720	3,100	12			
Tertiary air 1	49,600	950	1.292		28	71.8	0.2
Tertiary air 2	49,600	950	1.292		28	71.8	0.2
Primary air	16,200	80	1.292		28	71.8	0.2
Secondary air	33,065	950	1.292		28	71.8	0.2
Coal	14,811	60	1,300	50			
Hot gas from rotary kiln	110,600	1,100	1.292		8	72	20
Outlet	Static pressure	10^5 Pa					

Table 2 Variation of operating conditions for different cases

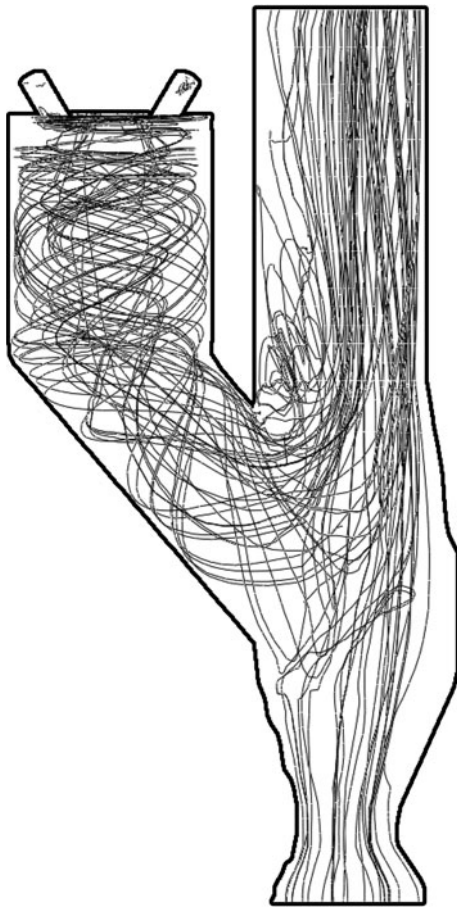| Calculation	Case 1 (%)	Case 2 (%)	Case 3 (%)	Case 4 (%)	Case 5
Tertiary air 1	−20	+20	–	–	–
Tertiary air 2	−20	+20	–	–	–
Coal	–	–	−10	+10	–
Adiabatic wall condition	–	–	–	–	Used

Fig. 2 Preview of flow characteristics inside the calculated calciner

are in the right cylinder part, due to the big mass flow of the hot gases coming from the rotary kiln and their mixing with the flow that is coming from calciner's left vertical cylinder. Lower velocities can be observed in the left part of the cylinder, where the recirculation region is positioned. Here, both decomposed limestone and burned coal particles are carried by the high velocity. These results give valuable information to plant operators, since high particle concentration on one side of the cylinder can cause wall wearing.

Figure 4 shows from left to right, the char, ash, limestone, and lime mass fraction in particles, and their distribution inside the calculated calciner for the reference case. The "empty" regions indicate the regions where conversion of char to CO, CO_2, and ash, and limestone to lime, to a large extent, has already been completed. In this figure, the decrease of char and limestone mass fraction and the corresponding increase of ash and lime mass fraction toward the inlet can be observed. Also, it can be seen that the char and ash particles are located in the middle of the burner chamber, while limestone and lime particles are located in the outer part of the burner chamber, close the calciner wall. Due to the location of limestone particles,

and since the calcination process is a strong endothermic reaction, the thermal load on calciner walls is reduced.

Figure 5 shows the CO mass fraction, temperature field, and NO mass fraction inside the calculated calciner for the reference case. It can be seen that highest concentrations of CO and NO occur close to the burner. The previous statement that due to the location of limestone particles in the outer part of the burner chamber, the thermal load on calciner walls is reduced, is confirmed when looking at the shown temperature field. Here, it can be seen that calcination lowered the temperature in the near wall region, and in that way protects the calciner walls.

Figure 6 shows the temperature field inside the calciner for the six calculated cases. In this figure from left to right the temperature fields for the reference case, cases 1–5 are shown. The figure shows that in all cases in the near wall regains the temperature is lower due to the calcination process. However, it can be seen that cases 2 and 4 have slightly higher temperatures in the connecting cylinder, meaning that the wall thermal load in those two cases is higher. Such results are valuable for plant operators, since they give information that can have an impact on calciners endurance.

Figure 7 shows the CO_2 mass fraction inside the calciner for the six calculated cases. In this figure from left to right the CO_2 mass fraction for the reference case, cases 1–5 are shown. The figure shows that in all cases the highest concentration of CO_2 is in the connecting cylinder, where most of the calcination process takes place. What can also be seen from this figure is that in cases 1, 4, and 5 a slightly higher concentration of CO_2 in the connecting cylinder and in the right vertical cylinder can be observed. This is also valuable information for plant operators, since it is known that the calcination process can extinguish the combustion process.

Although understanding of flow characteristics and thermo-chemical reactions inside cement calciners are important, plant operators and practical engineers are, due to increased environmental awareness, more and more interested in what comes out from the cement calciner. For that reason, in this study, six calculation cases with different parameters were calculated, in order to see the influence of these parameters on fuel efficiency and pollutant emissions. Due to asymmetric distribution of particles and pollutants on the calciner outlet, in Table 3 and Figs. 8 and 9 average values for observed parameters are given.

In Table 3, summarized results for six different cases are shown. As can be seen, for different cases the calciner outlet temperature is almost the same, and this corresponds to the values of calciner outlet temperatures that have been reported in the literature (Zhang et al. 2011). What can also be observed is that almost all cases give the same NO concentration on the calciner outlet.

Fig. 3 Velocity field inside two vertical cylinders of the calculated calciner
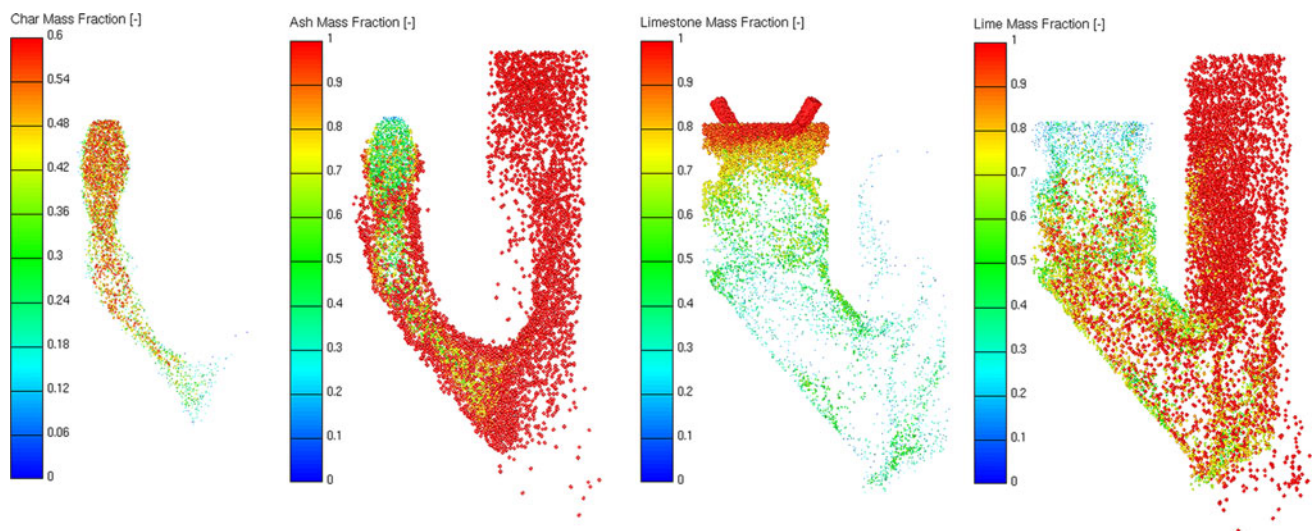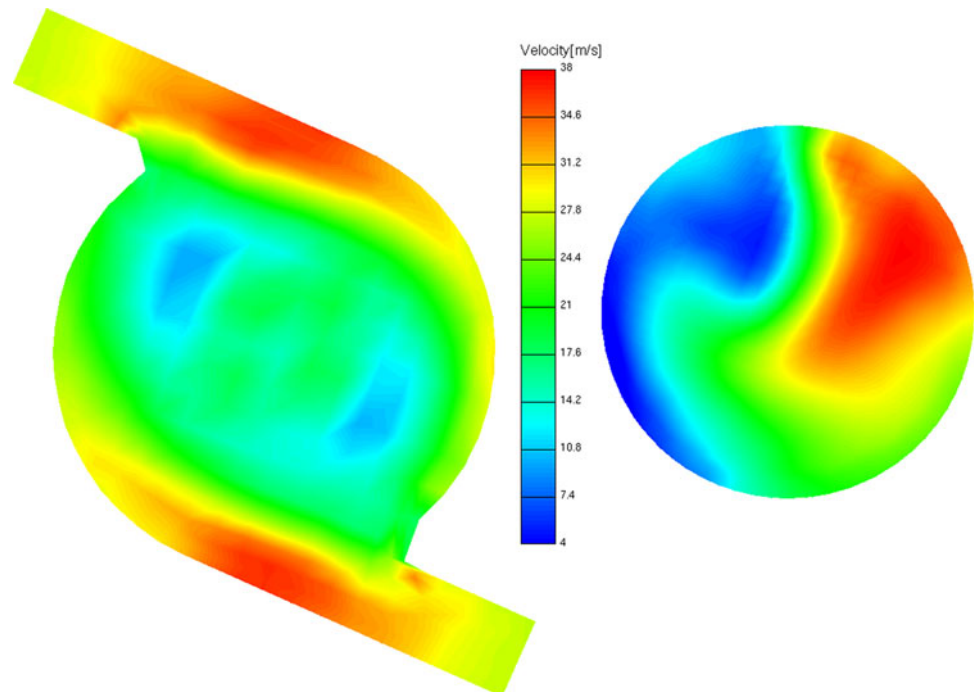

Fig. 4 Char, ash, limestone, and lime mass fraction in particles

Figure 8 shows the comparison of burnout and decomposition ratios on the calciner outlet. It can be seen that for the reference case and cases 1, 4, and 5 almost same values for burnout and decomposition ratio are obtained. However, in cases 2 and 3 lower decomposition ratios are obtained. For case 2, this can be explained due to shorter time limestone spends in the calciner. Limestone is carried by the tertiary air, and in this case higher mass flow of the tertiary air was used. For the case 3, the lower decomposition rate can be explained by the lack of the enthalpy needed for the calcination reaction. The enthalpy is provided by the combustion of fuel, and in this case 10 % less fuel was used.

Figure 9 shows the comparison of CO concentrations in terms of mass fraction on the calciner outlet. It can be seen that the reference case has the lowest CO emissions. It seems that in terms of CO emissions the reference case shows to be the optimal set-up of calciner's operating conditions.

To ensure the adequate conditions for a complete calcination reaction inside cement calciners, good mixing of limestone and pulverized fuel particles are essential for a
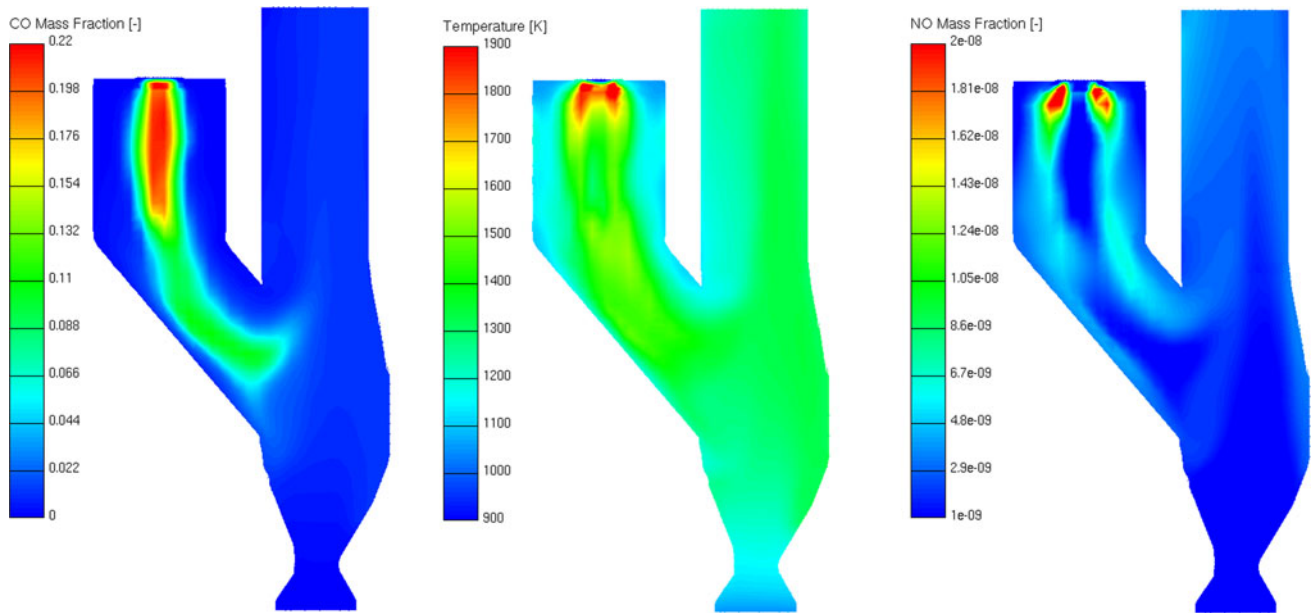
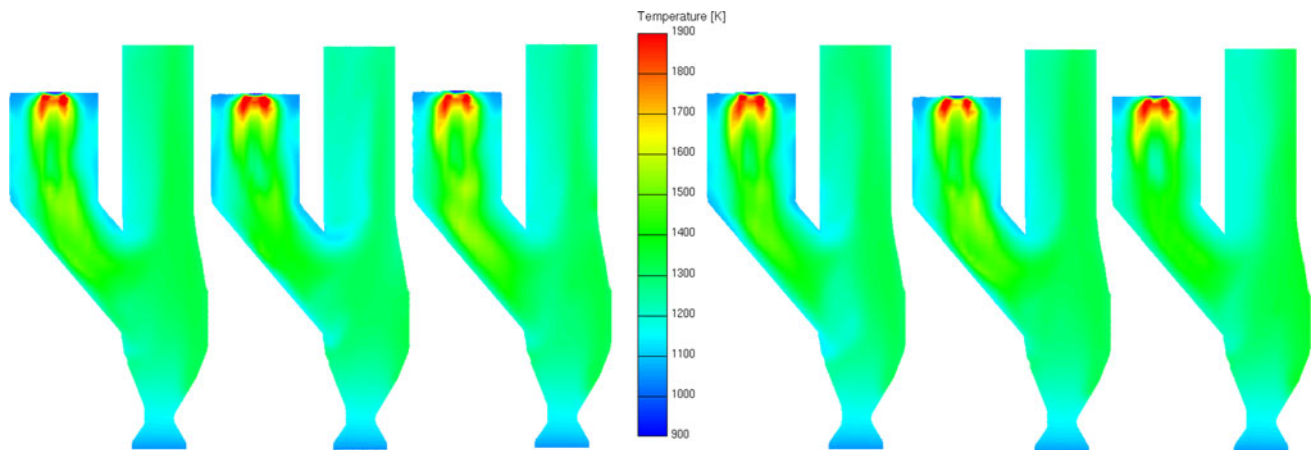**Fig. 5** CO mass fraction, Temperature field, and NO mass fraction inside the calculated calciner

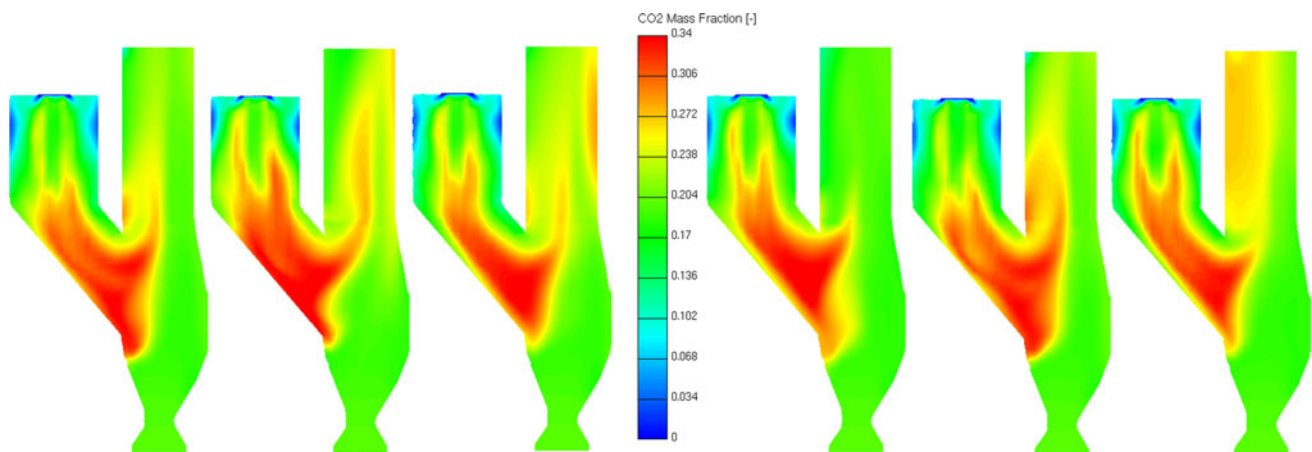**Fig. 6** Temperature fields inside the calciner for the six calculated cases

Fig. 7 CO_2 mass fraction inside the calciner for the six calculated cases

Table 3 Summarized calciner outlet results

	Reference case	Case 1 (−20 % tert. air)	Case 2 (+20 % tert. air)	Case 3 (−10 % fuel)	Case 4 (+10 % fuel)	Case 5 (adiabatic)
NO concentration (kg/kg)	3.329E−09	3.442E−09	3.453E−09	4.084E−09	2.999E−09	2.932E−09
CO concentration (kg/kg)	0.0031115	0.0095239	0.0075068	0.0071763	0.0107001	0.0096996
CO_2 concentrations (kg/kg)	0.2549952	0.2112467	0.2212173	0.2013529	0.2283265	0.2492649
O_2 concentration (kg/kg)	0.0893802	0.0912999	0.1110957	0.1112074	0.0960943	0.1006402
SO_2 concentration (kg/kg)	2.667E−06	1.648E−06	1.362E−06	1.152E−06	1.788E−06	1.676E−06
Outlet mean temperature (K)	1,171.8805	1,172.4826	1,174.7325	1,174.6059	1,172.9354	1,173.8705
Decomposition ratio (−)	0.9990101	0.9978904	0.9859680	0.9262303	0.9964629	0.9990001
Burnout ratio (−)	0.9990011	0.9990012	0.9990014	0.9990015	0.9990014	0.9990011
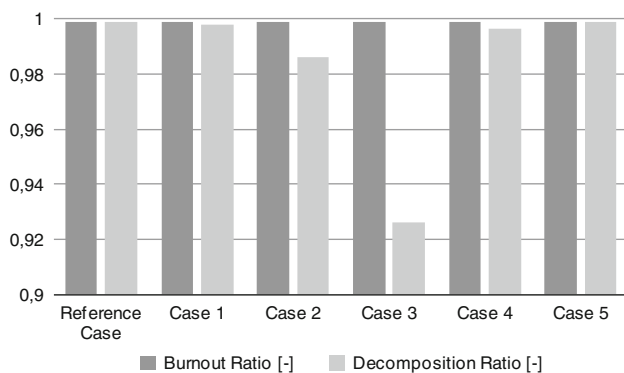
Fig. 8 Comparison of burnout and decomposition ratios
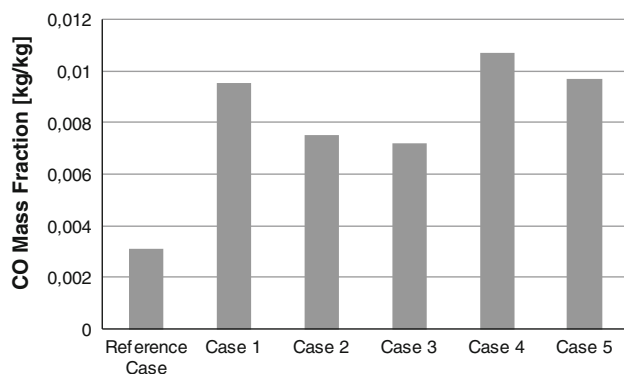
Fig. 9 Comparison of CO concentrations

more energy efficient cement production. The use of experimental methods to investigate the mixing phenomena is complex, expensive, and not that usual nowadays, thus the use of numerical techniques is a more attractive way to obtain the necessary information. Even more, results gained by the numerical investigations give detailed information about the flow characteristics and thermo-chemical reactions that occur inside a cement calciner.

The results gained by this study show some interesting features of the flow, and particle distribution which help to understand the operating conditions of the calculated cement calciner. The results show that the highly swirled flow in the left vertical cylinder and the connecting cylinder prolongs the particle residence time, and enhances the calcination process. The distribution of particles in the left vertical cylinder and the connecting cylinder shows that the wall is protected by the nature of the endothermic calcination process. By taking the heat, in the near wall region, provided by the combustion of pulverized coal, limestone particles decompose and lower the thermal load on the cement calciner wall. Furthermore, the gained results show that the developed models for the calcination process (Mikulčić et al. 2012b) and the pulverized coal combustion coupled with a commercial CFD code, form a promising tool for optimization of cement calciner's fuel consumption and pollutant emissions. That was the focus of this study. Although the comparison of numerically obtained results with experimental data is essential, experimental measurements were not available for this calciner. Nowadays, it is not usual to place measurement equipment in a fully operating industrial calciner. However, it will be very much desirable to have such experimental data in the future.

Conclusion

A numerical model for the prediction of the flow, temperature field, particle trajectories, calcination process, and pulverized coal combustion is presented. For the purpose of

numerical simulations, numerical model of calcination process and pulverized coal combustion was implemented into the commercial computational fluid dynamics code FIRE. Presented model is used to numerically study cement calciner's operating conditions and pollutant emissions. The study shows that it is possible to numerically simulate different thermo-chemical processes inside a cement calciner. By combining the information provided by the temperature field, the particle trajectories, and the decomposition and burnout rates, an interesting picture of the interdependence of their behavior is observed. The highly swirled flow enhances the mixing phenomena of pulverized limestone and coal particles, and prolongs the particle residence time. The highly decomposed limestone that comes out of the calciner suggests that this prolonged residence time is beneficial. Furthermore, the paper analyzes the influence of different parameters on the decomposition rate of limestone particles, burnout rate of coal particles, and pollutant emissions of a newly designed cement calciner. It can be concluded that most of the pollutants that are emitted from the calciner are related to the amount of fuel used. The results obtained by these simulations can be used for the optimization of cement calciner's fuel consumption, and thus its pollutant emissions. The paper demonstrates some important characteristics of cement calciner's operating conditions, which cannot be practically measured. The paper also show that CFD is a useful tool for plant design and process improvements, and that by using CFD engineers could gain an insight into process details. Together with experiments, CFD will be the basis for future cement calciners improvements.

References

Baburić M, Raulot A, Duić N (2004) Implementation of discrete transfer radiation method into SWIFT computational fluid dynamics code. Therm Sci 8:293–301

Baum MM, Street PJ (1971) Predicting the combustion behavior of coal particles. Combust Sci Techn 3:231–243

De Soete GG (1975) Overall reaction rates of NO and N_2 formation from fuel nitrogen, Proceeding 15th Int Symposium on Combust, The Combustion Institute, 1093–1102

Fidaros DK, Baxevanou CA, Dritselis CD, Vlachos NS (2007) Numerical modelling of flow and transport processes in a calciner for cement production. Powder Technol 171:81–95

FIRE_v2011_Manuals (2011), Graz, Austria

Fodor Z, Klemeš JJ (2011) Municipal solid waste as alternative fuel–minimising emissions and effluents. Chem Eng Trans 25:31–38

Fodor Z, Klemeš JJ (2012) Waste as alternative fuel–minimising emissions and effluents by advanced design. Process Saf Environ Prot 90:263–284

Giddings D, Eastwick CN, Pickering SJ, Simmons K (2000) Computational fluid dynamics applied to a cement precalciner. Proc Inst Mech Eng Part A: J Power Energy 214:269–280

Görner K (1991) Technical combustion systems: fundamentals, modelling, simulation. Springer/Heidelberg, Berlin/Germany

Hu Z, Lu J, Huang L, Wang S (2006) Numerical simulation study on gas–solid two-phase flow in pre-calciner. Commun Nonlinear Sci Numer Simul 11:440–451

Huang L, Lu J, Wang S, Hu Z (2005) Numerical simulation of pollutant formation in precalciner. Can J Chem Eng 83:675–684

Huang L, Lu J, Xia F, Li W, Ren H (2006) 3-D mathematical modeling of an in-line swirl-spray precalciner. Chem Eng Process 45:204–213

Huanpeng L, Wentie L, Jianxiang Z, Ding J, Xiujian Z, Huilin L (2004) Numerical study of gas–solid flow in a precalciner using kinetic theory of granular flow. Chem Eng J 102:151–160

Jones WP, Lindstedt RP (1988) Global reaction scheme for hydrocarbon combustion. Combust Flame 73:233–249

Maroušek J (2012) Study on agriculture decision-makers behavior on sustainable energy utilization. J Agric Environ Ethics. doi:10.1007/s10806-012-9423-x

Mikulčić H, Vujanović M, Fidaros DK, Priesching P, Minić I, Tatschl R, Duić N, Stefanović G (2012a) The application of CFD modelling to support the reduction of CO_2 emissions in cement industry. Energy 45:464–473

Mikulčić H, von Berg E, Vujanović M, Priesching P, Perković L, Tatschl R, Duić N (2012b) Numerical modelling of calcination reaction mechanism for cement production. Chem Eng Sci 69:607–615

Mikulčić H, Vujanović M, Duić N (2013) Reducing the CO_2 emissions in Croatian cement industry. Appl Energy 101:41–48

Mislej V, Novosel B, Vuk T, Grilc V, Mlakar E (2012) Combustion behaviour and products of dried sewage sludge—prediction by thermogravimetric analysis and monitoring the co-incineration process in a cement factory. Chem Eng Trans 29:685–690

Molina A, Murphy JJ, Winter F, Haynes BS, Blevins LG, Shaddix CR (2009) Pathways for conversion of char nitrogen to nitric oxide during pulverized coal combustion. Combust Flame 156:574–587

Sazhin SS, Sazhina EM, Faltsi-Saravelou O, Wild P (1996) The P-1 model for thermal radiation transfer: advantages and limitations. Fuel 75:289–294

Schnell U (1991) Calculation of the NOx emissions from pulverized coal combustion. VDI, Düsseldorf

Vad Mathiesen B, Lund H, Karlsson K (2011) 100 % Renewable energy systems, climate mitigation and economic growth. Appl Energy 88:488–501

Villar A, Arribas JJ, Parrondo J (2012) Waste-to-energy technologies in continuous process industries. Clean Technol Environ Policy 14:29–39

Zhang Y, Cao SX, Shao S, Chen Y, Liu SL, Zhang SS (2011) Aspen Plus-based simulation of a cement calciner and optimization analysis of air pollutants emission. Clean Technol Environ Policy 13:459–468

PAPER 5

Waste Management & Research

Numerical study of co-firing pulverized coal and biomass inside a cement calciner

Hrvoje Mikulcic, Eberhard von Berg, Milan Vujanovic and Neven Duic

Published by:

$SAGE

http://www.sagepublications.com

On behalf of:

ISWA
International Solid Waste Association

International Solid Waste Association

Additional services and information for ***Waste Management & Research*** can be found at:

Email Alerts: http://wmr.sagepub.com/cgi/alerts

Subscriptions: http://wmr.sagepub.com/subscriptions

Reprints: http://www.sagepub.com/journalsReprints.nav

Permissions: http://www.sagepub.com/journalsPermissions.nav

Citations: http://wmr.sagepub.com/content/32/7/661.refs.html

>> Version of Record - Jul 10, 2014

OnlineFirst Version of Record - Jun 24, 2014

What is This?

WM&R

Numerical study of co-firing pulverized coal and biomass inside a cement calciner

Hrvoje Mikulčić[1], Eberhard von Berg[2], Milan Vujanović[1] and Neven Duić[1]

Abstract

The use of waste wood biomass as fuel is increasingly gaining significance in the cement industry. The combustion of biomass and particularly co-firing of biomass and coal in existing pulverized-fuel burners still faces significant challenges. One possibility for the *ex ante* control and investigation of the co-firing process are computational fluid dynamics (CFD) simulations. The purpose of this paper is to present a numerical analysis of co-firing pulverized coal and biomass in a cement calciner. Numerical models of pulverized coal and biomass combustion were developed and implemented into a commercial CFD code FIRE, which was then used for the analysis. Three-dimensional geometry of a real industrial cement calciner was used for the analysis. Three different co-firing cases were analysed. The results obtained from this study can be used for assessing different co-firing cases, and for improving the understanding of the co-firing process inside the calculated calciner.

Keywords

Cement calciner, co-firing, coal, biomass, calcination process, CFD

Introduction

Over recent decades, the utilization of biomass for energy generation is constantly gaining more and more on importance (Sommer and Ragossnig, 2011). It is already an important mode of fuel utilization in the electric and heat power generation industry and in some process industries. The annual usage of biomass currently represents approximately 8–14% of the world final energy consumption (Ćosić et al., 2011; Williams et al., 2012). This is a result of increased environmental awareness, the effect of global warming and particularly because biomass is a unique renewable resource that directly replaces the use of fossil fuels (Vad Mathiesen et al., 2012). The cement industry is one of the largest carbon-emitting industrial sectors in the EU and in the world, accounting for approximately 4.1% of EU, and around 5% of world anthropogenic CO_2 emissions (Mikulčić et al., 2013a). In line with the EU commitment to combat climate change, the cement industry, as the third largest carbon-emitting industrial sector, needs to reduce its carbon emission significantly. Due to the need for lowering CO_2 emissions, biomass fuels are to some extent already replacing fossil fuels (Fodor and Klemeš, 2012). Unlike fossil fuels, biomass fuels are considered CO_2 neutral, and can be considered renewable, in the sense that the CO_2 generated by biomass combustion recycles from the atmosphere to the plants that replace the fuel, e.g. to the waste wood or energy crops. Since biomass, including biomass residue, decays and produces methane and other decomposition products that greatly exceed the potency of CO_2 as greenhouse gas, the use of biomass as fuel actually has the potential to decrease greenhouse gas impacts, and not just being neutral (Lu et al., 2008; Ragossnig et al., 2009). Combustion of biomass and especially co-combustion of biomass and coal are modes of fuel utilization that are increasingly gaining in significance in the cement industry (Schneider and Ragossnig, 2013; Thomanetz, 2012).

The development of appropriate combustion units is often very demanding, and time and cost consuming. One possibility for the control and investigation of the biomass combustion and co-combustion process involves computational fluid dynamics (CFD) simulations (Klemeš et al., 2010). Early comprehensive information, parametric studies and initial conclusions that can be gained from CFD simulations are very important in handling modern combustion units. Together with experiments and theory, CFD has become an integral component of combustion research. It has been used in the development process for understanding the complex phenomena occurring within the combustion units. However, CFD simulations of biomass combustion and co-combustion still face significant challenges.

[1]Faculty of Mechanical Engineering and Naval Architecture, University of Zagreb, Zagreb, Croatia
[2]AVL–AST, Hans List Platz 1, Graz, Austria

Corresponding author:
Hrvoje Mikulčić, Faculty of Mechanical Engineering and Naval Architecture, University of Zagreb, Ivana Lucica 5, 10000 Zagreb, Croatia.
Email: hrvoje.mikulcic@fsb.hr

There have been numerous studies that have investigated the biomass combustion on a single-particle level and in real industrial furnaces. Yang et al. (2008) investigated the combustion effects of a single biomass particle. That study showed that the isothermal particle assumption is no longer valid when the particle size exceeds 150–200 μm. This has profound implications on CFD modelling of biomass particles in pulverized fuel furnaces. Momeni et al. (2013) studied the ignition and combustion of biomass particles. That study showed that higher oxygen concentration and higher oxidizer temperature can greatly accelerate the ignition, devolatilization process and char combustion. Ma et al. (2007) using an Eulerian–Lagrangian frame of reference, numerically investigating the combustion of pulverized biomass in a 1-MW industrial test furnace. The numerical predictions obtained by that study showed good agreement with the measured data. However, the use of CFD for investigating the use of biomass as a fuel in cement pyroprocessing units has until now not been reported. The cement industry uses the biomass as a substitute fuel for coal in the rotary kiln or in the cement calciner (Friege and Fendel, 2011; Pomberger et al., 2012). Cement calciners are pyroprocessing units positioned prior to the rotary kiln, just after the cyclone preheating system. Inside them, the temperature range from 800° to 950°C, and the calcination process occurs (Mikulčić et al., 2013b). Controlling the calcination and the combustion process inside cement calciners is of great importance, as these two reactions have a direct effect on the clinker quality and the amount of energy consumed (Koumboulis and Kouvakas, 2003). For this reason, several studies numerically investigated cement calciners. Giddings et al. (2000) numerically analysed a fully operating cement calciner. The work showed the usefulness of the CFD as a research tool and some important flow characteristics of the simulated calciner, which cannot be experimentally investigated. Huang et al. (2006a) performed a three-dimensional simulation of a new type swirl-spray calciner. The work showed that predicted results for limestone decomposition, coal burnout and the temperature at the exit of the calciner agreed well with measured results. Also Huang et al. (2006b) investigated the cement calciner's operating conditions to lower the NO_x emissions. The study showed that together air and fuel staging can lower the NO_x emissions. Mujumdar et al. (2007) studied the processes occurring in the preheater, the calciner, kiln and cooler, and developed a model for the simulation of these processes. The study showed that with respect to overall energy consumption, for the kiln process studied in this work, the optimum value of calcination in calciner is about 70%. Fidaros et al. (2007) presented a mathematical model and a parametric study of fluid flow and transport phenomena in a cement calciner. The work showed good prediction capabilities for temperature, velocity and distribution of limestone and coal particles at the calciner exit, where measurements exist. Zheng et al. (2012), using the large eddy simulation (LES) simulation approach and the kinetic theory of granular flow, investigated the mixing of particles and the stability of production for the simulated cement calciner. The study showed that operating parameters needed to be set up very precisely to have an efficient and a stable production. Mikulčić

et al. (2013c) numerically investigated the influence of different amounts of fuel, mass flow of the tertiary air on the decomposition rate of limestone particles, burnout rate of coal particles and pollutant emissions of a newly designed cement calciner. The study showed that CFD is a useful tool for plant design and process improvements. All these studies show that there is still a need for further research of cement calciners, especially in the research of biomass combustion and co-firing in cement calciners.

The purpose of this paper is to present a CFD simulation of the co-combustion of biomass and coal in a cement calciner. Numerical models of pulverized coal and biomass combustion were developed and implemented into a commercial CFD code FIRE, which was then used for the analysis. By solving the governing set of conservation equations for mass, momentum and enthalpy, this code was used to simulate a turbulent flow field, interaction of particles with the gas phase, temperature field, and concentrations of the reactants and products. For biomass combustion, as well as for coal combustion, the effects of drying, the degradation during devolatilization, generation of gaseous species and char burnout were taken into account. Furthermore, three-dimensional geometry of a real industrial cement calciner was used for the CFD simulation of biomass and coal co-firing process.

Numerical model

The motion and transport of the solid particles are tracked through the flow field using the Lagrangian formulation, while the gas phase is described by solving conservation equations using the Eulerian formulation. Solid particles are discretized into finite numbers of particle groups, known as parcels, which are supposed to have same size and the same physical properties. The parcels are tracked as they move through the calculated flow field by using a set of equations derived from mass, momentum and enthalpy balances. The coupling between the parcels and the gaseous phase is taken into account by introducing appropriate source terms for mass, momentum and enthalpy exchange. The heterogeneous reactions of the mathematical model used for the calcination process, coal and biomass combustion calculation are treated in the Lagrangian spray module, where thermo-chemical reactions occur, involving particle components and gas phase species. The homogeneous reactions used for the coal and biomass combustion calculation are treated in the gas phase using the Eulerian formulation.

The developed models, together with thermo-physical properties of the limestone, the lime and the components of the biomass and coal particles, as well as a particle radiation model, were integrated into the commercial CFD code via user-functions written in the FORTRAN programming language, in order to simulate the named thermo-chemical reactions properly (Baburić et al., 2004).

Continuous phase

The equations of continuum mechanics are based on the conservation laws for mass, momentum and energy. The general form

of the time averaged conservation equation for any dependent variable φ, of the continuous phase in the differential form is:

$$\frac{\partial}{\partial t}(\rho \varphi) + \frac{\partial}{\partial x_j}(\rho \varphi u_j) = \frac{\partial}{\partial x_j}(\Gamma_\varphi \frac{\partial \varphi}{\partial x_j}) + S_\varphi, \quad (1)$$

where ρ is the density, u_j Cartesian velocity, Γ_φ diffusion coefficient and S_φ is the source term of the dependent variable φ. The source term S_φ is used for the coupling of the Eulerian and the Lagrangian phase.

Calcination process

In general, the following equation presents the calcination process:

$$CaCO_3(s) \xrightarrow{+\ 178\ kJ\ mol^{-1}} CaO(s) + CO_2(g). \quad (2)$$
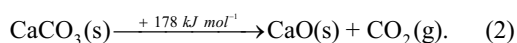
To describe the calcination process, a numerical model previously developed and validated was used (Mikulčić et al., 2012). The developed model takes into account the effects of decomposition pressure, temperature, diffusion and pore efficiency. It is detailed enough to contain the relevant physical and chemical processes, yet simple enough for detailed CFD simulations.

Pulverized coal and biomass combustion

The combustion of biomass can be considered, by analogy to coal combustion, as a four-step process: drying, devolatilization, char combustion and volatile combustion. For coal combustion models, the process of drying is incorporated in the devolatilization models. However, for biomass combustion, the water content is of significant importance and dominates the combustion process.

The evaporation of water vapour is related to the difference in water vapour concentration at the particle surface and in the gas:

$$N_w = k_w(C_p - C_g), \quad (3)$$

where N_w is the molar flux of water vapour, k_w is the mass transfer coefficient, C_p is the water vapour concentration at the particle surface and C_g is the water vapour concentration in the gas.

The water vapour concentration at the particle surface is evaluated by assuming that the partial pressure of water vapour at the particle surface is equal to the saturated water vapour pressure p_{sat}, at the particle temperature T_p:

$$C_p = \frac{p_{sat}}{RT_p}, \quad (4)$$

where R is the universal gas constant.

The concentration of vapour in the gas is known from solution of the following equation:

$$C_g = X_{H2O}\frac{p}{RT}, \quad (5)$$

where X_{H20} is the total local water mole fraction, which includes the air moisture, evaporated moisture, and combustion products

of coal and biomass, p is the local absolute pressure, and T is the local temperature in the gas. The mass transfer coefficient is calculated from the Sherwood number correlation:

$$Sh_{AB} = \frac{k_w d_p}{D_w} = 2.0 + 0.6\,Re_p^{1/2}\,Sc^{1/3}, \quad (6)$$

where d_p is the particle diameter, Re_p is the particle Reynolds number and Sc is the Schmidt number. The Schmidt number is calculated according the following equation:

$$Sc = \frac{\mu}{\rho D_w}, \quad (7)$$

where μ is the dynamic viscosity, ρ is the density and D_w is the diffusion coefficient of water vapour in the gas.

The water vapour flux becomes a source of water vapour in the gas phase species transport equation, and the mass flux of water vapour multiplied by the latent heat becomes a source in the energy equation.

$$m_p c_p \frac{dT_p}{dt} = \alpha A_p(T_g - T_p) +$$
$$\varepsilon_p \sigma A_p(T_g^4 - T_p^4) + \frac{dm_p}{dt}h_{latent} \quad (8)$$

In Eq. 8, m_p is the particle mass, c_p is the particle heat capacity, T_p is the particle temperature, T_g is the surrounding gas temperature, A_p is the particle surface, α is the convective heat transfer coefficient, ε_p is the particle emissivity, σ is the Stefan–Boltzmann constant and h_{latent} is the latent heat.

When the particle reaches the boiling temperature, i.e. 100°C, the boiling of particulate water starts. During the entire boiling process, the particle temperature remains the same, until the entire capillary bounded water is vaporized (Ma et al., 2007).

For devolatilization, a single rate expression is used meaning that the devolatilization rate $dc_{biomass}/dt$ is in a first-order dependency on the amount of biomass remaining in the particle:

$$\frac{dc_{biomass}}{dt} = -k_1 y_{biomass} \quad (9)$$

Here $y_{biomass}$ is the mass fraction of biomass remaining in the particle and k_1 is the kinetic rate defined by an Arrhenius-type expression, including a pre-exponential factor ($k_{0,1}$) and an activation energy (E_1):
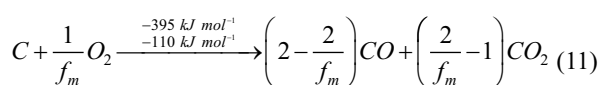
$$k_1 = k_{0,1}\exp\left(-E_1 / RT_p\right) \quad (10)$$

The values of the kinetic constants ($k_{0,1}$, the pre-exponential factor; E_1, the activation energy) for different biomass devolatilization are obtained from the literature (Ma et al., 2007).

Parallel to the devolatilization, char is oxidized to form CO and CO_2 taking into account a mechanism factor depending on char particle size and temperature:

Table 1. Boundary conditions.

	T (°C)	Reference case (100% coal combustion)	Case 1 (biomass 10% energy substitution)	Case 2 (biomass 20% energy substitution)	Case 3 (biomass 30% energy substitution)
		Mass flow rate (kg h⁻¹)			
Limestone 1+2	720	147 900			
Tertiary air 1	950	49 600			
Tertiary air 2	950	49 600			
Primary air	80	16 200			
Secondary air	950	33 065			
Coal	60	14 811	13 330	11 848	10 368
Biomass	60	–	3944	7888	11 833
Hot gas from rotary kiln	1100	110 600			
Outlet (Static Pressure)		10^5 Pa	10^5 Pa	10^5 Pa	10^5 Pa

$$C + \frac{1}{f_m}O_2 \xrightarrow[-110 \ kJ \ mol^{-1}]{-395 \ kJ \ mol^{-1}} \left(2 - \frac{2}{f_m}\right)CO + \left(\frac{2}{f_m} - 1\right)CO_2 \quad (11)$$

In Eq. 11, f_m represents the mechanism factor, which ranges between 1 and 2, causing predominant generation of CO for higher temperatures of approximately 900 K, and predominant production of CO_2 for temperatures lower than 900 K (Görner, 1991).

Char combustion (Eq. 11) is modelled according to the kinetics/diffusion limited reaction model of Baum and Street (1971). The model assumes that the reaction rate of char combustion is limited by either the kinetics of the heterogeneous reaction k_2^{ch} or the oxygen's diffusion into the particle's mass expressed by the value of k_2^{ph}:

$$\frac{dc_c}{dt} = -k_2 A_p p_{ox} y_c \quad (12)$$

$$k_2 = \frac{k_2^{ch} \cdot k_2^{ph}}{k_2^{ch} + k_2^{ph}} \quad (13)$$

$$k_2^{ch} = k_{0,2}^{ch} \cdot \exp\left(-E_2^{ch} / RT\right) \quad (14)$$

$$k_2^{ph} = \frac{24 \cdot f_m \cdot D_0}{R \cdot d_p \cdot T_0^{1.75}} T^{0.75} \cdot 10^5 \quad (15)$$

In Eq. 12 the char reaction rate dc_c/dt in terms of rate of change of mass fraction is given. Here y_c is the mass fraction of char remaining in the particle, A_p is the specific particle surface, p_{ox} is the oxygen partial pressure and k_2 is the overall kinetic rate of char combustion. In Eq. 14, the kinetics of the heterogeneous reaction k_2^{ch} is defined as an Arrhenius-type expression with a pre-exponential factor $k_{0,1}^{ch}$ and activation energy E_2^{ch}. In Eq. 15, D_0 is the oxygen diffusion coefficient, d_p is the particle diameter and T_0 is the reference temperature. The values of the kinetic constants for the char combustion model are obtained from the literature (Görner, 1991).

For the combustion of the volatiles released during the devolatilization process, a detailed chemistry approach is used for each of the homogeneous reaction. The source terms accounting for the gas phase reactions in the species transport equations and in the gas phase energy equation are calculated with reaction rates depending on species concentrations and temperature, e.g. reaction rates are defined by an Arrhenius law. The modelled homogeneous reactions include tar and CO oxidation, NO_x formation and the combustion of methane (Mikulčić et al., 2013c).

Computational details of the simulated cement calciner

To demonstrate the biomass combustion application, a three-dimensional geometry of an industrial cement calciner was used for a numerical simulation of biomass and coal co-firing. A detailed description of the geometry and the boundary conditions of the modelled calciner can be found in our previous study (Mikulčić et al., 2013c).

The grid-size dependency for calcination calculation was analysed in our previous study (Mikulčić et al., 2012), and based on these results, in the simulation of a cement calciner, 47 000 cells were employed to discretize the computational domain. The differencing scheme used for momentum, continuity and enthalpy balances was MINMOD Relaxed (FIRE Manuals, 2011) and for turbulence and scalar transport equations an Upwind scheme was applied. Turbulence was modelled by the standard $k - \varepsilon$ model. The P-1 radiation model was used to model the radiative heat transfer and the effects of the particle.

Since it is well known that the use of alternative fuels in existing pulverized burners alters the flame shape and the temperature profile inside the furnace (Beckmann et al., 2012), three different co-firing cases were simulated. The boundary conditions used for these three co-firing cases are given in Table 1. Furthermore, for consistency and better understanding of the amount of fuel that was substituted, in Table 1 the boundary conditions used for the reference coal combustion case are summarized. The values for the reference coal combustion case were the input data that were provided to the authors (Mikulčić et al., 2013c). The proximate and ultimate analyses of the used coal and biomass are tabulated in Table 2.

Result and discussion

Figure 1 shows the streamlines of the flow inside the calciner for the three calculated co-firing cases. It can be observed that in each case, in the left calciner part, the flow is highly swirled. The reason for this highly swirled flow is the large mass flow of the tertiary air that enters at the top of the calciner. The highly swirled flow enhances the mixing of particles, and the majority of reactions occur in this part of the calciner. What can also be observed is a small difference in the flow of the three co-firing cases. From left to right it can be observed that the streamlines are due to the larger fuel mass load in Case 1

Table 2. Proximate and ultimate analysis of the used coal and biomass.

	Coal	Biomass
Proximate (%wt raw)		
Moisture	0.5	33.00
Volatile matter	29.68	31.97
Fixed carbon	54.82	20.03
Ash	15.0	15.0
Ultimate (%wt daf)		
C	82.94	48.40
H	2.62	7.65
O	9.33	39.16
N	2.31	2.79
S	1.00	1.00
Lower heating value (MJ kg^{-1})	25.34	9.51

daf, dry ash free.

and Case 2 moved from the connecting cylinder top wall to its centre.

In Figure 2, the temperature field inside the calciner for the three calculated co-firing cases is shown. It can be seen that in all three cases in the left calciner part, temperatures in the near wall region are lower than in the centre. This is due to the calcination process, which is a strong endothermic reaction. Furthermore, when comparing the co-firing cases with the case where only the coal was combusted (Mikulčić et al., 2013c), it can be observed that in the co-firing cases in the near burner region the temperatures are roughly 100 K lower.

Figure 3 shows the CO_2 mole fraction inside the calciner for the three calculated co-firing cases. It is known that the majority of CO_2 emissions from cement manufacturing come from the calcination process. Since in modern cement plants calcination occurs in cement calciners, very high concentrations of CO_2 can be found in these units. In all three calculated cases, the highest concentration of CO_2 is in the connecting cylinder, where most of the calcination process takes place.

Figure 4 shows the limestone mass fraction in particles and their distribution inside the calciner for the three calculated co-firing cases. As can be observed, limestone mass fraction decreases from the calciner's inlet towards the outlet, and in all three cases the position of limestone particles is similar. The 'empty' calciner regions in this figure indicate the regions where conversion of limestone to lime has largely already been completed.

Figure 5 shows the lime mass fraction in particles and their distribution inside the calciner for the three calculated co-firing cases. As can be observed due to the available heat provided by the fuel combustion, the limestone decomposes and
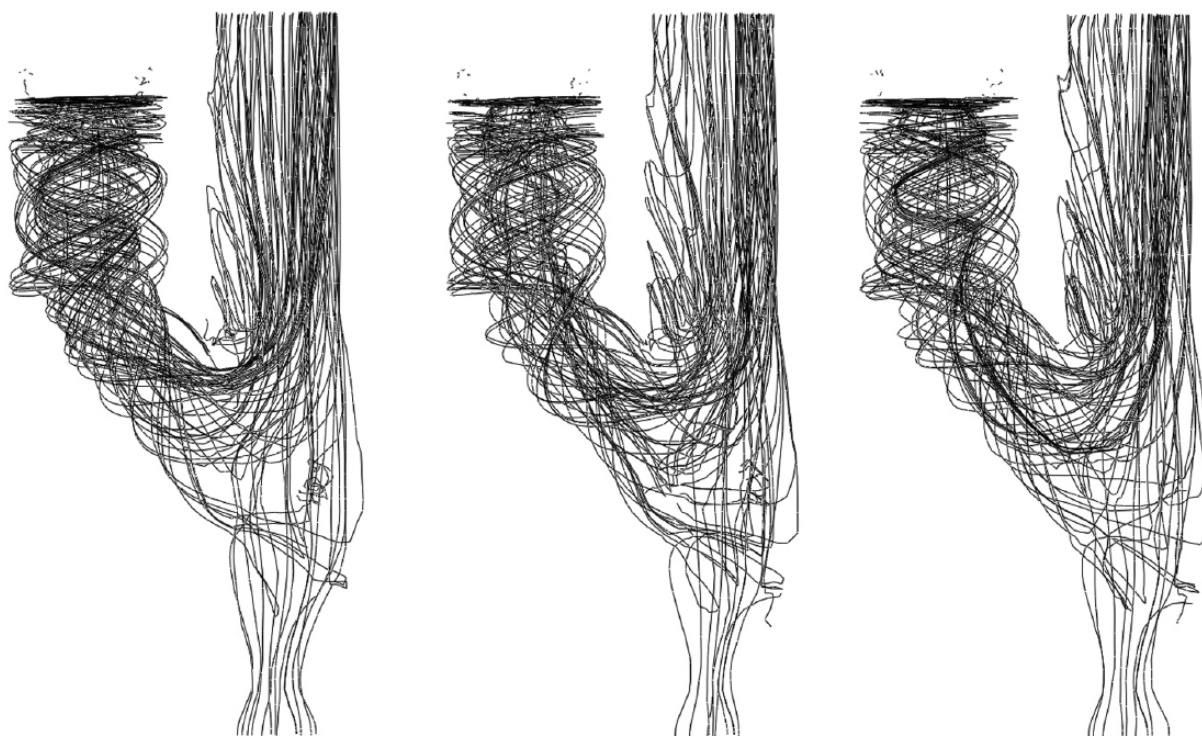

Figure 1. Flow characteristics inside the calciner: Case 1 (left); Case 2 (middle); Case 3 (right).

Figure 2. Temperature field inside the calciner: Case 1 (left); Case 2 (middle); Case 3 (right).
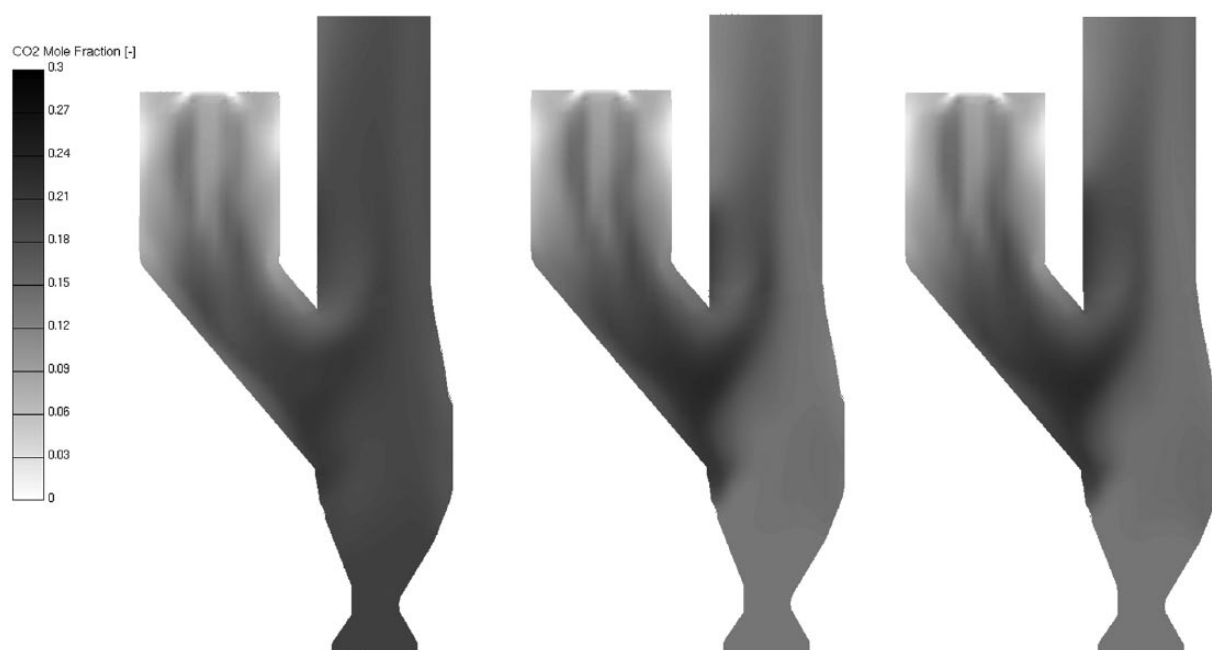

Figure 3. CO_2 mole fraction inside the calciner: Case 1 (left); Case 2 (middle); Case 3 (right).

the lime mass fraction increases from the calciner's inlet towards the outlet.

Figure 6 shows the char mass fraction in particles and their distribution inside the calciner for the three calculated co-firing cases. It can be seen that in all three cases the char particles are located in the middle of the left calciner part, where most of it oxidizes, and afterwards the high-velocity upward stream in the right part of the calciner blows them towards the outlet. Here it should be noted that in all three co-firing cases a small amount of unburned char particles exit the calciner, which was not observed

when just coal was combusted (Mikulčić et al., 2013c). The reason for this is the prolonged combustion time of the biomass particles. The biomass particles, which contain significantly more humidity than coal particle, first have to dry, then undergo devolitilization and after that the formed char particle needs to oxidize. For a plant operator, this information is essential, since it is not desirable to have some burnout char particles in the preheating system. The reason is that char particles can still oxidize in cement cyclones, causing destabilization of the preheating process and formation of undesirable pollutants.
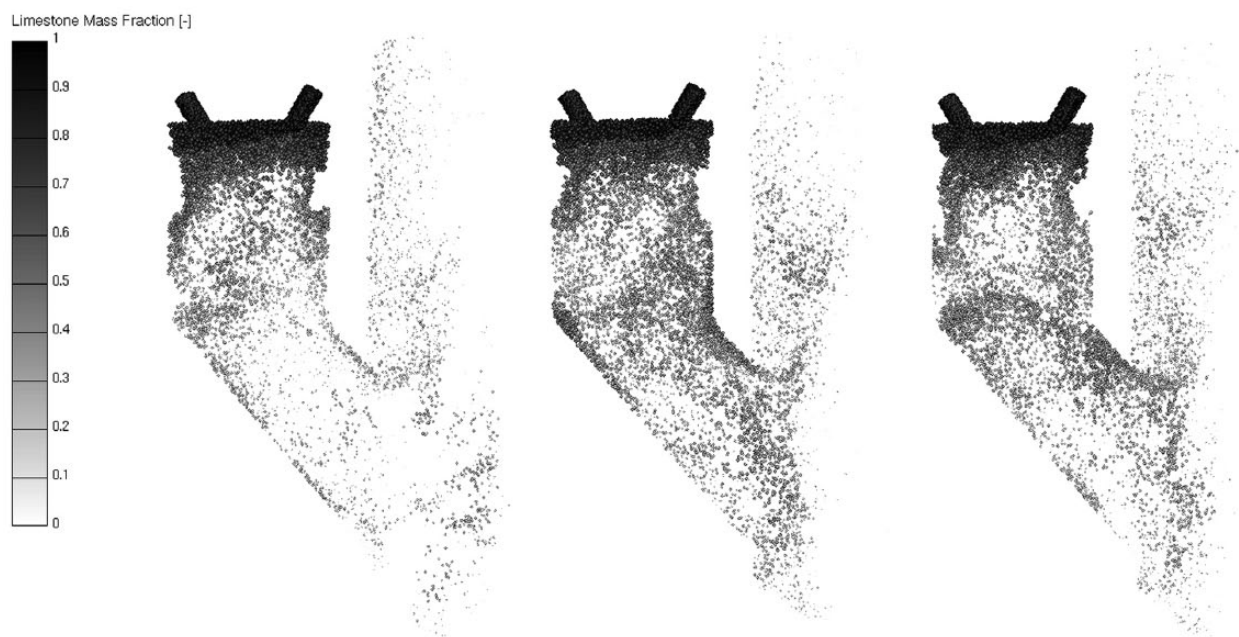
Figure 4. Limestone (CaCO₃) mass fraction in particles: Case 1 (left); Case 2 (middle); Case 3 (right).

Figure 5. Lime (CaO) mass fraction in particles: Case 1 (left); Case 2 (middle); Case 3 (right).

Figure 7 shows a comparison of the char burnout and limestone decomposition ratios on the calciner outlet for the three calculated co-firing cases. It can be seen that all three cases have similar burnout and decomposition ratios; however, when comparing these results with burnout and decomposition ratios of a calciner operating fully on coal, the difference can be seen. The co-firing cases have lower burnout and decomposition ratios. This can be explained by the prolonged combustion time of the biomass particles.

To ensure adequate conditions for a complete calcination reaction inside cement calciners, extensive understanding of the biomass and coal co-firing process is needed. Precisely the results gained by this study show that the developed models, coupled with a commercial CFD code, form a promising tool for improvement of the understanding of the co-firing process.

Conclusion

A numerical analysis of the co-firing of pulverized biomass and coal inside a cement calciner is presented. Numerical models of pulverized coal and biomass combustion were developed and

Figure 6. Char mass fraction in particles: Case 1 (left); Case 2 (middle); Case 3 (right).
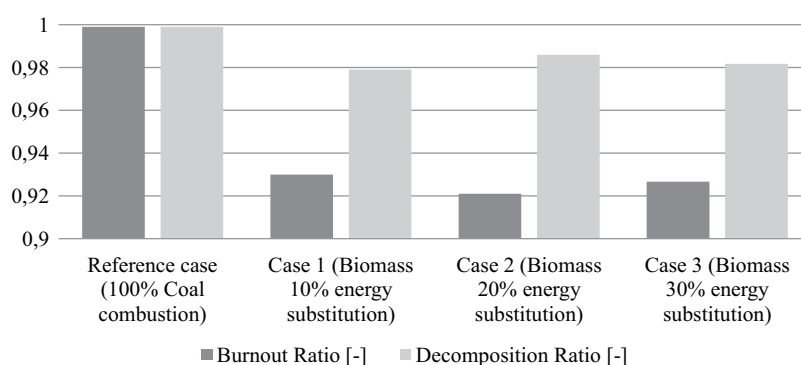

Figure 7. Comparison of burnout and decomposition ratios.

implemented into a commercial CFD code FIRE, which was then used for the analysis. The Eulerian–Lagrangian approach was used for coupling of the gaseous and particle phase. For the pulverized coal and biomass combustion, the effects of drying, devolatilization, char oxidation and volatile combustion are taken into account. For the calcination process, the effects of decomposition pressure, temperature, diffusion and pore efficiency are taken into account. Three-dimensional geometry of a real industrial cement calciner was used for the analysis. Three different co-firing cases were analysed. The results show that when combusting biomass in existing pulverized-fuel burners, special attention needs to be given to the complete oxidation of the char particles, in order to avoid undesirable instabilities in the preheating system. Furthermore, from the results shown it can be concluded that numerical modelling of the co-firing of biomass and coal can assist in improving the understanding of the co-firing process, in the investigation and better understanding of particle kinetics, in the optimization of cement calciner's

operating conditions and finally in reducing pollutant formation in combustion units.

Declaration of conflicting interests

The authors declare that there is no conflict of interest.

References

Baburić M, Raulot A and Duić N (2004) Implementation of discrete transfer radiation method into SWIFT computational fluid dynamics code. *Thermal Science* 8: 293–301.

Baum MM and Street PJ (1971) Predicting the combustion behaviour of coal particles. *Combustion Science and Technology* 3: 231–243.

Beckmann M, Pohl M, Bernhardt D and Gebauer K (2012) Criteria for solid recovered fuels as a substitute for fossil fuels – a review. *Waste Management & Research* 30: 354–369.

Ćosić B, Stanić Z and Duić N (2011) Geographic distribution of economic potential of agricultural and forest biomass residual for energy use: case study Croatia. *Energy* 36: 2017–2028.

Fidaros DK, Baxevanou CA, Dritselis CD and Vlachos NS (2007) Numerical modelling of flow and transport processes in a calciner for cement production. *Powder Technology* 171: 81–95.

FIRE v2011 Manuals (2011) Graz, Austria.

Fodor Z and Klemeš JJ (2012) Waste as alternative fuel – minimising emissions and effluents by advanced design. *Process Safety and Environmental Protection* 90: 263–284.

Friege H and Fendel A (2011) Competition of different methods for recovering energy from waste. *Waste Management & Research* 29: 30–38.

Giddings D, Eastwick CN, Pickering SJ and Simmons K (2000) Computational fluid dynamics applied to a cement precalciner. *Proceedings of the Institution of Mechanical Engineers, Part A: Journal of Power and Energy* 214: 269–280.

Görner K (1991) *Technische Verbrennungssysteme: Grundlagen, Modellbilung, Simulation* (*Technical combustion systems: fundamentals, modelling, simulation*), pp. 180–194. Berlin: Springer.

Huang L, Lu J, Xia F, Li W and Ren H (2006a) 3-D mathematical modeling of an in-line swirl-spray precalciner. *Chemical Engineering and Processing: Process Intensification* 45: 204–213.

Huang L, Lu J, Hu Z and Wang S (2006b) Numerical simulation and optimization of NO emissions in a precalciner. *Energy & Fuels* 20: 164–171.

Lu H, Robert W, Peirce G, Ripa B and Baxter LL (2008) Comprehensive study of biomass particle combustion. *Energy & Fuels* 22: 2826–2839.

Koumboulis FN and Kouvakas ND (2003) Model predictive temperature control towards improving cement precalcination. *Proceedings of the Institution of Mechanical Engineers, Part I: Journal of Systems and Control Engineering* 217: 147–153.

Klemeš JJ, Varbanov PS, Pierucci S and Huisingh D (2010) Minimising emissions and energy wastage by improved industrial processes and integration of renewable energy. *Journal of Cleaner Production* 18: 843–847.

Ma L, Jones JM, Pourkashanian M and Williams A (2007) Modelling the combustion of pulverized biomass in an industrial combustion test furnace. *Fuel* 86: 1959–1965.

Mikulčić H, von Berg E, Vujanović M, Priesching P, Perković L, Tatschl R and Duić N (2012) Numerical modelling of calcination reaction mechanism for cement production. *Chemical Engineering Science* 69: 607–615.

Mikulčić H, Vujanović M and Duić N (2013a) Reducing the CO_2 emissions in Croatian cement industry. *Applied Energy* 101: 41–48.

Mikulčić H, Vujanović M, Markovska N, Filkoski RV, Ban M and Duić N (2013b) CO_2 emission reduction in the cement industry. *Chemical Engineering Transactions* 35: 703–708.

Mikulčić H, von Berg E, Vujanović M, Priesching P, Tatschl R and Duić N (2013c) Numerical analysis of cement calciner fuel efficiency and pollutant emissions. *Clean Technologies and Environmental Policy* 15: 489–499.

Momeni M, Yin C, Kær SK and Hvid SL (2013) Comprehensive study of ignition and combustion of single wooden particles. *Energy & Fuels* 27: 1061–1072.

Mujumdar KS, Ganesh KV, Kulkarni SB and Ranade VV (2007) Rotary Cement Kiln Simulator (RoCKS): integrated modeling of pre-heater, calciner, kiln and clinker cooler. *Chemical Engineering Science* 62: 2590–2607.

Pomberger R, Klampfl-Pernold H and Abl C (2012) Current issues on the production and utilization of medium-calorific solid recovered fuel: a case study on SRF for the HOTDISC technology. *Waste Management & Research* 30: 413–420.

Ragossnig AM, Wartha C and Pomberger A (2009) Climate impact analysis of waste treatment scenarios – thermal treatment of commercial and pretreated waste versus landfilling in Austria. *Waste Management & Research* 27: 914–921.

Schneider DR and Ragossnig AM (2013) Biofuels from waste. *Waste Management & Research* 31: 339–340.

Sommer M and Ragossnig A (2011) Energy from waste in Europe: an analysis and comparison of the EU 27. *Waste Management & Research* 29: 69–77.

Thomanetz E (2012) Solid recovered fuels in the cement industry with special respect to hazardous waste. *Waste Management & Research* 30: 404–412.

Vad Mathiesen B, Lund H and Connolly D (2012) Limiting biomass consumption for heating in 100% renewable energy systems. *Energy* 48: 160–168.

Williams A, Jones JM, Ma L and Pourkashanian M (2012) Pollutants from the combustion of solid biomass fuels. *Progress in Energy and Combustion Science* 38: 113–137.

Yang YB, Sharifi VN, Swithenbank J, Ma L, Darvell LI, Jones JM, Pourkashanian M and Williams A (2008) Combustion of a single particle of biomass. *Energy & Fuels* 22: 306–316.

Zheng Jianxiang, Yan Tingzhi and Yang Jing (2012) Numerical simulation of gas and solid flow behaviour in the pre-calciner with large eddy simulation approach. *Energy Procedia* 17: 1535–1541.

PAPER 6

Improving the sustainability of cement production by using numerical simulation of limestone thermal degradation and pulverized coal combustion in a cement calciner

Hrvoje Mikulčić*, Milan Vujanović, Neven Duić

Faculty of Mechanical Engineering and Naval Architecture, University of Zagreb, Zagreb, Croatia

ABSTRACT

The cement industry sector is one of the largest carbon emitting industrial sectors, and due to the effect of global warming sustainable cement production is increasingly gaining on importance. Controlling the combustion of coal and the thermal degradation of limestone, the two main thermo-chemical processes that occur inside a cement calciner, is of significant importance, since these processes have a direct influence on the cement quality, pollutant formation and overall energy efficiency of the cement manufacturing process. One of the possibilities for the improvement and control of these thermo-chemical processes are Computational Fluid Dynamics – CFD simulations. The results gained from these simulations are being increasingly used to enhance the efficiency of cement production, since they improve the understanding of the flow characteristics and transport phenomena taking place inside the cement calciner. The purpose of this paper is to present that a more energy efficient and sustainable cement production can be achieved by deploying CFD simulations in the process of cement production. The numerical models of limestone thermal degradation, also known as the calcination process, and pulverized coal combustion were developed and implemented within the commercial computational fluid dynamics code FIRE, which was then used for the analysis. The developed models are based on the solution of Navier–Stokes equations for the gas phase, and on the Lagrangian dynamics for the discrete particles. A three dimensional complex geometry of a real industrial cement calciner was used for the CFD simulation. The information obtained from this numerical simulation, such as the distribution of particles, distribution of temperatures and the concentrations can be used for better understanding of particle kinetics and pollutant emissions from the given cement calciner and also for its further investigation and optimization.

© 2014 Elsevier Ltd. All rights reserved.

1. Introduction

Over the past five decades rapid increases in the concentrations of greenhouse gases – GHG in the atmosphere, mainly coming from the industrial sector, have resulted in global climate changes (IPCC, 2007). Due to this reason, cleaner and more sustainable production is becoming more and more important within all industrial sectors (Klemeš et al., 2012). The cement industry sector as an energy intensive industrial sector, where energy costs represent approximately 40% of the total production costs per ton of cement (Zhang et al., 2013), and one of the highest GHG emitting industrial sectors,

accounts for around 5% of global anthropogenic GHG emissions (Wang et al., 2013). Therefore, improvement in energy efficiency is becoming increasingly important for fulfilling the CO_2 emissions limitations coming from this industrial sector (Dovì et al., 2009).

Currently, the most energy efficient technology for cement production is a dry rotary kiln process with a multi-stage preheater and a cement calciner (Benhelal et al., 2013). The latter, cement calciner, is a pyroprocessing unit found in front of the rotary kiln, and inside of which the raw material, mainly composed of limestone, undergoes the calcination process. The calcination process is a strong endothermic reaction that requires combustion heat released by the fuel, indicating that endothermic limestone calcination and exothermic fuel combustion proceed simultaneously (Mikulčić et al., 2013a). Controlling of these two thermo-chemical processes is of significant importance, since they have a direct influence on the cement quality, pollutant formation and overall

energy efficiency of the cement manufacturing process. There are various approaches for controlling and improving of the energy efficiency within industrial furnaces. However, using CFD simulations (Klemeš et al., 2010) to investigate and improve thermo-chemical processes is becoming increasingly important. Together with experiments and theory, CFD simulations have become an integral component of pyroprocessing unit's research. The results gained from CFD simulations can be used for the optimization of turbulent reacting fluid flow, the design of the pyroprocessing unit, and finally for the enhancement of the fuel efficiency, e.g. energy efficiency, making the cement production more sustainable.

Several studies have examined some of the numerical aspects of complex multiphase flow inside cement calciners. Oh et al. (2004) analyzed the turbulent gas-particle flow, coal combustion and heat transfer within a cement calciner. Their work showed that the numerically predicted results agreed well with the measured results. Hillers et al. (2005) numerically investigated processes that occur in cement calciners, e.g. they modelled the turbulence, radiation, calcination process, coal combustion, and NOx formation. Their study showed that CFD shows a great potential regarding emission control and fuel savings. Zheng et al. (2005) studied the effects of primary jet velocity and throat diameter on the two-phase gas—solid flow inside a cement calciner. Their study showed that for the simulated cement calciner, these two effects have a strong influence on flow structure and particle concentration. Dou et al. (2009) investigated the coal combustion and the decomposition of raw material inside a cement calciner. Their work showed that in order to increase the raw material decomposition and optimise the temperature inside the calculated cement calciner, the direction of the tertiary inlet needs to be tangentially adjusted, and that the raw material inlet needs to be opposite the coal inlet. Ha et al. (2010) studied the separation of coal particles and its corresponding influence on the decomposition of limestone inside a cement calciner. Their study showed that by combusting finer coal particles a negligible influence can be observed on the decomposition of limestone. Nance et al. (2011) using the mineral interactive computational fluid dynamics investigated the "Hot-Reburn" conditions inside a cement calciner. Their work showed that the proposed method greatly assists in the optimization of a cement calciner's operating conditions and design. Mikulčić et al. (2013a) numerically studied the impact of different inlet mass flows and fuel amounts, on the coal burnout rate, limestone decomposition rate, and pollutant emissions. Their study showed that CFD is a useful tool for a cement calciner's process optimization. All of these studies show that despite ongoing efforts in the development of both physical and chemical modelling, CFD simulation of the complex multiphase flow inside the cement calciners cannot as yet be considered fully predictive on a quantitative level and further research is required.

The processes occurring inside a cement calciner have a direct influence on cement quality, pollutant formation and the overall energy efficiency of the cement manufacturing process. Appropriate numerical models need to be used to numerically study the role and interaction of pulverized coal combustion and limestone calcination within a cement calciner. In this study a numerical model of pulverized coal combustion was developed and implemented within the commercial finite volume based CFD code FIRE. This code was used to simulate turbulent fluid flow, temperature field, species concentrations and the interaction of particles with the gas phase inside the complex three dimensional geometry of a real cement calciner, by solving the set of mathematical equations that govern these processes. The numerical model is based on the solution of Navier—Stokes equations for the gas phase, and on the Lagrangian dynamics for the discrete particles. Actual plant data were used to verify the accuracy of the modelling approach. The

test of the numerical model's accuracy yielded satisfactory results and proper trends for the coal burnout rate as well as limestone degradation rate. The results gained by this real-plant example show that for better understanding of fluid flow, transport phenomena, and the thermo-chemical reactions taking place inside the cement calciner, the proposed model is a useful tool for investigation. Furthermore, the proposed model can assist in the improvement of the specific local conditions for the calcination process, the overall optimization of cement calciner's operating conditions, reduction of pollutant emissions, and the improvement of the cement calciner's design.

2. Numerical model

The continuous phase is described by solving conservation equations using the Eulerian formulation. These equations are based on the conservation laws for mass, momentum and energy. They are obtained by using the finite volume approach, where the fluid flow is divided into a number of control volumes and a mathematical description is developed for the finite control volume. The general form of conservation equation is fundamentally derived in integral form, taking into consideration the total amount of some property within the control volume:

$$\int_V \frac{\partial}{\partial t}(\rho\varphi)\mathrm{d}V + \int_S (\rho\varphi)u_j n_j \mathrm{d}S = \int_S \left(\Gamma_\varphi \frac{\partial\varphi}{\partial x_j}\right)n_j \mathrm{d}S + \int_V S_\varphi \mathrm{d}V,$$

(1)

where t is the time, ρ is the density, V is the volume, S is the surface, u_j velocity, n_j normal vector, x_j Cartesian coordinates, Γ_φ diffusion coefficient, and S_φ is the source term of the dependent variable φ. In Eq. (1) the first term is an unsteady term, the second term is convection, the third term is diffusion and the last term is source or sink. The first term on the left hand side represents the rate of change of the scalar property φ in the control volume. The second term on the left hand side is the net convective flux of this property across the control volume boundaries. The first term on the right hand side is the net diffusive flux across the control volume boundaries. The final term on the right hand side is the source or sink of the property φ. Two transport mechanisms can be distinguished across the control volume boundaries: convection — transport due to the motion of the fluid, and diffusion — transport due to the differences in concentration.

The motion and transport of the solid particles are tracked through the flow field using the Lagrangian formulation. Solid particles are discretized into finite numbers of particle groups, known as particle parcels, which are supposed to have same size and also the same physical properties. The trajectory of each particle parcel within the flow field is calculated using the Lagrangian scheme, which means that representative parcels are tracked by using a set of equations that describe their dynamic behaviour as they move through the calculated flow field. Furthermore, the equations of motion for each particle parcel based on the Lagrangian approach are coupled with the Eulerian representation of the continuous phase. This allows the decomposition of complicated and highly nonlinear systems of transport equations and describes the interactions between the control volumes and the system of equations that govern processes in individual control volumes, including the exchange between the solid particles and the gas phase. The systems of these equations are mainly integrated using a much shorter time step than the global time steps that are used for calculation of the gas phase. The coupling between the parcels and the gaseous phase is taken into account by introducing appropriate source terms for mass, momentum and enthalpy exchange.

The heterogeneous reactions of the mathematical model used for the calcination process, coal combustion calculation are treated in the Lagrangian spray module, where thermo-chemical reactions occur inside a particle involving particle components and gas phase species. The homogeneous reactions used for the coal combustion calculation are treated in the gas phase using the Eulerian formulation. In order to simulate the named thermo-chemical reactions properly, the developed models were integrated into the commercial CFD code via user-functions written in the FORTRAN programming language (FIRE, 2011).

2.1. Calcination process

Calcination is an industrial process that uses high temperature to change the chemical and physical properties of limestone, a sedimentary rock composed of the mineral calcite – calcium carbonate and other mineral dolomites. The calcination process is used in many different industries today, such as cement, chemical, pharmaceutical and sugar industry, where limestone $CaCO_3$ is converted by thermal decomposition into lime CaO and carbon dioxide CO_2. This reaction is highly endothermic and requires combustion heat released by the fuel where the temperature is between 780 °C and 1350 °C, indicating that endothermic limestone calcination and exothermic fuel combustion proceed simultaneously. The following equation is used to present the calcination process:

$$CaCO_3(s) \xrightarrow{+178 \text{ kJ/mol}} CaO(s) + CO_2(g). \tag{2}$$
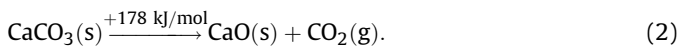
The previously developed and validated numerical model was used to describe the calcination process (Mikulčić et al., 2012). In the developed model, limestone calcination reaction is calculated using the Arrhenius rate equation for the liberation of CO_2 from the particle. The model takes into account the effects of temperature, decomposition pressure, diffusion, and particle porosity since dissociation of the limestone begins at the outer surface of the limestone particle and shifts inward, leaving a porous layer of lime at the surface.

2.2. Pulverized coal combustion

Pulverized coal combustion is a very significant mode of fuel utilization the cement industry. Due to the increase of environmental awareness, and the need for more sustainable coal utilization, plant operators are trying to lower greenhouse gas emissions. Moreover, due to the current energy crisis the need for the design of more powerful, fuel efficient, and environmentally friendly combustion systems is more and more highlighted. In addition to the influence on cement quality, pulverized coal combustion also affects the overall energy efficiency of the cement manufacturing process and the pollutant formation.

The combustion of coal can be considered, as a four step process: drying, devolatilisation process, combustion of char, and combustion of volatiles. In some extreme cases, different combustion stages may co-exist within a single particle (Backreedy et al., 2006).

2.2.1. Drying process

The evaporation of water vapour is related to the difference in water vapour concentration at the particle surface and in the gas:

$$N_w = k_w(C_p - C_g), \tag{3}$$

where N_w is the molar flux of water vapour, k_w is the mass transfer coefficient, C_p is the water vapour concentration at the droplet surface, and C_g is the water vapour concentration in the gas.

The water vapour concentration at the droplet surface is evaluated by assuming that the partial pressure of water vapour at the particle surface is equal to the water saturation pressure p_{sat}, at the particle temperature T_p:

$$C_p = \frac{p_{sat}}{RT_p}, \tag{4}$$

where R is the universal gas constant.

The concentration of vapour in the gas is known from solution of the following equation:

$$C_g = X_{H_2O}\frac{p}{RT}, \tag{5}$$

where X_{H_2O} is the local water mole fraction, p is the local absolute pressure, and T is the local temperature in the gas. The mass transfer coefficient is calculated from the Sherwood number correlation (Ranz and Marshall, 1952a,b):

$$Sh_{AB} = \frac{k_w d_p}{D_w} = 2.0 + 0.6Re_p^{\frac{1}{2}}Sc^{\frac{1}{3}}, \tag{6}$$

where d_p is the particle diameter, Re_p is the particle Reynolds number, and Sc is the Schmidt number. The Schmidt number is calculated according the following equation:

$$Sc = \frac{\mu}{\rho D_w}, \tag{7}$$

where μ is the dynamic viscosity, ρ is the density, and D_w is the diffusion coefficient of water vapour in the gas.

The water vapour flux becomes a source of water vapour in the gas phase species transport equation, and the mass flux of water vapour multiplied by the latent heat becomes a source in the energy equation.

$$m_p c_p \frac{dT_p}{dt} = \alpha A_p(T_g - T_p) + \varepsilon_p \sigma A_p\left(T_g^4 - T_p^4\right) + \frac{dm_p}{dt}h_{latent}. \tag{8}$$

In Eq. (8), m_p is the particle mass, c_p is the particle heat capacity, T_p is the particle temperature, T_g is the surrounding gas temperature, A_p is the particle surface area, α is the convective heat transfer coefficient, ε_p is the particle emissivity, σ is the Stefan–Boltzmann constant, and h_{latent} is the latent heat.

When the particle reaches the boiling temperature, i.e. 100 °C, the boiling process starts. During the whole boiling process particle temperature remains the same, until the entire capillary bounded water is vaporized (Agraniotis et al., 2010).

2.2.2. Devolatilisation process

For devolatilisation a single rate expression is used meaning that the devolatilisation rate dc_{coal}/dt is in a first order dependency on the amount of coal remaining in the particle (Eq. (9)).

$$\frac{dc_{coal}}{dt} = -k_1 y_{coal}. \tag{9}$$

Here y_{coal} is the mass fraction of coal remaining in the particle and k_1 is the kinetic rate defined by an Arrhenius type expression including a pre-exponential factor ($k_{0,1}$) and an activation energy (E_1) (Eq. (10)).

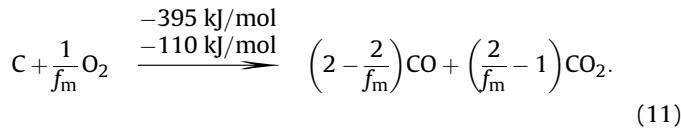$$k_1 = k_{0,1}\exp\left(-E_1/RT_p\right). \tag{10}$$

The values of the kinetic constants ($k_{0,1}$ – the pre-exponential factor and E_1 – the activation energy) for devolatilisation of different coals are obtained from the literature (Görner, 1991).

2.2.3. Volatile combustion

For the combustion of the volatiles released during the devolatilisation process, a detailed chemistry approach is used for each homogeneous reaction. The source terms in the species transport equations and in the gas phase energy equation, accounting for the gas phase reactions, are calculated with reaction rates depending on species concentrations and temperature, i.e. as defined by the Arrhenius law. The modelled homogeneous reactions include tar and CO oxidation, NO_x formation and the combustion of methane (Mikulčić et al., 2013b).

2.2.4. Char combustion

Parallel to the devolatilisation, coal char is oxidized to form CO and CO_2 taking into account a mechanism factor depending on char particle size and temperature.

$$C + \frac{1}{f_m}O_2 \xrightarrow[\substack{-395\ \text{kJ/mol} \\ -110\ \text{kJ/mol}}]{} \left(2 - \frac{2}{f_m}\right)CO + \left(\frac{2}{f_m} - 1\right)CO_2. \tag{11}$$

In Eq. (11), f_m represents the mechanism factor, which ranges between 1 and 2, and is calculated by the following expressions:

$$f_m = \frac{2f_{CO} + 2}{f_{CO} + 2}; \quad d_p < 50\ \mu m, \tag{12}$$

$$f_m = \frac{2f_{CO} + 2}{f_{CO} + 2} - \frac{f_{CO}(d_p - 50)}{(f_{CO} + 2) \cdot 950}; \quad 50\ \mu m < d_p < 1000\ \mu m. \tag{13}$$

Here d_p is the particle diameter, and the temperature dependence f_{CO} is defined as (Arthur, 1951)

$$f_{CO} = 2500 \cdot \exp(-6240/T), \tag{14}$$

where T is the temperature.

Char combustion (Eq. (11)) is modelled according to the kinetics/diffusion limited reaction model of Baum and Street (1971). The model assumes that the reaction rate of char combustion is limited either by the kinetics of the heterogeneous reaction k_2^{ch} or by the oxygen's diffusion into the particle's mass expressed by the value of k_2^{ph} as presented in Eqs. (15)–(18).

$$\frac{dc_c}{dt} = -k_2 A_p p_{ox} y_c, \tag{15}$$

$$k_2 = \frac{k_2^{ch} \cdot k_2^{ph}}{k_2^{ch} + k_2^{ph}} \tag{16}$$

$$k_2^{ch} = k_{0,2}^{ch} \cdot \exp\left(-E_2^{ch}/RT\right) \tag{17}$$

$$k_2^{ph} = \frac{24 \cdot f_m \cdot D_0}{R \cdot d_p \cdot T_0^{1.75}} T^{0.75} \cdot 10^5 \tag{18}$$

In Eq. (15) the char reaction rate dc_c/dt in terms of rate of change of mass fraction is given. Here y_c is the mass fraction of char remaining in the particle, A_p is the specific particle surface area, p_{ox} is the oxygen partial pressure, and k_2 is the overall kinetic rate of char combustion. In Eq. (16) the kinetics of the heterogeneous reaction k_2^{ch} is defined as an Arrhenius type expression with a pre-exponential factor $k_{0,1}^{ch}$ and activation energy E_2^{ch}. In Eq. (18) D_0 is

the oxygen diffusion coefficient, d_p is the particle diameter, and T_0 is the reference temperature. The values of the kinetic constants for the char combustion model are obtained from the literature (Görner, 1991).

3. Computational details

A complex geometry cement calciner used in the cement plant Lukavac, Bosnia and Herzegovina, was simulated and analyzed. Fig. 1 shows the calculated calciner's three dimensional geometry and the boundary conditions used in the CFD simulation. The calciner is 75 m high in total. The lower part of the calciner consists of two vertical tubes, of which one is used as the tertiary air inlet, and the other is used as an inlet for the hot flue gases coming from the rotary kiln. At the bottom of each of these tubes, inlets for coal and pre-dried limestone are positioned. Both tubes have an approximate diameter of 2 m, and they connect at the height of 25 m to form a rectangular shaped junction, where tertiary air and hot flue gases coming from the rotary kiln, together with the introduced limestone and coal particles, are mixed. After the rectangular shaped junction a single vertical tube, with diameter of 3.1 m, serves to direct the flow to the top of the calciner. The top of the calciner is designed in a way that it, by using the swirling effect, directs the upward stream to a downward stream. Finally after the flow is directed downwards, a tube, with diameter of 3.1 m, is used to direct the fluid flow together with now already calcined raw
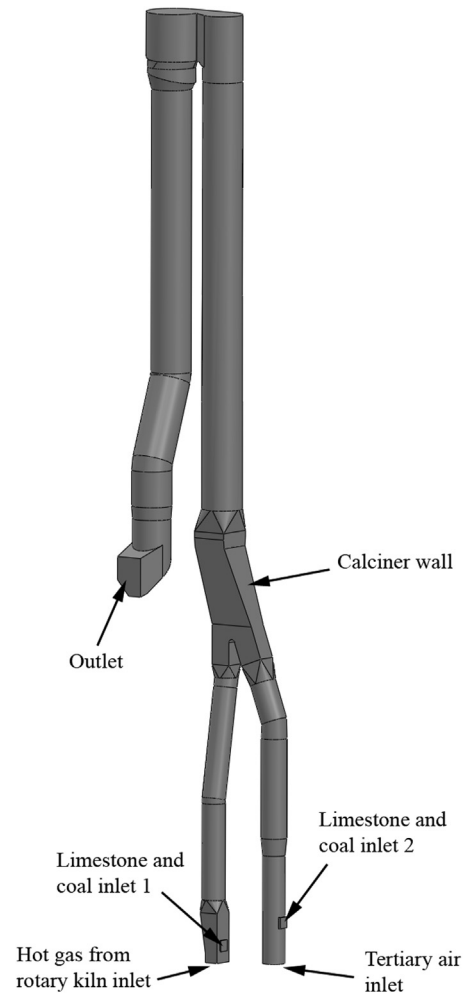

Fig. 1. Cement calciner's geometry and boundary conditions.

Table 1
Boundary conditions.

Notation		Mass flow rate [kg/h]	T [°C]	ρ [kg/m³]	d_p [μm]	O_2 [mass %]	N_2 [mass %]	CO_2 [mass %]
Limestone and coal inlet 1	Coal	5800	70	1300	50			
	Limestone	126,000	780	3100	50			
Limestone and coal inlet 2	Coal	1380	70	1300	50			
	Limestone	21,000	780	3100	50			
Tertiary air inlet		20,690	780	1.292		28	71.8	0.2
Hot gas from rotary kiln inlet		48,275	1060	1.292		8	72	20
Outlet	Static pressure	10^5 Pa						

material to the outlet of the calciner. The outlet of the calciner corresponds to the inlet of the fifth preheater cyclone, where measurement data are obtained. The total calciner volume is 603 m³.

The computational domain consists of 160,000 cells, which were employed to discretize the computational domain. The differencing scheme used for momentum, continuity and enthalpy balances was MINMOD Relaxed (FIRE, 2011) and for turbulence and scalar transport equations an Upwind scheme was applied. Turbulence was modelled by the standard $k-\varepsilon$ model. The P-1 radiation model was employed to model the radiative heat transfer. The P-1 radiation model takes into account the radiative heat exchanges between gas and particles, and is accurate in numerical simulations of pulverized coal combustion with radiation scattering (Sazhin et al., 1996). It has some disadvantage but it is advantageous in a way that it is easily applicable to the complicated geometries, like the one used in this study. The boundary conditions used for the cement calciner's simulation are given in Table 1. The values given in Table 1 were the input data that were provided to the authors.

The coal used in the cement plant Lukavac, comes from the coal quarry located close to the cement plant. Its composition was the input data that was provided to the authors. The proximate and ultimate analysis of used coal is tabulated in Table 2.

4. Result and discussion

CFD is an effective tool for the investigation of the multiphase flow inside the cement calciner. The results showed some interesting features of the flow, which help to understand the operating conditions of the simulated calciner.

Fig. 2 shows the flow streamlines inside the calculated calciner. As can be observed, in the lower part of the calciner, in the tertiary air tube and the hot flue gases coming from the rotary kiln tube, the flow streams are stable and uniform, and going upwards. Both streams join together in the rectangular shaped junction, after which they form one stream that is going upwards to the top of the calciner. In this part of the calciner the majority of the limestone thermal degradation, e.g. calcination process, occurs. At the top of the calciner, where the fluid flow changes the direction, from an upward to a downward direction, the flow becomes highly swirled. The reason for this highly swirled flow is the big mass flow of the stream that is coming to the top of the calciner and the design of the

calciner's top, that by using the swirling effect effectively changes the flow direction. After the flow is directed downwards, the flow gradually loses its swirling effect and together with now already calcined raw material goes to the outlet of the calciner. Understanding of the flow characteristics inside the calciner is of crucial

Fig. 2. Flow streamlines inside the calculated calciner.

Table 2
Proximate and ultimate analysis of the used coal.

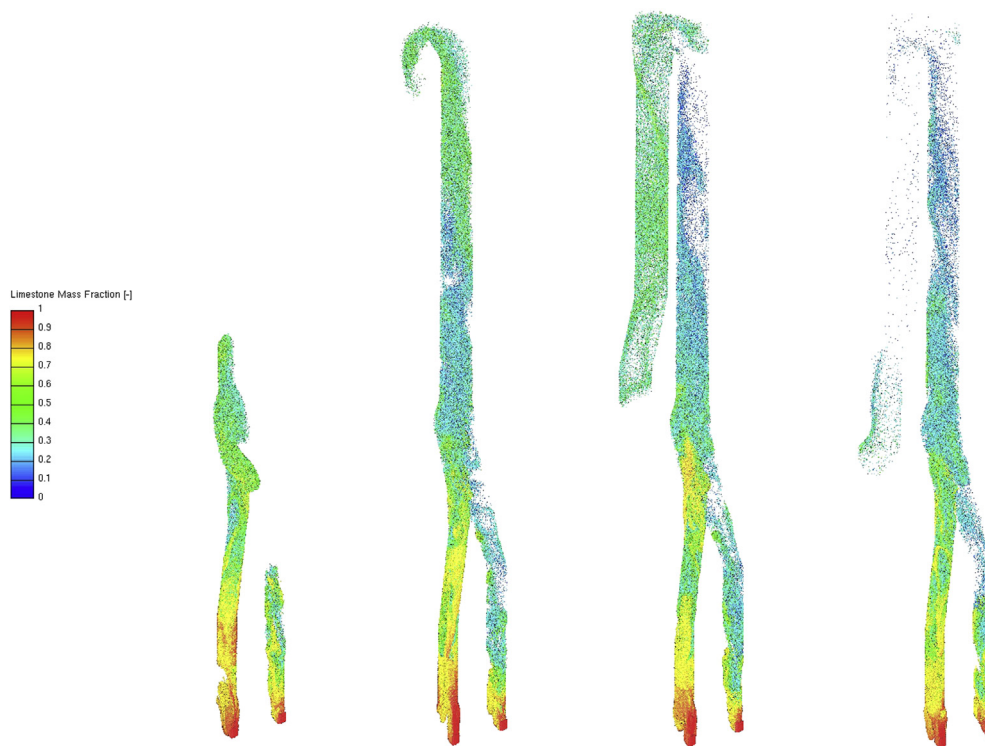| Proximate (%wt raw)		Ultimate (%wt daf)	
Moisture	7.64	C	77.94
Volatile matter	15.38	H	5.07
Fixed carbon	32.16	O	1.69
Ash	44.82	N	13.87
Lower heating value (MJ/kg)	23.34	S	1.43

Fig. 3. Limestone degradation at different particle residence time: 2 s (left); 4 s (second from left); 6 s (second from right); 8 s (right).

importance for plant operators, since the flow characteristics give a good estimation of the particle residence time. The particle residence time is important, since limestone and coal need several seconds to fully decompose and burn.

Fig. 3 shows, from the left hand side to the right hand side, the position of limestone particles and its degradation at 2, 4, 6 and 8 s of particle residence time. For each particle residence time, the limestone mass fraction in particles is shown. It can be seen that limestone particles need several seconds to fully decompose.

Fig. 4 shows, from the left hand side to the right hand side, the position of produced lime particles at 2, 4, 6 and 8 s of particle residence time. For each particle residence time, the lime mass
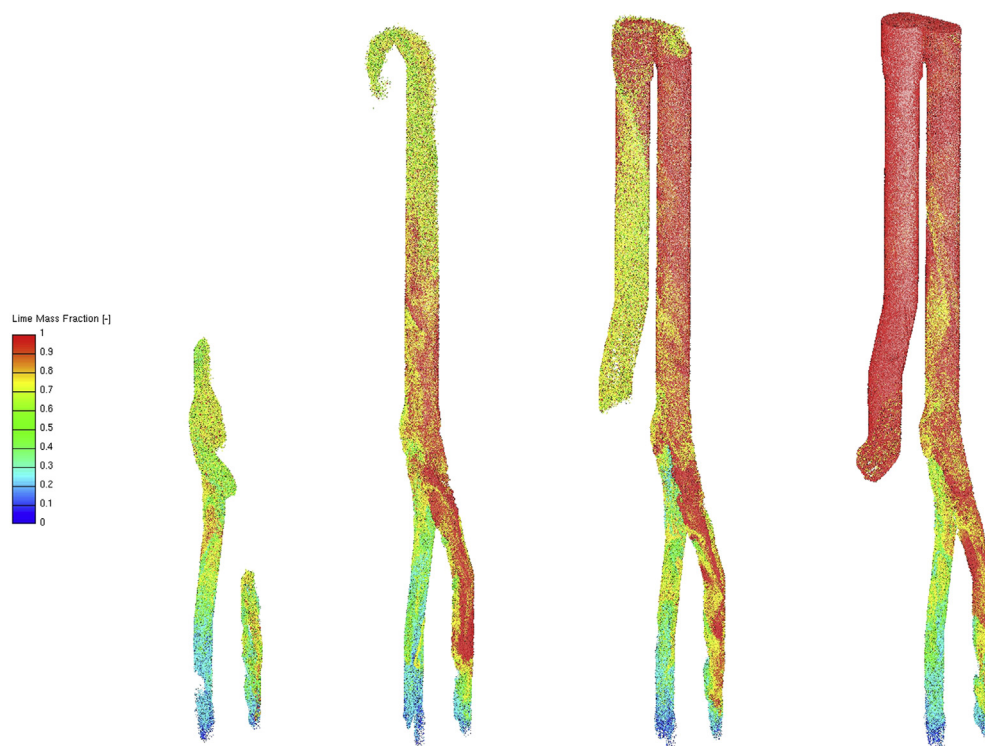

Fig. 4. Lime production at different particle residence time: 2 s (left); 4 s (second from left); 6 s (second from right); 8 s (right).
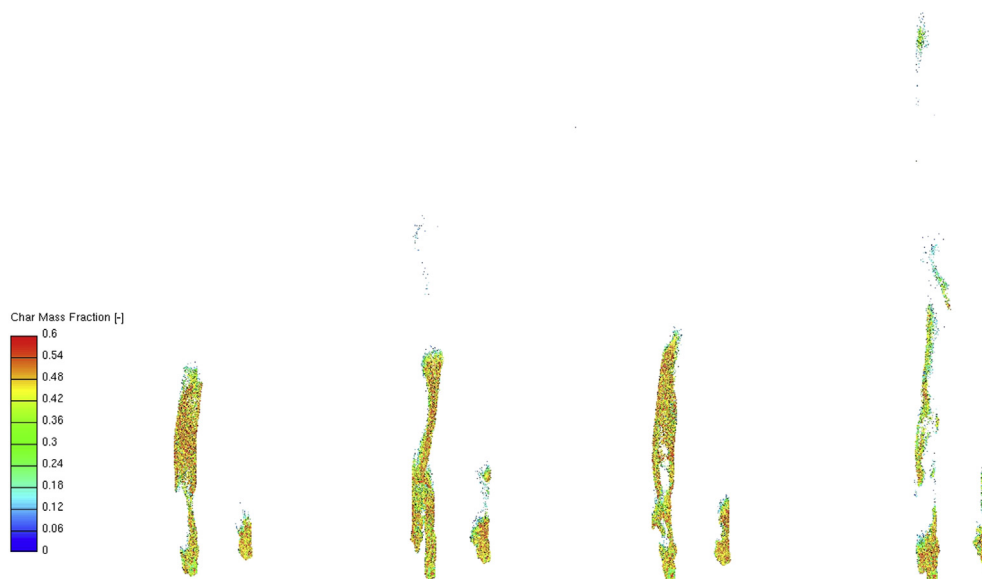
Fig. 5. Char oxidation at different particle residence time: 2 s (left); 4 s (second from left); 6 s (second from right); 8 s (right).

fraction in particles is shown. When compared to Fig. 3, the corresponding increase of the lime mass fraction at different particle residence time can be observed. In this figure, like in the previous one, it can be observed that the calcination process needs several seconds to finish.

Fig. 5 shows, from the left hand side to the right hand side, the position of char particles in the lower calciner part at 2, 4, 6 and 8 s of particle residence time. For each particle residence time, the char mass fraction in particles is shown. As can be observed, char particles combust in the lower part of the calciner, e.g. in two vertical tubes, of which one is used as the tertiary air inlet, and the other is used as an inlet of hot flue gases coming from the rotary kiln. Here it can be seen that unlike the calcination process, the char oxidation is a faster reaction and it does not need several seconds to fully react.

In Fig. 6 the particle residence time is shown. Due to increased environmental awareness, but also by increased environmental restrictions, plant operators and practical engineers are increasingly being interested in efficient cement production. Particle residence time is an important parameter for stabile and efficient operating cement calciner. As it was seen in previous figures raw material needs several seconds to fully decompose, by knowing the particle residence time inside the cement calciner plant operators can adjust the operating conditions for a more efficient operating calciner.

Due to the complex geometry of the calculated calciner, it is difficult to represent the concentration of species and the temperature field. For that reason, the back view of the calciner is shown in Figs. 7 and 8. Fig. 7 shows the combustion process inside the calculated calciner. The char mass fraction in particles is presented on the left hand side, in middle the temperature field is presented, and on the right side the ash mass fraction in particles is presented. Also the distribution of char and ash particles inside the calculated calciner is shown. The 'empty' regions for char mass fraction indicate the regions where conversion of char to CO, CO_2, and ash, to a large extent, has already been completed. In this figure the decrease of char mass fraction and the corresponding increase of ash mass fraction towards the outlet can be observed. Also, it can be seen that since the calcination process is a strong endothermic reaction, throughout the cement calciner the temperature field is uniform and there are no extreme temperature peaks inside the calciner. When looking at the shown temperature field, it can be
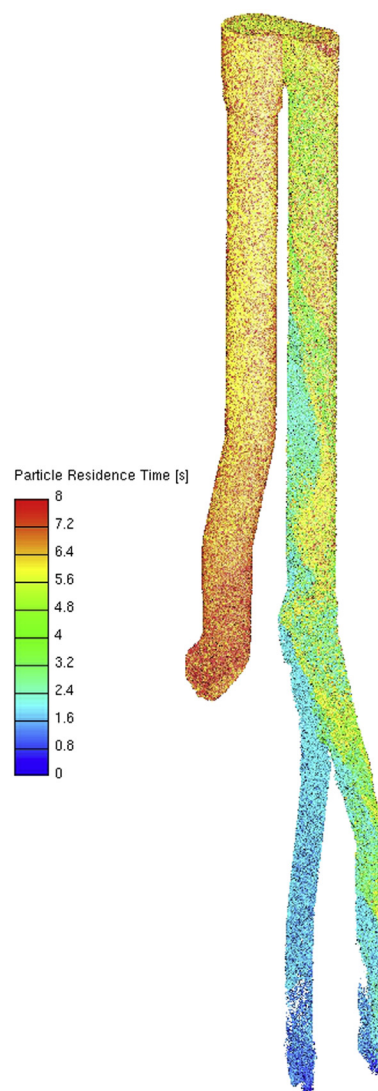

Fig. 6. Particle residence time.

observed that calcination process lowers the temperature, and in that way lowers the thermal load on the calciner's walls. Furthermore, from Fig. 7 the distribution of char and ash particle can be observed. It can be seen that the char particles are concentrated close to the inlets, and that the ash particles are found in the whole calciner.

Fig. 8 shows the thermal degradation of limestone inside the calculated calciner. On the left hand side the limestone mass fraction in particles is shown, in middle the CO_2 mass fraction is shown, and on the right hand side of the figure the produced lime mass fraction in particles is shown. It can be observed that as expected the limestone particles decompose from bottom of the calciner to its top and exit. The corresponding increase of the lime mass fraction can be observed on the right hand side of the figure. The mass fraction of lime in the particle increases as raw material particles move to the top of the calciner and its exit. The CO_2 mass fraction shown in the middle of the figure shows that the highest concentrations are located at the bottom of the calciner where the combustion of coal occurs, and between the rectangular junction and the top of the calciner where most of the calcination process occurs.

Comparison of numerically obtained results with experimental data is essential for the validation of the numerical model used. The measurement equipment of this fully operating industrial calciner was placed on its outlet. On the outlet of the calciner, coal burnout rate, limestone degradation rate and the outlet temperature was measured. In Table 3, the comparison of measurement data and numerical predictions is shown. As can be seen, the numerical predictions are in good correlation with the measured data. Coal burnout rate is the same, whereas for the limestone degradation rate and the outlet temperature numerical predictions are slightly higher, but still in good agreement with the measured data.

The results presented herein show that computer simulation method can serve as an advanced tool to analyze and improve understanding of complex turbulent reacting flow in real cement calciner. The proposed models and methods can assist plant operators and practical engineers in the optimization of cement calciner's operating conditions, which are crucial to ensure better plant efficiency and reduction of pollutant emissions.

5. Conclusion

Computer modelling of the combustion and calcination processes provides a valuable tool that can be used for the investigation and better understanding of particle kinetics and pollutant emissions from cement combustion systems. A numerical model for the prediction of the flow, temperature field, calcination process, and pulverized coal combustion was presented. The numerical model of the pulverized coal combustion, as well as the numerical model of the calcination process, was implemented into a
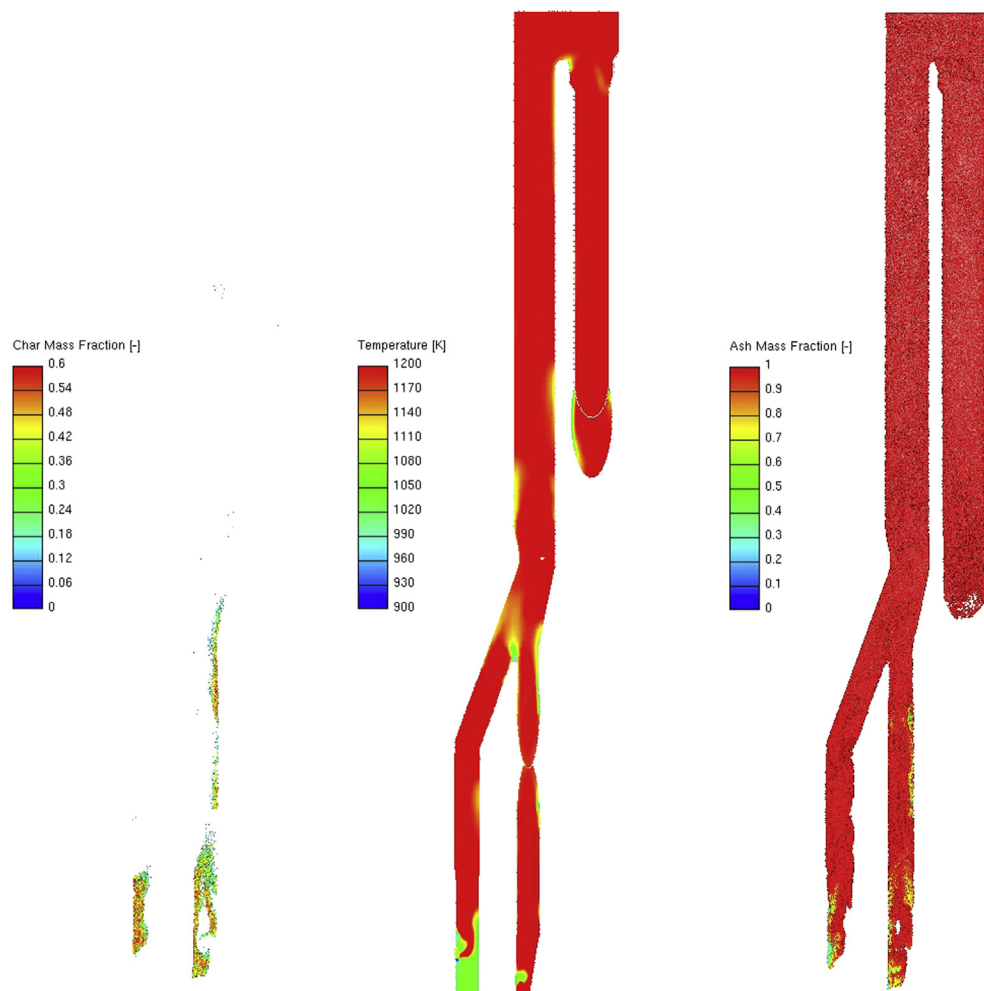

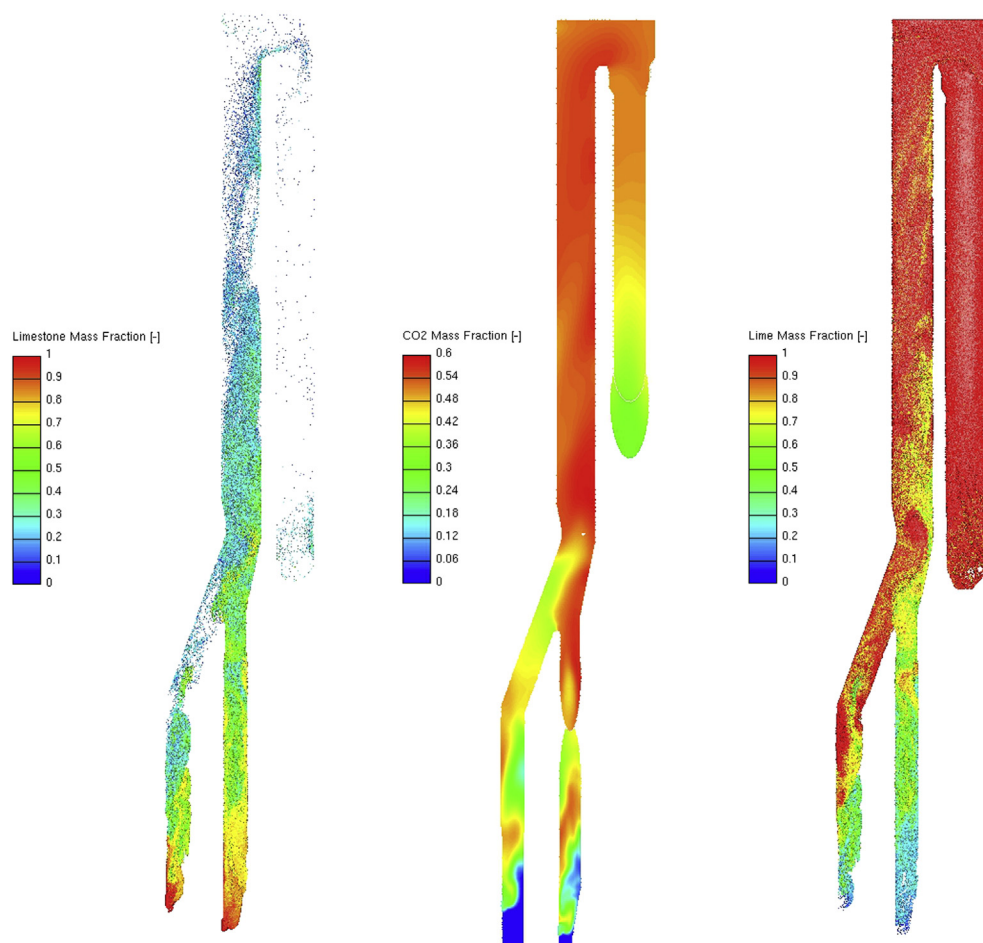**Fig. 7.** Combustion process inside the calculated calciner.

Fig. 8. Calcination process inside the calculated calciner.

commercial CFD code FIRE. The model takes into account the effects that dominate the named thermo-chemical reactions. For the pulverized coal combustion the effects of drying, the degradation during devolatilisation, generation of gaseous species and char oxidation are taken into account. For the calcination process the effects of decomposition pressure, temperature, diffusion, and particle porosity were taken into account. The model is detailed enough to contain the relevant physical and chemical processes, yet simple enough to run on the real industrial meshes needed for detailed CFD simulations of pyroprocessing units. The numerically obtained results were compared with available measurement data, and they are in good agreement. From the results shown it can be concluded that the presented model can be used for the investigation of reactive multiphase flows, and that numerical modelling can assist in the improvement of specific local conditions needed for the efficient calcination process. This paves the way for facilitating the reduction of pollutant emissions thus contributing to a more sustainable cement production.

Table 3
Comparison of measurement data and numerical predictions.

	Measurement data	Numerical predictions
Coal burnout rate [−]	1.0	0.999
Limestone degradation rate [−]	0.957	0.983
Outlet temperature [K]	1188	1213

References

Agraniotis, M., Nikolopoulos, N., Nikolopoulos, A., Grammelis, P., Kakaras, E., 2010. Numerical investigation of solid recovered fuels' co-firing with brown coal in large scale boilers − evaluation of different co-combustion modes. Fuel 89, 3693−3709.

Arthur, J.A., 1951. Reactions between carbon and oxygen. Trans. Faraday Soc. 47, 164−178.

Backreedy, R.I., Fletcher, L.M., Ma, L., Pourkashanian, M., Williams, A., 2006. Modelling pulverised coal combustion using a detailed coal combustion model. Combust. Sci. Technol. 178, 763−787.

Baum, M.M., Street, P.J., 1971. Predicting the combustion behavior of coal particles. Combust. Sci. Technol. 3, 231−243.

Benhelal, E., Zahedi, G., Shamsaei, E., Bahadori, A., 2013. Global strategies and potentials to curb CO_2 emissions in cement industry. J. Clean. Prod. 51, 142−161.

Dou, H., Chen, Z., Huang, J., 2009. Numerical study of the coupled flow field in a Double-spray calciner. In: Proceedings — 2009 International Conference on Computer Modeling and Simulation, ICCMS 2009, pp. 119—123 art. no. 4797367.

Dovì, V.G., Friedler, F., Huisingh, D., Klemeš, J.J., 2009. Cleaner energy for sustainable future. J. Clean. Prod. 17, 889—895.

FIRE v2011 Manuals, 2011. Graz, Austria.

Görner, K., 1991. Technical Combustion Systems: Fundamentals, Modelling, Simulation. Springer-Verlag, Berlin, Heidelberg, Germany (in German).

Ha, S., Li, Y., Zhang, H., Shi, H.-Y., Zhu, C., 2010. Study on a separation technology for more efficient utilization of pulverized coals in cement plants. Fuel Process. Technol. 91, 1261—1266.

Hillers, M., Severin, T., Görner, K., Scherer, V., 2005. Process optimization for a precalciner facility of the cement industry. VDI Berichte 1888, 553—558 (in German).

IPCC (Intergovernmental Panel on Climate Change), 2007. IPCC Fourth Assessment Report. Cambridge University Press, Cambridge, United Kingdom and New York, NY, USA. Available at: www.ipcc.ch/publications_and_data/publications_and_data_reports.shtml (accessed 06.11.13).

Klemeš, J.J., Varbanov, P.S., Pierucci, S., Huisingh, D., 2010. Minimising emissions and energy wastage by improved industrial processes and integration of renewable energy. J. Clean. Prod. 18, 843—847.

Klemeš, J.J., Varbanov, P.S., Huisingh, D., 2012. Recent cleaner production advances in process monitoring and optimization. J. Clean. Prod. 34, 1—8.

Mikulčić, H., von Berg, E., Vujanović, M., Priesching, P., Perković, L., Tatschl, R., Duić, N., 2012. Numerical modelling of calcination reaction mechanism for cement production. Chem. Eng. Sci. 69, 607—615.

Mikulčić, H., Vujanović, M., Duić, N., 2013a. Reducing the CO_2 emissions in Croatian cement industry. Appl. Energy 101, 41—48.

Mikulčić, H., von Berg, E., Vujanović, M., Priesching, P., Tatschl, R., Duić, N., 2013b. Numerical analysis of cement calciner fuel efficiency and pollutant emissions. Clean. Technol. Environ. Policy 15, 489—499.

Nance, G., Abbas, T., Lowes, T., Bretz, J., 2011. Calciner design for lower CO and NOx using MI-CFD analysis to optimize "Hot-Reburn" conditions. In: IEEE Cement Industry Technical Conference (Paper) art. no. 5934552.

Oh, S.C., Kim, D.W., Yoon, J.Y., Byun, S.J., Kwon, W.-T., Kim, S.-R., Kim, H.T., 2004. Numerical analysis of turbulent gas-particle flow and coal combustion in a fluidized-bed calciner. J. Ind. Eng. Chem. 10, 208—214.

Ranz, W.E., Marshall Jr., W.R., 1952a. Evaporation from drops, Part I. Chem. Eng. Prog. 48, 141—146.

Ranz, W.E., Marshall Jr., W.R., 1952b. Evaporation from drops, Part II. Chem. Eng. Prog. 4, 173—180.

Sazhin, S.S., Sazhina, E.M., Faltsi-Saravelou, O., Wild, P., 1996. The P-1 model for thermal radiation transfer: advantages and limitations. Fuel 75, 289—294.

Wang, Y., Zhu, Q., Geng, Y., 2013. Trajectory and driving factors for GHG emissions in the Chinese cement industry. J. Clean. Prod. 53, 252—260.

Zhang, H., Dewil, R., Degrève, J., Baeyens, J., 2013. The design of cyclonic pre-heaters in suspension cement kilns. Int. J. Sustain. Eng. http://dx.doi.org/10.1080/19397038.2013.843605.

Zheng, J., Lu, H., Sun, X., He, Y., Ding, J., Wang, S., 2005. Hydrodynamic modeling of gas-particle flows in D-D calciners. Ind. Eng. Chem. Res. 44, 3033—3041.